Study of the functional interplays between condensin and chromatin in fission yeast

Léonard Colin

▶ **To cite this version:**

Léonard Colin. Study of the functional interplays between condensin and chromatin in fission yeast. Biochemistry, Molecular Biology. Ecole normale supérieure de lyon - ENS LYON, 2023. English. NNT : 2023ENSL0094 . tel-04576113

HAL Id: tel-04576113
https://theses.hal.science/tel-04576113

Submitted on 15 May 2024

HAL is a multi-disciplinary open access archive for the deposit and dissemination of scientific research documents, whether they are published or not. The documents may come from teaching and research institutions in France or abroad, or from public or private research centers.

L'archive ouverte pluridisciplinaire **HAL**, est destinée au dépôt et à la diffusion de documents scientifiques de niveau recherche, publiés ou non, émanant des établissements d'enseignement et de recherche français ou étrangers, des laboratoires publics ou privés.

THESE

en vue de l'obtention du grade de Docteur, délivré par

l'ECOLE NORMALE SUPERIEURE DE LYON

Ecole Doctorale N° 340
Biologie Moléculaire, Intégrative et Cellulaire

Discipline :
Sciences de la vie et de la Santé

Soutenue publiquement le 01/12/2023, par :

Léonard COLIN

Study of the functional interplays between condensin and chromatin in fission yeast

Etude de l'interaction fonctionnelle entre la condensine et la chromatine chez la levure à fission

Devant le jury composé de :

MARCAND, Stéphane	DR-CEA	Institut de Biologie François Jacob	Rapporteur
UHLMANN, Frank	Research team leader	Francis Crick Institute	Rapporteur
BYSTRICKY, Kerstin	PR-UPS	CBI Toulouse	Examinatrice
LENGRONNE, Armelle	DR2	IGH Montpellier	Examinatrice
LOPPIN, Benjamin	DR	LBMC	Examinateur
BERNARD, Pascal	DR2	LBMC	Directeur de thèse

TABLE OF CONTENTS (p.2-4)

RESULTS

The scientific article was included in the sections **in blue** when relevant.

Authorship contribution indicated as **Léonard Colin** in the author list. # for equal contribution. PhD supervisor indicated as Pascal Bernard°.

Condensin positioning at telomeres by shelterin proteins drives sister-telomere disjunction in anaphase. eLife. **https://doi.org/10.7554/eLife.89812.1**

Léonard Colin#, Céline Reyes #, Julien Berthezene, Laetitia Maestroni, Laurent Modolo, Esther Toselli, Nicolas Chanard, Stephane Schaak, Olivier Cuvier, Yannick Gachet, Stéphane Coulon, Pascal Bernard°, Sylvie Tournier

RNA Pol II antagonises mitotic chromatin folding and chromosome segregation by condensin.
bioRxiv. https://doi.org/10.1101/2023.08.08.552486 In review
Jeremy Lebreton#, **Léonard Colin#**, Elodie Chatre, Pascal Bernard°

Evidence that nucleosomes antagonize condensin function. In preparation.

Léonard Colin#, Esther Toselli#, Laurent Modolo, Pascal Bernard°

Summary in french/Résumé en français

Les génomes du vivant sont organisés à plusieurs échelles de taille par différents composants protéiques – et ce d'une façon dynamique et régulée dans le temps. Les deux composants majeurs structurant l'ADN dans le noyau sont les nucléosomes et les complexes SMC (Structural Maintenance of Chromosome). Les nucléosomes constituent l'unité de base de la chromatine, qui compactent l'ADN par son enroulement autour d'un octamère de huits protéines (histones) chez les eucaryotes, et ce de façon répétée le long du génome. Les complexes SMC quant à eux, regroupent une famille diverse mais ancestrale de complexes protéiques avec des rôles clés dans l'organisation des génomes et la ségrégation des chromosomes, des bactéries aux eucaryotes multicellulaires. Le modèle actuel sur l'activité fonctionnelle *in vivo* des SMC repose sur un mécanisme d'extrusion de boucle (*loop extrusion* en anglais). In vitro, les complexes SMC sont capable d'élargir de façon progressive une boucle d'ADN en hydrolysant de l'ATP. Cette activité explique de façon pertinente plusieurs observations in vivo, bien que certains mécanismes, notamment celui de capture de segments d'ADN en trans (*diffusion capture* en anglais) aient été proposés plus récemment pour expliquer l'activité in vivo des SMC.

Bien que l'architecture des génomes soit vraisemblablement dictée par une combinatoire de la chromatine et des complexes SMC les études sur les interactions entre ces deux composants structuraux des génomes restent peu nombreuses. Lors de cette thèse, j'ai ainsi travaillé à explorer les interactions fonctionelles *in vivo* entre la chromatine et le complexe SMC condensine dont le rôle est de réorganiser l'ADN des noyaux interphasiques en chromosomes mitotiques condensés. En utilisant principalement des approches génétiques et de génomique fonctionelle, j'ai au cours de cette thèse travaillé sur trois aspects du micro-environnement chromatinien et de son impact sur la fonction de condensine chez la levure à fission *Schizosaccharomyces pombe*, en tant que co-premier auteur sur les trois sujets. Dans un premier temps, dans le cadre d'une collaboration avec d'autres équipes, j'ai contribué à décrire le rôle de condensine aux télomères. Spécifiquement, la chromatine aux télomères chez les eucaryotes est organisée par un complexe nommé shelterin. Nous fournissons des évidences suggérant que Taz1/TRF1 est important à la fois pour la localisation en *cis* de condensine aux télomères et contribuent à la séparation des télomères sœurs en anaphase car un mutant constitutif de Taz1 aggrave les défauts de ségrégation en anaphase aux télomères. Nous fournissons

également une évidence que Mit1, un remodelleur retirant les nucléosomes aux subtélomères, est partiellement responsable des défauts de ségrégation aux télomères lorsque condensine est partiellement défectueuse et que ce remodelleur limite également les niveaux de condensine aux télomères. Nous montrons également qu'une perte de fonction partielle de condensine menant à une mauvaise séparation des télomères mène également à un niveau de cohésine plus élevé aux télomères, et que ces niveaux plus élevés sont en partie responsables de la mauvaise séparation des télomères. Ainsi nous proposons que Shelterin chez *pombe* positionne condensine qui a un rôle spécifique pour séparer les télomères en mitose.

Dans un deuxième temps, grâce à des allèles conditionels générés lors de la thèse, j'ai participé à un projet visant à ré-explorer l'impact de la transcription par l'ARN polymérase II sur la fonction de condensine. Lors de la mitose chez les vertébrés, la transcription diminue de façon significative et condensine est positionnée en 5' des gènes au niveau des promoteurs. Cependant, chez *S. pombe* lors de la mitose la transcription reste active et la position des pics de condensine corrèle avec la position de l'ARN polymérase II. En prenant part de deux allèles conditionels pour dépléter à la fois rapidement l'ARN polymérase II ou augmenter artificiellement son niveau par translecture (en déplétant Dhp1^{XRN2}) nous montrons par ChIPseq calibrée que la position de condensine suit les pics d'ARN polymérase II. En revanche, la quantité totale de condensine associée aux chromosomes est indépendante du niveau d'ARN polymérase II présente sur la chromatine, suggérant que condensine est distribuée par l'ARN polymérase, évoquant des résultats précedents chez les SMC bactériens. Nous montrons de plus que dans ces deux conditions, la formation de contact à longues distances par Hi-C augmente quand la quantité d'ARN polymérase II diminue et la formation de contacts diminue quand la quantité d'ARN polymérase II est stabilisée. Nous corrélons également ces changements de niveau d'ARN polymérase II à des conséquences fonctionelles sur la ségrégation des chromosomes. Diminuer la quantité d'ARN polymérase II facilite la séparation des chromosomes lorsque condensine est en condition de perte de fonction partielle tandis que dans un contexte de translecture la séparation des chromosomes est appauvrie. Nous confirmons ainsi que l'ARN polymérase II influence négativement la translocation du complexe condensine en mitose chez *S. pombe* et fournissons une évidence indirecte sur le mécanisme assemblant les chromosomes mitotiques comme étant à priori un mécanisme processif argumentant pour une extrusion de boucles. Ainsi des complexes processifs comme l'ARN

polymérase qui doivent lire l'ADN chromatinien antagonisent la fonction de condensine pour former des chromosomes mitotiques.

Enfin, dans un troisième temps, nous explorons de façon plus directe les interactions fonctionelles entre les nucléosomes et le complexe condensine. Nous décrivons une interaction fonctionelle et physique entre la chaperone d'histone FACT et condensine. Une perte de fonction partielle de FACT facilite grandement la séparation des chromatides sœurs lorsqu'il y a une perte de fonction partielle de condensine, suggérant que FACT antagonise l'activité de condensine. En utilisant un allèle conditionnel pour dépléter FACT en mitose, nous montrons que le rôle de FACT est de stabiliser la chromatine, identiquement à son rôle décrit en interphase et que dans nos conditions une déplétion de FACT mène à une forte baisse du niveau d'histones associés à la chromatine. Une déplétion de FACT affecte la formation des chromosomes mitotiques en métaphase d'une façon qui a l'air *à priori* indépendante de condensine, car (1) ne change pas la distribution de condensine sur la chromatine et (2) affecte la formation de contacts en métaphase identiquement entre un fond sauvage et un fond où condensine a été déplétée. En revanche, la déplétion de FACT juste avant l'entrée en mitose facilite la séparation des chromatides sœurs dans un fond où condensine est partiellement non fonctionelle. De même, réduire la densité en nucléosomes sur la chromatine d'une autre manière, en réduisant le nombre de gènes d'histone facilite de façon significative l'activité de condensine en anaphase. Nos données suggèrent donc que les nucléosomes antagonisent l'activité de condensine (au minimum dans un fond où son activité n'est pas optimale).

En conclusion, nous montrons que l'activité de condensine *in vivo* est soumise à des contraintes particulières qui n'existeraient pas simplement sur de l'ADN nu. Ainsi, l'assemblage des chromosomes mitotiques doit être réalisé dans des conditions propices à l'arrivée massive de condensine en début de mitose et nous proposons que de futurs travaux doivent investiguer l'impact moléculaire des composants de la chromatine sur l'extrusion de boucle et potentiellement sur des mécanismes de capture en trans.

Preamble

This work was done over four years of PhD, including a 6 month internship during my masters study in the lab of Pascal Bernard. The main protagonist of this thesis is the condensin SMC complex, which is responsible for the large changes observed in vivo to reshape chromatin into rod shaped chromosomes upon M entry. I discovered condensin during my internship in Pascal's lab, although my initial interest in biology as a student had always been the nucleosome and "epigenetics" (which at the time I confused with chromatin remodelers and histone post-translational modifications).

In reviews recapitulating the work performed on either SMC complexes or nucleosomes, despite the fields being relatively separated (although more studies are considering crosstalks) the same key problem tends to be brought up during introductory sections. That is the dimensional analysis of linear length of genomes relative to nuclear size. One can estimate the linear length of a genome by multiplying the number of basepairs by 0.34nm. Very quickly this leads to lengthy molecules. Humans : ~2m (diploid) Aedes aegypti mosquito : ~1m (diploid) Yeasts : ~ 4.5 mm (haploid). Considering the nuclear size in eukaryotes tends to be 10^4-10^5 times smaller than this length scale, there must be active mechanisms, for cells to fit this DNA inside the nucleus. Each review then proposes that SMC complexes or nucleosomes participate in this process.

During the several projects I contributed to during my PhD the aim was always to explore the interplay between the condensin complex and its chromatinized template, formed by nucleosome-bound DNA and regulated by several other chromatin associated components such as shelterin at telomeres (Part 5), actively transcribing RNA pol II (Part 6) or the histone chaperone FACT (Part 7). Thus the work reported in this manuscript underlines the importance of integrating the functioning of condensin –and SMC complexes- with the chromatin environment.

In the introduction, I will present in a first part the nucleosome-based organization of eukaryotes, and in a second part will introduce SMC complexes in general. In a third part I will briefly introduce the cohesin SMC complex as an example of genome organizer and finally in a fourth part will address the organization of the mitotic chromosome and the structural and molecular roles of the condensin SMC complex in this process.

INTRODUCTION

Part 1 - EUKARYOTIC GENOMES ARE PACKAGED AND ORGANIZED INTO REPEATED UNITS OF NUCLEOSOMES

1.1 DNA is the support of life, but how is it packaged within chromosomes ?

The first recorded identification of deoxyribonucleic acid (DNA) in 1869 as nuclein by Miescher, the proposition of a polynucleotide model by Levene and finally the description of a double helix **(Watson and Crick, 1953)** were landmark discoveries that advanced our understanding of DNA structures and allowed the identification of DNA as the template for genetic information.

Histones were first identified by Albrecht Kossel in 1884, before chromatin had been described by Walther Flemming in 1890. There are four core histones, highly conserved among eukaryotes : H3, H4, H2A and H2B, with a fifth histone type, linker histone H1 which is more diverse or even absent from certain organisms (Schizosaccharomyces pombe for instance). They are key structural components of chromosomes : and account for a majority of the weight of chromosomal proteins in mitotic chromosomes **(Hirano and Mitchison, 1994; Ohta et al., 2010)** and their absence can lead to a certain extent to defects in the architecture of chromosomes post-mitotic assembly **(Shintomi et al., 2017).** A variety of histone post translational modifications (PTMs) and histone variants increase the complexity of chromatin across eukaryotes, and are discussed briefly later.

1.2 The canonical nucleosome core particle

Digestion of nuclei by endonucleases does not yield smears in agarose gels but rather multiples of size-specific bands **(Hewish and Burgoyne, 1973)**. This observation suggests a repetitive pattern of obstacles to the DNA cleavage activity of the enzyme. The source of these patterns can also be isolated with micrococcal nuclease (Mnase) which led to the first identification of these structures by electron microscopy experiments **(Oudet et al., 1975)** and their visualization as 'beads on a string' **(Olins and Olins, 1978; Oudet et al., 1975)**. As it turns out, these repetitive structures emerged from the assembly of DNA around histone proteins. The folding of DNA around histone octamers is an autonomous process, driven by the acidic surfaces of histone subunits leading to interactions with the

DNA backbone. The structure of DNA bound to histones follows a superhelical architecture that can be stretched and reformed **(Richards and Pardon, 1970)**. Core histones form dimers, H3 associating with H4 and H2A associating with H2B **(Kornberg and Thomas, 1974)**. As a fully formed octamer, two of each H3, H4, H2A and H2B subunits form a globular structure around which 145-147bp of DNA wraps around into a nucleosome core particle (NCP) **(Luger et al., 1997) (Fig. I1)**. The rest of the DNA which does not directly contact the histone octamer is called the linker DNA. The center of symmetry for this structure is the dyad, a reference point to position contacts between the major groove of DNA and the positive histone surface. These points are called SHL for Super Helix Location (dyad = SHL 0) and range from SHL -7 to +7 in a manner that respects the 10bp periodicity of the DNA superhelix. In this fully assembled, DNA-wrapped octamer, the H2A-H2B surface is readily accessible by the solvent and composes an acidic patch which is negatively charged. From each histone subunit, N-terminal tails protrude outward of the NCP. In general, these N-terminal tails are particularly important surfaces for post-translational modifications as well as to establish higher order organization. In the canonical nucleosome H3 N-terminal tails contact the DNA gyres at the entry/exit sites of DNA.

Fig. I1 Structure of the nucleosome core particle
See text for details. a/ Color-coded molecular structure of the NCP. b/ Electrostatic potential of the nucleosome surface. c/ Organisation of the linker DNA in the NCP crystal. Taken from Zhou et al, 2019

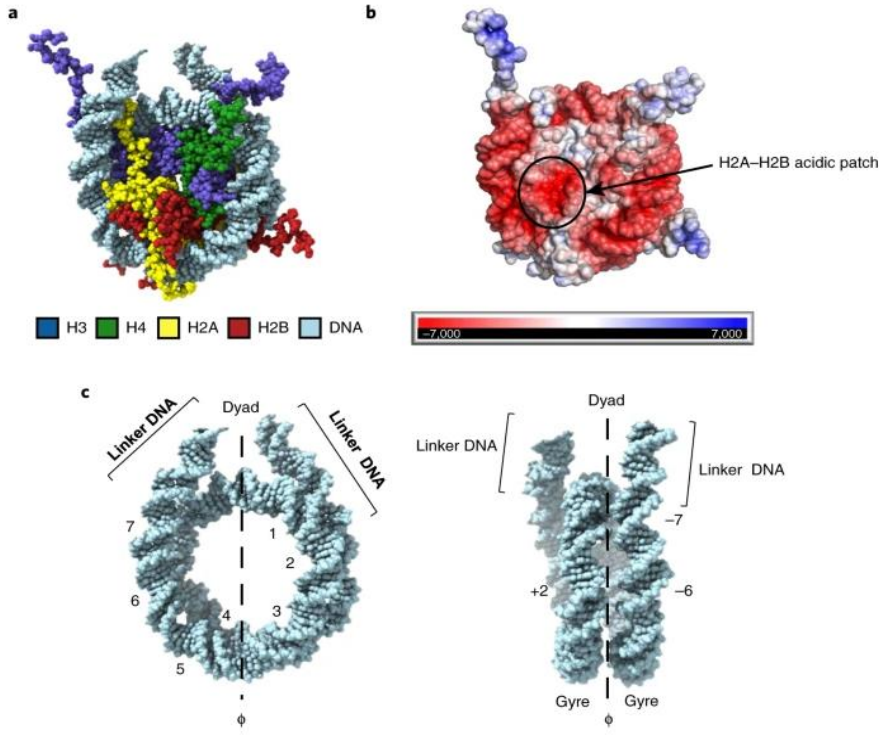

PROKARYOTIC, ARCHAEAL AND SPERM CHROMATIN

An important point is that eukaryotic nucleosomes appear quite different to their prokaryotic and bacterial counterparts. Prokaryotic species, to be brief, do not code for histones but a diversity of basic DNA binding proteins (Nucleoid Associated Proteins, NAP) that participate in chromatin folding at multiple scales **(Lioy et al., 2018)**. Archaeal chromatin on the other hand, is composed of histones, of NAPs, or both. It is sensitive to MNase and showcases similar promoter structures with -1 and +1 nucleosomes flanking a NDR and some degree of phasing downstream in *Haloferax volcanii* **(Ammar et al., 2012)**. While MNase digestion in eukaryotes yields bands of sizes multiples of ~150 bp (or more depending on tissue specific linker lengths), the bands in archaea seem to be multiples of ~30bp with 60bp minima **(Ammar et al., 2012; Maruyama et al., 2020; Pereira et al., 1997)** implying a fundamental structural difference in the underlying DNA wrapping around archaeal histones. Structural data has shown that these histone-like proteins form dimers that mimic tertiary eukaryotic DNA/histone contacts but hold a symmetry allowing continuous polymerization and formation of a 'superhelix' with adjacent dimers. Substitution of residues responsible for contacts between polymers of this helix in vivo leads to the loss of higher order polymers observed after MNase digestion and altered gene expression **(Mattiroli et al., 2017)**. This organization has been described as 'hypernucleosomal' **(Henneman et al., 2018)** or 'archaeasomal' **(Laursen et al., 2021, p. 201)** However, certain species of archaea like crenarchenota do not encode histones and do not display repetitive banding patterns on gels after MNase digestion **(Maruyama et al., 2020)**. In the case of coexistence of both histones and archaeal NAPs, current experiments suggest that archaeasome mediated compaction is in competition with the DNA binding of Alba, a dsDNA specific NAP which rigidifies DNA segments **(Maruyama et al., 2020)**. It is important to acknowledge that the environmental conditions of extremophiles is restrictive for typical eukaryotic chromatin transactions (high temperatures may lead to excessive DNA melting for instance), necessitating adapted machineries.

Another physiologically specific context in which DNA is compacted differently to typical nucleosomal chromatin in eukaryotes occurs in the male germline. At a certain point during spermatogenesis, sperm chromatin becomes compacted with protamines or a mix of protamines and histones, although exceptions where sperm chromatin is nucleosomal exist such as zebrafish. Protamines are small basic proteins which lead to drastic compaction of sperm chromatids **(Orsi et al., 2023)**. In certain species (for instance Xenopus) some histones are retained on sperm chromatin but for the most part protamines must be removed just after sperm has fertilized eggs arrested in meiosis II (or meiosis I in insects) to ensure proper embryonic development.

These observations suggest that evolutionarily there is more diversity in the strategies to package chromatin, while the motors enabling chromosome segregation (see Part 2) during cell division appear more conserved.

1.3 Nucleosome structure and nucleosomal DNA are dynamic

While the canonical structure of a nucleosome crystal **(Luger et al., 1997)** was essential for the understanding of chromatin biology, it does not convey the full dynamic structure of a nucleosome. In eukaryotes, an additional level of organization can be added to the organization of the NCP by the addition of linker histone H1. Linker histones are non-canonical histones that can bind on the axis of

symmetry of the nucleosome (on-dyad) or slightly up/down-stream of the axis of symmetry (off-dyad) **(Zhou et al., 2021, 2015)** to convert the nucleosome into a 'chromatosome'.

The nucleosome structure by itself is dynamic and can 'breathe' ; i.e the DNA unwraps and rewraps rapidly around the octamer under physiological salt conditions **(Bilokapic et al., 2018; Li and Widom, 2004)**. Certain moieties of histone subunits such as histone tails are crucial for establishing the energy cost of unwinding/winding DNA **(Parsons and Zhang, 2019)**. Histone tails are dynamic and can regulate contacts with the wrapped DNA by differential binding/unbinding kinetics **(Peng et al., 2021)**. They also act as outward protrusions from the nucleosomal core particle that make them prime targets for histone modifying and chromatin remodeling enzymes as well as important for higher order folding of chromatin. Trypsin digestion experiments suggests these tails are important for the three dimensional compaction of a chromatin fiber with or without linker histone H1 **(Allan et al., 1982)**.

Increasing salt concentrations of buffers containing nucleosomal particles shift reaction equilibrii and suggest that the disassembly of a nucleosomal particle hinges on the sequential release of each H2A-H2B dimer, leading to partially disassembled intermediates **(Chen et al., 2017)**. These intermediates, named hexasomes **(Arimura et al., 2012; Kato et al., 2017)** or tetrasomes/hemisomes **(Furuyama et al., 2013)** are not simply artefacts of buffer conditions because they can be generated by the activity of specific factors as will be described in a section downstream. Similar release patterns of H2A-H2B can be observed with positive supercoiling **(Sheinin et al., 2013)** and if sufficiently strong, positive supercoiling can even induce a chiral transition from a left handed wrapping of DNA around the octamer to a right handed one **(Bancaud et al., 2006)**. Importantly, evidence in vivo suggests non canonical nucleosomes are a major fraction of chromatin in yeast **(Cai et al., 2018b; Yang et al., 2023)** but it was reported to not be the case in HeLa cells **(Cai et al., 2018a)**.

1.4 Individual histone subunits can show structural variation

The NCP can be the subject of structural variation by two active mechanisms in cells, the first are post-translational modifications (PTMs) of histones and the second is the replacement of canonical

NCP histone subunits by specific variants. These structural variations can impact the dynamics of nucleosomes and lead to crosstalks with other chromatin bound activities. Note that a large amount of histone residues can be modified by PTMs, producing complex networks that are impossible to fully parse or quickly explain, and a similar observation can be made for the complexity of histone variants. I will therefore only briefly introduce a couple of examples to illustrate the structural diversity of the NCP. I have selected classical examples that I present below to introduce the concept of structural variations of the NCP : histone methylations and H2A.Z and CENP-A histone variants, with other examples mentioned later in the introduction to illustrate other properties of the chromatin *in vivo*.

Post-translational modification of histones : histone methylation

Di- and tri-methylation of Lysine 9 of core histone H3 (H3K9me2/3) are established by histone methyltransferases Suppressor of Variegation 3.9 in Drosophila and human, Su(var)3-9/SUV39H **(Tschiersch et al., 1994)** and Cryptic loci Regulator 4, Clr4 in fission yeast **(Ivanova et al., 1998)**. This histone modification is recognized by Heterochromatin Protein 1 (HP1)/Swi6 **(Bannister et al., 2001)** and thus form the core PTMs of constitutive heterochromatin, which can spread as adjacent nucleosomes are methylated but can also be restricted by local depletion of nucleosomes, dynamic turnover or antagonized by histone acetylation **(Allshire and Madhani, 2018)**. Evidence *in vitro* and *in vivo* in drosophila also suggests that HP1 can undergo liquid-liquid phase separation **(Strom et al., 2017)**, but not in mouse **(Erdel et al., 2020)**. Tri- methylation of lysine 27 of core histone H3 (H3K27me3) by the PRC2 methyltransferase (part of the Polycomb complex) on the other hand establishes facultative heterochromatin **(Piunti and Shilatifard, 2021)**.

Histone variants : H2A.Z and CENP-A

H2A.Z is a variant of the canonical H2A histone. It is conserved in metazoans and is essential during development in flies and mice **(Faast et al., 2001; Ibarra-Morales et al., 2021; van Daal and Elgin, 1992)**. Structurally H2A.Z leads to a similar path of the DNA around the nucleosome, however it does induce subtle differences in terms of interactions between H2A.Z-H2B dimers and between H2A.Z-H2B and H3-H4 tetramers **(Suto et al., 2000)**. Simulations suggest H2A.Z enhances DNA unwrapping **(Li et al., 2022)** and increases flexibility of DNA ends in H2A.Z containing nucleosomes

observed by cryo-EM **(Lewis et al., 2021)**. In vivo ChIP experiments suggest H2A.Z nucleosomes can be heterotypic (a single H2A.Z-H2B dimer in the NCP) or homotypic (two H2AZ-H2B dimer in the NCP) **(Nekrasov et al., 2012; Weber et al., 2010)**. H2A.Z can be found at heterochromatin **(Rangasamy et al., 2003)** and at promoters and tend to favor the pausing of RNAPII there **(Mylonas et al., 2021)**. The SWi2/Snf2 Related 1 Complex (SWR1C) from the INO80 family loads H2A.Z in nucleosomes in a manner that is less dependent on replication than canonical H2A **(Tachiwana et al., 2021)**. Both the proportion of heterotypic nucleosomes and the quantities of H2A.Z at subtelomeres and centromeres are higher in M compared to G1/S **(Nekrasov et al., 2012)**.

At the centromere, a variant of canonical histone H3 called CENP-A is preferentially deposited, as canonical H3 histones appear to be destabilized at centromeres **(Shukla et al., 2018)**. Low levels of CENP-A allow nucleation of the kinetochore **(Fachinetti et al., 2013)** and this nucleosome variant acts as a platform upon which the kinetochore can assemble, with linker DNA being gripped by the kinetochore complex **(Yatskevich et al., 2022)**. CENP-A however is not required for kinetochore function once it has been assembled **(Hoffmann et al., 2016)**.

1.5 Nucleosomes are actively repositioned on chromatin in vivo

Many a paper has reproduced the ladder of in vivo chromatin after nuclease digestion, nowadays mostly with MNase. Aligning sequenced reads produced by MNase digestion on a reference genome, particularly along the length of genes, yields peaks and valleys assigning average nucleosome positions. Over a cell population average, a specific locus can be overrepresented in the library (i.e a position of high nucleosome occupancy). One can also determine whether the signal is biased towards a specific nucleotide (i.e the nucleosome has a very-well defined position). It could be that a specific locus, over the population average, is highly bound by a specific nucleosome, but its position varies in each cell (high occupancy but low positioning). It is also possible for a nucleosome to be well positioned, but not be frequently observed (low occupancy and high positioning).

These nucleosomal patterns are determined in some form by the GC content of the underlying DNA, particularly at promoters. AT-rich DNA tends to disfavor the formation of nucleosomes – and would therefore tend to produce valleys in Mnase-seq data **(Basu et al., 2021)**. However overall the

pattern of nucleosome occupancy is mostly independent of DNA sequence. When centering Mnase-protected signals around the promoters, a depletion of signal prior to the TSS marks a Nucleosome Depleted Region (NDR), characteristic of transcribed genes. From this region, successive peaks and valleys starting from the TSS can be observed, reminiscent of wave-like functions with a specific phase. This average phase can be interpreted as the average spacing between nucleosomes and is defined as a Nucleosome Repeat Length (NRL). The nucleosomes flanking the NDR of the promoter are labelled as +1, +2… (towards the transcription termination site) and -1, -2… (in the other direction). Note that this phased pattern can be observed when the signal is centered on other genomic features, such as CTCF sites **(Zhang et al., 2023)** or Reb1-bound sites **(Oberbeckmann et al., 2021)**.

This pattern within genes seems to be conserved among eukaryotes, although the nucleosome repeat length (NRL, distance between peaks) measured varies between species and cell types. The NRL of mouse ESC cells is 186 bp, with an increase of 5-7 bp upon differentiation **(Teif et al., 2012)**, 154 bp for S. pombe and 167 bp for S. cerevisae **(Lantermann et al., 2010)**. Note that on top of these shorter NRL, budding and fission yeast do not seem to have linker histone H1, although these organisms may have replaced this metazoan linker with Hmo1p **(Panday and Grove, 2016)**. Variations within genomes can be observed : for instance, actively transcribed genes tend to be more susceptible to MNase digestion particularly at the 5' end **(Levy and Noll, 1981)**. Strikingly, it is possible to obtain very similar phasing patterns after MNase digestion of DNA with budding yeast chromatin factors by switching the DNA to that of genomes from fission yeast or even E. Coli **(Oberbeckmann et al., 2021)**. It is even possible to replace all core histones of budding yeast with human histones in vivo, and observe on average similar nucleosome repeat length (NRL) to wild-type although nucleosome stability (resistance to MNase) seems to increase **(Truong and Boeke, 2017)**. These striking observations underline the conserved nature of nucleosome positioning.

Nonetheless, such genome-wide repetitions can reasonably only occur by consistent forces driving their maintenance. The key driving factor to maintain regular internucleosomal distances along the genome is an ATP-dependent process **(Zhang et al., 2011)** that relies on ATP-dependent chromatin remodelers **(Oberbeckmann et al., 2021)**. For more on chromatin remodelers, we refer the reader

to adress specific reviews (for reference **(Clapier et al., 2017; Reyes et al., 2021)**). Briefly, chromatin remodelers in eukaryotes can be divided in 4 families : ISWI, INO80, SWI/SNF and CHD. ISWI and CHD complexes appear to mostly space the nucleosomes while the SWI/SNF family (containing the Remodeling Structure of Chromatin) evicts nucleosomes and the INO80 family seems to edit nucleosome by introducing histone variants. While the specificities of these complexes rely on the presence of different regulatory domains **(Patel et al., 2019)** as well as the local chromatin environment and the presence of additional factors, they share the same main mechanism. All of these complexes associate to SHL –2 of a NCP and translocate DNA along the nucleosome using the energy of ATP **(Reyes et al., 2021)**. This mechanism is defined as an inchworming mechanism as the DNA is moved 1bp per hydrolysis cycle and allows the sliding of DNA along the histone octamer **(Clapier et al., 2017)**.

1.6 Nucleosomes are chaperoned for chromatin transactions

In addition to chromatin remodelers, another process which participates in the steady-state composition of chromatin are histone chaperones which participate in histone transactions involved in assembly and disassembly of nucleosomes, and they do so without having an ATP-dependent enzymatic activity themselves. Histone chaperones can introduce histone variants into the chromatin template, for instance Holliday Junction Recognition Protein (HJURP) is a histone chaperone introducing CENP-A/H4 tetramers at centromeres **(Foltz et al., 2009)**. Histone chaperones can also recycle histone subunits into the nucleosome after destabilizing processes or participate in the assembly of nucleosome on DNA. For instance, the histone chaperone Chromatin Assembly Factor 1 (CAF-1) is specific to a pathway which occurs during replication, when newly synthesized H3-H4 histones are assembled onto replicating DNA **(Smith and Stillman, 1989)**. Anti Silencing Function 1 (Asf1) on the other hand, participates in both replication-coupled and independent pathways by its ability to bind H3-H4 dimers and assemble nucleosomes **(English et al., 2006, 2005)**. These pathways are complex and histone chaperones tend to function by competing for contacts between histones and DNA with poor conservation of histone chaperone folds **(Hammond et al., 2017)**. Notably, CAF-1 and Asf1 appear to be H3-H4 specific chaperones, but this is not the case for the FACT histone chaperone which is able to establish contacts with both H3-H4 and H2A-H2B dimers (see

below). I will therefore focus only on the assembly and disassembly of histone subunits by histone chaperones using the example of 1/ chromatin assembly upon fertilization and 2/ introduce the histone chaperone FACT, relevant to Part 7.

Sperm chromatin is converted to nucleosomal chromatin by histone chaperones

Sperm chromatin enters the egg as a highly compacted structure, with a protamine-based organization. In many species, core histones H3-H4 are retained at low levels on sperm chromatin and are positioned at intergenic regions and retain methylation marks at specific genomic loci **(Yamaguchi et al., 2018).** For proper embryonic development however, large scale chromatin remodeling must occur with the removal of protamines and the assembly of nucleosomes which is *a priori* guaranteed by the sole concerted activities of histone chaperones, at least in a minimal system. The subsequent removal of protamines and assembly into a nucleosome-based chromatin sensitive to MNase **(Ohsumi and Katagiri, 1991)** requires the activity of the chaperone nucleoplasmin (Np) in frogs **(Ohsumi and Katagiri, 1991)** but not mouse **(Burns et al., 2003)**. In vertebrates, HIRA is essential for proper chromatin assembly upon fertilization **(Lin et al., 2014)**. In a minimal system, assembly of chromatin onto mouse sperm can be performed by the combined activity of Np and the histone chaperone Nap-1 **(Shintomi et al., 2015)** while in Xenopus egg extracts, assembly of chromatin on mouse sperm requires the presence of the Asf1 H3-H4 histone chaperone **(Shintomi and Hirano, 2021)**. The same histone chaperones are involved in other physiological contexts where nucleosomes must be assembled, such as replication-coupled and independent nucleosome assembly by Asf1 or replication and transcription dependent nucleosome assembly by Nap-1. Strikingly, after the conversion of sperm chromatin into embryonic nucleosomal chromatin in a minimal system, mitotic condensation of this template requires the activity of the FACT histone chaperone **(Shintomi et al., 2015)**.

The FACT histone chaperone

One of the most studied histone chaperone is FAcilitates Chromatin Transcription/Transaction (FACT). FACT is an ATP-independent conserved histone chaperone in eukaryotes, composed of the two

subunits Pob3/SSRP1 (Polymerase One Binding/Structure Specific Recognition Protein 1) and Spt16/SUPT16H (Suppressor of Ty 16/Suppressor of Ty 16 Homolog) **(Fig. I2)**.

Spt16 structure is subdivided as four domains : an N-terminal domain (NTD), a dimerization domain (DD), a middle domain (MD) and a C-terminal domain (CTD). Pob3 structure is subdividied in a N-terminal DD, a MD, an intrinsically disordered domain (IDD), a high mobility group box (HMGB) and a CTD. In yeast, the IDD and HMGB domains are missing, and the Nhp6 protein appears to be an analog of the HMG domain from SSRP1.

The two subunits form a heterodimer by DD-mediated interactions and bind a single nucleosome as a two subunit complex, although in vivo a fission yeast *pob3Δ* is viable and Spt16 binds to chromatin **(Murawska et al., 2020)**. Spt16-NTD by itself binds to H3 and H4 via their tail and their globular structure but not to H2A-H2B dimers **(Stuwe et al., 2008)**. The MD of Spt16 binds to H3 and H4 and is organized by two Pleckstrin homology groups (PH) which can also be found in other chaperones like Rtt106 **(Kemble et al., 2013)**. The MD of Pob3 while it has low sequence resemblance to Spt16, also has two PH domains **(Kemble et al., 2013; VanDemark et al., 2006)**.

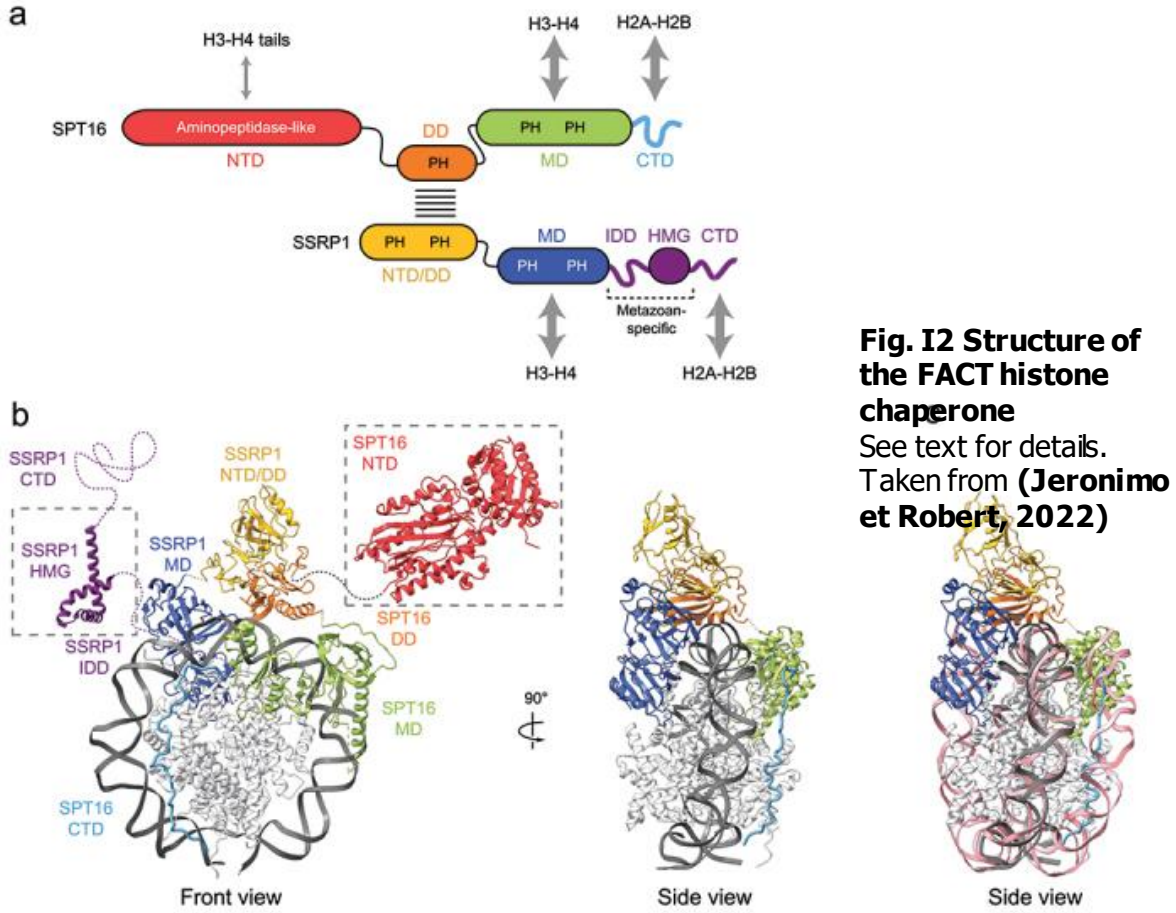

Fig. I2 Structure of the FACT histone chaperone
See text for details.
Taken from **(Jeronimo et Robert, 2022)**

Both CTD of Spt16 and Pob3 by themselves bind H2A-H2B dimers. Moreover, the Spt16-CTD and H2A-H2B interaction surface aligns quite well to similar interaction structures observed for the ANP32E H2A.Z-H2B histone chaperone and the SWR1 H2A.Z-H2B chromatin remodeller **(Kemble et al., 2015)**. Some histone chaperone folds in FACT are therefore conserved in other chaperones/remodellers. The full structure in the presence of a nucleosome shows FACT binding as a 'unicycle', on top of the nucleosome or a hexasome **(Liu et al., 2020)** demonstrating its ability to establish contacts with all histone subunits.

The Nhp6 (non histone chromatin protein) HMG-box protein weakly binds to yFACT with unclear stoichiometry **(Formosa et al., 2001; Sivkina et al., 2022)**. To allow binding of yFACT in vitro to nucleosomes fusing Nhp6 to Pob3 is not sufficient and at least three HMGB must be fused. Additionally, human FACT requires Nhp6 in vitro to bind nucleosomes suggesting the excess of Nhp6 required in vitro does not recapitulate the function of the SSRP1 HMG box **(McCullough et al., 2018)**. FACT appears to favor the binding of destabilized nucleosomes, as HMGB domains favor the bending of DNA, likely promoting unwrapping of nucleosomes **(McCauley et al., 2022, 2019)** and this extra moiety is likely required for yFACT and hFACT association to nucleosomes as otherwise even hFACT does not change the structure of an intact nucleosome **(Valieva et al., 2017)**. In the presence of Nhp6, FACT can fully unfold a nucleosome **(Sivkina et al., 2022)** and FACT can accelerate the loss of H2A-H2B dimers from a nucleosomal fiber under tension **(McCauley et al., 2022)**. However, FACT also stabilizes the structure of the chromatin for a higher number of strectching and relaxation cycles relative to a fiber stretched and relaxed without FACT **(McCauley et al., 2022)**. Favored models of FACT function therefore propose that it stabilizes the intermediate state between a histone octamer and a disassembled nucleosome.

1.7 The nucleosomal fiber is the template for the activity of chromatin factors and enzymes

The steric hindrance and coiling constraints imposed by nucleosomes on DNA - both at the scale of a single NCP but also on higher orders of chromatin fibers - seem intuitively incompatible with certain enzymatic activities. In the context of DNA replication **(Demeret et al., 2001)** and DNA repair

(Price and D'Andrea, 2013) specific chromatin remodeling pathways are involved to ensure the function of these processes. In this section I will describe this principle by using the example of the transcriptional process through a nucleosome by RNA polymerase II (RNAPII).

Due to the wrapping of DNA around the canonical nucleosome structure RNA polymerases must locally compete with putative DNA-histone contacts. When considering transcription at the scale of a gene, RNA polymerases must access loci which can be wrapped into several (in yeast) to hundreds of NRLs (in humans). Indeed, chromatin inhibits the activity of either transcription by RNAPII or replication by DNA pol α **(Kireeva et al., 2002; Kurat et al., 2017)**. Strikingly, the frequency of nucleosome arrays using an *in vitro* chromatin system is increased upon Pol II depletion **(Singh et al., 2021)** and active promoters are known to be sites of nucleosome depletion **(Boeger et al., 2003)** suggesting there are transcription-dependent activities that weaken nucleosome arrays in cells. Therefore, activities in cells that can remodel and/or destabilize nucleosomes appear essential for genetic programs to be regulated and maintained across cell divisions. Aditionally, apart from pioneer transcription factors **(Zaret and Mango, 2016)**, an overwhelming majority of transcription factors are bound at DNase accessible site, interpreted as nucleosome depleted **(Thurman et al., 2012)** suggesting transcription factor binding requires chromatin remodeling at the level of its binding site.

The sequence-flexibility of DNA is higher on the TSS proximal side of the nucleosome dyad positions, where RNAPII invades nucleosomes during transcription **(Basu et al., 2021)**, providing potentially a way for RNAPII to invade the nucleosome. Despite this, *in vitro* transcription shows that RNAPII + TFIIS elongation factor stalls at SHL -5 suggesting in this system additional factors are required **(Ehara et al., 2019)**. Adjunction of elongation factors enables RNAPII to bypass the nucleosomal barriers (i.e : stalling at precise SHL), such as addition of Spt4/5 and Elf1, which could potentially provide basic residues allowing for a competition between histone/DNA in the case of Elf1 **(Ehara et al., 2019)**. Evidence suggests that transcription associated methyltransferases promotes the methylation of lysine 36 of core histone H3 (H3K36me) to recruit histone deacetylases. This will favor chromatin closure after transcription has occurred, potentially to prevent cryptic transcription *in vivo* **(Carrozza et al., 2005; Keogh et al., 2005; Li et al., 2009)**, suggesting that while nucleosomes are obstacles to elongation, they must also be maintained to ensure the integrity of chromatin.

The FACT histone chaperone also participates in similar functional roles during transcription. It is known that transcription by RNAPII leads to the loss of a single H2A-H2B dimer (hexasome formation) at 300mM KCl **(Kireeva et al., 2002)**. Loss of a H2A-H2B dimer can be stimulated during transcription in vitro with the histone chaperone FACT **(Belotserkovskaya et al., 2003).** The same histone chaperone FACT enhances transcription by RNAPII through the nucleosome and binds the destabilized NCP following nucleosome opening **(Farnung et al., 2021)**. However, in vivo phenotypes of FACT are consistent with a role of FACT in maintenance of chromatin structure at actively transcribed genes **(Jamai et al., 2009)** and FACT maintains chromatin in vitro from repeated stretching forces induced on nucleosome fibers **(McCauley et al., 2022)**.

Interestingly it has been argued that RNAPIII simply displaces the octamer to transcribe **(Studitsky et al., 1997)**. Simple displacement of the histone octamer is also observed for bacteriophage RNA polymerase **(Kireeva et al., 2002)**. FACT is not found at RNAPIII genes **(Saunders et al., 2003)** suggesting it may have been selected to maintain H2A-H2B dimers in the wake of RNAPII. FACT however is also required for the replisome to progress through chromatin in vitro **(Kurat et al., 2017)** and to promote assembly of replication origins by evicting H1 **(Falbo et al., 2020)**.

Hence, enzymatic activities that require access to contiguous DNA sequences must intrinsically involve themselves with nucleosome dynamics to ensure proper transcription or replication occurs.

1.8 The nucleosome fiber can organize in higher order structures

Individual nucleosomes can organize into higher order structures *in vivo* mediated notably by nucleosome stacking mediated by H4-tails, which can be key targets for acetylation. Histone tails, particularly H4 tails, mediate higher order interactions. Indeed, digestion of tails by trypsin **(Allan et al., 1982)** or tail-less H4 **(Dorigo et al., 2003; Shogren-Knaak et al., 2006)** impairs the higher-order compaction of chromatin. Molecular structures show that the H4 tail and the acidic patch of H2A-H2B interact to drive higher order compaction **(Davey et al., 2002; Dorigo et al., 2004)**. A H4K16 acetylated histone tail (H4K16ac) phenocopied tail-less H4 suggesting H4K16ac is a key driver of higher order compaction **(Shogren-Knaak et al., 2006)**. The larger acidic patch in H2A.Z can

also drives higher order compaction via HP1 **(Fan et al., 2004)** consistent with its localization at heterochromatin **(Rangasamy et al., 2003)**.

In vitro folding of oligonucleosomes can lead to the formation of the so-called 30nm-fiber organized as a solenoid structure **(Finch and Klug, 1976; Song et al., 2014)**, with n and n+1 nucleosomes facing each other via their linker and n and n+2 nucleosomes stacking on top of each other **(Song et al., 2014)**. This 30nm fiber model is however controversial, both because *in vivo* it had not been convincingly observed **(Eltsov et al., 2008; Maeshima et al., 2010)**, and also because at higher cations concentrations relative to these studies (~1-2mM MgCl2) oligonucleosomes form a condensate like structure. *In situ* chelation of cations in nuclei also leads to loss of eu- and hetero-chromatin **(Maeshima et al., 2016)** suggesting proper chromatin organization as condensates depends on the presence of cations *in vivo*. Recent observations however have provided evidence that chromatin fibers may indeed follow a two start structure with n/n+2 stacking *in vivo* **(Beel et al., 2021; Li et al., 2023)**.

While heterochromatin was reported to follow properties consistent with liquid-liquid phase separation in drosophila **(Strom et al., 2017)**, the opposite was reported for mouse heterochromatin **(Erdel et al., 2020)**. *In vitro* it is possible for chromatin to behave as a solid or a liquid depending on the conditions **(Gibson et al., 2019; Strickfaden et al., 2020)** and chromatin was proposed to behave as a solid *in vivo* **(Strickfaden et al., 2020)**. Consistent with their roles in higher order compaction, both linker histone H1 **(Maeshima et al., 2016)** and histone acetylation **(Gibson et al., 2019; Schneider et al., 2022; Strickfaden et al., 2020)** respectively favor and antagonize the formation of compacted mesoscale structures of 200-300 nm which can be observed *in vivo* **(Miron et al., 2020; Nozaki et al., 2017)**. Whether these structures are solid or liquid is unclear due to conflicting reports on the physical nature of chromatin **(Gibson et al., 2023; Strickfaden et al., 2020)**. Evidence suggests at least that there is a sharp size limit of DNA density in mesoscale domains *in vivo*, beyond which nanometer-sized tracer beads cannot diffuse at relevant timescales **(Gelléri et al., 2023)** suggesting that compacted chromatin if not solid, is highly viscous.

1.9 Genomes are organized into diverse higher order structures

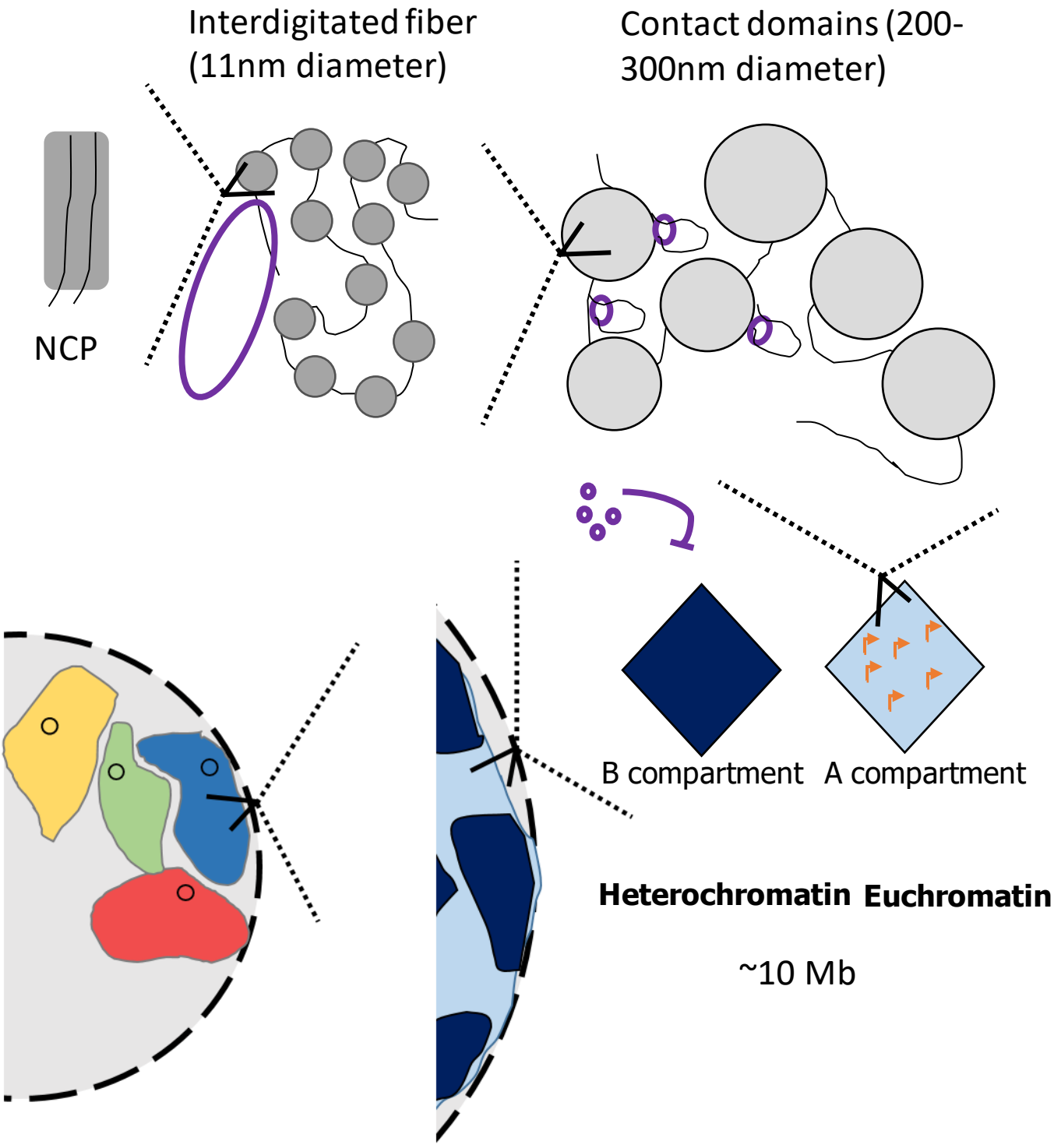

Fig. I3 The genome is organized at multiple scales by different principles
The nucleosomal core particle is the basic subunit of a nucleosomal 11-nm fiber, which forms mesoscale contact domains. These chromatin domains can organize into large scale domains which tend to self interact and are correlated with levels of gene expression. At larger scale, chromosomes are inidivdualized in the nucleus and form their own territories and tend to limit intermingling. This organization is counterbalanced by the loop formation activity of SMC complexes (typically cohesin, in purple)

With a more general view of genome organization, a complex and multi-scale genome structure inside the nucleus can be described **(Fig. I3)**. Individual chromosomes are physically separated as "chromosome territories" although there is some intermingling of the chromatin between these regions with potential implications in gene expression **(Branco and Pombo, 2006)**. Within chromosomes, large scale so called "A/B" compartments, which tend to correspond to euchromatin and heterochromatin, tend to associate with themselves but not to each other. A/B compartments are generally a measure of the chromatin states and correlate respectively with active/repressed regions in terms of transcription, early/late replicating regions or LTR poor/LTR rich regions **(Solovei et al., 2016)**. Moreover, heterochromatin tends to be located towards the periphery of the nucleus, where inactive genes can be found **(Croft et al., 1999)**. Note that A/B compartment size determined by chromosome conformation capture (3C) is also highly dependent on the resolution of the experiment, and the biocomputing analysis **(Harris et al., 2023)**. At a smaller scale, topologically associated domains (TADs) were described by 3C approaches as domains that tended to interact preferentially together **(Dixon et al., 2012; Lieberman-Aiden et al., 2009)**. These tens to hundreds kb long TADs are formed by SMC complex-driven genome folding, which will be described in the following sections (Part 2 - 4). This higher order architecture of genomes has multi-faceted roles in gene expression, DNA repair or gene expression and potentially many other functions intricated with each other which are far outside the scope of this manuscript **(Davidson et al., 2019; Solovei et al., 2016)**.

During mitosis, chromosomes are reshaped in a striking manner into rod-like structures in vertebrates. While the basic unit of chromatin at the mesoscale, that of contact domains, is retained during mitosis **(Nozaki et al., 2017)**, the mitotic chromosome is also shaped by loop forming SMC complexes **(Gibcus et al., 2018)**. The reshaping of interphase chromosomes into mitotic chromosomes makes them into a platforms competent for the accurate and precise segregation of sister chromatids to the respective daughter cells. First, it enables linear compaction of each individual chromosomes and generates a stiffer structure amenable for crosstalks with cytoskeletal components. Second, and crucially, the process of condensation also must involve some activity to separate each DNA molecule generated after the process of replication, removing entanglements that would antagonize this

process **(Nasmyth, 2001)**. This must be done while keeping them in close proximity to ensure daughter cells receive each the appropriate chromatids to maintain their karyotypes. Additionally, in the context of meiosis, for sexual reproduction, the rod shaped chromosomes provide the opportunity for meiotic bivalents to cross-over to introduce variation in the offspring. Finally, the mitotic chromosome has roles in ensuring the proper architecture of the following interphase **(Fig. I4)**. Evidence suggest that the position of chromosome territories themselves is retained throughout mitosis – or at least that chromosomes segregated earlier tend to migrate towards the pole of the nucleus **(Gerlich et al., 2003)** and that the organization of centromeres and heterochromatin in interphase partially relies on a function of condensin II (see following sections) in mitosis **(Hoencamp et al., 2021)**.

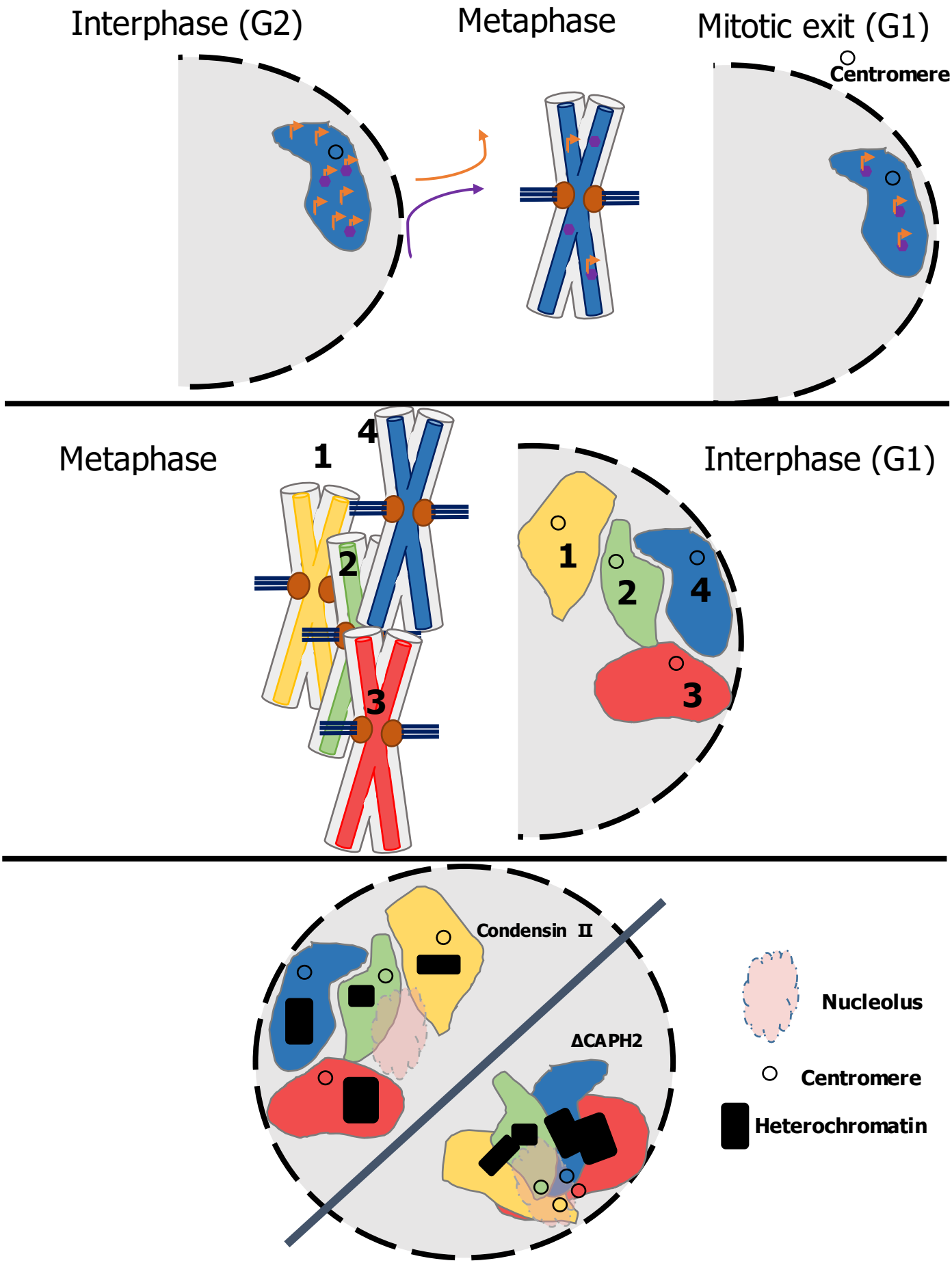

Fig. I4 The mitotic chromosome must support genome architecture after mitotic exit.
Top : Bookmarking factors (purple) enable the reexpression of genetic programs (orange) even after transcriptional downregulation. Middle : position of chromosome territories is correlated with position of chromosomes on the metaphase plate. Bottom : Condensin II prevents clustering of remarkable genomic loci.

Part 2 - THE SMC COMPLEXES FOLD CHROMATIN

2.1 The *cut* mutants and discovery of the SMC complexes

The lab of Mitsuhiro Yanagida performed genetic screens in *Schizosaccharomyces pombe* of historical importance for the field of chromosome assembly and segregation during mitosis. Temperature sensitive mutants from those mutagenetic screens allowed the study of essential genes by conditional loss of function. Their work identified a striking phenotype during cell division. Mutants of the topoisomerase 2 (topo II) gene enter into the mitotic process but the segregation of chromosomes is incomplete and the DNA remains associated as a chromatin bridge, until it is cleaved by the septum **(Uemura and Yanagida, 1984)**. This phenotype prompted their team to search similar candidates by a genetic screen, with thermosensitive alleles generating chromatin bridges which they called Cell Untimely Torn (cut) phenotypes **(Hirano et al., 1986)** with candidate genes participating in chromosome segregation. This striking phenotype implied an uncoupling in fission yeast between chromosome segregation and cytokinesis. Speculatively, these defects in mitosis could therefore occur not because of a defect in timing of mitosis, but perhaps because of the underlying structure of the DNA. Importantly, chromatin bridges can be observed in human cells, extend to very long distances and do not break unless the formation of the cleavage furrow is induced. This can cause genome variability in contexts such as cancer by inducing DNA damage responses and/or leading to chromothripsis, either immediately following the bridge or following further cell divisions **(Umbreit et al., 2020)**. From the initial screen, many key cell-cycle regulators were also identified, such as Cut1/separase, Cut2/securin, Cut4 and Cut9 as Anaphase Promoting Complex (APC)/C subunits **(Hirano et al., 1986)**. More importantly, from those screens, the essential genes *cut3* and *cut14* were identified, **(Saka et al., 1994)** whose protein homologs were identified in Xenopus in the same year as coiled-coil SMC proteins **(Hirano and Mitchison, 1994).** The characterization of the full complex called condensin a few years later was performed in Xenopus **(Hirano et al., 1997).**

In parallel, other labs discovered SMC-like genes. The first bacterial SMC gene, MukB, was discovered in E. coli **(Niki et al., 1991)**. Later in budding yeast, characterization of subunits of cohesin SMC **(Guacci et al., 1997; Michaelis et al., 1997; Strunnikov et al., 1993)** followed by the identification of the five subunit complex described in Xenopus and budding yeast **(Losada et al.,**

1998; Tóth et al., 1999). Finally SMC5/6 subunits were identified in another screen **(Fousteri and Lehmann, 2000)**, completing the discovery of canonical eukaryotic SMC complexes.

2.2 SMC complexes are a conserved feature of all branches of life

The SMC proteins themselves appear conserved in all eukaryotes that have been currently looked at. In eukaryotes, cohesin participates in genome folding in interphase and cohesion of sister chromatids, condensin reshapes interphase chromosomes into their mitotic form and SMC5/6 plays as of yet poorly understood roles in DNA repair. Functional SMC complexes also exist in archaea and bacteria, where they play a role in chromosome segregation and genome organization, underlining their ancestral nature. This strongly suggests that an ancestral SMC complex gave rise to the diversity of SMC complexes observed in other species.

SMC complexes follow highly conserved structural principles : they organize around coiled-coil SMC proteins which dimerize in all organisms at the hinge **(Hirano and Hirano, 2002) (Fig. I5)**. These coiled-coil proteins fold on themselves at the hinge and bring together Walker A and Walker B domains, reminiscent of ABC-ATPase transporter cassettes. This forms globular ATPase heads which hold two chambers that can accommodate one ATP molecule each. These globular heads can be brought together to enable ATP hydrolysis. The SMC dimer then associates to a flexible kleisin subunit which contacts the ν-SMC neck (neck gate) via its N-terminal extremity and the κ-SMC cap via its C-terminal extremity **(Fig. I5)**. This SMC-kleisin structure forms a topologically closed entity termed the S-K ring. While this S-K is called a ring, the coiled-coil SMC proteins are very flexible and can be observed in a variety of conformations, such as a ring-like 'O' shape or an 'I' shape where coiled-coils are juxtaposed closely together **(Bauer et al., 2021; Ryu et al., 2020)**. Moreover, the coiled-coils can bend in a way that brings the dimerized hinge domain closer to the ATPase heads **(Bauer et al., 2021; Ryu et al., 2020)**. The uniformity of this S-K structure nonetheless, across SMC complexes and species suggests a conserved core function. On top of this tripartite ring, SMC complexes always display additional regulatory subunits in all species and forms of the complex **(Fig. I5, I6)**. In bacteria, these subunits are termed KITEs while in eukaryotes they are called HAWKs **(Fig. I6)**.

In vertebrate cohesin, two major variants can be defined by the presence of SA1/SA2, also known as STAG1/STAG2 **(Table I1) (Kojic et al., 2018)** and a specific form of cohesin during meiosis bears a

variant SMC1β, a variant kleisin subunit called REC8, and variant HEAT protein called SA3 **(Ishiguro, 2019).** In vertebrate condensin, two different forms of the complex exist called condensin I and condensin II. While condensin I is essential and conserved across all eukaryotes, the same cannot be

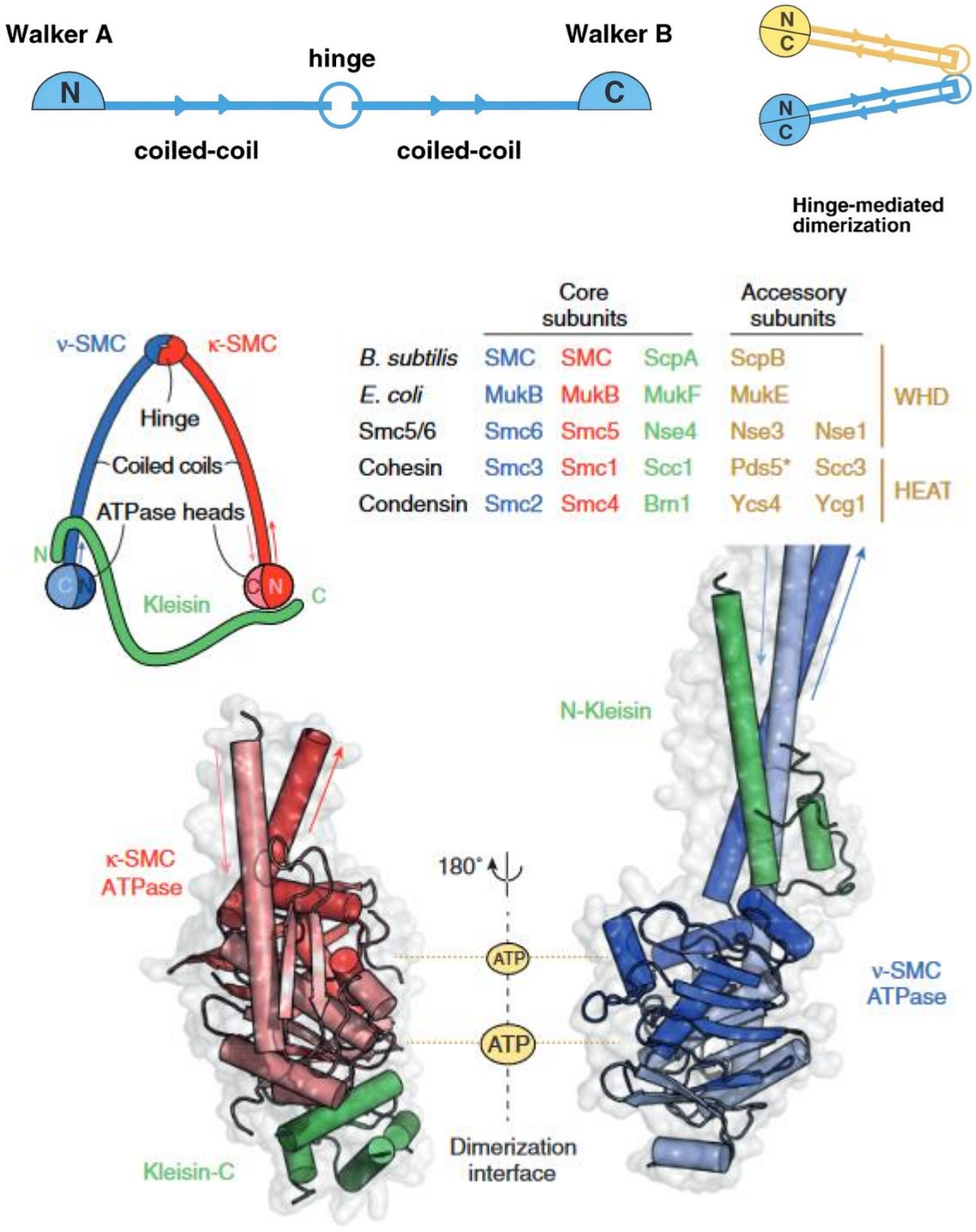

Fig. I5 General structure of SMC complexes (1)
Top : SMC coiled coils fold as antiparallel units at the level of the hinge and form a globular ATPase head by associating their N- and C-ter domains together. Taken from Hirano., 2002. Middle : SMC dimers associate with a flexible kleisin subunit to form an S-K ring and can accomodate additional subunits. Bottom : Globular ATPase heads can accomodate two ATP molecules. Taken from Hassler et al., 2018.

said for condensin II **(Hoencamp et al., 2021)**. Condensin complexes vary by their HEAT proteins and their kleisin subunit **(Table I1)** but both play a role during mitosis.

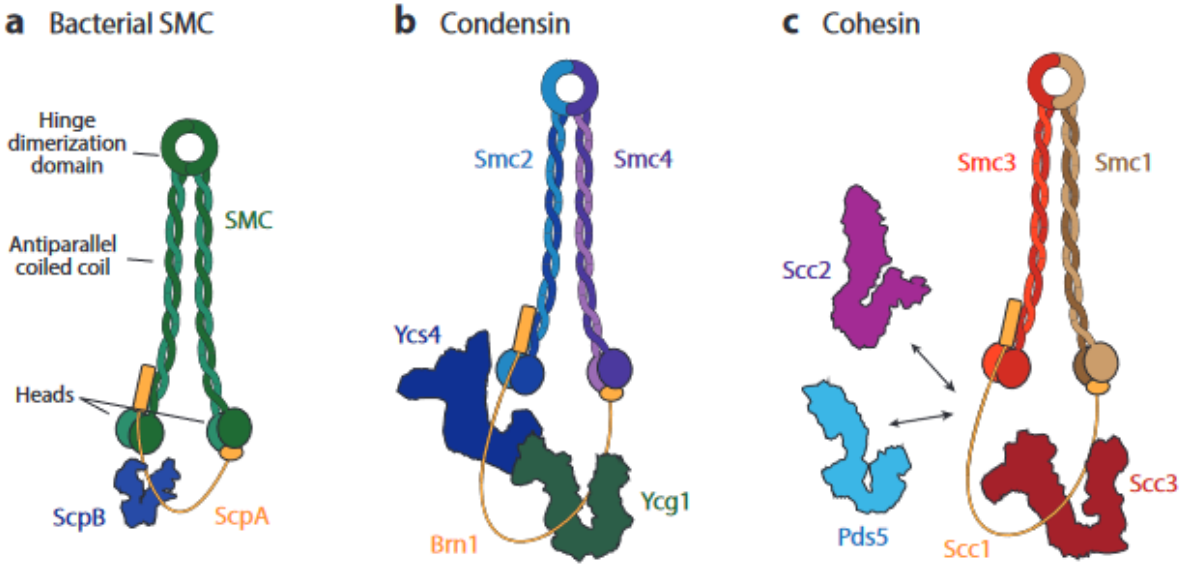

Fig. I6 General structure of SMC complexes (2)
SMC subunits fold at the level of the hinge on themselves to form anti-parallel coiled-coil structures along their lengths. Bringing their C- and N-ter extremities together they assemble ATPase heads. SMC subunits then either homodimerize in bacteria or heterodimerize in eukaryotic SMC complexes. A kleisin subunit binds to the ATPase heads of each SMC subunit to form a tripartite ring (S-K for SMC-Kleisin). In bacteria, additional subunits called Kites associate with the SMC complex while in eukaryotes, regulatory subunits called HAWKs (Heat-Repeat Associated with Kleisin) associate to the complex. Taken from Yatskevich et al., 2019.

SMC complexes are DNA binding machines, and all complexes associate to DNA in the presence of ATP. Moreover, this DNA binding is retained after high-salt washes **(Cuylen et al., 2011; Gutierrez-Escribano et al., 2020; Murayama et al., 2018; Niki and Yano, 2016)** suggesting the complex is topologically binding DNA, with topological entrapment demonstrated for the cohesin complex **(Haering et al., 2008; Srinivasan et al., 2018)**. This DNA-binding property is essential for the ability of SMC complexes to perform their main function of genome folding.

Note that the function of SMC complexes are diverse, and many complexes remain poorly understood (and some may even remain to be discovered). Other types of SMC complexes in eukaryotes, such as Mre11-Rad50-Nbs1 (MRN) **(Kinoshita et al., 2009)** or SMCHD1 **(Gurzau et al., 2020)** are non-canonical eukaryotic members of the SMC complexes with functions in double strand break repair and

gene silencing. In C. elegans, a third condensin complex was identified, specifically involved in dosage compensation – hence called condensin DC – which is a different form of condensin I with the SMC4 subunit replaced by a SMC called DPY-27 **(Csankovszki et al., 2009)**.

Table I1. Diversity of cohesin and condensin subunits
Taken from Oldenkamp et al., 2022

			H. *Sapiens* (Human)	S. *Cerevisiae* (Budding yeast)	S. *Pombe* (Fission yeast)
Cohesin					
Subunits	κ-SMC		SMC1	Smc1	Psm1
	ν-SMC		SMC3	Smc3	Psm3
	α-kleisin		SCC1 (RAD21)	Scc1 (Mcd1)	Rad21
	Heat-A^{Scc2}		SCC2 (NIPBL)	Scc2	Mis4
	Heat-A^{Pds5}		PDS5A or PDS5B	Pds5	Pds5
	Heat-B		STAG1 or STAG2	Scc3	Psc3
Condensin					
Subunits	κ-SMC		SMC4	Smc4	Smc4
	ν-SMC		SMC2	Smc2	Smc2
	Condensin I	γ-kleisin	CAPH	Brn1	Cnd2
		Heat-IA	CAP-D2	Ycs4	Cnd1
		Heat-IB	CAP-G	Ycg1	Cnd3
	Condensin II	β-kleisin	CAPH2	-	-
		Heat-IIA	CAP-D3	-	-
		Heat-IIB	CAP-G2	-	-

The euryarcheota *H. volcanii* folds its chromosomes in an SMC dependent fashion **(Cockram et al., 2021)** and crenarchea *Sulfolobus* shows enrichment in B-compartments of low transcription (analogous to B compartments of eukaryotes) of the SMC complex coalescin ClsN **(Takemata et al., 2019; Takemata and Bell, 2021)**. In prokaryotes, the main SMC complexes organizing genomes which are currently studied are the *E. coli* MukBEF **(Lioy et al., 2018)** promoting long-range interactions and the *B. subtilis* SMC-ScpA/ScpB complex which juxtaposes chromosome arms **(Wang et al., 2018, 2017)**. As argued by **(Hirano, 2016)** chromosome segregation in bacteria is performed at the same time as replication occurs. Hence while the SMC complex is important for

segregation it does not appear to play a role in organizing a scaffold-like structure as seen in vertebrate mitosis (see Part 4). Additionally, some bacteria have evolved SMC-derived complexes termed Wadjet, recently characterized, **(Deep et al., 2022; Liu et al., 2022)** acting as "immune complexes" preventing the transformation of bacteria by foreign circular dsDNA **(Doron et al., 2018)**.

2.3 SMC complexes are DNA motors and crosslinkers

Despite a shared property of binding DNA and of the conserved S-K ring structure, the diversity of SMC complexes, of their regulatory subunits, and of their function bring into question whether all these activities are orchestrated by a same molecular mechanism.

The main model favored currently proposes that SMC complexes act as loop extruding factors (LEF), i.e they processively enlarge loops of DNA by the process of binding and hydrolyzing ATP **(Fig. I7)**.

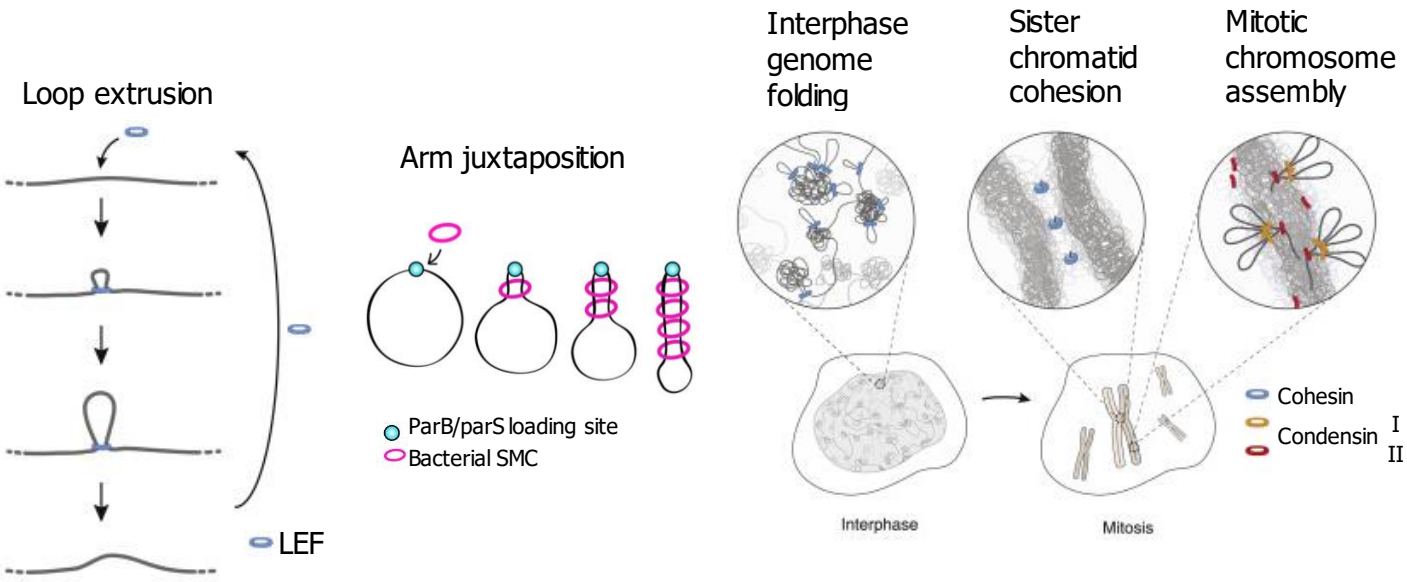

Fig. I7 Basic functions of SMC complexes
Left : SMC complexes in the favored model act as loop extruding factors (LEF). Taken from Oldenkamp et al., 2022. Middle : In bacteria, SMC complexes juxtapose chromosome arms during cell division. Taken from Wang., et al 2017. Right : In eukaryotes, SMC complexes form loops in interphase by the activity of cohesin and in mitosis by the activity of condensin. Additionally, cohesin ensures sister chromatids are cohered together just before anaphase onset. Taken from Oldenkamp et al., 2022

This leads to translocation of the SMC complex, or of the DNA template depending on the observer's point of view, and importantly this mechanism explains observations in vivo regarding the juxtaposition of chromosome arms in bacteria **(Wang et al., 2017, Fig. I7),** the loop structures formed by cohesin in interphase (Rao et al., 2017a) and the loops formed by condensin in mitosis **(Gibcus et al., 2018, Fig. I7)**. While this loop extrusion activity has not been shown directly *in vivo*, it was observed *in vitro* in real-time for the condensin complex first **(Ganji et al., 2018)**, then for cohesin **(Davidson et al., 2019; Kim et al., 2019)** and more recently for SMC5/6 **(Pradhan et al., 2023)**. The loop extrusion process is thought to occur in two main steps : the first is that the SMC complex associates to DNA in a salt-sensitive manner but then involves an initial reaction which allows its loading onto DNA. After this loading, ATP hydrolysis by the SMC complex can render its association salt-resistant **(Eeftens et al., 2017)** and proceed to processive ATP-driven loop extrusion **(Ganji et al., 2018)**. On the other hand, different models based on theoretical simulations and fit to experimental data **(Cheng et al., 2015; Gerguri et al., 2021, Fig. I8)** propose that SMC complexes perform their function as DNA crosslinkers in trans, by capturing a second fragment of DNA. A known example in vivo of this activity, called diffusion capture, is cohesin which has been shown to entrap two DNA molecules **(Murayama et al., 2018; Srinivasan et al., 2018)** and tethers the products of replication together by a distinct mechanism to loop extrusion **(Nagasaka et al., 2023)**. Additionally, diffusion capture could be performed indirectly by contacts between different SMC complexes. This could be the case for clusters of cohesin **(Ryu et al., 2021a)**, for proposed interactions between condensin complexes **(Kinoshita et al., 2022)** or as reported directly by condensin **(Tang et al., 2023)**, for the functioning of bacterial SMC as multimers **(Hirano and Hirano, 2004)**, or SMC5/6 as a dimer **(Pradhan et al., 2023)**.

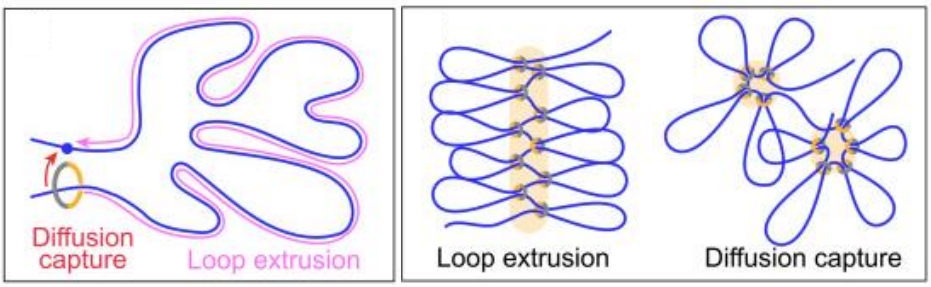

Fig. I8 Loop extrusion and diffusion capture
While loop extrusion relies on a processive mechanism and the translocation of the complex, diffusion capture relies on capture of DNA in trans. Both mechanisms can in theory produce loops to fold chromosomes. Taken from Higashi et al. 2022

In the following section I will discuss in more detail the cohesin complex, which has received the most attention in experimental studies to understand the functioning of SMC complexes as genome organizers.

Part 3 – THE COHESIN SMC COMPLEX STRUCTURES THE GENOME IN INTERPHASE

3.1 The cohesin complex holds replicated sister chromatids together

Cohesin is loaded on chromosomes concomitantly with the reappearance of TADs following mitotic exit **(Abramo et al., 2019)** and also during S-phase **(Zheng et al., 2018)**, but cohesin establishes cohesion of sister chromatids only if it was present during S phase **(Uhlmann and Nasmyth, 1998**). The ability of cohesins to perform cohesion (in other words, to act as a 'cohesive' cohesin) can be explained by the ability of a single complex to entrap two DNA molecules **(Murayama et al., 2018; Srinivasan et al., 2018)**, in a manner that relies likely on specific residues of the cohesin SMC hinge **(Nagasaka et al., 2023)**. Cohesive cohesin can be converted from pre-existing chromatin bound cohesin or loaded de-novo during S-phase **(Srinivasan et al., 2020)**. The cohesive form of cohesin is characterized by acetylation at specific residues of SMC3 which are driven by the acetyltransferase Eco1 **(Ivanov et al., 2002)**. Favored models propose that cohesive cohesin is stabilized by this acetylation which prevents the binding of Wapl, a factor promoting the unloading of cohesin, **(Feytout et al., 2011; Sutani et al., 2009)** and by the binding of Sororin which competes with Pds5/Wapl in vertebrates **(Hoencamp and Rowland, 2023)**. This cycle of loading/unloading determines the steady-state residence time of chromatin-bound cohesin and is key to establish cohesion, although the molecular details of cohesion remain under investigation. In the context of cohesin loading during replication, acetylation relies on the replication fork structure interplaying with the cohesin SCC2/SCC4 "loader" subunits **(Delamarre et al., 2020; Gillespie and Hirano, 2004; Minamino et al., 2023; Psakhye et al., 2023)** although whether the HEAT SCC2 is a loader is currently under discussion **(Alonso-Gil and Losada, 2023)**. The pool of stabilized cohesive cohesin remains on chromosomes until early mitosis **(Gerlich et al., 2006b)**, with some pools retained specifically at centromeres **(Kitajima et al., 2004)** and at inter-sister chromatid bridges **(Chu et al., 2022)**. As cells leave metaphase stage, the conjoined activity of the APC/C and separase then cleaves cohesin to promote the separation of sister chromatids **(Uhlmann et al., 1999)**.

The timely control of cohesive cohesin maintenance and subsequent removal is therefore crucial for the proper segregation of mitotic chromosomes.

3.2 The cohesin complex folds interphase genomes by forming loops

While the molecular activity had been proposed much earlier **(Nasmyth, 2001)** seminal in vitro work demonstrated in 2018 that the condensin complex could processively enlarge loops of DNA *in vitro* **(Ganji et al., 2018)** – an activity called loop extrusion thereafter. We discuss the relevance of loop extrusion in the introduction on condensin and during the Discussion.

This activity was shown *in vitro* for the cohesin complex **(Davidson et al., 2019; Kim et al., 2019)** and is proposed to be a driver of genome folding. In fact, recent evidence argues that cohesion-specific mutants can be generated in cell lines **(Nagasaka et al., 2023)** and that loop extrusion does not require entrapment of DNA since closure of the S-K ring does not prevent loop expansion **(Davidson et al., 2019)** strongly suggesting distinct molecular mechanisms. *In vitro*, loop extrusion by cohesin requires both HEAT protein NIPBL and the additional HEAT protein MAU2 **(Davidson et al., 2019)** and enlarges a loop in a symmetrical fashion, by reeling in DNA from both sides.

The loop extrusion hypothesis argues that cohesin progressively grows a loop over time on chromatin *in vivo*. Such structures can be seen in Hi-C maps as Topologically Associated Domains (TADs) or dots **(Rao et al., 2017a)** and also as stripes **(Vian et al., 2018)**. Removal of cohesin abolishes these structures in populations of cells as seen by Hi-C (Rao et al., 2017b). The residence time of cohesin is a key determinant for the size of these loops and in theory these loops can grow until:

- Their characteristic turnover is reached and cohesin is released from DNA. In cells this residence time is estimated to ~30mn but removal of Wapl, the cohesin unloader, extends this residence time by approximately twenty fold **(Tedeschi et al., 2013)**. The canonical phenotype of Wapl loss is the

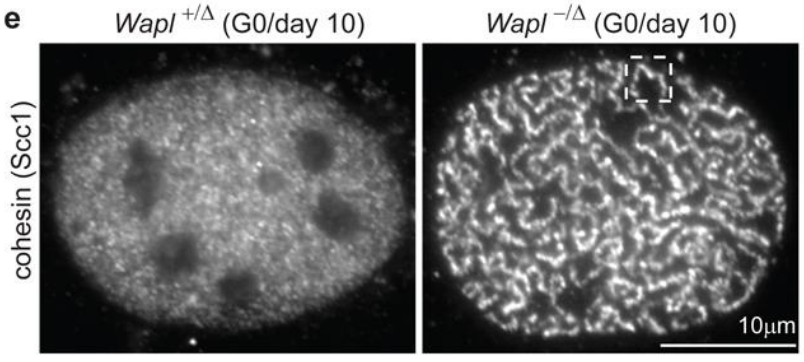

Fig. I9 Wapl prevents the formation of visible chromosomes
See text for details. Taken from Tedeschi et al., 2013

formation of visible chromosomes (*vermicelli*) in quiescent cells under the microscope, akin to mitotic chromosomes **(Fig. I9)**, implying a similar molecular mechanism may exist to form mitotic chromosomes by condensin.

- The cohesin complex encounters an obstacle, which blocks their translocation. The canonical examples of this type of obstacle is CTCF, an 11-zinc finger protein that binds to a specific sequence motif in mammals. *In vivo* CTCF are found at boundaries of TADs in a convergent manner mostly **(Rao et al., 2014)** and the orientation of CTCF is key to block translocation of cohesin *in vitro* **(Davidson et al., 2023, Fig. I10).** This provides indirect evidence that cohesin anchors loops by processively extruding them, since *in vivo* if cohesin were simply capturing long-distance sites to bring them together it would be difficult to explain why most loop anchors would be biased towards convergence of CTCF motifs and not divergent or other motifs. The physical interaction between cohesin and CTCF competes with a Wapl binding interface suggesting cohesin is stabilized at CTCF sites **(Li et al., 2020)** in a manner dependent on the integrity of the ring **(Liu and Dekker, 2022)**. Convincing evidence for loop extrusion by cohesin can be found in the literature describing the role of CTCF orientation in V(D)J recombination. Briefly, in the Igh locus convergent CTCF sites enable recombination of V(D)J segments, and a specific transcription factor can downregulate Wapl to increase cohesin residence time and lead to recombination of more distal sites, correlated with a longer loop **(Hill et al., 2020; Peters, 2021)**. Additional evidence *in vivo* for loop extrusion are the property of active transcription to stall translocating SMC complexes. This was demonstrated convincingly in bacteria **(Tran et al., 2017; Wang et al., 2017)** and several reports provide evidence that similar properties of SMC cohesin can be found in budding yeast **(Jeppsson et al., 2022a; Lengronne et al., 2004)** and in vertebrates (Banigan et al., 2023; Busslinger et al., 2017).

Finally, cohesive cohesin is also likely found enriched at CTCF sites as suggested by the bias of ring integrity at CTCF sites, and that CTCF sites are biased with sites of cohesion as determined by sister-chromatid-sensitive Hi-C **(Liu and Dekker, 2022; Mitter et al., 2020).** Convergent or divergent CTCF sites appear to be positions of early replication origins **(Emerson et al., 2022)**, suggesting perhaps that while loop extrusion and cohesion are independent molecular mechanisms, blockage of loop extruding cohesin at CTCF sites may also constitute hotspots of cohesion initation.

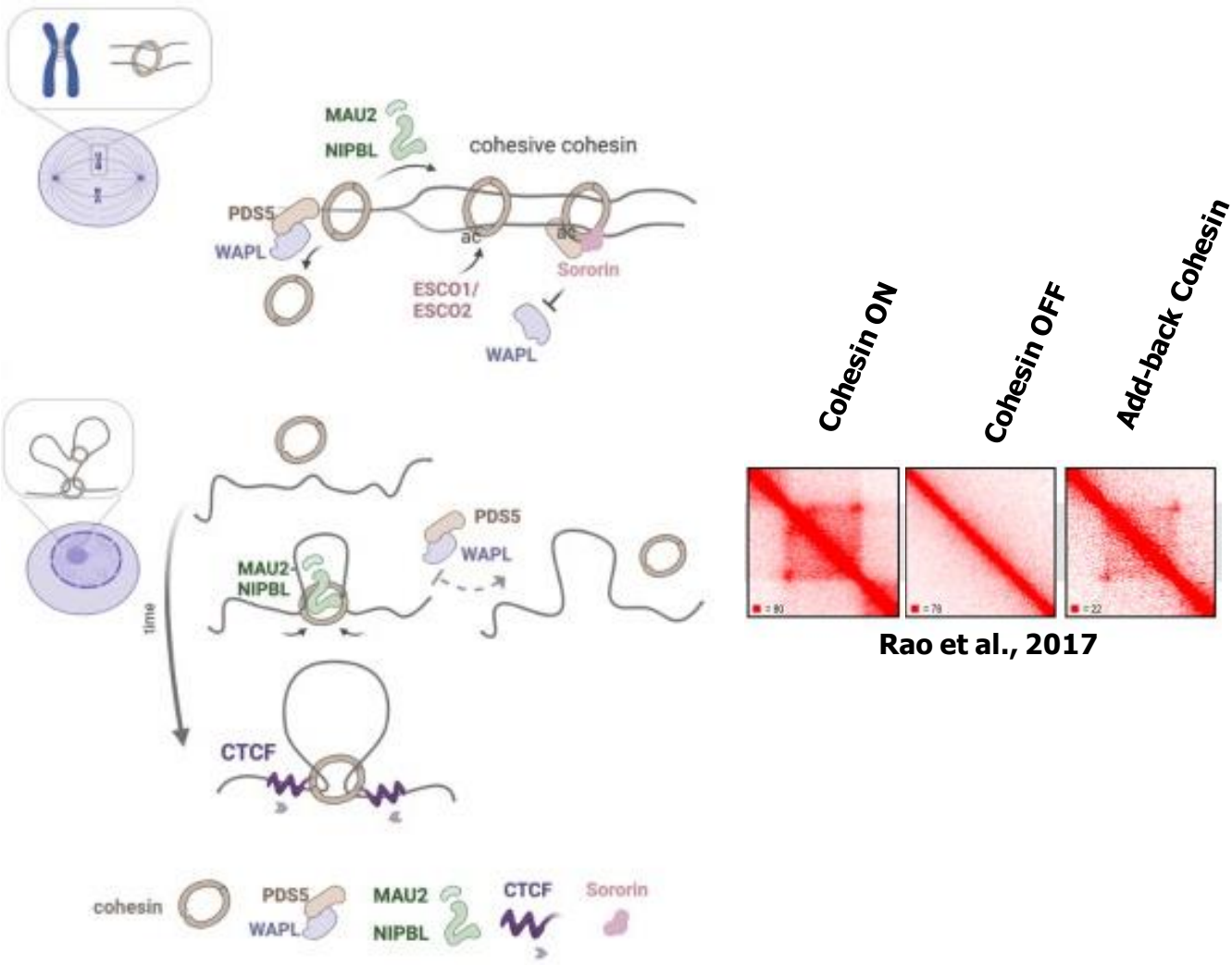

Fig. I10 Cohesion and loop extrusion by cohesin regulation
Cohesin residence time on chromatin is determined by its regulatory activities, with PDS5/WAPL promoting the unloading of cohesin from chromatin. Taken from Alonso-Gil et al., 2022. Top : Products of replication are maintained by cohesin from S-phase onwards. Acetylation by acetyltransferase and sororin in vertebrates stabilize the topological entrapment of DNA by cohesin. Bottom : Processive loop extrusion is stimulated by NIPBL/SCC2 and MAU2 and unloaded by WAPL and PDS5. A specific oriented motif of the CTCF protein blocks translocation of cohesin and stabilizes it by competing with Wapl binding, explaining how convergent CTCF sites are hotspots of cohesin-anchored loops. Right : TAD/dot structure disappears after cohesin depletion by degron and reappears after auxin removal in cells. 800kb box. Taken from Rao et al., 2017.

Part 4 – THE ASSEMBLY OF MITOTIC CHROMOSOMES BY CONDENSIN AND TOPO II

4.1 Mitotic chromosomes have a scaffold and loops of chromatin

While under a light microscope the contents of a housing the DNA can appear diffuse and perhaps even disorganized, during M-phase the DNA is converted in visible rod-shaped structures. During the XIXth century Walther Flemming provided key drawings of rod-shaped mitotic chromosomes following observations of chromosomes stained by DNA dyes. This reshaping of the contents of a seemingly disorganized interphase nucleus preceded the segregation of two sets of rods to each daughter cell. A century after Walter Flemming's initial observation, Laemmli and colleagues provided striking images of mitotic chromosomes under electron microscopy after full **(Paulson and Laemmli, 1977)** or partial **(Earnshaw and Laemmli, 1983)** histone depletion. This work argued that the mitotic chromosome is structured by an electron dense core at the center from which chromatin loops emanate and can be seen individually on the grid. Both sister chromatids could be observed in these samples, which appeared to be held together by the core as well. These fibers form loops that protrude outward and remain partially assembled by individual nucleosomes **(Earnshaw and Laemmli, 1983)**. The scaffold persisted in 2M NaCl suggesting a tethering component, likely proteic in nature, held together the metaphase chromosome. The key components of the scaffold were then purified as Scaffold Component 1 & 2 **(Lewis and Laemmli, 1982)**. Sc1 was identified first as topoisomerase II **(Earnshaw et al., 1985)** and Sc2 was then described as a coiled-coil protein **(Hirano and Mitchison, 1994; Saitoh et al., 1994)** and later characterized as the SMC2 subunit of the condensin complex **(Hirano et al., 1997)**.

More recent studies of vertebrate mitotic chromosomes show that metaphase chromosomes are covered by a peripheral layer. This structure contributes anywhere from one third to almost half of the volume of metaphase chromosomes **(Booth et al., 2016)** and is composed of a multitude of proteins originating from the nucleolus which all depend on the presence of Ki-67 **(Stenström et al., 2020)**. Ki-67 has been proposed to act as an electrostatic surfactant preventing the intermingling of individual chromosomes in cells **(Cuylen et al., 2016; Takagi et al., 2018)** but the function of this peripheral layer remains relatively unexplored, although it appears non-essential.

These Sc proteins assembled into mitotic chromosome and formed an internal structure and were essential for the structure of the rod shaped chromosome and their function **(Hirano and Mitchison, 1994)** which made them as a key candidate for the mitotic chromosome scaffold. Indeed, staining of condensin on metaphase chromosomes suggest it is enriched along an axis internal to the chromosome **(Chu et al., 2020a; Maeshima and Laemmli, 2003; Ono et al., 2003)**. Topo II (read section below) is also found enriched in this axis **(Chu et al., 2020a; Maeshima and Laemmli, 2003)**. The staining of condensin also show it is present on this internal axis in a punctate, discontinuous manner **(Maeshima and Laemmli, 2003; Sun et al., 2018; Walther et al., 2018)**. Consistent as a key player of this scaffold structure identified by Laemmli and colleagues, condensin association and activity in vivo is defined by a central axis from which loops emanate **(Gibcus et al., 2018; Houlard et al., 2021)** at least in vertebrates. Similarly to vertebrates, conditional depletion in metaphase suggest that the assembly of mitotic chromosomes is completely dependent on condensin in fission yeast **(Kakui et al., 2017)**. While the proteinaceous scaffold of mitotic sister chromatids is described as being composed of condensin, topo II and Kif4A in vertebrates **(Paulson et al., 2021)** it could also be argued that the scaffold structure itself results from the activity of SMC complexes and topo II.

4.2 The condensin complex

Condensin works as a key chromosomal organizer of the genome and functions on chromatin as a pentameric complex **(Kimura and Hirano, 2000)**. Crucially, phosphorylation of condensin by Cdk 1/Cdc2 is required to promote its activity **(Kimura et al., 1998)**. Furthermore, to condense assembly of chromatin into mitotic chromosomes in a minimal system, the sole phosphorylation of condensin by Cdk1 is sufficient, while phosphorylation by Aurora B is not **(MacCallum et al., 2002; Shintomi et al., 2015)**. Note that the picture in vivo and depending on the species might be different. Hyperactivation of condensin by Polo-kinase (Plk1)-dependent phosphorylation is required in anaphase **(St-Pierre et al., 2009)**.

In vertebrates two versions of the pentameric condensin complex exist, named condensin I and condensin II **(Ono et al., 2003)**. In both complexes there are two common subunits SMC2 and SMC4. Kleisin in condensin I (CAP-H/Cnd2/Brn1) or in condensin II (CAP-H2) is a long flexible protein

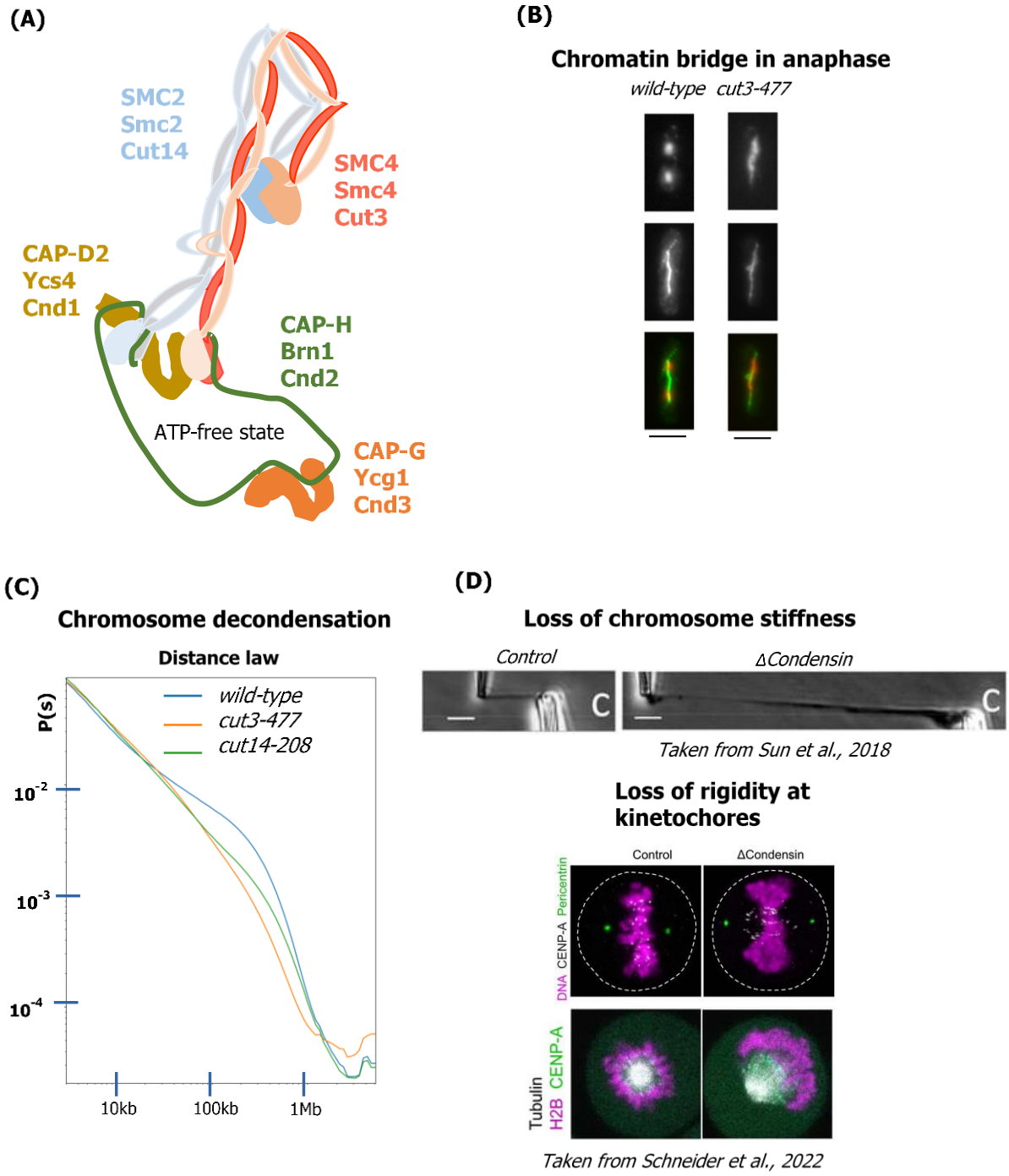

Fig. I11 Condensin structure and defects upon condensin loss of function
(A) Scheme of the pentameric condensin complex with names in vertebrate, budding yeast and fission yeast from top to bottom. (B) Left : Cytological stages of anaphase in *wild-type* Right : Chromatin bridge phenotype during anaphase. Scale bars are 5µm. (C) Representative Hi-C distance law and its slope showing defects in mitotic chromosome folding associated with the temperature sensitive alleles *cut3-477* and *cut14-208*. (D) Phenotypes associated to the rheology of mitotic chromosomes.

and will bind the SMC2 neck (the coiled coil region just above the ATPase head) via its N-terminal extremity and the SMC4 cap (at the bottom of the SMC4 head) via its C-terminal extremity. The coiled-coil structure is flexible. It has been observed in different species in a "rod" or "open" conformation **(Eeftens et al., 2016; Ryu et al., 2020)** and the hinge can bend towards the ATPase

heads thanks to local flexibility at an 'elbow' region in the coiled coil arms **(Eeftens et al., 2016; Lee et al., 2020; Ryu et al., 2020)**. The SMC4 hinge contacts the SMC2 coiled-coil and this bend is particularly pronounced in condensin (2/3 of the length) **(Lee et al., 2020)** while it is shorter in cohesin complexes and bacterial SMC complexes. Each of the three subunits then associates with HAWK subunits (Heat-Repeat Associating With Kleisin) which differ between condensin I and condensin II. These are CAP-D2/Ycs4/Cnd1 and CAP-G/Ycg1/Cnd3 for condensin I and CAP-D3, CAP-G2 in condensin II.

The functional specificities between these two variant complexes have not been fully elucidated. Both complexes associate to chromatin with large differences in residence time in vivo (~5mn vs ~25mn+) **(Gerlich et al., 2006a)** but associate at different stages of mitosis. Condensin II is nuclear during interphase and binds to DNA as early as S-phase **(Ono et al., 2013)** and remains bound until the start of mitosis and is not significantly enriched upon progression through M **(Gerlich et al., 2006a; Samejima et al., 2022)**. Condensin I however is cytoplasmic, gains access to chromosomes upon Nuclear Enveloppe BreakDown (NEBD) and is enriched on chromosomes from prometaphase onwards **(Ono et al., 2004; Shintomi and Hirano, 2011).** Both condensin complexes control different condensation phenotypes of mitotic chromosomes **(Ono et al., 2003)**, with condensin II establishing longer-range structures than condensin I **(Gibcus et al., 2018)** and being more internal within chromosomes than condensin I **(Shintomi et al., 2017; Walther et al., 2018)**. Condensin I and II appear to be mostly non-overlapping particularly at centromeres where condensin II appears bound specifically **(Ono et al., 2004)** and also along arms although there is some overlap **(Ono et al., 2004; Sun et al., 2018; Walther et al., 2018).** Condensin II is present in prophase and leads to individualized, long chromosomes, which become shorter and fatter upon NEBD (Liang et al., 2015) at prometaphase when condensin I gains access to the nucleus **(Gerlich et al., 2006a)**. Condensin I is more abundant than condensin II and the 5:1 I:II ratio is important for the shape of chromosomes **(Shintomi and Hirano, 2011)** and from metaphase to anaphase the ratio of condensin I/II increases **(Walther et al., 2018)**.

Finally, attributed loop sizes of 80kb to condensin I and 400 kb to condensin II **(Gibcus et al., 2018)** coincidentally respect the stoichiometric 5:1 ratio of condensin I:II in metaphase **(Shintomi and**

Hirano, 2011). The current model of vertebrate chromosomes **(Gibcus et al., 2018; Walther et al., 2018)** proposes that condensin II binds to form loops of 400kb and condensin I binds in late prophase to form nested loops of 80kb, with condensin II contributing to axial shortening while condensin I in lateral compaction **(Shintomi and Hirano, 2011)**.

SMC/Condensin is required for viability in all organisms with a few exceptions, notably E.coli MukBEF is not strictly essential **(Niki et al., 1991)**, similarly for SMC in B. subtilis **(Bürmann et al., 2017)**, H. volcanii **(Cockram et al., 2021)** and condensin II in some species like red algae **(Fujiwara et al., 2013)**.

Defects in mitotic condensin function leads to several defects in the architecture of metaphase chromosomes and their ability to segregate during anaphase **(Fig. I11)**. The most obvious is the stereotypical phenotype of chromatin bridges **(Gerlich et al., 2006a; Hirano et al., 1986; Piskadlo et al., 2017)**. Loss of condensin also leads to centromere stretching by microtubules **(Piskadlo et al., 2017; Schneider et al., 2022)** and to lower stiffness of the chromatid in general when probed by micropipettes **(Sun et al., 2018)**. This mechanical property can also be observed in budding yeast anaphase where a partial deficiency of condensin prevents the recoiling of sister chromatids once separated **(Renshaw et al., 2010)**. Other, less investigated roles in cell physiology have been described. An early report suggested that the kleisin subunit played a role in DNA replication and repair **(Aono et al., 2002)**. More recent work shows that condensin II promotes the disjunction of replicated sister chromatids as early as S phase **(Ono et al., 2013)** and depletion of condensin in G2 phase has been shown to trigger both increased chromatin mobility and potentially double strand breaks **(Kakui et al., 2020).** Unexpected roles of condensin outside of mitosis are yet to be investigated more deeply. Importantly, condensin II provides more mechanical stiffness to metaphase chromosomes than condensin I **(Sun et al., 2018)**. Moreover, condensin II appears to specifically be involved in the prevention of ultrafine bridges **(Elbatsh et al., 2019)**. While eukaryotic condensin is conserved in all species, this is not the case for condensin II subunits, which are not conserved in all lineages. Fungi such as fission yeast and budding yeast only have a single kind of condensin complex, which resembles condensin I, although while condensin in fission yeast gains access to chromosomes during mitosis, condensin in budding yeast is already nuclear at S phase

similarly to condensin II **(Bhalla et al., 2002)**. In general, condensin II appears to have been lost multiple times across evolution **(Hirano, 2016; Hoencamp et al., 2021)** which could potentially be responsible for reproductive barriers during fertilization **(Yakoubi and Akera, 2022)**.

4.3 Condensin structure and the ATPase cycle

The condensin complex (but this rationale can be extended to other SMC complexes) requires functional ATP binding and hydrolysis to assemble mitotic chromosomes. The ATPase heads in the condensin complex resemble the Walker motifs found in other protein complexes, such as ABC transporter cassettes or other motors like kinesins or dyneins.

The ATPase heads can theoretically accomodate 2 ATP molecules per hydrolysis events, but the binding events are asymmetric. Indeed, the SMC2 head by itself in a complex cannot bind or hydrolyse ATP and ATP binding at the SMC2 head requires a comformational change determined by a previous ATP binding at the SMC4 head **(Hassler et al., 2019)**. Complexifying this, the two ATPase sites formed by SMC2-SMC4 head engagement appear to have different functions in condensin. Mutants in the ATPase site AS2, show hypercondensation phenotypes while mutants in the other site AS1 show hypocondensation **(Elbatsh et al., 2019)** consistent with AS1 being the site that can initate ATP binding **(Hassler et al., 2019, Fig. I12)**. Although mechanistic and structural explanations for this remain unclear, the AS2LV mutant appears to form less Z-loops **(Elbatsh et al., 2019)** which have therefore been proposed to limit loop size to explain the condensation phenotypes.

Nonetheless, ATP binding drives a conformational change which can bring the far apart SMC ATPase heads closer together and lead to the bending of the coiled coils into a more open state **(Lee et al., 2020)** which can accommodate dsDNA inside the ring just above the ATPase heads **(Lee et al., 2022; Shaltiel et al., 2022)**. This position of dsDNA just above the heads, covered by kleisin, is functionally relevant as it is conserved in cohesin complexes **(Higashi et al., 2020; Shi et al., 2020)** and E.coli and B. subtilis bacterial SMC complexes **(Bürmann et al., 2021; Vazquez Nunez et al., 2019)**. Importantly, ATP binding drives a chemical change leading to high resistance to pulling force within the SMC complex, consistent with SMC heads brought closer together **(Pobegalov et al.,**

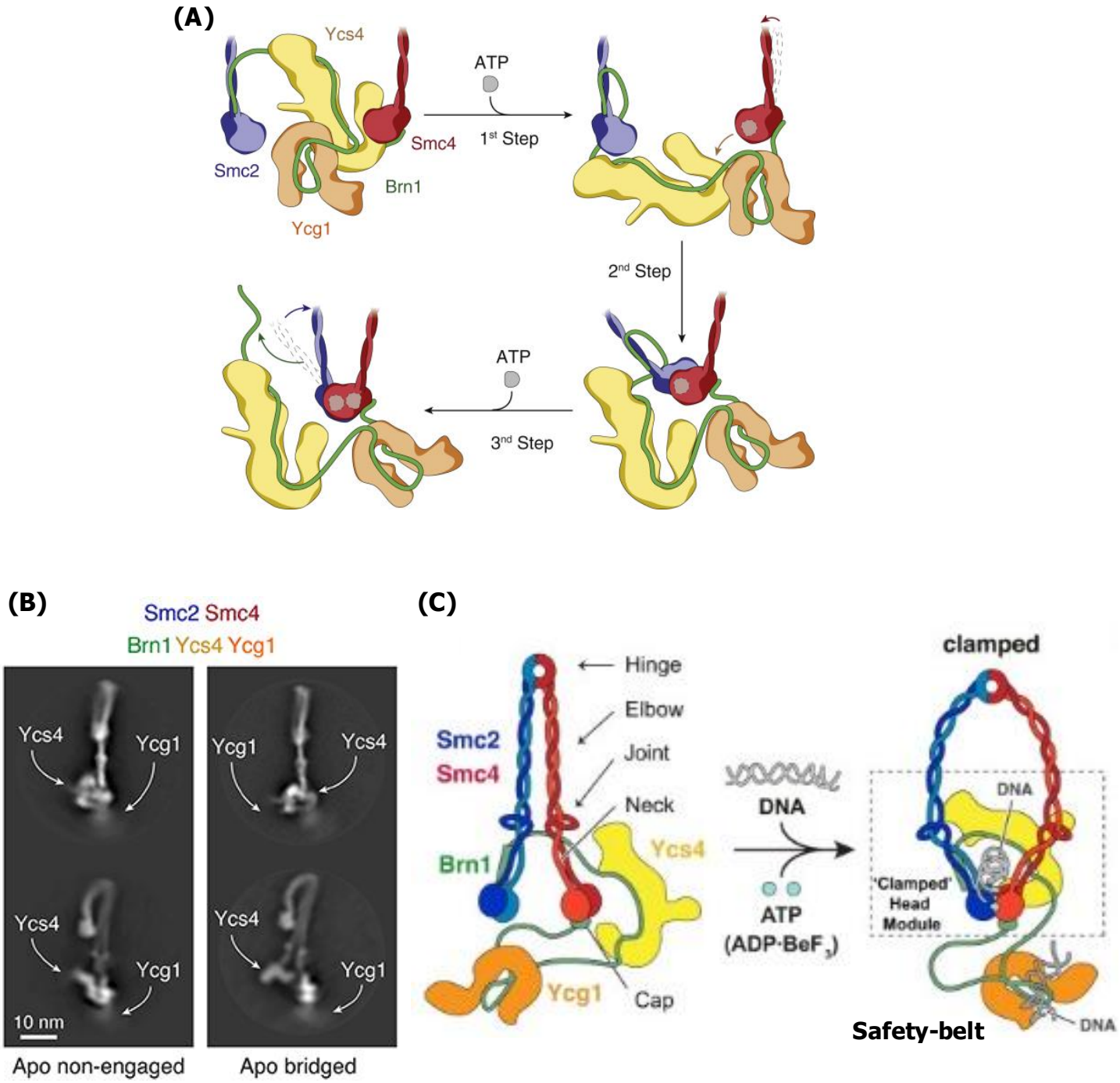

Fig. I12 Structure of the condensin complex
See text for details. (A) In an apo state, CAP-D2/Cnd1/Ycs4 KG-loop interacts with Smc4 W-loop. Upon ATP binding, SMC2 and SMC4 heads bind together, excluding CAP-D2/Cnd1/Ycs4. A second ATP binding event can occur and leads to the opening of the neck-gate between SMC2 and CAP-H/Cnd2/Brn1. Taken from Hassler et al., 2019 (B) Cryo-EM of condensin complex without ATP, with the visible rod shape and bend. In cryo-EM images, it is challenging to visualize a class-average of the kleisin subunit due to its flexibility. Taken from Lee et al., 2020 (C) Condensin complex in the presence of ATP and DNA. Condensin binds to the DNA via the safety belt and clamps DNA just above the ATPase heads but this binding appears to disfavor opening of the neck gate. Taken from Lee et al., 2022

2023). Additionally, ATP binding in vitro is the step required for stepwise compaction by condensin

(Ryu et al., 2021b) suggesting that ATP binding and not hydrolysis is the event generating the

power stroke necessary for processive loop extrusion observed in vitro **(Ganji et al., 2018)**.

The position of HAWK subunits relative to the rest of the complex is flexible, potentially due to their association with kleisin, and are thus not often well resolved in cryo-EM images. Without DNA, when condensin is in an apo state, CAP-G/Ycg1/Cnd3 is not well resolved while CAP-D2/Ycs4/Cnd1 is close to the ATPase heads. Ycs4 contacts SMC4 with its HEAT repeats 18-19 forming a conserved KG-loop interacting with a SMC4 W-loop **(Hassler et al., 2019)**. Upon ATP binding however, Ycs4 is not seen close to the ATPase heads and instead Ycg1 is brought closer **(Lee et al., 2020)**. Consistent with this, ATP binding prevents the copurification of CAP-D2/Ycs4/Cnd1 with CAP-G/Ycg1/Cnd3, a minimal kleisin and SMC2/4 heterodimers **(Lee et al., 2020)**. Importantly, the KG-loop/W-loop interaction described above has been proposed to mediate interactions between different condensin complexes **(Kinoshita et al., 2022)**.

Strikingly, ATP binding also leads to the opening of the kleisin gate near the neck of SMC2 as shown by TEV cleavage experiments **(Hassler et al., 2019)**. However this same phenomenon is not seen when the complex binds ATP in the presence of DNA **(Lee et al., 2022)**. In the same vein, an ATP-bound condensin complex in the presence of DNA does not prevent the association of CAP-D2/Ycs4/Cnd1 to the SMC head gate **(Shaltiel et al., 2022)**. Recent evidence has suggested that the N-terminal tail of CAP-H prevents the opening of the SMC2 neck-CAP-H gate, and that this is relieved upon phosphorylation by Cdk1 **(Tane et al., 2022)** which could provide an initial DNA loading activity onto chromatin. These features underline the possibility of different conformations for the loading of condensin on DNA versus processive loop expansion once bound. CAP-G/Ycg1/Cnd3 associates with kleisin to form a "safety belt" structure **(Fig. I12C)** which can entrap DNA via positively charged surfaces of the HEAT-repeat. This domain is also important to provide a DNA dependent stimulation of condensin ATPase activity **(Kschonsak et al., 2017)**. Importantly this safety belt is the domain anchoring the condensin complex to DNA during the loop extrusion reaction **(Shaltiel et al., 2022)**. How the DNA is moved relative to the condensin holocomplex during the process of loop expansion remains unclear, but it must accommodate DNA at two positions (at the very least, but could be more). One of these being the CAP-G/CAP-H safety belt as an anchor point,

the remaining known DNA binding sites are likely candidates to investigate for the other positions for DNA loop expansion.

Certain models have proposed the hinge domain as an anchor point since it has flexibility **(Eeftens et al., 2016)** to potentially grab DNA**.** However, the flexibility is driven by thermal motion **(Pobegalov et al., 2023)** and it is far more parsimonious for head-head engagement by ATP binding to generate the power stroke necessary to extrude the loop. Despite this, the length of the coiled-coil is under strong selective pressure to respect a certain phasing **(Bürmann et al., 2017)** potentially hinting at a physiologically relevant function of the hinge movement. Another DNA contact could be the observed position of dsDNA just above the ATPase heads **(Lee et al., 2022)** but what kind of motion of DNA starting from this position would lead to processive expansion is not known.

4.4 Condensin molecular activities

Many molecular activities, all seemingly different, have been attributed to condensin. It is clear that the ATP-dependent hydrolysis activity of condensin is required for its function but whether some of these activities can be uncoupled from each other or can be differentiated on structural basis of the condensin complex is not clear.

Loop extrusion hypothesis

The main activity attributed to condensin which has gained a lot of traction remains it's ability to translocate on DNA *in vitro* **(Terakawa et al., 2017)** and to initiate and then enlarge loops of DNA **(Ganji et al., 2018)** both in an ATP-dependent fashion. The experiment from Ganji et al., led to the innovation of the loop extrusion assay, allowing the visualization of processive loop enlargement from a DNA tethered on a flowcell upon SMC addition. At the base of these loops single condensin complexes are found **(Kong et al., 2020)**, although examples with two complexes were also described **(Kim et al., 2020; Kong et al., 2020)**. This loop extrusion activity is in major part asymmetric in the case of condensin I **(Ganji et al., 2018; Golfier et al., 2020; Kong et al.,**

2020), meaning once condensin is bound and begins to enlarge a loop it does so only from one side in contrast with human cohesin which enlarges loops symmetrically **(Davidson et al., 2019; Kim et al., 2019)**. In the system of Ganji and colleagues condensin hydrolyzes ~2 ATP molecules per second and on average extrudes a loop at an average speed of ~600b per second. This processivity is highly dependent on the tension/slack of the DNA molecule as very low forces ~1pN can stall condensin loop formation **(Ganji et al., 2018)** but these parameters potentially do not reflect the mitotic activity of condensin as it was recovered from cycling cells. When Xenopus egg extracts (with the majority of histones removed) are provided instead of minimally purified components **(Golfier et al., 2020)** the speed of loop extrusion reaches an average of ~2kb/s, remains in majority asymmetric and displays even lower stall forces on average ~0.15pN.

While loop extrusion has not been observed *in vivo* several lines of supporting evidence have suggested it is a bona fide activity of condensin :

1/ This activity was convincingly shown *in vitro* with single molecule assays in real-time and is conserved in the cohesin complex **(Davidson et al., 2019; Kim et al., 2019)** and in the SMC5/6 complex **(Pradhan et al., 2023)**. Accumulating evidence suggests that loop extrusion is a mechanism shaping chromosomes during interphase (see Part 3) and in bacteria **(Wang et al., 2017)**.

2/ This activity *in vitro* can be abolished by mutations preventing the binding of ATP **(Ganji et al., 2018)** or using safety-belt mutants which lead to events of anchor slippage and loss of translocation directionality **(Ganji et al., 2018; Shaltiel et al., 2022)**.

3/ It provides a consistent way of compacting linearly the DNA **(Banigan and Mirny, 2020)** while resolving sister entanglements in a single mechanism in mitotic chromosomes **(Brahmachari and Marko, 2019)** consistent with the interplay between condensin and topo II **(Baxter et al., 2011; Charbin et al., 2014)**. In vivo structures **(Earnshaw and Laemmli, 1983; Paulson and Laemmli, 1977)** are consistent with loops and were confirmed to be condensin-dependent units of

mitotic chromosomes **(Gibcus et al., 2018)**. Additionally, while NGS approaches cannot provide time-sensitive information, certain features associated to cohesin fit with a processive activity to form domains; such as stripes in Hi-C maps (Costantino et al., 2020; Dauban et al., 2020; Gibcus et al., 2018; Rao et al., 2017b) ; or convergent CTCF barriers which prevents loop extrusion **(Davidson et al., 2023)** where cohesin accumulates in vivo **(de Wit et al., 2015)**.

4/ Finally, extending the residence time of an SMC complex also increases the size of these structures, as seen for both cohesin **(Haarhuis et al., 2017; Tedeschi et al., 2013)** and condensin II **(Houlard et al., 2021)** which promotes the formation of 'mitotic-like' chromosomes in interphase. Nonetheless, *in vivo* evidence for loop extrusion by condensin remains more scarce than for cohesin.

A recent preprint **(Guérin et al., 2023)** however reports that yeast expressing a loop extrusion mutant form of cohesin grows on plates as well as wild-type, bringing into question the physiological relevance of cohesin loop extrusion at least in budding yeast.

Diffusion capture

An alternative model to the activity of condensin by loop extrusion is a stochastic pair-wise interaction model, called diffusion capture **(Cheng et al., 2015; Gerguri et al., 2021)**. In this model, condensin, after binding to one site on a genome, would then establish a contact with a second locus on the genome and bring far-apart sites closer together. Theoretical simulations of this model reproduce more efficiently experimental features of mitotic Hi-C maps and changes in DNA compaction compared to loop extrusion in fission yeast **(Gerguri et al., 2021)**.

Multimerization

A recent report suggests that the assembly of the axis relies, at least in part, on an activity that is not loop extrusion and relies on interactions between condensin complexes **(Kinoshita et al., 2022)**. Said tetrameric ΔCAP-G condensin complex is incapable of loop extrusion **(Kinoshita et al., 2022)**

yet it can participate in mitotic chromosome assembly through a function performed by CAP-D2 **(Kinoshita et al., 2022)** which is consistent with opposite roles of CAP-G and CAP-D2 subunits in axis assembly described previously and the ability of CAP-G less complex to bind to chromosomes **(Kinoshita et al., 2015)**. This activity has been proposed to be established due to interactions mediated between the CAP-D2 KG-loop and the SMC4 head W-loop, which should also exist for condensin Ⅱ **(Kinoshita et al., 2022)**. These results are striking and have further implications : they give molecular weight to proposed models of mitotic chromosome condensation by diffusion capture **(Gerguri et al., 2021)**. Condensin multimerization could therefore stabilize, or provide a mechanism for, these long-range interactions without a loop extrusion mechanism. Indeed, clustering of condensin would be consistent with observations regarding cohesin complexes **(Ryu et al., 2021a)**, BsSMC **(Kim and Loparo, 2016)** and some proposed condensin-condensin interactions **(Eeftens et al., 2016; Kim et al., 2020)** in vitro and could provide a mechanism to organize large domains, or to stabilize them.

Supercoiling and DNA reannealing

Condensin can promote the positive supercoiling of DNA *in vitro* **(Kimura et al., 1999; Kimura and Hirano, 1997; Martínez-García et al., 2022)** but this is observed at high concentrations of condensin, at more than 1 complex per 100bp **(Martínez-García et al., 2022)**. However, supercoiling could be a consequence of the activity of a single complex as seen *in vitro* **(Bazett-Jones et al., 2002; Kim et al., 2022),** although whether this supercoiling would be positive is unclear, and whether it exists in a condensin-dependent manner *in vivo* as well.

Condensin has also been shown to reanneal single stranded DNA in a manner that requires only the SMC heterodimer **(Akai et al., 2011; Sakai et al., 2003; Sutani and Yanagida, 1997)** which are presumably binding to ssDNA. This activity is not seen with a cohesin heterodimer and is seen at relatively high concentrations of condensin ~40nM **(Sakai et al., 2003)**, despite cohesin being reported to capture ssDNA only during second strand capture assays **(Murayama et al., 2018).** Crucially this activity becomes temperature sensitive when ts mutants (*cut14-208* and *cut3-477* used in our studies) of the heterodimer are purified and used for the assay **(Sutani and Yanagida,**

1997). This activity has been proposed to be important during the segregation of chromosomes in anaphase **(Nakazawa et al., 2019; Sutani et al., 2015)** but remains to this day unexplored.

Topological entrapment

Experiments have also suggested the structural integrity of the S-K ring **(Cuylen et al., 2013, 2011)** is important for retaining DNA within the complex consistent with what is observed for bacteria **(Wilhelm et al., 2015)**. As discussed by **(Yatskevich et al., 2019)**, in papers claiming condensin establishes topological entrapment **(Cuylen et al., 2013, 2011; Tane et al., 2022)**, the complex simply retains DNA under high salt washes. While topological entrapment was demonstrated by crosslinking experiments for cohesin **(Haering et al., 2008; Srinivasan et al., 2018)** similar experimental proof remains lacking for condensin. Recent experimental evidence in loop extrusion assays suggest the path of DNA to be likely pseudo-topological (Pradhan et al., 2022) bringing into question topological entrapment of DNA by condensin.

4.5 The architectural changes of mitotic chromosomes

While the mitotic chromosome is well understood to contain a proteinaceous scaffold forming two axes (one within each sister-chromatids), with loops of DNA emanating from this scaffold, and a peripheral layer in metaphase, there are multiple complexities underlying the shape of mitotic chromosomes.

Over the course of mitosis, the chromosome does not simply become more and more compact in a progressive fashion, but experiences significant morphological changes in cells. I provide a scheme describing the morphological changes chromosomes experience (mostly in M) with description of the presence of SMC structural components.

First is the apparent condensation of G2 chromosomes into visible, individual units during prophase. Chromosomes condense into bent structures during early/mid prophase (Kireeva et al., 2004; Liang et al., 2015) and overall tend to straighten from late prophase onwards and well into metaphase (Liang et al., 2015). While sister chromatids cannot be discerned very well in early prophase images (Kireeva et al., 2004; Liang et al., 2015) they can be distinguished in late prophase **(Chu et al., 2020a;**

Kireeva et al., 2004). These observations are consistent with the modulation of SMC complexes during early mitosis. In G2/early prophase, condensin II and cohesin are bound to chromosomes. Cohesin removal from chromosome arms by Wapl coincides with the appearance of 'bubbles' in late prophase which helps resolve sister chromatids **(Chu et al., 2020a)** and coincides with a reported expansion in volume **(Chu et al., 2020a; Kireeva et al., 2004)**. Moreover, the progressive macroscopic straightening of chromosomes from G2 to metaphase is consistent with the proposed function of condensin II as shortening the axis **(Shintomi and Hirano, 2011)** and to its presence on chromosomes at the very start of mitosis. During this resolution of sister chromatids in late prophase, links between sister chromatids (bridges) remain and retain cohesin **(Chu et al., 2020a)** but are removed during anaphase **(Chu et al., 2022)**, after the conserved cohesin tethers at centromeres.

After NEBD, chromosomes progress through prometaphase to metaphase. Chromosomes appear straightened and take on a rod shape (although they show some flexibility, as pictures of chromosomes aggregating in metaphase plates suggest). They are thicker and shorter, and they tend to become more so as metaphase progresses **(Gibcus et al., 2018)**. In metaphase chromosomes, condensin I has gained access to the DNA and drives lateral compaction of the chromosome **(Shintomi and Hirano, 2011)** and its proper activity in chromosome morphology likely relies on the presence of a pre-existing condensin II axis **(Shintomi et al., 2017)**.

The exact shape of the mitotic chromosome is still under investigation. The main model argues that chromatin loops emanate radially in a helical manner from the internal axis of metaphase chromosome **(Gibcus et al., 2018)**. In this landmark study, modelling approaches combined with Hi-C data suggest that the best fit for mitotic chromosomes are loops with correlated orientations and that the appearance of a second diagonal band in metaphase Hi-C maps, suggesting a periodic structure, can be most parsimoniously explained by a helical structure. The helical structure of mitotic chromosomes is an old model **(de la Tour and Laemmli, 1988)** and is consistent with optical sectioning data. However this data was obtained from extracted chromosomes in metaphase, and does not necessarily accurately reflect the picture of mitotic chromosomes in vivo **(Kireeva et al., 2004)**. This helical organization has in fact been brought into question by another group with the following arguments

(Chu et al., 2020a): a/ the centroid of axis components (here topo II) does not follow a helix but a planar path (with bends) b/ Z stacking of chromosomes is not consistent with the shape of a helix c/ helical coiling of chromatin would generate mechanical constraints on the sister chromatid. Other

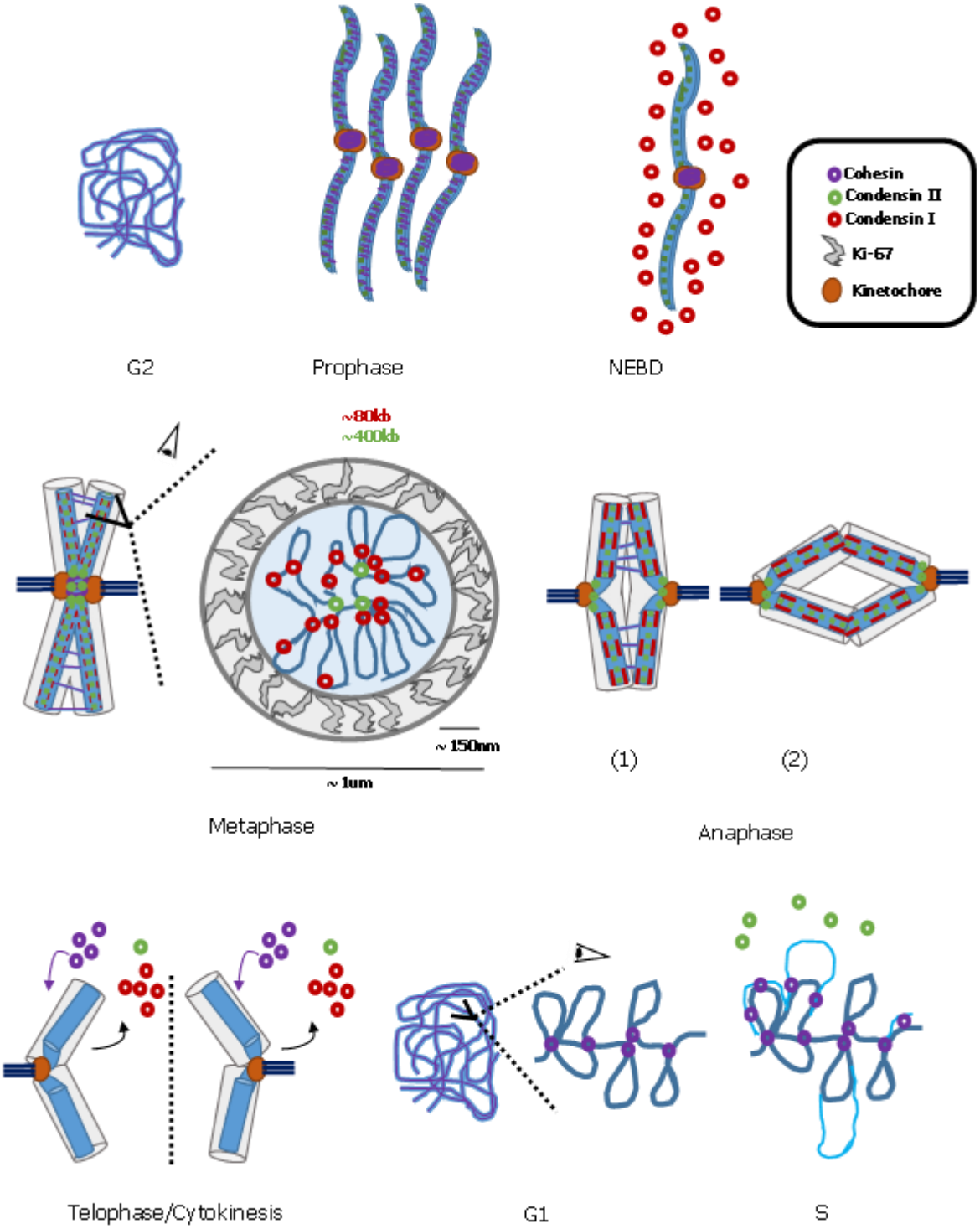

Fig. I13 Scheme of SMC-driven organization of a vertebrate chromosome during the cell cycle of an actively dividing cell.
See text for details.

studies after Gibcus and colleagues have provided experimental evidence consistent with a helical

scaffold in vertebrate cells **(Kubalová et al., 2023; Phengchat et al., 2019).** 3D-SIM of fixed chromosomes also suggest a double stranded helix per chromatid **(Poonperm et al., 2015)**. Perhaps these apparent contradictions underscore a difference in organization between early mitotic chromosomes and metaphase chromosomes.

4.6 Topoisomerase II is a required complementary activity of condensin

Historically the cut phenotype which described the function of condensin SMC proteins was identified earlier as a phenotype of topoisomerase II (topo II) deficiency **(Uemura and Yanagida, 1984)**.

Topo II is found in the vicinity of condensin, on the mitotic chromosome **(Cuvier and Hirano, 2003; Maeshima and Laemmli, 2003; Nielsen et al., 2020; Shintomi and Hirano, 2021)** although whether it has a scaffolding role has been the source of conflicting observations **(Hirano and Mitchison, 1993; Nielsen et al., 2020)**. What is clear is that topo II on mitotic chromosomes is resistant to 600 mM NaCl when chromosomes have undergone replication beforehand but detach from mitotic chromosomes otherwise **(Cuvier and Hirano, 2003).**

Despite this context-dependent association, topo II is absolutely required for the condensation of mitotic chromosomes even when it is not resistant to salt **(Cuvier and Hirano, 2003; Shintomi et al., 2015; Shintomi and Hirano, 2021)**. Topo II participates in both individualization of mitotic chromosomes and their thickening, with the step required to generate thickening requires on intra-chromatid contacts established in a manner dependent on the C-terminal domain of Topo II, which maintains its association to chromatin **(Shintomi and Hirano, 2021)**. Importantly, topo II has been shown to interplay with condensin function. Topo II stimulates the positive supercoiling activity of condensin **(Kimura et al., 1999)** and promotes the proper positioning of condensin **(Morao et al., 2022),** while condensin drives the activity of topo II towards decatenation **(Baxter et al., 2011; Charbin et al., 2014; Piskadlo et al., 2017)**.

This interplay provides a potential pathway for the importance of resolving entanglements between sister chromatids prior to anaphase onset, as decatenation via topo II would resolve these entanglements and prevent the formation of chromatin bridges.

Cohesin has recently been shown to resolve entanglements of sister chromatids in G2 **(Batty et al., 2023)**, underlining the possibility that topo II activity may also be important for decatenation in a manner that relies on cohesin activity (at least just after S phase). Nonetheless, as chromosomes progress through mitosis, sister chromatids split during prophase in a manner that depends on topo II activity **(Chu et al., 2020b)** and condensin II **(Nagasaka et al., 2016)**. Then, the final step of sister chromatid separation relies on topo II activity as adjunction of ICRF193 during anaphase prevents its completion **(Chu et al., 2022)** although we argue that the final step, being telomere resolution **(Chu et al., 2022)** is actually independent of topo II (see Part 5).

4.7 Condensin localization

While microscopy suggests condensin bounds across the axis of chromosomes in vertebrates, ChIP-seq studies have systematically found among eukaryotes that condensin is enriched at highly expressed genes in C.elegans **(Kranz et al., 2013)** fission yeast and human **(Sutani et al., 2015)**, budding yeast (D'Ambrosio et al., 2008), chicken **(Kim et al., 2013)** and potentially many others. In vertebrates this enrichment is found at the 5' end of genes, specifically at promoters **(Kim et al., 2013; Sutani et al., 2015; Yuen et al., 2017)** while in fission yeast whose transcription is not downregulated this enrichment is significant at the 3' end of transcribed genes **(Sutani et al., 2015)**. Additional factors have been shown to position condensin in cis at the rDNA **(Nakazawa et al., 2008)** and at the centromere **(Nakazawa et al., 2008; Tada et al., 2011)**. Several examples of transcription factors such as TFIIIC (D'Ambrosio et al., 2008; Yuen et al., 2017) or fission yeast-specific transcription factors (Kim et al., 2016) appear to position condensin. The hosting lab also showed that chromatin remodelers acting at the promoter were important for condensin association genome-wide and for condensation **(Toselli-Mollereau et al., 2016)**.

Despite peaks visible by ChIP-seq, there is no obvious bias for the establishment of long-range contacts from these loci in chicken **(Gibcus et al., 2018)** or a very mild one in fission yeast **(Kakui et al., 2017)**, bringing into question the biological significance of this peak, which we discuss in Part 6.

4.8 The chromatin of mitotic chromosomes

As cells enter mitosis, multiple alterations to chromatin can be reported.

Transcription

In vertebrates transcription in mitosis is downregulated **(Palozola et al., 2017)** even on viral DNA that has infected a cell **(Spencer et al., 2000)** and this downregulation is likely established at least in part by Cdk1 **(Gebara et al., 1997; Leresche et al., 1996)**. Low levels of transcription can be observed however, and even some subset of genes are reported to be maintained/upregulated in M **(Palozola et al., 2017)**. Specific transcription at the kinetochore in mitosis can be observed, and this transcriptional activity appears to have a role in preventing lagging chromosomes in anaphase **(Chan et al., 2012)**. Specific phosphorylation of threonine 4 of the RNAPII CTD is potentially mediated by Polo-like kinase 1 for localization of RNAPII at the centromere and for proper progression through mitosis **(Hintermair et al., 2016)**. Interestingly, only a minority of genes appear regulated in fission yeast mitosis, and no obvious strong decrease of transcription is reported **(Rustici et al., 2004)**.

While accumulating evidence suggests that RNA polymerase transcription drives the positioning of cohesin, evidence exists as well for condensin although this is less of a trend in the field **(D'Ambrosio et al., 2008; Johzuka and Horiuchi, 2007; Rivosecchi et al., 2021; Sutani et al., 2015)**.

Change in chromatin remodeler binding

In early mitosis, nucleolar chromatin factors as well as components of the nuclear membrane are depleted from chromatin, before NEBD **(Samejima et al., 2022)**. As cells progress into mitosis, metaphase chromosomes observe a reduction of the association of chromatin remodelers in large part **(Funabiki et al., 2017)**, as early as prometaphase **(Samejima et al., 2022)**. Whether these components are fully removed is not clear. For instance, chromatin bound ISWI is reduced to ~25% of interphase levels in metaphase chromosomes in replicating xenopus egg extracts **(MacCallum et al., 2002)** while some components like the FACT histone chaperone **(Jenness et al., 2018)** and specific SWI/SNF subunits **(Zhu et al., 2023)**.

Phosphorylation of chromatin

Threonine 3 of core histone H3 appears as an important amino acid phosphorylated upon mitotic entry by Haspin, one of the targets of the Cdk1-cyclin, in a Polo-like kinase 1 dependent manner **(Zhou et al., 2014)**. This mitotic phosphorylation is important to enable the binding of the Aurora B/Chromosomal Passenger Complex (CPC) at centromeres **(Wang et al., 2010)**. H3 appears to be a substrate for mitotic cascades of phosphorylation via H3T3 which supports the assembly of the CPC and activation of Aurora B to form the spindle **(Kelly et al., 2010; Zierhut et al., 2014)**. Moreover, dephosphorylation of H3T3ph and removal of the CPC appear required to decondense chromosomes **(Kelly et al., 2010)**. In that context, H3T3ph seems to play a signaling role. Another histone phosphorylation which occurs in mitosis is phosphorylation of serine 10 of core histone H3 (H3S10ph). In interphase, this modification is present at promoters of more highly expressed genes and also regions of early replication timing **(Chen et al., 2018)** but waves of phosphorylation of Serine 10 of core histone H3 seem to occur in early mitosis **(Van Hooser et al., 1998)** by an Aurora B dependent mechanism, potentially downstream of H3T3ph. In budding yeast it was proposed that H3S10ph promotes compaction by recruiting a histone deacetylase **(Wilkins et al., 2014)** although this histone modification seems not required for the proper transmission of mitotic chromosomes to daughter cells as H3S10A show little phenotype **(Hsu et al., 2000)**, although this same mutation causes defects in chromosome segregation in mitosis of Tetrahymena micronuclei **(Wei et al., 1999)**,

HP1 is also a target of phosphorylation during mitosis **(Nishibuchi et al., 2019)** and is removed from mitotic chromatin concomitantly by Aurora B-dependent H3S10ph **(Fischle et al., 2005; Hirota et al., 2005)**. Despite this, a subset of HP1α is retained on mitotic chromosomes at centromeres **(Serrano et al., 2009)**. HP1α provides mechanical stiffness to chromosomes and its depletion leads to defects in chromosome segregation **(Strom et al., 2021)**. This has been argued to be independent of histone methylation which can also bring stiffness to mitotic chromosomes **(Biggs et al., 2019; Strom et al., 2021)**.

Compaction and chromatin structure

Inhibiting deacetylation in mitosis does reduce the compaction of chromosomes **(Cimini et al., 2003; Schneider et al., 2022)** and a deacetylase mutant *hst2Δ* in budding yeast seems to reduce compaction **(Kruitwagen et al., 2015)**. Defects in anaphase seem relatively mild, with low number of lagging chromosomes induced by TSA treatment **(Cimini et al., 2003; Schneider et al., 2022)**. Hence decompaction by favoring increased acetylation does not seem to impair significantly chromosomes segregation. Vertebrate mitotic chromatin is capable of greater compaction than interphase **(Zhiteneva et al., 2017)**, but the exact importance of compaction during mitosis is not clear. No obvious difference at the average nucleosome scale are observed between interphase and metaphase chromatin – except for a stable binding of linker histone H1.8 at the dyad in Xenopus **(Arimura et al., 2021)**, contact domains from interphase are still observed in mitosis **(Nozaki et al., 2017)** and remarkably the accessibility of chromatin from interphase to mitosis remains largely unchanged in vertebrates **(Djeghloul et al., 2020; Hsiung et al., 2015)**, although one can note enhancers lose accessibility in M **(Hsiung et al., 2015)** and do not form contacts with promoters **(Hsiung et al., 2016)**, although promoters remain accessible **(Hsiung et al., 2015)**. Hence compaction is driven in mitosis by an activity acting at a mesoscale level, consistent with internucleosomal interactions disfavored by acetylation.

4.9 Key problems in the condensin field and biological question of the PhD thesis

Since the characterization of condensin by Tatsuya Hirano **(Hirano et al., 1997)**, key information was obtained on the complex, namely :

- Its role during mitosis in eukaryotes, particularly in condensing and segregating sister chromatids.
- Its organization within the scaffold and how it is found at the base of loops.
- Its loop extruding activity shown *in vitro.*
- Recent evidence for condensin-condensin interactions.
- The molecular structure of the condensin holocomplex, with key features identified dependent on the presence of ATP and DNA.

In the field currently, several key questions remain, notably :

- A deeper understanding of the link between the cell cycle and the condensin complex, beyond simply our canonical knowledge on phosphorylation ; and their function.
- The full description of the architectural changes of condensin in the presence of DNA during an ATP hydrolysis cycle, i.e how is the DNA manipulated to form a loop ?
- Further characterization of key condensin partners and their mechanistic interplays, specifically topoisomerase II and to a lesser extent the vertebrate specific Kif4A and how they impact condensin function.
- Disentangling and elucidating specific activities of the condensin complex, namely a/ what is the relative contribution of loop extrusion and diffusion capture b/ can condensin topologically entrap DNA in the S-K ring akin to cohesin c/ can so-far poorly explained molecular activities of condensin such as supercoiling or the reannealing activity be pertinent *in vivo* ?
- Addressing comprehensively the role of condensin outside of M, as suggested by reports on condensin loss of function phenotypes in G2 **(Kakui et al., 2020)** in S phase **(Aono et al., 2002)** and in post-mitotic neurons **(Hassan et al., 2020)**.

The last problem (at least, in this list which I formulate from my own knowledge of the field), which has formed the basis of my 4-year PhD and the key question of the hosting lab relates to the integrated functioning of condensin within the nucleus. Specifically, how can condensins (and SMC complexes) perform their function in a crowded environment, with a chromatin substrate assembled into nucleosomal fibers which can be remodeled by various activities and other processive enzymes ? Does condensin simply ignore this parameter and assembles chromosomes with no impact from the nucleosomal fiber **(Fig. I14)** ? Are processive activities such as RNA polymerases an obstacle for eukaryotic condensin ? Is condensin loaded at specific loci modulated by chromatin structure on chromosomes ? And can we glean information regarding the molecular mechanism by which condensin assembles mitotic chromosomes from these questions ?

Single cell Hi-C show that TADs form independently of the presence of cohesin **(Bintu et al., 2018)**, suggesting that some other chromatin associated function forms these domains, but cohesin drives a bias in the position of TAD formation which can explain why TADs disappear in population averages

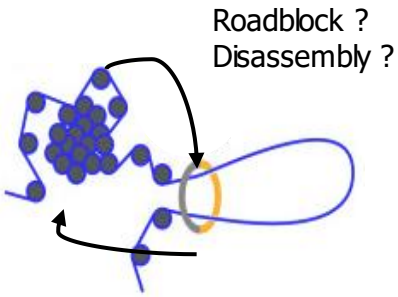

Fig. I14 Interplay between chromatin and loop extrusion
Taken from Higashi et al. 2022

(Bintu et al., 2018; Rao et al., 2017b). Consistent with this observation, 200-300nm contact domain topology is reported to be independent of cohesin SMC **(Miron et al., 2020)** however in another report cohesin depletion had comparable effects to TSA treatment on decondensation of these domains **(Nozaki et al., 2017)**. Chromatin movement (i.e the diffusive motion of nucleosomes) is restrained by condensin in interphase and mitosis of fission yeast **(Kakui et al., 2020, 2017)** and cohesin also restricts chromatin motion in interpase **(Bailey et al., 2023)**. The general effect of cohesin on chromatin remains unclear, although we do know that cohesin negatively impacts the steady-state level of heterochromatin. Enhancing cohesin stability by Wapl depletion disfavors the formation of heterochromatin-rich B compartments and clearly impairs large-scale H3K9me3 domain levels **(Haarhuis et al., 2022)** consistent with reports suggesting cohesin degradation enhances compartmentalization **(Liu and Dekker, 2022; Rao et al., 2017b)**. Similarly, condensin II loss during mitosis leads to increased centromere and heterochromatin domains clustering seen by microscopy in the following G1 **(Hoencamp et al., 2021)**, or clustering in drosophila **(Bauer et al., 2012)** suggesting cohesin and condensin II may play a role in heterochromatin physiology.

Conversely, is the packaging of DNA into nucleosomes a process which facilitates SMC activity ? Or is it antagonistic and are there activities that facilitate SMC function in vivo ?

One convincing example of the impact of chromatin on SMC function is the impact of transcription on the translocation of SMC complexes. Highly transcribed genes negatively impact translocation of bacterial SMC in B. subtilis **(Brandão et al., 2019; Wang et al., 2017)**. Strikingly, similar results can be observed for cohesin in yeast **(Jeppsson et al., 2022b)** and in mammals when CTCF and Wapl are removed (Banigan et al., 2023; Busslinger et al., 2017)**.** These data demonstrate that processive, chromatin bound activities can antagonize genome folding by SMC complexes. Whether

this is also the case for condensin when transcription is known to be downregulated in vertebrate mitosis **(Palozola et al., 2017)** is not entirely clear.

Regarding the nucleosomal template itself, an early report suggested that histones acted as receptors of condensin **(Tada et al., 2011)** although this appeared contradictory with the existing literature. Evidence suggests that binding of DNA to nucleosomes is disfavored **(Kong et al., 2020; Piazza et al., 2014)** and sterically the anchor site for loop extrusion cannot accommodate a nucleosome **(Kschonsak et al., 2017)**. However, evidence suggested that the proper activity of nucleosomes and condensin II was required for the function of condensin I **(Shintomi et al., 2017)**. Evidence from the hosting lab and others have also implicated chromatin remodelers setting up NDR at promoters as important for condensin **(Toselli-Mollereau et al., 2016)** and cohesin **(Huang et al., 2004; Muñoz et al., 2019)** association to chromosomes. Notably, recovery of loop formation after cohesin depletion also appears faster at regions with active histone marks, notably H4K16ac, and slower at repressive marks (Rao et al., 2017b).

Each Results section addresses a scientific paper regarding the impact of the chromatin environment (telomeres, transcription, FACT) on condensin function with a very brief introduction acting as a reminder to the biological question.

RESULTS

Contributions for each study

While I present three different studies in this PhD thesis my contribution has not covered the entirety of the experiments and analyses. I would like to thank all contributors and underscore that while I have contributed to these three studies I am co-first author on all of them. In other words, this was only possible thanks to collaborations within my hosting lab and with others, and with the major contributions of t.he other first and secondary authors. Below is a quick summary of the contribution for the data

° I have done both data collection and analysis.

* I have only collected the data.

I have only analyzed the data.

~ I have not contributed significantly to this figure.

Part 7 – TELOMITO PROJECT

The cytological experiments with telomere foci were done by the Tournier lab, and some NGS data sets were generated by Esther Toselli.

Fig. 1 A-B ~ C # D # E Fig. S1 A-B ~ C # D # E#

Fig. 2 ~ Fig. S2 ~

Fig. 3 A-D° E* Fig. S3 A-D° E*

Fig. 4° Fig. S4°

Fig. 5~ Fig. S5°

Fig. 6 A~ B° Fig. S6~

Part 6 - DHP1-RPB1 PROJECT

For this project all genomic and cytological data on Rpb1 was collected by me and on Dhp1 by Jeremy Lebreton and we analyzed the data together.

For other experiments/analysis specifically done by Jeremy :

Fig. 2 ~ Fig. S2 ~ Fig. 4 A-C~ S4 ~ Fig. 5 ~

Part 7 – FACT PROJECT

The raw data I have not generated myself was generated by Esther Toselli.

Fig. 1 A~ B-C°

Fig. 2 ° S2 °

Fig. 3A ° B# C° S3 ~ B-C°

Fig. 4°

FIg. 5 A-B# C-D° Fig. S5 A-C~ D-F°

Fig. 6° S6°

Fig. 7° S7°

Fig. 8°

FIg. 9#

DISCUSSION

Fig D1-3 ° Fig D4#

PART 5 – TELOMITO PROJECT. Colin et al., 2023

This project was done in collaboration with people from the CBI Toulouse which I warmly thank. The Tournier lab in particular performed all the microscopy experiments which are key for the functional aspect of the project. I also would like to thank Laure Cuby who helped me with this telomere project at the start when I mentored her for her undergraduate internship. Concerning Part 5, the people at the CBI Toulouse in the **Cuvier lab** who provided data analysis on the Hi-C, the **Tournier lab** for the key microscopy data and the **Coulon lab** in Marseille for expertise on telomere blots.

5.1 Telomere disjunction in anaphase

Sister chromatids that are segregated in mitosis are held together at the centromere by cohesin **(Tanaka et al., 2000)** and at chromosome arms along thin bridges **(Chu et al., 2022, 2020a)**. As cells are being segregated, the centromeres separate first, then the chromosome arms and finally at the end the edges of sister chromatids, the telomeres, are separated last **(Chu et al., 2022)**. This final linkage between telomeres in wild-type cells is resolved during anaphase B.

Whether the segregation of telomeres is 1/ an active process requiring a specialized mechanism 2/ an active process, but requiring the same known factors promoting segregation of chromosome arms such as topo II and condensin or 3/ a passive mechanism resolving entanglements by being the physical end of the chromosome and benefitting from chromosome arm separation is not clear.

The linkages between sister telomeres appear to remain for a few minutes during anaphase, hinting at slow disassembly **(Chu et al., 2022)**. These linkages between telomeres are also observed in anaphases of telocentric pig cells, suggesting proximity to centromeres does not facilitate separation which is inconsistent with hypothesis 3/ **(Chu et al., 2022)**. Additionally, accumulating evidence suggests that in mammals the poly-ADP-ribosyl transferase Tankyrase 1 TNKS1 is required for sister telomere separation **(Canudas et al., 2007; Dynek and Smith, 2004)**, implicating the cohesin variant subunit STAG1 **(Canudas et al., 2007)**, while in fission yeast condensin function appears important to disjoin sister telomeres in anaphase **(Reyes et al., 2015)**. It is not clear whether in this system, the function of condensin acts *in cis* or promotes a separation of sister arms amenable to telomere segregation.

Telomeres are the physical extremity of chromosome in cells. As such, they are subject to specific constraints leading to evolutionary adaptations which are outside of the scope of this thesis. In brief, the two classically described constraints are that 1/ telomeres must not be recognized as a site of DNA damage such as a break in a DNA duplex 2/ telomere structure must also be maintained during replication, which can lead to a shortening of their sequence if not maintained by specific mechanisms. These two constraints have likely led during evolution to the emergence of specialized chromatin composition at telomeres, relying on the conserved shelterin complex.

Scheme of the telomere-associated Shelterin complex in eukaryotes. Taken from De Lange et al., 2018

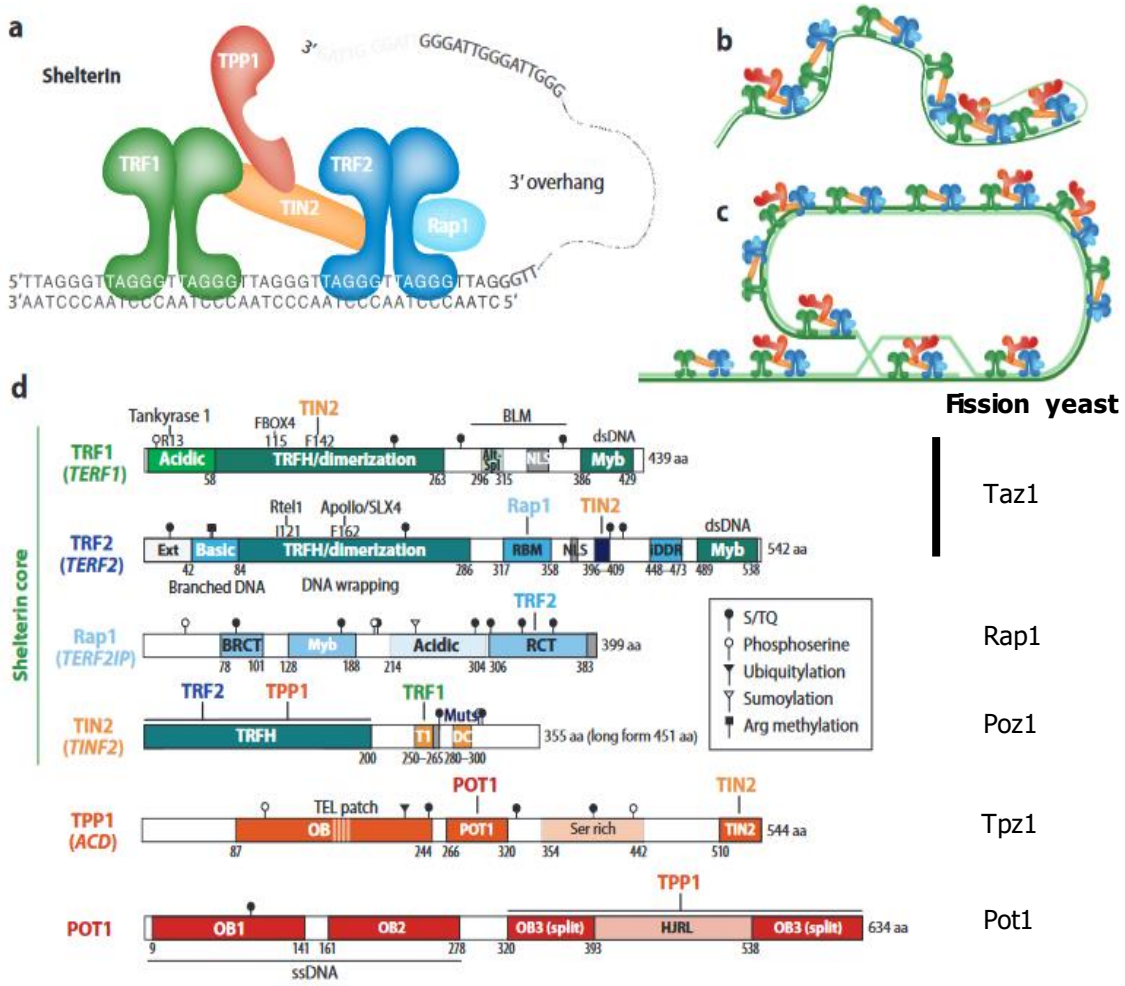

In the following paper we provide evidence that telomere segregation relies on a Topo II independent mechanism and that shelterin complex components position condensin at telomeres and are important for its function in telomere disjunction, arguing for a mechanism *in cis* involving condensin.

5.2 Condensin positioning at telomeres by Taz1 promotes telomere disjunction in anaphase Colin et al., 2023. https://doi.org/10.7554/eLife.89812.1

bioRxiv preprint doi: https://doi.org/10.1101/2022.03.18.484892; this version posted September 11, 2023. The copyright holder for this preprint (which was not certified by peer review) is the author/funder, who has granted bioRxiv a license to display the preprint in perpetuity. It is made available under aCC-BY-NC-ND 4.0 International license.

Condensin positioning at telomeres by shelterin proteins drives sister-telomere disjunction in anaphase

Léonard Colin [2, 3 †], Céline Reyes[1†], Julien Berthezene[1], Laetitia Maestroni [4], Laurent Modolo [2,3], Esther Toselli [2,3], Nicolas Chanard [1,5], Stephane Schaak[1,5], Olivier Cuvier [1,5], Yannick Gachet [1*], Stéphane Coulon* [4], Pascal Bernard [2, 3*], Sylvie Tournier [1*]

[1] MCD, Centre de Biologie Intégrative, Université de Toulouse, CNRS, UPS, 31062 Toulouse Cedex, France.
[2] CNRS - Laboratory of Biology and Modelling of the Cell, UMR 5239, Lyon, France.
[3] ENS de Lyon, Univ. Lyon, 46 allée d'Italie, site Jacques Monod, F-69007, Lyon, France.
[4] CNRS, INSERM, Aix Marseille Univ, Institut Paoli-Calmettes, CRCM, Equipe labellisée par la Ligue Nationale contre le Cancer, Marseille, F-13009, France.
[5] CBI, MCD-UMR5077, CNRS, Chromatin dynamics team, 31062, Toulouse.

* Co-corresponding authors: Sylvie Tournier sylvie.tournier-gachet@univ-tlse3.fr , Pascal Bernard pascal.bernard@ens-lyon.fr , Stéphane Coulon stephane.coulon@inserm.fr and Yannick Gachet yannick.gachet@univ-tlse3.fr

[†] These authors participate equally to this work.

ABSTRACT

The localization of condensin along chromosomes is crucial for their accurate segregation in anaphase. Condensin is enriched at telomeres but how and for what purpose had remained elusive. Here we show that fission yeast condensin accumulates at telomere repeats through the balancing acts of Taz1, a core component of the shelterin complex that ensures telomeric functions, and Mit1, a nucleosome-remodeler associated with shelterin. We further show that condensin takes part in sister-telomere separation in anaphase, and that this event can be uncoupled from the prior separation of chromosome arms, implying a telomere-specific separation mechanism. Consistent with a cis-acting process, increasing or decreasing condensin occupancy specifically at telomeres modifies accordingly the efficiency of their separation in anaphase. Genetic evidence suggests that condensin promotes sister-telomere separation by counteracting cohesin. Thus, our results reveal a shelterin-based mechanism that enriches condensin at telomeres to drive in cis their separation during mitosis.

bioRxiv preprint doi: https://doi.org/10.1101/2022.03.18.484892; this version posted September 11, 2023. The copyright holder for this preprint (which was not certified by peer review) is the author/funder, who has granted bioRxiv a license to display the preprint in perpetuity. It is made available under aCC-BY-NC-ND 4.0 International license.

INTRODUCTION

In eukaryotes, mitotic entry is marked by the profound reorganization of chromatin into mitotic chromosomes driven by the condensin complex (Hirano, 2016). It is acknowledged that this process, namely mitotic chromosome assembly or condensation, is an absolute pre-requisite for the accurate transmission of the genome to daughter cells, but our understanding of the mechanisms by which condensin associates with chromatin, shapes mitotic chromosomes and contributes to their accurate segregation in anaphase remains incomplete.

Condensin is a ring-shaped ATPase complex that belongs to the Structural Maintenance of Chromosomes (SMC) family of genome organizers, which also includes the cohesin complex involved in chromatin folding during interphase and in sister-chromatid cohesion (Hirano, 2016; Davidson & Peters, 2021). Condensin is composed of a core ATPase heterodimer, made of the SMC2 and SMC4 proteins, associated with a kleisin and two HEAT-repeat subunits. Most multicellular eukaryotes possess two condensin variants, named condensin I and II, made of a same SMC2/4 core but associated with distinct sets of non-SMC subunits (Ono *et al*, 2003; Hirano, 2012). Budding and fission yeasts, in contrast, possess a single condensin complex, similar to condensin I. Thereafter, condensin complexes will be collectively referred to as condensin, unless otherwise stated. There is robust evidence that condensin shapes mitotic chromosomes by massively binding to DNA upon mitotic entry and by folding chromatin into arrays of loops (Gibcus *et al*, 2018; Kakui *et al*, 2017). Thereby, condensin conceivably reduces the length of chromosomes, confers to chromosome arms the stiffness to withstand the spindle traction forces (Sun *et al*, 2018), and promotes the removal of catenations between chromosomes and sister-chromatids by orientating the activity of Topoisomerase II (Topo-II) towards decatenation (Baxter *et al*, 2011; Charbin *et al*, 2014). Hence, when condensin is impaired, sister-centromeres often reach the opposite poles of the mitotic spindle in anaphase but chromosome arms fail to separate, forming stereotypical chromatin bridges. *In vitro* studies have shown that condensin anchors itself on naked DNA through sequence-independent electrostatic interactions and uses the energy of ATP hydrolysis to extrude adjacent DNA segments into a loop of increasing size (Kschonsak *et al*, 2017; Ganji *et al*, 2018; Kong *et al*, 2020). Although such a loop extrusion reaction convincingly explains the structural properties of mitotic chromosomes (Nasmyth, 2017; Davidson & Peters, 2021), we still ignore whether and how it could take place in the context of a chromatinized genome, crowded with potential hindrances.

bioRxiv preprint doi: https://doi.org/10.1101/2022.03.18.484892; this version posted September 11, 2023. The copyright holder for this preprint (which was not certified by peer review) is the author/funder, who has granted bioRxiv a license to display the preprint in perpetuity. It is made available under aCC-BY-NC-ND 4.0 International license.

There is robust evidence that chromatin micro-environments impinge upon the localization of condensin. ChIP-seq studies performed on species ranging from yeasts to mammals have revealed a conserved condensin pattern along the genome, constituted of a broad and basal distribution punctuated by peaks of high occupancy at centromeres, rDNA repeats and in the vicinity of highly expressed genes (D'Ambrosio *et al*, 2008; Kim *et al*, 2013; Kranz *et al*, 2013; Dowen *et al*, 2013; Sutani *et al*, 2015). Various factors such as the chromokinesin Kif4 (Samejima *et al*, 2012), the zinc-finger protein AKAP95 (Steen *et al*, 2000), transcription-factors and chromatin remodelers (for review see (Robellet *et al*, 2017) have been involved in the binding of condensin to chromatin in yeasts or vertebrate cells. Additional cis-acting factors that increase condensin's local concentration at centromeres and/or at rDNA repeats have been identified in budding or fission yeast (Tada *et al*, 2011; Johzuka & Horiuchi, 2009; Verzijlbergen *et al*, 2014). Such enrichments are likely to play a positive role since there is clear evidence that condensin contributes to the stiffness of centromeric chromatin and to the bilateral attachment of centromeres in early mitosis (Ono *et al*, 2004; Gerlich *et al*, 2006; Nakazawa *et al*, 2008; Ribeiro *et al*, 2009; Verzijlbergen *et al*, 2014; Piskadlo *et al*, 2017). Likewise, the segregation of the rDNA is acutely sensitive to condensin activity (Freeman *et al*, 2000; Nakazawa *et al*, 2008; Samoshkin *et al*, 2012). Highly expressed genes, in contrast, are thought to constitute a permeable barrier where active condensin complexes stall upon encounters with DNA-bound factors such as RNA polymerases (Brandão *et al*, 2019; Rivosecchi *et al*, 2021). Consistent with a local hindrance, in fission yeast, attenuating transcription that persists during mitosis improves chromosome segregation when condensin is impaired (Sutani *et al*, 2015). Further evidence in budding yeast indicates that dense arrays of protein tightly bound to DNA can constitute a barrier for DNA-translocating condensin (Guérin *et al*, 2019). Thus, depending on the context, condensin enrichment can reflect either positive or negative interplays.

Microscopy studies have clearly shown that condensin I is enriched at telomeres during mitosis and meiosis in mammalian cells (Walther *et al*, 2018; Viera *et al*, 2007), and ChIP-seq has further revealed that condensin I accumulates at telomere repeats in chicken DT40 cells, but the mechanisms underlying such enrichment as well as its functional significance have remained unknown. We and others previously showed that the separation of sister-telomeres in anaphase involves condensin regulators such as Cdc14 phosphatase in budding yeast (Clemente-Blanco *et al*, 2011), and Aurora-B kinase in fission yeast (Reyes *et al*, 2015; Berthezene *et al*, 2020), but

bioRxiv preprint doi: https://doi.org/10.1101/2022.03.18.484892; this version posted September 11, 2023. The copyright holder for this preprint (which was not certified by peer review) is the author/funder, who has granted bioRxiv a license to display the preprint in perpetuity. It is made available under aCC-BY-NC-ND 4.0 International license.

whether and how condensin could play a role has remained unclear.

In the present study, we sought to determine how and why condensin is enriched at telomeres by using the fission yeast *Schizosaccharomyces pombe* as a model system. Telomeres contain G-rich repetitive sequences that are protected by a conserved protein complex called Shelterin (de Lange, 2018; Lim & Cech, 2021), which is composed, in fission yeast, of Taz1 (a myb-domain DNA-binding protein homologous to human TRF1 and TRF2), Rap1, Poz1 (a possible analog of TIN2), Tpz1 (an ortholog of TPP1), Pot1, and Ccq1. Whilst Taz1 binds to double-stranded G-rich telomeric repeats, Pot1 binds to 3′ single-stranded overhang. Rap1, Poz1, and Tpz1 act as a molecular bridge connecting Taz1 and Pot1 through protein–protein interactions. Ccq1 contributes to the recruitment of the nucleosome remodeler Mit1 and of telomerase (for review on fission yeast shelterin see Moser & Nakamura, 2009; Dehé & Cooper, 2010). We found that Taz1 plays the role of a cis-acting enrichment factor for condensin at telomeres, whilst Mit1 antagonized condensin's accumulation. Thus, telomeres are a remarkable chromosomal environment where condensin is enriched by a shelterin-dependent cis-acting mechanism. Our results further indicate that the level of condensin at telomeres, set up by Taz1 and Mit1, is instrumental for their proper disjunction during anaphase, hence associating a key biological function to this local enrichment. Based on these data, we propose that condensin is enriched at telomeres *via* interplays with shelterin proteins to drive sister telomere separation in anaphase.

RESULTS

Fission yeast condensin is enriched at telomeric repeats during metaphase and anaphase

Fission yeast condensin, like vertebrate condensin I, is largely cytoplasmic during interphase and binds genomic DNA during mitosis (Sutani *et al*, 1999). At this stage, it shows high level of occupancy at centromeres, at rDNA repeats and in the vicinity of highly transcribed genes (Sutani *et al*, 2015; Nakazawa *et al*, 2015). However, unlike vertebrate condensin I (Kim *et al*, 2013; Walther *et al*, 2018), whether fission yeast condensin is present at telomeres had not been reported. To assess this, we performed chromatin immunoprecipitation of the kleisin subunit Cnd2 tagged with GFP (Cnd2-GFP) and analyzed the co-immunoprecipitated DNA by quantitative real time PCR (ChIP-qPCR). Figure 1A provides a reference map for the right telomere of chromosome 2 (TEL2R). *cnd2-GFP cdc2-as* shokat mutant cells were blocked at the G2/M transition and released into a synchronous mitosis. Cnd2-GFP was hardly detectable at TEL2R and along chromosome

bioRxiv preprint doi: https://doi.org/10.1101/2022.03.18.484892; this version posted September 11, 2023. The copyright holder for this preprint (which was not certified by peer review) is the author/funder, who has granted bioRxiv a license to display the preprint in perpetuity. It is made available under aCC-BY-NC-ND 4.0 International license.

arms during the G2 arrest (Fig. 1B, t = 0 min). However, during early mitosis, Cnd2-GFP was clearly bound to telomeric repeats (the tel0 site), and to a lesser extent at more distal sites within subtelomeric elements (Fig. 1B, t = 7 min post-release). Cnd2-GFP occupancy at tel0 was in the range of the highly expressed genes *cdc22* and *exg1* used as control for enrichment (Sutani *et al*, 2015). Cnd2-GFP level further increased in anaphase (15 min post-release from the G2 block), consistent with the maximum folding of fission yeast chromosomes achieved in anaphase (Petrova *et al*, 2013) and reminiscent of the second wave of condensin binding observed during anaphase in human cells (Walther *et al*, 2018). These data show that the kleisin subunit of condensin is enriched at TEL2R during mitosis in fission yeast cells.

In order to thoroughly describe condensin's localization at telomeres, we generated calibrated ChIP-sequencing (ChIP-seq) maps of Cnd2-GFP from metaphase-arrested cells (Fig. 1 C-D). Since the current version of the fission yeast genome lacks telomere-proximal DNA and telomeric repeats, we generated a version comprising a full-length TEL2R sequence according to the described sub-telomeric and telomeric sequences (Sugawara, 1988), (Fig. S1A). Then, we measured the binding of Cnd2-GFP by calculating, at each base, the ratio of calibrated read-counts between the IP and Total (Input) fractions (Fig. S1B and Materials and Methods). As shown for centromere outer-repeats and rDNA repeats (Fig. S1C), this method allows for a better quantification of occupancy at repeated DNA sequences by correcting for biases in coverage in the Total fraction. We found Cnd2-GFP clearly enriched at telomere repeats of TEL2R in metaphase arrested cells (Fig. 1C). Cnd2-GFP binding declined rapidly over the proximal STE1 element and remained at a basal level throughout more distal elements such as STE2, STE3 and the heterochromatic *thl2* gene (Fig. 1C and Fig. S1D). To ascertain that such enrichment at telomeric repeats reflected the binding of the condensin holocomplex, we used the thermosensitive *cut14-208* and *cut3-477* mutations in the Cut14^{SMC2} and Cut3^{SMC4} ATPase subunits of condensin (Saka *et al*, 1994). Consistent with previous ChIP-qPCR data (Nakazawa *et al*, 2015), we found that the *cut14-208* mutation reduced the binding of Cnd2-GFP at centromeres (Fig. 1C), along chromosome arms (Fig. 1D), and at TEL2R (Fig. 1D and S1C). We observed similar genome-wide reduction in *cut3-477* cells, though of a smaller amplitude at TEL2R (Fig. S1E). Note that a reduction of the steady state level of Cnd2 is unlikely to explain such reductions in binding (Fig. 1E). Taken together, our data indicate that condensin accumulates at telomeric repeats during metaphase and anaphase in fission yeast.

bioRxiv preprint doi: https://doi.org/10.1101/2022.03.18.484892; this version posted September 11, 2023. The copyright holder for this preprint (which was not certified by peer review) is the author/funder, who has granted bioRxiv a license to display the preprint in perpetuity. It is made available under aCC-BY-NC-ND 4.0 International license.

Condensin is required for sister-telomere disjunction in anaphase

To investigate the function of condensin at telomeres, we inactivated condensin using the thermosensitive mutations *cut14-208* or *cut3-477*, in cells whose telomeres were fluorescently labelled with Taz1-GFP. Fission yeast has three chromosomes that adopt a Rabl configuration during interphase, with telomeres clustered into 1 to 3 foci at the nuclear periphery (Chikashige *et al*, 2009; Funabiki *et al*, 1993). We previously showed that telomeres dissociate in two steps during mitosis (Reyes *et al*, 2015). In wild-type cells, the number of Taz1-GFP foci increases from 1 to up to 6 as cells transit from prophase to metaphase, i.e. when the distance between the spindle pole bodies (SPBs) increased from 0 to 4 µm (Fig. 2A, middle panel). This reflects the declustering of telomeres. During anaphase, when the distance between SPBs increases above 4 µm, the appearance of more than 6 Taz1-GFP foci indicates sister-telomere separation, and 12 foci full sister-telomere disjunction (Fig. 2A, right panel). Strikingly, *cut14-208* cells shifted to 36°C almost never showed more than six telomeric dots in anaphase, despite their centromeres being segregated at the opposite poles of the mitotic spindle (Fig. 2A and 2B). Such severe telomere dissociation defect correlates with condensin loss of function as it was not observed at the permissive temperature (25°C) (Fig. S2A). Sister-telomere disjunction was also clearly impaired in *cut3-477* mutant cells, though at milder level (Fig. 2B). To confirm the role of condensin in sister-telomere disjunction, we simultaneously visualized the behavior of LacO repeats inserted in the vicinity of telomere 1L (Tel1-GFP) together with TetO repeats inserted within centromere 3L (imr3-tdTomato) and Gar1-CFP (nucleolus) during mitotic progression (Figure S2B). After anaphase onset, as judged by the separation of sister-centromeres 3L, control cells always displayed two sister telomeric 1L foci (n=43) while 82% of *cut14-208* mutant cells (n=51) grown at non-permissive temperature remained with a single telomeric foci confirming a striking defect in the disjunction of Tel1L.

Next, we wondered whether a change in telomere length could cause telomere disjunction defects as described previously (Miller & Cooper, 2003). We measured telomere length in various condensin mutant cells including *cut14-208* and *cut3-477* mutants. We only observed little variation of telomere length (Fig. 2C), unlikely to be responsible for the failure to disjoin sister-telomeres when condensin is impaired. An alternative and more likely possibility was that persistent entanglements left between chromosome arms upon condensin loss of function

bioRxiv preprint doi: https://doi.org/10.1101/2022.03.18.484892; this version posted September 11, 2023. The copyright holder for this preprint (which was not certified by peer review) is the author/funder, who has granted bioRxiv a license to display the preprint in perpetuity. It is made available under aCC-BY-NC-ND 4.0 International license.

prevented the transmission of traction forces from centromeres to telomeres in anaphase. To test this hypothesis, we assessed telomere disjunction in cold-sensitive *top2-250* mutant cells, whose Topo II decatenation activity becomes undetectable at 20°C (Uemura *et al*, 1987). As expected, *top2-250* cells cultured at the restrictive temperature exhibited frequent chromatin bridges during anaphase (Fig. 2D, compare *top2-250* at 19°C with *cut3-477* at 36°C), and lagging centromeres (Fig. S2B). Yet, and remarkably, telomere disjunction remained effective during anaphase at 19°C, even within chromatin bridges (Fig. 2D-E). The decatenation activity of Topo II and the full separation of chromosome arms are therefore largely dispensable for telomere disjunction. Thus, these results indicate (1) that the function of condensin in sister-telomere separation is mostly independent of Topo II decatenation activity, and (2) that the separation of chromosome arms is not a prerequisite for the disjunction of sister-telomeres. Condensin might therefore play a specific role at telomeres for their proper separation during anaphase.

Condensin takes part in the declustering of telomeres during early mitosis

To assess whether condensin might shape telomere organization prior to anaphase, we generated Hi-C maps of cells arrested in metaphase (Fig. 3A). As previously reported (Kakui *et al*, 2017), we observed frequent centromere-to-centromere and telomere-to-telomere contacts between the three chromosomes in wild-type cells (Fig. 3B). In the *cut14-208* condensin mutant at restrictive temperature, contact frequencies within chromosome arms were reduced in the range of 100 kb to 1 Mb (Fig. 3C-D), as expected from an impaired mitotic-chromosome folding activity. In contrast, contacts frequencies between telomeres were increased, both within chromosomes (intra) and in-between chromosomes (inter) (Fig. 3D). Contacts frequencies between centromeres exhibited no significant change. Aggregating Hi-C signals at chromosome ends further revealed that intra-chromosomal contacts dominate over inter-chromosomal contacts in wild-type cells and were increased in the mutant (Fig. 3E, see material and methods). Similar results obtained from a second biological and technical replicate are shown in Figure S3. Taken together these data suggest that fission yeast chromosomes enter mitosis in a Rabl configuration, with telomeres clustered together and that condensin drives their declustering into pairs of sister-telomeres as cells progress towards metaphase (Fig. 3 and S3) and their full-separation in anaphase (Fig. 2).

bioRxiv preprint doi: https://doi.org/10.1101/2022.03.18.484892; this version posted September 11, 2023. The copyright holder for this preprint (which was not certified by peer review) is the author/funder, who has granted bioRxiv a license to display the preprint in perpetuity. It is made available under aCC-BY-NC-ND 4.0 International license.

Condensin enrichment at telomeres result from positive and negative interplays with telomeric proteins

To further investigate how condensin takes part in telomere disjunction in anaphase, we sought for a cis-acting factor controlling condensin localisation specifically at telomeres. We first considered the shelterin complex and assessed Cnd2-GFP binding by calibrated ChIP-qPCR in *taz1*Δ or *rap1*Δ cells arrested in metaphase (Fig. 4A and Material and Methods). In cells lacking Taz1, Cnd2-GFP occupancy was reduced almost twofold at telomeres (tel0 site) and sub-telomeres (tel2.4 site), while remaining unchanged at the kinetochore and within chromosome arms. In contrast, the *rap1*Δ mutant showed no change compared to wild-type. A different normalization method produced similar results (Fig. S4A). Since telomere size is increased to similar extents in *taz1*Δ and *rap1*Δ mutants (Cooper *et al*, 1997; Miller *et al*, 2005), it is unlikely that condensin is titrated out from the tel0 site by supernumerary telomeric repeats in *taz1*Δ cells. Taz1 directly binds to telomeric repeats but also to non-repeated DNA motifs within chromosome arms (Zofall *et al*, 2016; Toteva *et al*, 2017). However, the binding of Cnd2-GFP was basal and independent of Taz1 at such non-telomeric Taz1-islands (Fig.4B-C and Fig. S4B-C), suggesting that Taz1 is unlikely to directly recruit condensin onto chromosomes. In line with this, we observed no physical interaction between condensin and Taz1, either by co-IP or by yeast two-hybrid assay (our unpublished data). Thus, the density of Taz1 binding sites and/or the telomeric context might be instrumental for locally enriching condensin. We therefore conclude that the core shelterin protein Taz1 plays the role of a cis-acting enrichment factor for condensin at telomeres.

The ATP-dependent chromatin remodeler Mit1 was another telomeric factor of interest. Indeed, Mit1 maintains nucleosome occupancy through its association with the shelterin and *mit1*Δ cells show a reduced histone H3 occupancy at sub-telomeres (van Emden *et al*, 2019). Since we previously reported that nucleosome eviction underlies condensin's binding to chromosomes (Toselli-Mollereau *et al*, 2016), we assessed condensin binding at telomeres in cells lacking Mit1. As expected, we observed an increased condensin occupancy at telomeres and sub-telomeres by calibrated-ChIP-seq (Fig. 4D) and ChIP-qPCR (Fig. S4-D). ChIP-seq further showed that such increase was largely, if not strictly, restricted to chromosome ends (Fig. 4D-E and Fig. S4E). These data strongly suggest that Mit1 counteracts condensin localization at telomeres. Thus, taken together, our results suggest that the steady state level of association of condensin with telomeres results from the balancing acts of shelterin proteins and associated factors, amongst which Taz1

bioRxiv preprint doi: https://doi.org/10.1101/2022.03.18.484892; this version posted September 11, 2023. The copyright holder for this preprint (which was not certified by peer review) is the author/funder, who has granted bioRxiv a license to display the preprint in perpetuity. It is made available under aCC-BY-NC-ND 4.0 International license.

and Mit1.

Condensin acts in *cis* to promote telomere disjunction in anaphase

Since the *cut14-208* and *cut3-477* mutations reduce condensin binding all along chromosomes, it was difficult to ascertain the origin of the telomere disjunction defect in these mutants. However, the finding that condensin localization at telomeres partly relies on Taz1 and Mit1 provided a means to assess whether condensin could drive telomere disjunction in *cis*. If it were the case, then removing Taz1 in a sensitized *cut3-477* background, to further dampen condensin at telomeres, should strongly increase the frequency of sister-telomere non-disjunctions compared to single mutants. Conversely, removing Mit1 in *cut3-477* cells should rescue sister-telomere disjunctions. We observed very few non-disjunction events during anaphases in *taz1*Δ single mutant cells at 32°C (Fig. 5A). We speculate that the residual amount of condensin that persists at telomeres when Taz1 is lacking might be sufficient to ensure their efficient disjunction. However, combining *cut3-477* and *taz1*Δ caused a synergistic increase of the frequency of sister-telomere non-disjunction (Fig. 5A) that correlated with a synthetic negative growth defect at 32°C and 34°C (Fig. 5B). Conversely, eliminating Mit1 rescued sister-telomere disjunction in *cut3-477* mutant cells (Fig. 5C). Taken together, these data indicate that the level of condensin bound to telomeres is a limiting parameter for their efficient separation in anaphase, suggesting therefore that condensin controls sister-telomeres disjunction in *cis*.

Condensin counteracts cohesin at telomeres

We previously showed that eliminating the heterochromatin protein $Swi6^{HP1}$ alleviates the telomere separation defect caused by the inhibition of Ark1 (Reyes *et al*, 2015). Since Ark1 controls condensin association with chromosomes (Petersen & Hagan, 2003; Tada *et al*, 2011), and Swi6 enriches cohesin at heterochromatin domains, including telomeres (Bernard *et al*, 2001), we asked whether interplays between condensin and cohesin might underlie telomere separation during anaphase. To test this, we assessed the impact of the cohesin mutation *rad21-K1*, known to weaken sister-chromatid cohesion (Bernard *et al*, 2001), on telomere disjunction. First, we observed that sister-telomere separation occurs at a smaller mitotic spindle size in the *rad21-K1* mutant as compared to wild-type, indicating an accelerated kinetics during mitosis (Fig. 6A). Second, weakening cohesin partly rescued telomere disjunction when condensin was impaired, as

bioRxiv preprint doi: https://doi.org/10.1101/2022.03.18.484892; this version posted September 11, 2023. The copyright holder for this preprint (which was not certified by peer review) is the author/funder, who has granted bioRxiv a license to display the preprint in perpetuity. It is made available under aCC-BY-NC-ND 4.0 International license.

suggested by the increased number of telomeric dots displayed by *cut3-477 rad21-K1* double mutant cells in anaphase (Fig. 6A). A similar rescue was observed when Rad21 was inactivated in early G2 cells purified using a lactose gradient (Fig. S6), indicating that cohesin inactivation post cohesion establishment complemented the telomere disjunction defects of a condensin mutant. These observations indicate that cohesin hinders the separation of sister-telomeres, suggesting therefore that condensin might counteract cohesin at telomeres. To test this hypothesis, we assessed cohesin binding to chromosomes in the *cut3-477* condensin mutant. Cells were arrested at the G2/M transition, shifted to the restrictive temperature to inactivate condensin while maintaining the arrest, and released into a synchronous mitosis (Fig. 6B). Cohesin binding was assessed by calibrated ChIP-qPCR against the $Psm3^{SMC3}$ subunit of cohesin tagged with GFP (Psm3-GFP). We observed no strong change in cohesin occupancy between G2 and anaphase in wild-type cells, consistent with the idea that solely 5-10% of the cohesin pool is cleaved by separase at the metaphase to anaphase transition in fission yeast (Tomonaga *et al*, 2000). In *cut3-477* mutant cells, however, we observed a strong increase in Psm3-GFP levels at telomeres (tel0 site) and sub-telomeres (tel1.2 site), but no change at further distal sites, nor within chromosome arms or at centromeres (Fig. 6B and S5). This specific increase in occupancy at telomeres and sub-telomeres in the condensin mutant was readily visible both during G2 and anaphase. Altogether, our data indicate that cohesin restrain telomere disjunction in anaphase and that condensin prevents the accumulation of cohesin at telomeres.

DISCUSSION

With this work, we show that condensin is enriched at fission yeast telomeres during mitosis and that such enrichment results from the balancing acts of telomeric proteins. We also show that the separation of sister-telomeres is not the mere consequence of the separation of chromosome arms and that condensin acts in cis at telomeres to drive their disjunction during anaphase. We provide evidence that condensin might achieve this task by counteracting cohesin.

Previous work has shown that the kleisin subunit of condensin II (CAPH2) binds human TRF1, a counterpart of Taz1, in RPE-1 cells (Wallace *et al*, 2019), but since no physical or functional link has been described between TRF1 and other subunits of the condensin II holocomplex, it was unclear whether CAPH2 might act at telomeres independently of condensin II. Hence, the biological significance of the presence of condensin complexes at telomeres remained enigmatic.

bioRxiv preprint doi: https://doi.org/10.1101/2022.03.18.484892; this version posted September 11, 2023. The copyright holder for this preprint (which was not certified by peer review) is the author/funder, who has granted bioRxiv a license to display the preprint in perpetuity. It is made available under aCC-BY-NC-ND 4.0 International license.

Here we show that the kleisin subunit of fission yeast condensin is bound to the telomere repeats of TEL2R in metaphase and anaphase and that such binding relies on the Cut14^{SMC2} and Cut3^{SMC4} ATPases (Saka *et al*, 1994), arguing therefore that the condensin holocomplex is bound to TEL2R. Since southern blotting and FISH experiments have shown that chromosome I and II contains similar sub-telomeric elements (Funabiki *et al*, 1993; Oizumi *et al*, 2021), our observations made using TEL2R DNA are likely to be relevant to most fission yeast telomeres.

We further show that condensin occupancy at telomeres is controlled by the telomeric proteins Taz1 and Mit1. Taz1 being a core component of the shelterin complex, we cannot formally rule out that the reduced binding of condensin stems from a collapse of the overall telomeric structure in cells lacking Taz1. However, two observations argue against such scenario. First, the fact that deleting Rap1, another key component of shelterin, does not impair condensin localisation and, second, our finding that condensin binding to telomeres is also controlled, negatively, by the nucleosome remodeler Mit1, which associates with telomeres *via* the Ccq1 subunit of shelterin (Sugiyama *et al*, 2007; van Emden *et al*, 2019). Such negative regulation by Mit1 not only strengthens our previous work suggesting that nucleosome arrays are an obstacle for condensin binding to DNA *in vivo* (Toselli-Mollereau *et al*, 2016), but also strongly suggests that condensin localisation at telomeres relies on a dedicated pathway that involves interplays with telomeric components. However, and in sharp contrast with the human TRF1 and CAP-H2 (Wallace *et al*, 2019), we detected no protein-to-protein interactions between Taz1 and Cnd2/condensin. Together with our observation that Taz1 does not enrich condensin at discrete Taz1-DNA binding sites located outside telomeres, this suggests that Taz1 is not a cis-acting recruiter for condensin at telomeres. Rather, by analogy with the accumulation of condensin at highly expressed genes (Brandão *et al*, 2019; Rivosecchi *et al*, 2021), we speculate that arrays of Taz1 proteins tightly bound to telomere repeats might create a permeable barrier onto which condensin molecules accumulate. However, unlike highly expressed genes that most likely hinder condensin-mediated chromosome segregation in anaphase (Sutani *et al*, 2015), the Taz1 barrier would play a positive role in chromosome segregation by promoting sister-telomere disjunction in anaphase.

Using Hi-C and live cell imaging, we provide evidence that condensin takes part in telomere declustering during the early steps of mitosis and in sister-telomere disjunction in anaphase. It is tempting to speculate that condensin promotes the dissociation of telomeric clusters, inherited from the Rabl organisation of chromosomes in interphase, by folding chromatin into mitotic

bioRxiv preprint doi: https://doi.org/10.1101/2022.03.18.484892; this version posted September 11, 2023. The copyright holder for this preprint (which was not certified by peer review) is the author/funder, who has granted bioRxiv a license to display the preprint in perpetuity. It is made available under aCC-BY-NC-ND 4.0 International license.

chromosomes. As condensation proceeds, axial shortening and stiffening of chromosome arms would drive the movement of the pairs of telomeres located at the opposite ends of a chromosome away from each other. The separation of sister-telomeres during anaphase, in contrast, cannot be the passive consequence of the separation of sister chromatids. Indeed, the striking observation that sister-telomere disjunction can be uncoupled from the separation of chromosome arms, as seen in the decatenation-defective *topo-250* mutant, implies the existence of a mechanism independent of chromosome arms, driving sister-telomere disjunction. In fission yeast, condensin must play a key role within such telomere-disjunction pathway (TDP) since modulating its occupancy at telomeres whilst leaving chromosome arms largely unchanged, using *taz1*Δ or *mit1*Δ mutations, is sufficient to change accordingly the efficiency of sister-telomeres disjunction. The fact that condensin occupancy at telomeres is a limiting parameter for their disjunction argues for a role played in *cis*. This finding is reminiscent of telomere separation in human cells that specifically relies on the activity of the poly(ADP-ribose) polymerase tankyrase 1 (Dynek & Smith, 2004), and suggest therefore that the existence of a dedicated pathway for sister-telomere disjunction is a conserved feature of eukaryotic cells. We therefore conclude that condensin enriched at telomeres *via* the balancing acts of Taz1 and Mit1 drives the separation of sister-telomeres in anaphase. The corollary is that failures to disjoin sister-telomeres most likely contribute to the stereotypical chromatin bridge phenotype exhibited by condensin-defective cells. Our results do not rule out the possibility that Topo II contributes to telomeres disentanglements, but nevertheless imply that Topo II catalytic activity is dispensable for telomere segregation provided that condensin is active. The close proximity of DNA ends could explain such a dispensability. It has been reported in budding yeast that the segregation of LacO repeats inserted in the vicinity of TelV is impaired by the *top2-4* mutation (Bhalla *et al*, 2002). At first sight, this appears at odds with our observations made using the telomere protein Taz1 tagged with GFP. However, since LacO arrays tightly bound by LacI proteins constitute a barrier for the recoiling activity of budding yeast condensin in anaphase (Guérin *et al*, 2019), the insertion of such a construct might have created an experimental condition in which condensin activity was specifically impaired at TELV, hence revealing the contribution of Topo II. In addition, the telomere structure in budding and fission yeast is significantly different. Budding yeast protects its telomeres *via* two independent factors, Rap1 and the Cdc13-Stn1-Ten1 complex, whereas in fission yeast Taz1 and Pot1 are bridged by a complex protein interaction network (Rap1-Poz1-Tpz1). This is a remarkable conserved structural feature

bioRxiv preprint doi: https://doi.org/10.1101/2022.03.18.484892; this version posted September 11, 2023. The copyright holder for this preprint (which was not certified by peer review) is the author/funder, who has granted bioRxiv a license to display the preprint in perpetuity. It is made available under aCC-BY-NC-ND 4.0 International license.

between the shelterin of *S. pombe* and the human shelterin. Notably, it was recently shown that the telomeric components of *S. pombe* can dimerize leading to a higher complex organization of the shelterin (Sun *et al*, 2022). It is thus likely that dimerization of Taz1, Poz1, and the Tpz1-Ccq1 subcomplex may also contribute to the clustering of sister and non-sister chromatid telomeres. The architectural differences in telomere organization between budding and fission yeast may require different mechanisms to properly segregate telomeres during mitosis.

Understanding how condensin takes part in the disjunction of sister-telomeres will require identifying the ties that link them. Cohesin has been involved in telomere cohesion in budding yeast (Antoniacci & Skibbens, 2006; Renshaw *et al*, 2010), but in human cells the situation remains unclear. Although $Scc3^{SA1}$ is a likely target of the tankyrase 1 pathway for telomere disjunction (Canudas & Smith, 2009), telomeric cohesion appears independent of other cohesin subunits (Bisht *et al*, 2013). Our finding that *rad21-K1*, a loss-of-function mutation in the kleisin subunit of fission yeast cohesin, accelerates sister-telomere disjunction in an otherwise wild-type genetic background would be consistent with a role for cohesin in ensuring cohesion between sister-telomeres in fission yeast. Alternatively, *rad21-K1* might indirectly increase the impact of condensin at chromosome ends, for instance by altering the structure of sub-telomeric heterochromatin (Dheur *et al*, 2011). However, such an indirect effect seems less likely because the kinetics of sister-telomere disjunction is not accelerated in cells lacking the core heterochromatin protein Swi6 (Reyes *et al*, 2015). Therefore, we favour the conclusion that condensin drive sister-telomere disjunction by counteracting cohesin at chromosome ends. Whether it could be cohesive- or loop-extruding- cohesin remains to be determined, but we note that an antagonism between condensin and cohesin for the folding of interphase chromatin as well as for telomere segregation in anaphase has been reported in Drosophila and budding yeast, respectively (Rowley *et al*, 2019; Renshaw et al. 2010). Thus, unravelling the mechanism by which condensin drives telomere disjunction in anaphase will require further investigations not only on the interplays between condensin and cohesin at telomeres, but also on the role played or not by condensin loop-extrusion activity and on the dynamics of shelterin. Because of its ability to organize telomeres into various structures (Lim & Cech, 2021), the shelterin complex may link sister-telomeres together and loop extrusion by condensin may provide the power stroke to disentangle such structures. Thus, as speculated in Figure 7, the accumulation of condensin against $Taz1^{TRF1}$ barriers, together with a possible up-regulation by Aurora-B kinase in anaphase (Reyes

bioRxiv preprint doi: https://doi.org/10.1101/2022.03.18.484892; this version posted September 11, 2023. The copyright holder for this preprint (which was not certified by peer review) is the author/funder, who has granted bioRxiv a license to display the preprint in perpetuity. It is made available under aCC-BY-NC-ND 4.0 International license.

et al, 2015), might allow condensin-mediated DNA translocation to pass a threshold beyond which the ties between sister-telomeres would be eliminated, be it cohesin- and/or shelterin-mediated. Whatever the mechanism, given the conservation of shelterin, and the abundance of condensin complexes at telomeres during mitosis and meiosis in mammals (Viera *et al*, 2007; Walther *et al*, 2018), we speculate that condensin specifically drives the separation of telomeres in other living organisms.

REFERENCES AND NOTES

Antoniacci LM & Skibbens RV (2006) Sister-chromatid telomere cohesion is nonredundant and resists both spindle forces and telomere motility. *Curr Biol CB* 16: 902–906

Aoi Y, Kawashima SA, Simanis V, Yamamoto M & Sato M (2014) Optimization of the analogue-sensitive Cdc2/Cdk1 mutant by in vivo selection eliminates physiological limitations to its use in cell cycle analysis. *Open Biol* 4

Bahler J, Wu JQ, Longtine MS, Shah NG, McKenzie 3rd A, Steever AB, Wach A, Philippsen P & Pringle JR (1998) Heterologous modules for efficient and versatile PCR-based gene targeting in Schizosaccharomyces pombe. *Yeast* 14: 943–951

Baxter J, Sen N, Martinez VL, De Carandini ME, Schvartzman JB, Diffley JF & Aragon L (2011) Positive supercoiling of mitotic DNA drives decatenation by topoisomerase II in eukaryotes. *Science* 331: 1328–1332

Bernard P, Maure JF, Partridge JF, Genier S, Javerzat JP & Allshire RC (2001) Requirement of heterochromatin for cohesion at centromeres. *Science* 294: 2539–42

Berthezene J, Reyes C, Li T, Coulon S, Bernard P, Gachet Y & Tournier S (2020) Aurora B and condensin are dispensable for chromosome arm and telomere separation during meiosis II. *Mol Biol Cell* 31: 889–905

Bhalla N, Biggins S & Murray AW (2002) Mutation of YCS4, a budding yeast condensin subunit, affects mitotic and nonmitotic chromosome behavior. *Mol Biol Cell* 13: 632–645

Bisht KK, Daniloski Z & Smith S (2013) SA1 binds directly to DNA through its unique AT-hook to promote sister chromatid cohesion at telomeres. *J Cell Sci* 126: 3493–3503

Brandão HB, Paul P, van den Berg AA, Rudner DZ, Wang X & Mirny LA (2019) RNA polymerases as moving barriers to condensin loop extrusion. *Proc Natl Acad Sci U S A* 116: 20489–20499

Canudas S & Smith S (2009) Differential regulation of telomere and centromere cohesion by the Scc3 homologues SA1 and SA2, respectively, in human cells. *J Cell Biol* 187: 165–173

Charbin A, Bouchoux C & Uhlmann F (2014) Condensin aids sister chromatid decatenation by topoisomerase II. *Nucleic Acids Res* 42: 340–348

Chikashige Y, Yamane M, Okamasa K, Tsutsumi C, Kojidani T, Sato M, Haraguchi T & Hiraoka Y (2009) Membrane proteins Bqt3 and -4 anchor telomeres to the nuclear envelope to ensure chromosomal bouquet formation. *J Cell Biol* 187: 413–427

Clemente-Blanco A, Sen N, Mayan-Santos M, Sacristan MP, Graham B, Jarmuz A, Giess A, Webb E, Game L, Eick D, *et al* (2011) Cdc14 phosphatase promotes segregation of telomeres through repression of RNA polymerase II transcription. *Nat Cell Biol* 13: 1450–6

Cooper JP, Nimmo ER, Allshire RC & Cech TR (1997) Regulation of telomere length and function

bioRxiv preprint doi: https://doi.org/10.1101/2022.03.18.484892; this version posted September 11, 2023. The copyright holder for this preprint (which was not certified by peer review) is the author/funder, who has granted bioRxiv a license to display the preprint in perpetuity. It is made available under aCC-BY-NC-ND 4.0 International license.

by a Myb-domain protein in fission yeast. *Nature* 385: 744–747

D'Ambrosio C, Schmidt CK, Katou Y, Kelly G, Itoh T, Shirahige K & Uhlmann F (2008) Identification of cis-acting sites for condensin loading onto budding yeast chromosomes. *Genes Dev* 22: 2215–2227

Davidson IF & Peters J-M (2021) Genome folding through loop extrusion by SMC complexes. *Nat Rev Mol Cell Biol* 22: 445–464

Dehé P-M & Cooper JP (2010) Fission yeast telomeres forecast the end of the crisis. *FEBS Lett* 584: 3725–3733

Dheur S, Saupe SJ, Genier S, Vazquez S & Javerzat JP (2011) Role for cohesin in the formation of a heterochromatic domain at fission yeast subtelomeres. *Mol Cell Biol* 31: 1088–97

Dowen JM, Bilodeau S, Orlando DA, Hübner MR, Abraham BJ, Spector DL & Young RA (2013) Multiple Structural Maintenance of Chromosome Complexes at Transcriptional Regulatory Elements. *Stem Cell Rep* Vol. I: 371–378

Dynek JN & Smith S (2004) Resolution of Sister Telomere Association Is Required for Progression Through Mitosis. *Science* 304: 97–100

van Emden TS, Forn M, Forné I, Sarkadi Z, Capella M, Martín Caballero L, Fischer-Burkart S, Brönner C, Simonetta M, Toczyski D, *et al* (2019) Shelterin and subtelomeric DNA sequences control nucleosome maintenance and genome stability. *EMBO Rep* 20: e47181

Freeman L, Aragon-Alcaide L & Strunnikov A (2000) The condensin complex governs chromosome condensation and mitotic transmission of rDNA. *J Cell Biol* 149: 811–824

Funabiki H, Hagan I, Uzawa S & Yanagida M (1993) Cell cycle-dependent specific positioning and clustering of centromeres and telomeres in fission yeast. *J Cell Biol* 121: 961–76

Ganji M, Shaltiel IA, Bisht S, Kim E, Kalichava A, Haering CH & Dekker C (2018) Real-time imaging of DNA loop extrusion by condensin. *Science* 360: 102–105

Gerlich D, Hirota T, Koch B, Peters JM & Ellenberg J (2006) Condensin I stabilizes chromosomes mechanically through a dynamic interaction in live cells. *Curr Biol* 16: 333–44

Gibcus JH, Samejima K, Goloborodko A, Samejima I, Naumova N, Nuebler J, Kanemaki MT, Xie L, Paulson JR, Earnshaw WC, *et al* (2018) A pathway for mitotic chromosome formation. *Science* 359

Grallert A & Hagan IM (2017) Preparation of Protein Extracts from Schizosaccharomyces pombe Using Trichloroacetic Acid Precipitation. *Cold Spring Harb Protoc* 2017: pdb.prot091579

Guérin TM, Béneut C, Barinova N, López V, Lazar-Stefanita L, Deshayes A, Thierry A, Koszul R, Dubrana K & Marcand S (2019) Condensin-Mediated Chromosome Folding and Internal Telomeres Drive Dicentric Severing by Cytokinesis. *Mol Cell* 75: 131-144.e3

Hirano T (2012) Condensins: universal organizers of chromosomes with diverse functions. *Genes Dev* 26: 1659–78

Hirano T (2016) Condensin-Based Chromosome Organization from Bacteria to Vertebrates. *Cell* 164: 847–857

Hu B, Petela N, Kurze A, Chan K-L, Chapard C & Nasmyth K (2015) Biological chromodynamics: a general method for measuring protein occupancy across the genome by calibrating ChIP-seq. *Nucleic Acids Res* 43: e132

Johzuka K & Horiuchi T (2009) The cis element and factors required for condensin recruitment to chromosomes. *Mol Cell* 34: 26–35

Kakui Y, Rabinowitz A, Barry DJ & Uhlmann F (2017) Condensin-mediated remodeling of the mitotic chromatin landscape in fission yeast. *Nat Genet* 49: 1553–1557

Kanoh J, Sadaie M, Urano T & Ishikawa F (2005) Telomere binding protein Taz1 establishes Swi6 heterochromatin independently of RNAi at telomeres. *Curr Biol* 15: 1808–1819

bioRxiv preprint doi: https://doi.org/10.1101/2022.03.18.484892; this version posted September 11, 2023. The copyright holder for this preprint (which was not certified by peer review) is the author/funder, who has granted bioRxiv a license to display the preprint in perpetuity. It is made available under aCC-BY-NC-ND 4.0 International license.

Kim JH, Zhang T, Wong NC, Davidson N, Maksimovic J, Oshlack A, Earnshaw WC, Kalitsis P & Hudson DF (2013) Condensin I associates with structural and gene regulatory regions in vertebrate chromosomes. *Nat Commun* 4: 2537

Kong M, Cutts EE, Pan D, Beuron F, Kaliyappan T, Xue C, Morris EP, Musacchio A, Vannini A & Greene EC (2020) Human Condensin I and II Drive Extensive ATP-Dependent Compaction of Nucleosome-Bound DNA. *Mol Cell* 79: 99-114.e9

Kranz AL, Jiao CY, Winterkorn LH, Albritton SE, Kramer M & Ercan S (2013) Genome-wide analysis of condensin binding in Caenorhabditis elegans. *Genome Biol* 14: R112

Kschonsak M, Merkel F, Bisht S, Metz J, Rybin V, Hassler M & Haering CH (2017) Structural Basis for a Safety-Belt Mechanism That Anchors Condensin to Chromosomes. *Cell* 171: 588-600.e24

de Lange T (2018) Shelterin-Mediated Telomere Protection. *Annu Rev Genet* 52: 223–247

Liang J, Lacroix L, Gamot A, Cuddapah S, Queille S, Lhoumaud P, Lepetit P, Martin PGP, Vogelmann J, Court F, *et al* (2014) Chromatin immunoprecipitation indirect peaks highlight long-range interactions of insulator proteins and Pol II pausing. *Mol Cell* 53: 672–681

Lim CJ & Cech TR (2021) Shaping human telomeres: from shelterin and CST complexes to telomeric chromatin organization. *Nat Rev Mol Cell Biol* 22: 283–298

Madeira F, Park YM, Lee J, Buso N, Gur T, Madhusoodanan N, Basutkar P, Tivey ARN, Potter SC, Finn RD, *et al* (2019) The EMBL-EBI search and sequence analysis tools APIs in 2019. *Nucleic Acids Res* 47: W636–W641

Miller KM & Cooper JP (2003) The telomere protein Taz1 is required to prevent and repair genomic DNA breaks. *Mol Cell* 11: 303–313

Miller KM, Ferreira MG & Cooper JP (2005) Taz1, Rap1 and Rif1 act both interdependently and independently to maintain telomeres. *Embo J* 24: 3128–3135

Moreno S, Klar A & Nurse P (1991) Molecular genetic analysis of fission yeast Schizosaccharomyces pombe. *Methods Enzym* 194: 795–823

Moser BA & Nakamura TM (2009) Protection and replication of telomeres in fission yeast. *Biochem Cell Biol* 87: 747–758

Nakazawa N, Nakamura T, Kokubu A, Ebe M, Nagao K & Yanagida M (2008) Dissection of the essential steps for condensin accumulation at kinetochores and rDNAs during fission yeast mitosis. *J Cell Biol* 180: 1115–31

Nakazawa N, Sajiki K, Xu X, Villar-Briones A, Arakawa O & Yanagida M (2015) RNA pol II transcript abundance controls condensin accumulation at mitotically up-regulated and heat-shock-inducible genes in fission yeast. *Genes Cells* 20: 481–499

Nasmyth K (2017) How are DNAs woven into chromosomes? *Science* 358: 589–590

Oizumi Y, Kaji T, Tashiro S, Takeshita Y, Date Y & Kanoh J (2021) Complete sequences of Schizosaccharomyces pombe subtelomeres reveal multiple patterns of genome variation. *Nat Commun* 12: 611

Ono T, Fang Y, Spector DL & Hirano T (2004) Spatial and temporal regulation of Condensins I and II in mitotic chromosome assembly in human cells. *Mol Biol Cell* 15: 3296–3308

Ono T, Losada A, Hirano M, Myers MP, Neuwald AF & Hirano T (2003) Differential contributions of condensin I and condensin II to mitotic chromosome architecture in vertebrate cells. *Cell* 115: 109–121

Petersen J & Hagan IM (2003) S. pombe aurora kinase/survivin is required for chromosome condensation and the spindle checkpoint attachment response. *Curr Biol* 13: 590–7

Petrova B, Dehler S, Kruitwagen T, Heriche JK, Miura K & Haering CH (2013) Quantitative analysis of chromosome condensation in fission yeast. *Mol Cell Biol* 33: 984–98

bioRxiv preprint doi: https://doi.org/10.1101/2022.03.18.484892; this version posted September 11, 2023. The copyright holder for this preprint (which was not certified by peer review) is the author/funder, who has granted bioRxiv a license to display the preprint in perpetuity. It is made available under aCC-BY-NC-ND 4.0 International license.

Piskadlo E, Tavares A & Oliveira RA (2017) Metaphase chromosome structure is dynamically maintained by condensin I-directed DNA (de)catenation. *eLife* 6: e26120

Rao SSP, Huntley MH, Durand NC, Stamenova EK, Bochkov ID, Robinson JT, Sanborn AL, Machol I, Omer AD, Lander ES, *et al* (2014) A 3D map of the human genome at kilobase resolution reveals principles of chromatin looping. *Cell* 159: 1665–1680

Renshaw MJ, Ward JJ, Kanemaki M, Natsume K, Nedelec FJ & Tanaka TU (2010) Condensins promote chromosome recoiling during early anaphase to complete sister chromatid separation. *Dev Cell* 19: 232–244

Reyes C, Serrurier C, Gauthier T, Gachet Y & Tournier S (2015) Aurora B prevents chromosome arm separation defects by promoting telomere dispersion and disjunction. *J Cell Biol* 208: 713–727

Ribeiro SA, Gatlin JC, Dong Y, Joglekar A, Cameron L, Hudson DF, Farr CJ, McEwen BF, Salmon ED, Earnshaw WC, *et al* (2009) Condensin regulates the stiffness of vertebrate centromeres. *Mol Biol Cell* 20: 2371–2380

Rivosecchi J, Jost D, Vachez L, Gautier FD, Bernard P & Vanoosthuyse V (2021) RNA polymerase backtracking results in the accumulation of fission yeast condensin at active genes. *Life Sci Alliance* 4: e202101046

Robellet X, Vanoosthuyse V & Bernard P (2017) The loading of condensin in the context of chromatin. *Curr Genet* 63: 577–589

Rowley MJ, Lyu X, Rana V, Ando-Kuri M, Karns R, Bosco G & Corces VG (2019) Condensin II Counteracts Cohesin and RNA Polymerase II in the Establishment of 3D Chromatin Organization. *Cell Rep* 26: 2890-2903.e3

Saka Y, Sutani T, Yamashita Y, Saitoh S, Takeuchi M, Nakaseko Y & Yanagida M (1994) Fission yeast cut3 and cut14, members of a ubiquitous protein family, are required for chromosome condensation and segregation in mitosis. *Embo J* 13: 4938–52

Samejima K, Samejima I, Vagnarelli P, Ogawa H, Vargiu G, Kelly DA, de Lima Alves F, Kerr A, Green LC, Hudson DF, *et al* (2012) Mitotic chromosomes are compacted laterally by KIF4 and condensin and axially by topoisomerase IIalpha. *J Cell Biol* 199: 755–70

Samoshkin A, Dulev S, Loukinov D, Rosenfeld JA & Strunnikov AV (2012) Condensin dysfunction in human cells induces nonrandom chromosomal breaks in anaphase, with distinct patterns for both unique and repeated genomic regions. *Chromosoma* 121: 191–9

Steen RL, Cubizolles F, Le Guellec K & Collas P (2000) A kinase-anchoring protein (AKAP)95 recruits human chromosome-associated protein (hCAP)-D2/Eg7 for chromosome condensation in mitotic extract. *J Cell Biol* 149: 531–536

Sugawara N (1988) DNA sequences at the telomeres of the fission yeast S. pombe.

Sugiyama T, Cam HP, Sugiyama R, Noma K, Zofall M, Kobayashi R & Grewal SIS (2007) SHREC, an Effector Complex for Heterochromatic Transcriptional Silencing. *Cell* 128: 491–504

Sun H, Wu Z, Zhou Y, Lu Y, Lu H, Chen H, Shi S, Zeng Z, Wu J & Lei M (2022) Structural insights into Pot1-ssDNA, Pot1-Tpz1 and Tpz1-Ccq1 Interactions within fission yeast shelterin complex. *PLoS Genet* 18: e1010308

Sun M, Biggs R, Hornick J & Marko JF (2018) Condensin controls mitotic chromosome stiffness and stability without forming a structurally contiguous scaffold. *Chromosome Res* 26: 277–295

Sutani T, Sakata T, Nakato R, Masuda K, Ishibashi M, Yamashita D, Suzuki Y, Hirano T, Bando M & Shirahige K (2015) Condensin targets and reduces unwound DNA structures associated with transcription in mitotic chromosome condensation. *Nat Commun* 6: 7815

Sutani T, Yuasa T, Tomonaga T, Dohmae N, Takio K & Yanagida M (1999) Fission yeast condensin complex: essential roles of non-SMC subunits for condensation and Cdc2

bioRxiv preprint doi: https://doi.org/10.1101/2022.03.18.484892; this version posted September 11, 2023. The copyright holder for this preprint (which was not certified by peer review) is the author/funder, who has granted bioRxiv a license to display the preprint in perpetuity. It is made available under aCC-BY-NC-ND 4.0 International license.

phosphorylation of Cut3/SMC4. *Genes Dev* 13: 2271–83

Tada K, Susumu H, Sakuno T & Watanabe Y (2011) Condensin association with histone H2A shapes mitotic chromosomes. *Nature* 474: 477–83

Tomonaga T, Nagao K, Kawasaki Y, Furuya K, Murakami A, Morishita J, Yuasa T, Sutani T, Kearsey SE, Uhlmann F, *et al* (2000) Characterization of fission yeast cohesin: essential anaphase proteolysis of Rad21 phosphorylated in the S phase. *Genes Dev* 14: 2757–2770

Toselli-Mollereau E, Robellet X, Fauque L, Lemaire S, Schiklenk C, Klein C, Hocquet C, Legros P, N'Guyen L, Mouillard L, *et al* (2016) Nucleosome eviction in mitosis assists condensin loading and chromosome condensation. *Embo J* 35: 1565–1581

Toteva T, Mason B, Kanoh Y, Brøgger P, Green D, Verhein-Hansen J, Masai H & Thon G (2017) Establishment of expression-state boundaries by Rif1 and Taz1 in fission yeast. *Proc Natl Acad Sci U S A* 114: 1093–1098

Uemura T, Ohkura H, Adachi Y, Morino K, Shiozaki K & Yanagida M (1987) DNA topoisomerase II is required for condensation and separation of mitotic chromosomes in S. pombe. *Cell* 50: 917–925

Verzijlbergen KF, Nerusheva OO, Kelly D, Kerr A, Clift D, de Lima Alves F, Rappsilber J & Marston AL (2014) Shugoshin biases chromosomes for biorientation through condensin recruitment to the pericentromere. *eLife* 3: e01374

Viera A, Gómez R, Parra MT, Schmiesing JA, Yokomori K, Rufas JS & Suja JA (2007) Condensin I reveals new insights on mouse meiotic chromosome structure and dynamics. *PLoS ONE*

Wallace HA, Rana V, Nguyen HQ & Bosco G (2019) Condensin II subunit NCAPH2 associates with shelterin protein TRF1 and is required for telomere stability. *J Cell Physiol* 234: 20755–20768

Walther N, Hossain MJ, Politi AZ, Koch B, Kueblbeck M, Ødegård-Fougner Ø, Lampe M & Ellenberg J (2018) A quantitative map of human Condensins provides new insights into mitotic chromosome architecture. *J Cell Biol* 217: 2309–2328

Zofall M, Smith DR, Mizuguchi T, Dhakshnamoorthy J & Grewal SIS (2016) Taz1-Shelterin Promotes Facultative Heterochromatin Assembly at Chromosome-Internal Sites Containing Late Replication Origins. *Mol Cell* 62: 862–874

ACKNOWLEDGMENTS

We thank the National BioResource-Yeast Project, J. Cooper, JP. Javerzat, M. Yanagida and J. Kanoh for strains; J. Baxter and N. Minchell for teaching the rudiments of Hi-C to L.C., J.P. Javerzat, F. Beckouet, V. Vanoosthuyse and A. Piazza for helpful discussions.

FUNDING

L.C. and J.B. are supported by PhD studentships from respectively la Ligue contre le cancer, and a University MRT and la Fondation pour la Recherche Médicale. This work was funded by the CNRS, Inserm (O.C. and S.S.), ANR-blanc120601, ANR-16-CE12-0015-TeloMito, la Fondation ARC (PJA 20191209370 to PB; 20161204921 to ST) and la ligue régionale contre le cancer –

bioRxiv preprint doi: https://doi.org/10.1101/2022.03.18.484892; this version posted September 11, 2023. The copyright holder for this preprint (which was not certified by peer review) is the author/funder, who has granted bioRxiv a license to display the preprint in perpetuity. It is made available under aCC-BY-NC-ND 4.0 International license.

comité Auvergne-Rhône-Alpes et Saône-et-Loire to PB.

AUTHOR CONTRIBUTIONS

Conceptualization and Methodology: S.T.; P.B., S.C., Y.G.

Investigation: all authors

Visualization: L.C., C.R., J.B, S.T., P.B., S.C., Y.G.

Funding acquisition: S.T., P.B., S.C., Y.G.

Project administration: S.T., P.B.

Supervision: S.T., P.B., S.C., Y.G., O.C.

Writing – original draft: S.T., P.B.

Writing – review & editing: S.T., P.B., S.C., Y.G., O.C.

COMPETING INTERESTS

Authors declare that they have no competing interests.

FIGURE LEGENDS

Figure 1. Fission yeast condensin is enriched at telomeres during metaphase and anaphase. (**A**) The telomere and sub-telomere of the right arm of chromosome 2 (Tel2R) as an example of chromosome end sequence in fission yeast. Sub-telomeric elements (STE), the heterochromatic gene *tlh2*, the domain bound by Taz1 (orange) (Kanoh *et al*, 2005) and primers for ChIP-qPCR (blue arrows) are shown. (**B**) Cnd2-GFP ChIP-qPCR from cells synchronized at G2/M (time post release 0 min) and upon their release in mitosis (time post release 7 min and 15 min). Left panel: cell cycle stages determined by scoring the accumulation of Cnd2-GFP in the nucleus (metaphase) and by DAPI staining (anaphase). Right panel: ChIP-qPCR results, *cdc22*, *exg1* and *gly05* loci, being high or low condensin binding sites which are used as controls. Shown are the averages and standard deviations (sd) from 3 independent biological and technical replicates. (**C-D**) Cnd2-GFP calibrated ChIP-seq in metaphase arrests at 36°C. (C) left panel: mitotic indexes of the two independent biological and technical replicates used. Right panel: genome browser views of replicate #1. The second is shown in Figure EV1C-D. (D) Metagene profiles of all condensin binding sites along chromosome arms from replicates #1 and #2; TSS (Transcription Start Site),

bioRxiv preprint doi: https://doi.org/10.1101/2022.03.18.484892; this version posted September 11, 2023. The copyright holder for this preprint (which was not certified by peer review) is the author/funder, who has granted bioRxiv a license to display the preprint in perpetuity. It is made available under aCC-BY-NC-ND 4.0 International license.

TES (Transcription End Site). (**E**) Western blot showing Cnd2-GFP steady state level in indicated cells arrested in metaphase for 3h at 36°C. Tubulin (Tub.) serves as loading control.

Figure 2. Condensin takes part in telomere disjunction during anaphase in a decatenation-independent manner. (**A**) left panel: WT or *cut14-208* condensin mutant cells shifted to the restrictive temperature of 36°C for three hours were fixed with formaldehyde and directly imaged. Telomeres were visualized via Taz1-GFP (green), kinetochores/centromeres via Mis6-RFP (red), and spindle pole bodies (SPBs) via Cdc11-CFP (blue). Right panel: number of telomeric foci according to the distance between SPBs at 36°C (n>90 cells for each strain). The data shown are from a single representative experiment out of three repeats. (**B**) Same procedure as in (A) applied to the *cut3-477* condensin mutant. (**C**) Genomic DNA from the indicated strains cultured at 32°C was digested with *Apa*I and Southern blotted using a telomeric probe (green), as represented by the grey bar. The relative gain or loss of telomeric DNA compare to WT is indicated. (**D**) Cells expressing Taz1-GFP and Cdc11-CFP, cultured at 25°C, were shifted to 19°C (restrictive temperature of *top2-250*) or 36°C (restrictive temperature of *cut3-477*), further incubated for 3 hours and fixed with formaldehyde. DNA was stained with DAPI, chromosome and telomere separation in anaphase (distance between the SPBs > 5 µm) were assessed. Shown are averages and SD obtained from three independent experiments (n=100 cells for each condition). (**E**) Left panel: Live imaging of telomere separation according to the length of the mitotic spindle (distance between the SPBs) in *top2-250* cells undergoing mitosis at 25°C or after a shift to the restrictive temperature of 19°C using fast microfluidic temperature control. Right panel: number of telomeric foci according to the distance between SPBs at 25°C or 19°C in the *top2-250* mutant. Shown is a representative experiment out of three replicates with n>70 cells, each.

Figure 3. Condensin deficiency increases contact frequencies between telomeres in metaphase. (**A**) Mitotic indexes of cell cultures used for Hi-C. (**B**) Hi-C contact probability matrix at 25 kb resolution of wild-type metaphase arrests at 33°C. Contacts between telomeres (arrows) and centromeres (circles) are indicated. (**C**) Median contact probabilities as a function of distance along chromosomes for wild-type and *cut14-208* metaphases at 33°C. (**D**) Differential Hi-C contact map between wild-type and *cut14-208*. (**E**) Measurements of aggregated contact frequencies at high resolution (5 kb) over the ends of chromosomes in metaphase arrests at 33°C.

bioRxiv preprint doi: https://doi.org/10.1101/2022.03.18.484892; this version posted September 11, 2023. The copyright holder for this preprint (which was not certified by peer review) is the author/funder, who has granted bioRxiv a license to display the preprint in perpetuity. It is made available under aCC-BY-NC-ND 4.0 International license.

Boxes indicate the median, 1st and 3rd quartiles, whiskers the minimum and maximum, and notches represent the 95% confidence interval for each median. Data points are shown as grey circles. The significance in contact frequencies was confirmed statistically by Mann-Whitney-Wilcoxon test between *cut14-208* and wild-type conditions.

Figure 4. Condensin enrichment at telomeres results from positive and negative interplays with telomeric factors. (**A**) Cnd2-GFP calibrated ChIP-qPCR from cells arrested in metaphase at 30°C. Shown are averages and standard deviations (SD) of mitotic indexes and ChIP-qPCRs for 3 biological and technical replicates. *cnt1* is the kinetochore domain of *cen1*, *exg1*, *gas1* and *cnd1* are high or low occupancy binding sites on chromosome arms. (**B-C**) Cnd2-GFP occupancy assessed at non-telomeric Taz1 islands (isl) in the same samples as in Figure 1C & S1-D and Figure 4A, respectively. (**D-E**) Cnd2-GFP calibrated ChIP-seq in metaphase arrests. (D) left panel: mitotic indexes of the two independent biological and technical replicates used. Right panel: genome browser views of replicate #1. The second replicate is shown in Figure S4. (E) Metagene profiles of all condensin binding sites along chromosome arms from replicates #1 and #2; TSS (Transcription Start Site), TES (Transcription End Site).

Figure 5. Condensin level at telomeres is a limiting parameter for their disjunction during anaphase. (**A**) Cells were grown at 25°C or shifted to 32°C for 3 hours, fixed with formaldehyde and stained with DAPI to reveal DNA. Left panel: example of anaphase cells showing chromatin bridges and non-disjoined telomeres in late anaphase in the *cut3-477 taz1*Δ double mutant. Right panel: telomere non-disjunction events were scored in anaphase cells. Shown are averages and standard deviation from 3 independent biological and technical replicates with n=100 cells, each. (**B**) Cells of indicated genotypes were serially diluted 1/5 and spotted onto YES plates at indicated temperatures for 7 (18°C), 3 (25°C) and 2 (32 and 34°C) days. (**C**) Left panel: *cut3-477* or *cut3-477 mit1*Δ mutant cells shifted to the restrictive temperature of 36°C for three hours were fixed with formaldehyde and directly imaged. Telomeres were visualized via Taz1-GFP (green) and spindle pole bodies (SPBs) via Cdc11-CFP (blue). Right panel: number of telomeric foci according to the distance between SPBs at 36°C (n>90 cells for each strain). The data shown are from a single representative experiment out of three repeats.

bioRxiv preprint doi: https://doi.org/10.1101/2022.03.18.484892; this version posted September 11, 2023. The copyright holder for this preprint (which was not certified by peer review) is the author/funder, who has granted bioRxiv a license to display the preprint in perpetuity. It is made available under aCC-BY-NC-ND 4.0 International license.

Figure 6. Condensin counteracts cohesin at telomeres. (A) Top panel: WT, *rad21-K1* or *rad21-K1 cut3-477* cells were shifted to the restrictive temperature of 36°C for three hours, fixed with formaldehyde and directly imaged. Telomeres were visualized via Taz1-GFP (green) and spindle pole bodies (SPBs) via Cdc11-CFP (blue). Lower panels: number of telomeric foci according to the distance between SPBs at 36°C (n>90 cells for each strain). The data shown are from a single representative experiment out of three repeats. (**B**) Psm3-GFP calibrated ChIP-qPCR from cells synchronized in G2/M and shifted at 36°C to inactivate condensin during the G2 block (time 0 min) and upon their release in anaphase (time 30 min). Left panel: cell cycle stages determined by DAPI staining. Right panel: ChIP-qPCR results. *cendh1, kgd1* and *lvs1* are cohesin binding sites, while *exg1, gas1* and *rRNA37* are condensin binding sites. Percentage of IP with Psm3-GFP have been normalized using *S. cerevisiae* (S.c.) CEN4 locus. Shown are the averages and standard deviations from 3 independent biological and technical replicates.

Figure 7. Model for condensin-driven sister-telomere disjunction. Loop extruding condensin accumulates against a barrier formed by arrays of Taz1 proteins bound to telomeric repeats, allowing condensin-mediated DNA translocation to pass a threshold beyond which the ties between sister-telomeres such as cohesin would be eliminated. See Discussion for details.

SUPPLEMENTARY DATA

Figure S1. Fission yeast condensin is enriched at telomeres during metaphase and anaphase. (A) Telomeric plasmid pNSU70 (Sugawara, 1988) aligned against the *S. pombe* genome (ASM294v2) using Blast shows a best hit with cosmid SPBCT2R1 that corresponds to the right end of chromosome 2 (nucleotides 4500619 to 4539800 in the ASM294v2 genome). SPBCT2R1 was aligned with pNSU70 using Clustal Omega (Madeira *et al*, 2019) and the nucleotides 4137 to 7223 of pNSU70 were added to the sequence of chromosome 2 at position 4539800 to create a TEL2R-extended version of the genome, which is available under the accession number GSE196149. **(B)** Principle of the base per base normalisation method applied to ChIPs to assess the occupancy of Cnd2-GFP from *S. pombe* (S.p.) at repeated DNA elements using chromatin from *S. cerevisiae* (S.c.) cells expressing SMC3-GFP for internal calibration. (**C**) Results of the base per base normalization method applied to calibrated ChIP-seq data to correct for biases in coverage

bioRxiv preprint doi: https://doi.org/10.1101/2022.03.18.484892; this version posted September 11, 2023. The copyright holder for this preprint (which was not certified by peer review) is the author/funder, who has granted bioRxiv a license to display the preprint in perpetuity. It is made available under aCC-BY-NC-ND 4.0 International license.

in the IP and Total (T) fractions. Calibrated read counts obtained in the IP and Total (T) fractions, and their base per base ratios (IP/T) obtained at centromere 2 (*cen 2*), composed of a central core (cc) flanked by repetitive heterochromatic outer repeats (otr) and at rDNA repeats are shown. The single-copy gene *exg1* serves as a non-repetitive control. (**D**) Calibrated read-counts and base per base IP/T ratios obtained at TEL2R for two biological and technical replicates. Data from replicate #1 are also shown in Figure 1C. (**E**) Results from calibrated ChIP-seq against Cnd2-GFP in metaphase arrests WT and *cut3-477* condensin mutant. Shown are the base per base ratios and metagene profiles obtained from two biological and technical replicates. Mitotic indexes of cell cultures were: WT (77% ± 6%), *cut3-477* (70% ± 5%).

Figure S2. Condensin takes part in telomere disjunction during anaphase in a decatenation-independent manner. (**A**) left panel: Condensin mutant cells *cut14-208* grown at the permissive temperature (25°C) or shifted to the restrictive temperature of 36°C for three hours were fixed with formaldehyde and stained with calcofluor to reveal the septum. Telomeres were visualized via Taz1-GFP (green), kinetochores/centromeres via the colocalization of Mis6-RFP (red) and Ndc80-GFP (green), and spindle pole bodies (SPBs) via Cdc11-CFP (blue). Right panel: number of telomeric foci according to the distance between SPBs at 25°C and 36°C in the *cut14-208* mutant (n>90 cells for each strain). The data shown are from a single representative experiment out of three repeats. (**B**) Left panel: WT or *cut14-208* condensin mutant cells shifted to the restrictive temperature of 36°C for three hours were fixed with formaldehyde and directly imaged. Sister telomeres 1L (Tel1-GFP, green), sister centromeres 3L (imr3-tdTomato, red) and the nucleolus (Gar1-CFP) were visualized. Right panel: number of telomeric foci according to the distance between sister-centromeres 3L at 36°C (n>43 cells for each strain). The data shown are from a single representative experiment out of three repeats. (**C**) Kymograph representation of kinetochore dynamics in live *top2-250* mutant cells at permissive temperature (25°C) or restrictive temperature (18°C). Kinetochores are visualized via Ndc80-GFP (green) and SPBs via Cdc11-CFP (red). Right panel. Quantification of the percentage of *top2-250* anaphase cells showing lagging centromeres. Error bars indicate SD obtained from three independent experiments (n=100 for each condition).

bioRxiv preprint doi: https://doi.org/10.1101/2022.03.18.484892; this version posted September 11, 2023. The copyright holder for this preprint (which was not certified by peer review) is the author/funder, who has granted bioRxiv a license to display the preprint in perpetuity. It is made available under aCC-BY-NC-ND 4.0 International license.

Figure S3. Condensin deficiency increases contact frequencies between telomeres in metaphase. Data from the biological and technical replicate of those shown in Fig. 3. (**A**) Mitotic indexes of cell cultures used for Hi-C. (**B**) Hi-C contact probability matrix at 25 kb resolution of wild-type cells arrested in metaphase at 33°C. Contacts between telomeres (arrows) and centromeres (circles) are indicated (**C**) Median contact probabilities as a function of distance along the chromosomes for wild-type and *cut14-208* cells arrested in metaphase at 33°C. (**D**) Hi-C difference map at 25 kb resolution comparing *cut14-208* and wild-type cells. (**E**) Aggregation of contact frequencies at chromosome ends in wild-type and *cut14-208* mutant cells in metaphase at 33°C. Boxes indicate the median, 1st and 3rd quartiles, whiskers extend to minimum and maximum values and notches represent the 95% confidence interval for each median. Data points are shown as grey circles.

Figure S4. Taz1 specifically enriches condensin at telomeres. (A) Cnd2-GFP calibrated ChIP-qPCR shown in Figure 1C were normalized with respect to their corresponding IP/T ratios of budding yeast SMC3-GFP at CEN4. *cnt1* is the kinetochore domain of *cen1* while *exg1*, *gas1* and *cnd1* loci are high or low occupancy binding sites on chromosome arms. Shown are the average and standard deviations from n=3 biological and technical replicates. (**B**) Cnd2-GFP occupancy at non-telomeric Taz1 islands in wild-type or *cut14-208* mutant cells arrested in metaphase, as determined by calibrated ChIP-seq (n =2 biological and technical replicates). (**C**) Summary of the ChIP-seq results obtained at several representative Taz1 islands (Zofall *et al*, 2016). (**D**) Cnd2-GFP calibrated ChIP-qPCR from indicated metaphase arrests. Left panel: mitotic indexes of cell cultures used for ChIP. Right panel: results of calibrated ChIP-qPCR. Shown are averages and sd from 6 independent biological and technical replicates. (**E**) Left panel: genome browser views of Cnd2-GFP calibrated ChIP-seq in indicated metaphase arrests, with two independent biological and technical replicates (#). Replicate #1 is shown in Figure 4. Right panel: metagene profile of all condensin binding sites along chromosome arms from replicate #2. TSS (Transcription Start Site), TES (Transcription End Site).

Figure S5. Condensin counteracts cohesin at telomeres

Psm3-GFP calibrated ChIP-qPCR from cells synchronized at G2/M (time 0 min; top panel) and

bioRxiv preprint doi: https://doi.org/10.1101/2022.03.18.484892; this version posted September 11, 2023. The copyright holder for this preprint (which was not certified by peer review) is the author/funder, who has granted bioRxiv a license to display the preprint in perpetuity. It is made available under aCC-BY-NC-ND 4.0 International license.

upon their release in anaphase (time 30 min; bottom panel). *cendh1*, *kgd1* and *lvs1* loci are cohesin binding sites, while *exg1*, *gas1* and *rRNA37* loci are condensin binding sites. Percentage of IP with Psm3-GFP has been normalized using *S. cerevisiae* (S.c.) CARIV locus. Shown are the averages and standard deviations (sd) from 3 independent biological and technical replicates.

Figure S6. Condensin counteracts cohesin at telomeres

cut3-477 and *cut3-477 rad21-K1* mutants were grown at permissive temperature and small, early G2 cells were purified using a lactose gradient. After synchronization, the entire cell population was in G2 (0% of cells in mitosis or cytokinesis). Purified early G2 cells were shifted to the restrictive temperature of 36°C and telomeric foci were scored according to the distance between SPBs (n>80 cells for each strain). The data shown are from a single representative experiment out of three repeats.

DATA AND MATERIALS AVAILABILITY

Raw and processed data from calibrated-ChIP-seq, Hi-C and the TEL2R-extended ASM294v2 version of the fission yeast genome, are available at the NCBI Gene Expression Omnibus (GEO) repository under the accession number GSE196149.

MATERIALS AND METHODS

Media, molecular genetics and cell culture

Media, growth, maintenance of strains and genetic methods were as described (Moreno *et al*, 1991). Standard genetics and PCR-based gene targeting method (Bahler *et al*, 1998) were used to construct *S. pombe* strains. All fluorescently tagged proteins used in this study are expressed from single-copy genes under the control of their natural promoters at their native chromosomal locations. Strains used in this study are listed in Table S1. For metaphase arrests used in ChIP and Hi-C experiments, cells expressing the APC/C co-activator Slp1 under the thiamine-repressible promoter *nmt41* (Petrova *et al*, 2013) were cultured in synthetic PMG medium at 30°C, arrested in metaphase for 2h at 30°C by the adjunction of thiamine (20 µM final) and shifted at indicated restrictive temperatures for 1 hour. For Hi-C, the cultures were arrested for 3h at 33°C. Mitotic indexes were determined by scoring the percentage of cells exhibiting Cnd2-GFP fluorescence in

bioRxiv preprint doi: https://doi.org/10.1101/2022.03.18.484892; this version posted September 11, 2023. The copyright holder for this preprint (which was not certified by peer review) is the author/funder, who has granted bioRxiv a license to display the preprint in perpetuity. It is made available under aCC-BY-NC-ND 4.0 International license.

their nucleoplasm (Sutani *et al*, 1999). G2/M block and release experiments were performed using an optimized cdc2-as allele (Aoi *et al*, 2014). Cells were arrested in late G2 by 3h incubation in the presence of 3-Br-PP1 at 2 µM final concentration (#A602985, Toronto Research Chemicals). Cells were released into synchronous mitosis by filtration and 3 washes with prewarmed liquid growing medium. For the viability spot assay, cell suspensions of equal densities were serially diluted five-fold and spotted on solid YES medium, the first drop containing 10^7 cells. For microscopy, cells were grown in yeast extract and centrifuged 30 sec at 3000 g before mounting onto an imaging chamber. Total protein extractions for western blotting were performed by precipitation with TCA as previously described (Grallert & Hagan, 2017).

Lactose gradient for G2 cells purification

Cell synchrony was achieved by lactose gradient size selection. Log phase cells (50ml of 5.10^6 cells) were concentrated in 2ml and loaded onto a 50ml 7-35% linear lactose gradient at 4°C. After 10min centrifugation at 1600rpm at 4°C, 3ml of the upper of two visible layers was collected and washed twice in cold YES media before being resuspended in fresh medium. At this stage, cells were released at 36°C and fixed every 20min until the first mitotic peak.

Cell imaging and fast microfluidic temperature control experiments

Live cell analysis was performed in an imaging chamber (CoverWell PCI-2.5, Grace Bio-Labs, Bend, OR) filled with 1 ml of 1% agarose in minimal medium and sealed with a 22 × 22-mm glass coverslip. Time-lapse images of Z stacks (maximum five stacks of 0.5 µm steps, to avoid photobleaching) were taken at 30 or 60 sec intervals. Images were acquired with a CCD Retiga R6 camera (QImaging) fitted to a DM6B upright microscope with a x100 1.44NA objective, using MetaMorph as a software. Intensity adjustments were made using the MetaMorph, Image J, and Adobe Photoshop packages (Adobe Systems France, Paris, France). Fast microfluidic temperature control experiments were performed with a CherryTemp from Cherry Biotech. To determine the percentage of chromatin bridges with unseparated telomeres, cells were fixed in 3.7% formaldehyde for 7 min at room temperature, washed twice in PBS, and observed in the presence of DAPI/calcofluor.

Image processing and analysis

bioRxiv preprint doi: https://doi.org/10.1101/2022.03.18.484892; this version posted September 11, 2023. The copyright holder for this preprint (which was not certified by peer review) is the author/funder, who has granted bioRxiv a license to display the preprint in perpetuity. It is made available under aCC-BY-NC-ND 4.0 International license.

The position of the SPBs, kinetochores/centromeres and telomeres were determined by visualization of the Cdc11–CFP, Ndc80–GFP/Mis6-RFP and Taz1-GFP/Ccq1-GFP signals. Maximum intensity projections were prepared for each time point, with the images from each channel being combined into a single RGB image. These images were cropped around the cell of interest, and optional contrast enhancement was performed in MetaMorph, Image J or Photoshop where necessary. The cropped images were exported as 8-bit RGB-stacked TIFF files, with each frame corresponding to one image of the time-lapse series. For both channels, custom peak detection was performed. The successive positions of the SPBs were determined. The number of telomeres during spindle elongation was determined by visual inspection.

Telomere length analysis by Southern blotting

Genomic DNA was prepared and digested with *Apa*I. The digested DNA was resolved in a 1.2% agarose gel and blotted onto a Hybond-XL membrane. After transfer, DNA was crosslinked to the membrane with UV and hybridized with a radiolabelled telomeric probe. The telomeric DNA probe was extracted by digestion of pIRT2-Telo plasmid by *Sac*I/*Pst*I.

ChIP and calibrated-ChIP

Fission yeast cells, expressing either Cnd2-GFP or NLS-GFP, and arrested in metaphase by the depletion of Slp1, were fixed with 1% formaldehyde for 5 min at culture temperature and 20 min at 19°C in a water bath, quenched with glycine 0.125 M final, washed twice with PBS, frozen in liquid nitrogen and stored at -80°C until use. For calibration, *Saccharomyces cerevisiae* cells expressing Smc3-GFP were grown in Yeast Peptone Dextrose liquid medium at 30°C in log phase and fixed with 2.5% formaldehyde for 25 min. 2.10^8 fission yeast cells were used per ChIP experiment. To perform calibrated ChIP the same amount of fission yeast cells was mixed with 4.10^7 budding yeast cells. Cells were resuspended in lysis buffer (50 mM Hepes KOH pH 7.5, NaCl 140 mM, EDTA 1 mM, Triton X-100 1%, sodium deoxycholate 0.1%, PMSF 2mM) supplemented with a protease inhibitor cocktail (cat. 11836170001, Roche), and lysed with Precellys ®. Chromatin was sheared to ~ 300 bp fragments with Covaris ® S220 (18 min at duty factor 5%, 200 cycles per burst, and 140W peak power), clarified twice by centrifugation at 9600 g at 4°C and adjusted to 1 mL final with lysis buffer. For ChIP, two 60 µl aliquots of chromatin each served as Total (input) fractions, while two aliquots of 300 µl of chromatin (IPs) were

bioRxiv preprint doi: https://doi.org/10.1101/2022.03.18.484892; this version posted September 11, 2023. The copyright holder for this preprint (which was not certified by peer review) is the author/funder, who has granted bioRxiv a license to display the preprint in perpetuity. It is made available under aCC-BY-NC-ND 4.0 International license.

incubated each with 35 µl of Dynabeads™ protein A (cat. 10002D, Invitrogen) and 8 µg of anti-GFP antibody (cat. A111-22, Invitrogen). For calibrated-ChIP-seq one 60 µl aliquot of chromatin served as Total (T) fraction and IP was performed on 600 µl of chromatin using 75 µl of Dynabeads™ proteinA and 16 µg of anti-GFP antibody. T and IP samples were incubated overnight in a cold room, IPs being put on slow rotation. IPs were washed on a wheel at room temperature for 5 min with buffer WI (Tris-HCl pH8 20 mM, NaCl 150 mM, EDTA 2 mM, Triton X-100 1%, SDS 0.1%), WII (Tris-HCl pH8 20 mM, NaCl 500 mM, EDTA 2 mM, Triton X-100 1%, SDS 0.1%) and WIII (Tris-HCl pH8 10 mM, sodium deoxycholate 0.5%, EDTA 1 mM, Igepal 1%, LiCl 250 mM) and twice with TE pH8 without incubation. Immunoprecipitated materials on beads and T samples were brought to 100 µl in TE pH8, supplemented with RNAse A at 1µg/µl and incubated 30 min at 37°C. 20 µg of proteinase K was added and tubes were incubated 5h at 65°C. For calibrated-ChIPseq, IPs on beads were eluted in Tris 50 mM, EDTA 10 mM, SDS 1% 15 min at 65°C. Supernatants were transferred to a new tube supplemented with RNAse A at 1µg/µl and incubate 1h at 37°C. 200 µg of proteinase K was added followed by an incubation of 5h at 65°C. DNA was recovered using QIAquick PCR Purification Kit, following manufacturer's instructions. For calibrated ChIP-qPCR, real time quantitative (q) PCRs were performed on a Rotor-Gene PCR cycler (Qiagen) using Quantifast (Qiagen) SYBR Green. The ratios (IP/T) calculated for fission yeast DNA sequences where normalized to their associated IP/T ratio calculated for budding yeast CARIV or CEN4 DNA sequences bound by SMC3-GFP. For calibrated ChIP-seq, Total and IPed DNA samples were washed with TE pH8 and concentrated using Amicon® 30K centrifugal filters, and libraries were prepared using NEBNext® Ultra™ II DNA Library Prep Kit for Illumina® kits according to the manufacturer's instructions. DNA libraries were size-selected using Ampure XP Agencourt beads (A63881) and sequenced paired-end 150 bp with Novaseq S6000 (Novogene®).

Hi-C sample preparation

Fission yeast cells, expressing Cnd2-GFP and arrested in metaphase by the depletion of Slp1 were fixed with 3% formaldehyde for 5 min at 33°C followed by 20 min at 19°C, washed twice with PBS, frozen in liquid nitrogen and stored at -80°C. 2.10^8 cells were lysed in ChIP lysis buffer with Precellys ®. Lysates were centrifuged 5000 g at 4°C for 5 min and pellets were resuspended once in 1 ml lysis buffer and twice in NEB® 3.1 buffer. SDS was added to reach 0.1% final and samples

bioRxiv preprint doi: https://doi.org/10.1101/2022.03.18.484892; this version posted September 11, 2023. The copyright holder for this preprint (which was not certified by peer review) is the author/funder, who has granted bioRxiv a license to display the preprint in perpetuity. It is made available under aCC-BY-NC-ND 4.0 International license.

were incubated for 10 min at 65°C. SDS was quenched on ice with 1% Triton X-100 and DNA digested overnight at 37°C with 200 Units of *Dpn*II restriction enzyme. Samples were incubated at 65°C for 20 min to inactivate *Dpn*II. Restricted-DNA fragments were filled-in with 15 nmol each of biotin-14-dATP (cat. 19524016, Thermofisher), dTTP, dCTP and dGTP, and 50 units of DNA Klenow I (cat. M0210M, NEB) for 45 min at 37°C. Samples were diluted in 8 ml of T4 DNA ligase buffer 1X and incubated 8 hours at 16°C with 8000 Units of T4 DNA ligase (NEB). Crosslinks were reversed overnight at 60°C in the presence of proteinase K (0.125 mg / ml final) and SDS 1% final. 1 mg of proteinase K was added again and tubes were further incubated for 2 hours at 60°C. DNA was recovered by phenol-chloroform-isoamyl-alcohol extraction, resuspended in 100 µl TLE (Tris/HCl 10 mM, 0.1 mM EDTA, pH8) and treated with RNAse A (0.1 mg / ml) for 30 min at 37°C. Biotin was removed from unligated ends with 3 nmol dATP, dGTP and 36 Units of T4 DNA polymerase (NEB) for 4 hours at 20°C. Samples were incubated at 75°C for 20 min, washed using Amicon® 30k centrifugal filters and sonicated in 130 µl H_2O using Covaris® S220 (4 min 20°C, duty factor 10%, 175W peak power, 200 burst per cycle). DNA was end-repaired with 37.5 nmol dNTP, 16.2 Units of T4 DNA polymerase, 54 Units of T4 polynucleotide kinase, 5.5 Units of DNA Pol I Klenow fragment for 30 min at 20°C and then incubated for 20 min at 75°C. Ligated junctions were pulled-down with Dynabeads® MyOne™ Streptavidin C1 beads for 15 min at RT and DNA ends were A-tailed with 15 Units of Klenow exo- (cat. M0212L, NEB). Barcoded PerkinElmer adapters (cat. NOVA-514102) were ligated on fragments for 2 hours at 22°C. Libraries were amplified with NextFlex PCR mix (cat. NOVA-5140-08) for 5 cycles, and cleaned up with Ampure XP Agencourt beads (A63881). Hi-C libraries were paired-end sequenced 150bp on Novaseq6000.

Calibrated ChIP-seq data analysis

Scripts and pipelines are available in the git repository https://gitbio.ens-lyon.fr/LBMC/Bernard/chipseq (tag v0.1.0). Analyses have been performed based on the method described by Hu et al. (Hu *et al*, 2015), using a modified version of the nf-core/chipseq (version 2.0.0) pipeline (https://doi.org/10.1038/s41587-020-0439-x) executed with `nextflow` (version 23.02.1). We used the *S. pombe* genome (ASM294v2, or its TEL2-R extended version available at Omnibus GEO GSE196149) and the *S. cerevisiae* genome (sacCER3 release R64-1-1).) for internal calibration. Technical details regarding our calibrated-ChIP-seq pipeline are available in

bioRxiv preprint doi: https://doi.org/10.1101/2022.03.18.484892; this version posted September 11, 2023. The copyright holder for this preprint (which was not certified by peer review) is the author/funder, who has granted bioRxiv a license to display the preprint in perpetuity. It is made available under aCC-BY-NC-ND 4.0 International license.

the Appendix Supplementary Methods section. Of note, we noticed a sharp decrease in the number of reads passed the coordinate 4,542,700 at the right end of chromosome II, i.e. within the telomeric repeats of TEL2R, in Total extracts. Thus, to avoid any biased enrichment in our IP/Total ratios, all calibrated ChIP-seq results concerning TEL2R have been taken within the limit of the position 4,542,700 within telomeric repeats of TEL2R.

Hi-C data analysis

Computational analyses of Hi-C data were performed with R (version 3.4.3). Reads were aligned on the genome of *S. pombe* version ASM294v2 using bwa (version 0.7.17-r1188) with default settings. Hi-C contacts matrices of DpnII digested genomic fragments were normalized and processed using Juicer (version 1.6: https://github.com/aidenlab/juicer). Hi-C reads were binned to a resolution of 5 kb using a square root vanilla count normalization. 2D plots were performed for normalized (observed/expected) Hi-C read counts using Juicebox. Differential 2D plots were visualized in Log2 (of normalized Hi-C reads in mutants / normalized Hi-C reads in wild-type control). Aggregation of Hi-C data was performed essentially as previously described (Liang *et al*, 2014; Rao *et al*, 2014) with the following modified parameters for adaptation to 3D contacts at telomeres: Hi-C reads were counted over bins of 5 kb over a 150 kb distal region covering both telomeres of each chromosome. Long-range interactions were assessed for all combinations of telomeres over a sliding matrix (21x21 bins). To optimize detection of long-range interactions between telomeres, a quantilization was performed by ranking the 21x21 bins of every sub-matrix contributing to the aggregation, allowing to assess interactions from averaged values. Statistical analyses were performed both for the corresponding quantilized matrices, and verified with non-quantilized matrices, using a Mann-Whitney-Wilcoxon test using R (Stats4) and validated for each of the replicates made for every mutant and wild-type conditions.

bioRxiv preprint doi: https://doi.org/10.1101/2022.03.18.484892; this version posted September 11, 2023. The copyright holder for this preprint (which was not certified by peer review) is the author/funder, who has granted bioRxiv a license to display the preprint in perpetuity. It is made available under aCC-BY-NC-ND 4.0 International license.

1000

Table S1. Strain list used in this study

Strain	Genotype	Figures
LY4682	*h- leu1-32 ura4D18 cdc2asM17*	Fig. 1B
LY4731	*h- leu1-32 ura4D cdc2asM17 cnd2-GFP-LEU2*	Fig. 1B
LY6281	*Mata ade2-1 his3-11 his3-15 ura3 leu2-3 trp1-1 can1-100 SMC3-GFP-KanR*	Fig. 1C-D, S1, 4 & S4
LY4483	*h- leu1-32 ura4D-18 ura4-Pnmt41-slp1+ cnd2-GFP-LEU2*	Fig. 1C-E, S1, 3 & S3, 4 & S4
LY6305	*h- leu1-32 ura4D cut14-208 ura4-Pnmt41-slp1+ cnd2-GFP-LEU2*	Fig. 1C-E, S1D, 3 & S3, S4B
LY6304	*h+ leu1-32 ura4D cut3-477 ura4-Pnmt41-slp1+ cnd2-GFP-LEU2*	Fig. 1E, S1E
LY5480	*leu1- ura4- ade6- ura4-Pnmt41-slp1+ aur1::padh21-NLS-GFP-9PK::aur1R*	Fig. 4A, 4C, S4A & S4D
LY5298	*h? leu1-32 ura4D18 ade6-21? KanR-Pnmt1-slp1+ taz1Δ::ura4+ cnd2-GFP-LEU2*	Fig. 4A, 4C, S4A
LY5948	*h- leu1-32 ura4D ura4-Pnmt41-slp1+ rap1Δ::KanR cnd2-GFP-LEU2*	Fig. 4A, 4C, S4A
LY5898	*h+ leu1-32 ura4D ura4-Pnmt41-slp1+ mit1Δ::KanR cnd2-GFP-LEU2*	Fig. 4D-E, S4D-E
ST1711	*h+ cdc11-CFP::KanR taz1-GFP::KanR mis6-2mRFP::hph*	Fig. 2A-B
ST2624	*h?cut3-477 cdc11-CFP::KanR taz1-GFP::KanR mis6-2mRFP::hph*	Fig. 2B
ST1738	*h? cut14-208 cdc11-CFP::KanR taz1-GFP::KanR mis6-2mRFP::hph*	Fig2A & Fig.S2A
ST2622	*h?cut3-477 cdc11-CFP::KanR taz1-GFP::KanR*	Fig.2D, 5C, 6A
ST1665	*h? top2-250 cdc11-CFP:: KanR taz1-GFP:: KanR*	Fig.2D-E
FY24566	*h+ imr3L-tetO-ura4+ Z:adh31-tetR-tdTomato<<natr his7+<<Pdis1-GFP-lacI leu1 ade6 tel1L-lacO-kanr C:adh21-gar1-CFP<<hygr* (Tada et al. 2011)	Fig.S2B
ST2640	*h? cut14-208 imr3L-tetO-ura4+ Z:adh31-tetR-tdTomato<<natr his7+<<Pdis1-GFP-lacI leu1 ade6 tel1L-lacO-kanr C:adh21-gar1-CFP<<hygr*	Fig.S2B
PR109	*h- leu1-32 ura4D-18*	Fig. 5B, S2C
SC388	*h- leu1-32 ura4D-18 ade6-M210 taz1 ::ura4+*	Fig. 5B

bioRxiv preprint doi: https://doi.org/10.1101/2022.03.18.484892; this version posted September 11, 2023. The copyright holder for this preprint (which was not certified by peer review) is the author/funder, who has granted bioRxiv a license to display the preprint in perpetuity. It is made available under aCC-BY-NC-ND 4.0 International license.

LY999	*h- leu1-32 ura4D ade6-M210 cut3-477 :NatR*	Fig. 5B, S2C
SC1432	*h ? leu1-32 ura4D-18 taz1::ura4+ cut3-477 :NatR*	Fig. 5B
ST1928	*h? taz1::ura+ cut3-477 ccq1-GFP::KanR cdc11-CFP:: KanR ura4D-18*	Fig. 5A
ST1664	h? *top2-250 ndc80-GFP:: KanR cdc11-CFP:: KanR mis6-RFP-hyg*	Fig. S2C
ST1172	*h? ccq1-GFP:: KanR cdc11-CFP:: KanR*	Fig. 5A
ST1183	*h- taz1::KanR ccq1-GFP::KanR cdc11-CFP:: KanR*	Fig. 5A
ST1657	*h- cut3-477 ccq1-GFP:: KanR cdc11-CFP :: KanR*	Fig. 5A
ST2636	*h? mit1::hph cdc11-CFP:: KanR taz1-GFP:: KanR*	Fig. 5C
LY646	*h- leu1-32 ura4D-18 cut14-90*	Fig. 2C
LY140	*h- leu1-32 ura4D cut14-208*	Fig. 2C
LY1252	*h- leu1-32 ura4D ade6-M210 cut14-180*	Fig. 2C
LY3185	*h- ura4D ade6-M210 cut3-M26*	Fig. 2C
LY3186	*h- ura4D ade6-M210 cut3-I23-GFP:his7+*	Fig. 2C
LY4681	*h+ leu1-32 ura4D18 cdc2asM17*	Fig. 6B, S5
LY7260	*h+ leu1-32 ura4D? ade6-210 cdc2asM17 psm3-GFP-NatR*	Fig. 6B, S5
LY7262	*h+ leu1-32 ura4D? ade6-210 cdc2asM17 psm3-GFP-NatR cut3-477*	Fig. 6B, S5
STCS138	*h? rad21-K1 cdc11-CFP:: KanR taz1-GFP:: KanR*	Fig.6A, S6A
ST2638	*h? rad21-K1 cut3-477 cdc11-CFP:: KanR taz1-GFP:: KanR*	Fig.6A, S6A

1005

bioRxiv preprint doi: https://doi.org/10.1101/2022.03.18.484892; this version posted September 11, 2023. The copyright holder for this preprint (which was not certified by peer review) is the author/funder, who has granted bioRxiv a license to display the preprint in perpetuity. It is made available under aCC-BY-NC-ND 4.0 International license.

Table S2. Primers used for qPCR

Site	Forward primer	Reverse primer
cnt1	ACCGTTGCAACTTACATCAGC	GGTCGCCAAATAGCAATGAG
exg1	CACATAGACGGACCACTTTGAG	ATATGTCACCTGTGGCTGAGTG
gas1	AATAGCATGTCGAGGTTGTATGG	TGTCATCGCGAAACCTTACC
cnd1	AGCAATTAGCCGAACGTCTG	CACCACATGATCCCATTGAC
cdc22	CGGGCTAAATTGAGGTATGG	CGCAGTTGCACTTTTCAAAC
gly05	GACGTTGTGCTAAAAGGTGTTG	GGAAATCGAGCAGAGGTCAG
rRNA37	TAGGATCGCTGAGAATCCATC	TGGATTAAAACACATTGCTTGC
arg04	CATTAATCCGCCGTGGATAG	TTCACCTAATAGTTGCCAAACG
cendh1	CGCTTTGTTGTCGTGGACTA	AACACGGCGATAAGAAATGG
kgd1	GCTTCAGATCATTTGGTCCAG	GGAATTCATGGCATTGGAAC
lvs1	GGCATTTGTCGGTAACACTC	GTTTGCAGCGACTGTGTTTC
tel30	GAAATTGTGCCACGTTGGAG	GACAGGGTCCTTGCTAAGTTTC
tel19	CGGGATAACACACATGCAAC	GCTTTGATGGCAACTGGTTC
tel13	CCAATCCCCAGGTTTCTTTC	TTTCGACCTATCAGCGGTTG
tel9.2	ACACGCTCTGACAACATTCG	CGCAATCTCGATTACCGAAC
tel6.1	AAACAACTGCAAGCGGTAGG	CGCATTTACCATTCCTCCAC
tel2.4	AGCAGGGGACTATATTGGAGTG	CCCCTTCAATTACCAAAGTCCAC
tel0	GTGTGGAATTGAGTATGGTGAA	CGGCTGACGGGTGGGGCCCAATA
isl7	ACACTTGTTTCAGCCGATTTC	AAGCATTGCTCCATTAAAACAAC
isl13	ATGAAGGTACGGAAGCAACG	TAGCCCTTTCATTAATAGCTTCG
isl15	AGAAAAGGCAATGCGAGAGC	CGCAAATCATCTGACATTGG
scCARIV	TCAGGGAAGGTACGGAAATG	GCATGACTATTCGCGTTTGAG
scCEN4	AAATGCCGAGGCTTTCATAG	GTGACGATAAAACCGGAAGG

Table S3. Antibodies used in this study

Antibody	target	experiment
A-11122 (Invitrogen)	Anti-GFP	ChIP
Tat-1 (a gift from Keith Gull)	Anti-α-Tubulin	Western blot
Cnd2 (euromedex, GTX64102)	Anti-Cnd2 fission yeast	Western blot
anti-rabbit NA9340V Amersham	Anti-rabbit secondary	Western blot
anti-mouseNA931 -1ml Amersham	Anti-mouse secondary	Western blot

bioRxiv preprint doi: https://doi.org/10.1101/2022.03.18.484892; this version posted September 11, 2023. The copyright holder for this preprint (which was not certified by peer review) is the author/funder, who has granted bioRxiv a license to display the preprint in perpetuity. It is made available under aCC-BY-NC-ND 4.0 International license.

Appendix Supplementary Methods

Scripts and pipelines are available in the git repository https://gitbio.ens-lyon.fr/LBMC/Bernard/chipseq (tag v0.1.0). Pipelines were executed with `nextflow` (version 23.02.1). In the subsequent section, *genome* refers to the *S. pombe* genome (*ASM294v2, or its TEL2-R extended version available at* Omnibus GEO GSE196149), while *calibration genome* refers to the genome of *S. cerevisiae* (sacCER3 release R64-1-1) used for internal calibration. To perform the analyses, we use a modified version of the nf-core/chipseq (version 2.0.0) pipeline (https://doi.org/10.1038/s41587-020-0439-x). We modified this pipeline as follows: We added an optional `--fasta_calibration` parameter to pass the calibration genome. We modified the subworkflow `prepare_genome.nf` to run `GUNZIP_FASTA` on both the `--fasta` and `--fasta_calibration` files and merge the two fasta file with the `MIX_FASTA` process, while adding a `cali_` prefix to the names of the chromosome of the calibration genome. The workflow chipseq.nf was modified to run a new process, `BAM_CALIB` (replacing `BEDTOOLS_GENOMECOV`), on the IP bam file and their corresponding Total (INPUT) bam file to generate calibrated IP and INPUT bigwig files. The workflow chipseq.nf was modified to then run `BIGWIG2BAM` to generate synthetic bam files from the output of `BAM_CALIB`. These synthetic bam files are single-end and replace the output of the mapping step in the next parts of the pipeline. The `BIGWIG2BAM` outputs are indexed with a `SAMTOOLS_INDEX` process. The `BAM_CALIB` tool (https://gitbio.ens-lyon.fr/LBMC/Bernard/bamcalib v0.1.5) takes into inputs a sorted bam file for the IP data and a sorted bam file for the TOTAL data (mapped on the concatenation of the two genomes), and output a calibrated bigwig for the reference genome. For the normalization, we modified a previously described method (Hu *et al*, 2015) in order to account for biases in coverages in the TOTAL fractions. We introduce the following notation: $IP_x(t)$ is the coverage at position t in the IP sample on the reference genome, $IP_c(t)$ is the coverage at position t in the IP sample on the calibration genome, $WCE_x(t)$ is the coverage at position t in the TOTAL (whole cell extract) sample on the reference genome, and $WCE_c(t)$ the coverage at position t in the TOTAL sample on the calibration genome. In a reference genome of size T_x (ignoring the chromosome segmentation), and in a calibration genome of size T_c, Hu et al. compute the Occupancy Ratio (OR) as follows (Hu *et al*, 2015):

bioRxiv preprint doi: https://doi.org/10.1101/2022.03.18.484892; this version posted September 11, 2023. The copyright holder for this preprint (which was not certified by peer review) is the author/funder, who has granted bioRxiv a license to display the preprint in perpetuity. It is made available under aCC-BY-NC-ND 4.0 International license.

$$\mathrm{OR} = \frac{10^6 \sum_{t'=1}^{T_c} WCE_c\left(t'\right)}{\sum_{t'=1}^{T_c} IP_c\left(t'\right) \sum_{t'=1}^{T_x} WCE_x\left(t'\right)}$$

Instead, we used the following formula with β (default to 10^3) an arbitrary scaling factor.

$$\mathrm{norm}IP\left(t\right) = IP_x\left(t\right) \frac{\beta \frac{1}{T_c} \sum_{t'=1}^{T_c} WCE_c\left(t'\right)}{\frac{1}{T_c} \sum_{t'=1}^{T_c} IP_c\left(t'\right) \frac{1}{T_x} \sum_{t'=1}^{T_x} WCE_x\left(t'\right)}$$

This formula can be described as follows:

The technical variations on the IP efficiencies are corrected by scaling $\mathrm{IP}_x\left(t\right)$ by the calibration genome coverage:

$$\frac{1}{\frac{1}{T_c} \sum_{t'=1}^{T_c} IP_c\left(t'\right)}$$

To account for variations in cells proportion, we correct by a scaled WCE coverage:

$$\frac{\frac{1}{T_c} \sum_{t'=1}^{T_c} WCE_c\left(t'\right)}{\frac{1}{T_x} \sum_{t'=1}^{T_x} WCE_x\left(t'\right)}$$

To be able to analyze the coverage information at repetitive regions of the genome, we propose to normalize the signal nucleotide by nucleotide and introduce the OR ratio:

$$\mathrm{ratio}IP\left(t\right) = \frac{\mathrm{norm}IP\left(t\right)}{\mathrm{norm}WCE\left(t\right)}$$

with:

$$\mathrm{norm}WCE\left(t\right) = WCE_x\left(t\right) \frac{1}{\frac{1}{T_c} \sum_{t'=1}^{T_c} WCE_c\left(t'\right)} \alpha$$

We then find α such that (not to distort the $\mathrm{norm}IP$ signal on average):

$$E\left(\mathrm{norm}IP\left(t\right)\right) = E\left(\frac{\mathrm{norm}IP\left(t\right)}{\mathrm{norm}WCE\left(t\right)}\right)$$

which gives

$$\mathrm{norm}WCE\left(t\right) = WCE_x\left(t\right) \frac{1}{\sum_{t'=1}^{T_x} IP_x\left(t'\right)} \sum_{t'=1}^{T_x} \frac{IP_x\left(t'\right)}{WCE_x\left(t'\right)}$$

With this method, we retain the internal calibration developed by Hu et al. (Hu *et al*, 2015) and we account for variations in read density at each base in WCE samples.

In the BAM_CALIB tools, the coverage does not correspond to the number of read covering a given position like in classical tools outputting bigwig. Instead we compute the number of fragments for paired-end data. To compute the coverage density $\mathrm{X}_y(t)$ with $\mathrm{X} \in [IP, WCE]$ and

bioRxiv preprint doi: https://doi.org/10.1101/2022.03.18.484892; this version posted September 11, 2023. The copyright holder for this preprint (which was not certified by peer review) is the author/funder, who has granted bioRxiv a license to display the preprint in perpetuity. It is made available under aCC-BY-NC-ND 4.0 International license.

$y \in [c, x]$ we count the number of reads $r(t)$ overlapping with position t. For properly paired reads (with a mate read on the same chromosome and with a starting position ending after the end of the read) we also count a density of 1 between the end of the first reads and the start of his mate read $g(t)$. $X_y(t) = r(t) + g(t)$. Some fragment can be artificially long (with reads mapping to repeated regions at the start and end of a chromosome), therefore, we compute a robust mean μ of the gap size, between two reads of a pair, by removing the 0.1 upper and lower quantile of the fragment length distribution. Fragments with a size higher than $\phi^{-1}(0.95, \mu, 1.0)$ are set to end at the $\phi^{-1}(0.95, \mu, 1.0)$ value, with $\phi()$ the Normal CDF function. For fragments shorter than the read length, we don't count the overlapping reads region as a coverage of 2 fragments but as the coverage of 1 fragment. The BIGWIG2BAM Tools (https://gitbio.ens-lyon.fr/LBMC/Bernard/bamcalib v0.1.1), generate a synthetic bam file from a bigwig file and a reference genome. The purpose of this tool is to create a bam file having the same coverage profile as the one described in the input bigwig file. Therefore, we can run any chip-seq tools working with bam file instead of bigwig file on our normalized data.

(which was not certified by peer review) is the author/funder, who has granted bioRxiv a license to display the preprint in perpetuity. It is m
available under aCC-BY-NC-ND 4.0 International license.

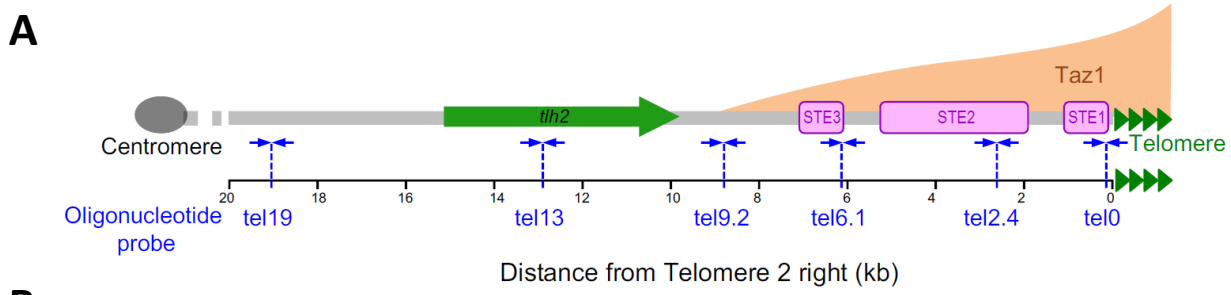

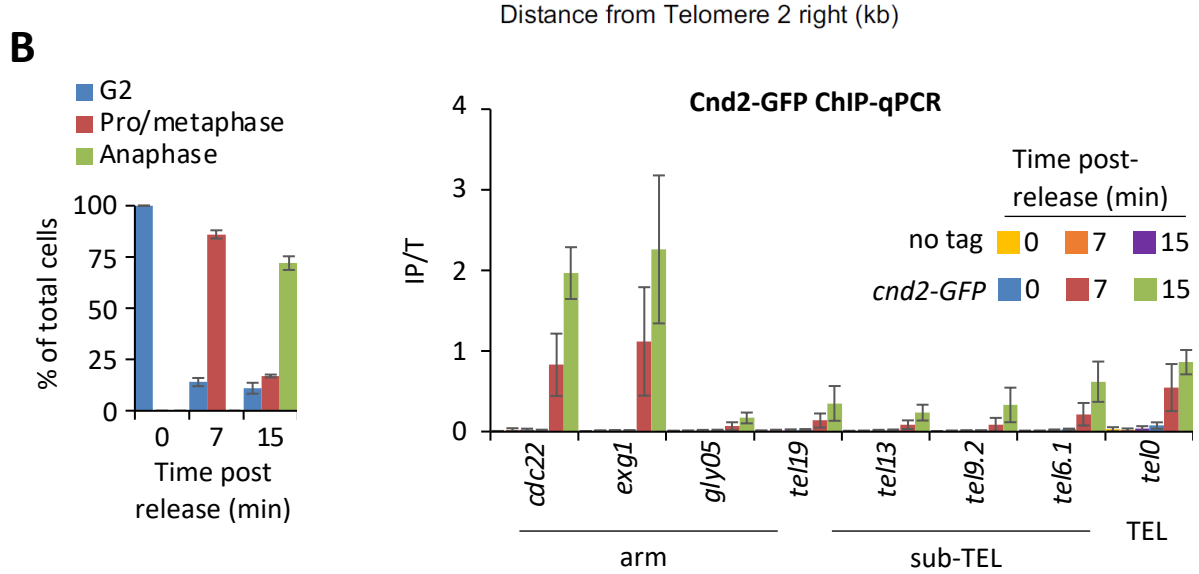

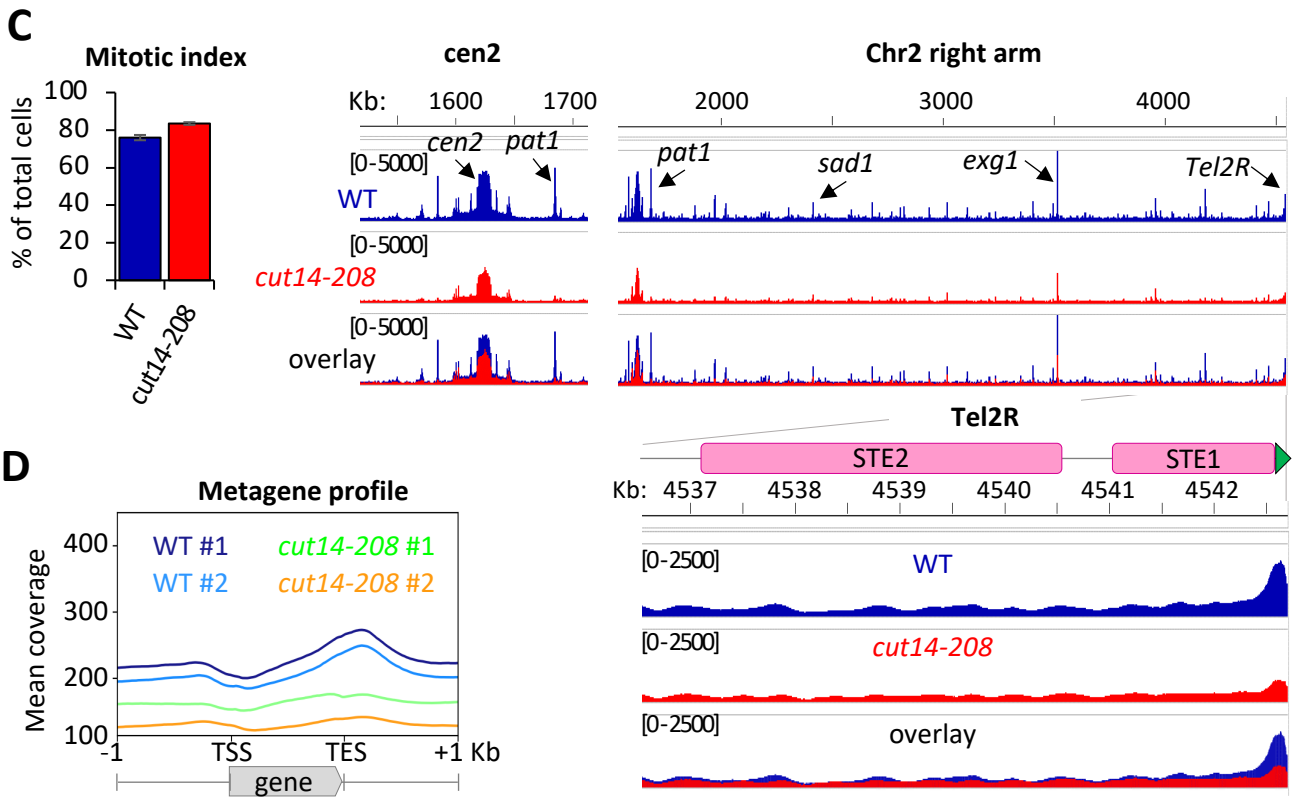

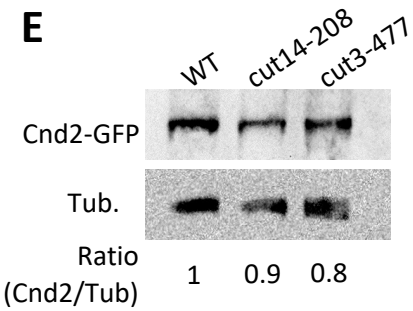

Figure 1

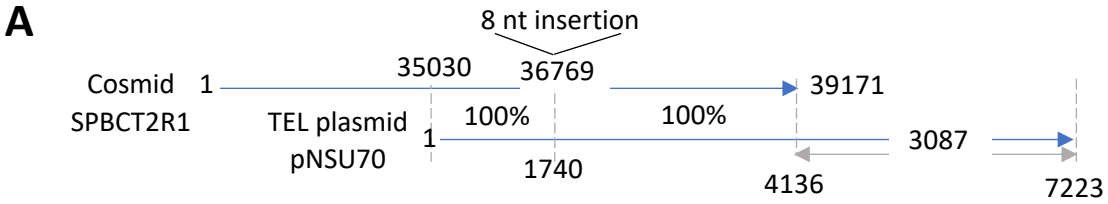
A
8 nt insertion
35030
36769
Cosmid
SPBCT2R1
1
39171
TEL plasmid
pNSU70
1
100%
100%
3087
1740
4136
7223

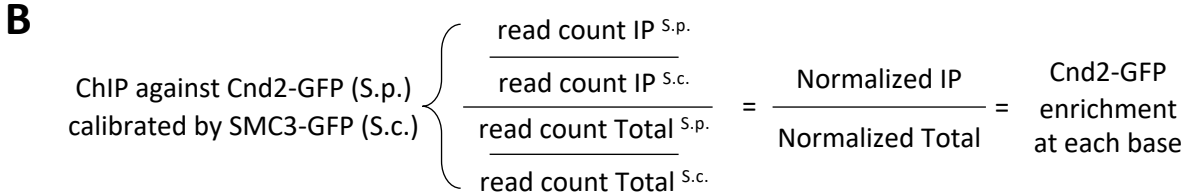
B
ChIP against Cnd2-GFP (S.p.)
calibrated by SMC3-GFP (S.c.)
read count IP S.p.
read count IP S.c.
read count Total S.p.
read count Total S.c.
=
Normalized IP
Normalized Total
=
Cnd2-GFP
enrichment
at each base

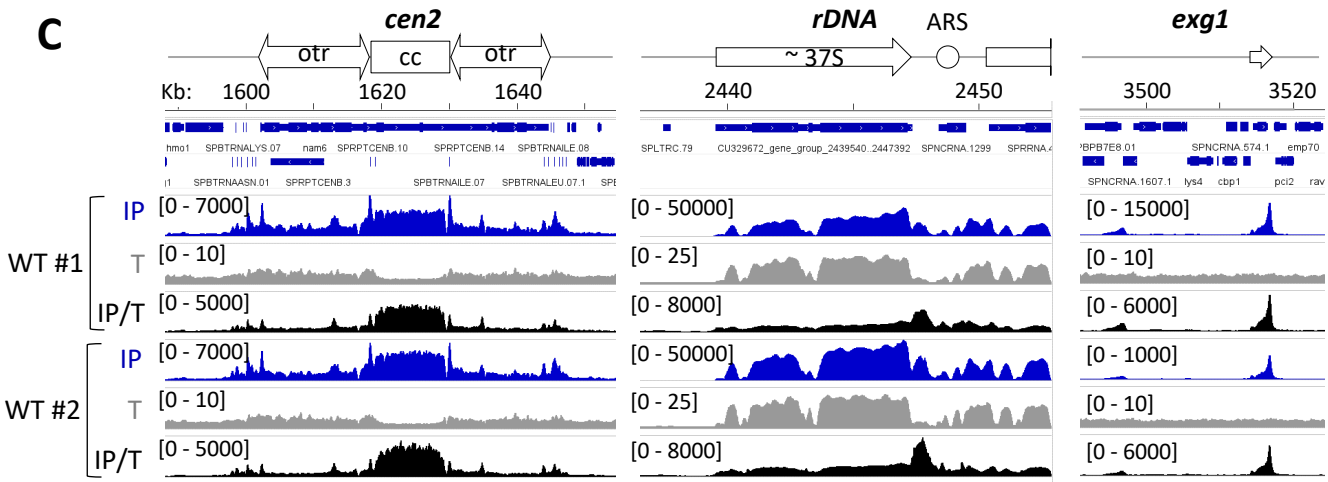
C
cen2
otr
cc
otr
Kb: 1600 1620 1640
rDNA
ARS
~ 37S
2440 2450
exg1
3500 3520
WT #1
WT #2
IP
T
IP/T
[0 - 7000]
[0 - 10]
[0 - 5000]
[0 - 50000]
[0 - 25]
[0 - 8000]
[0 - 15000]
[0 - 6000]
[0 - 1000]

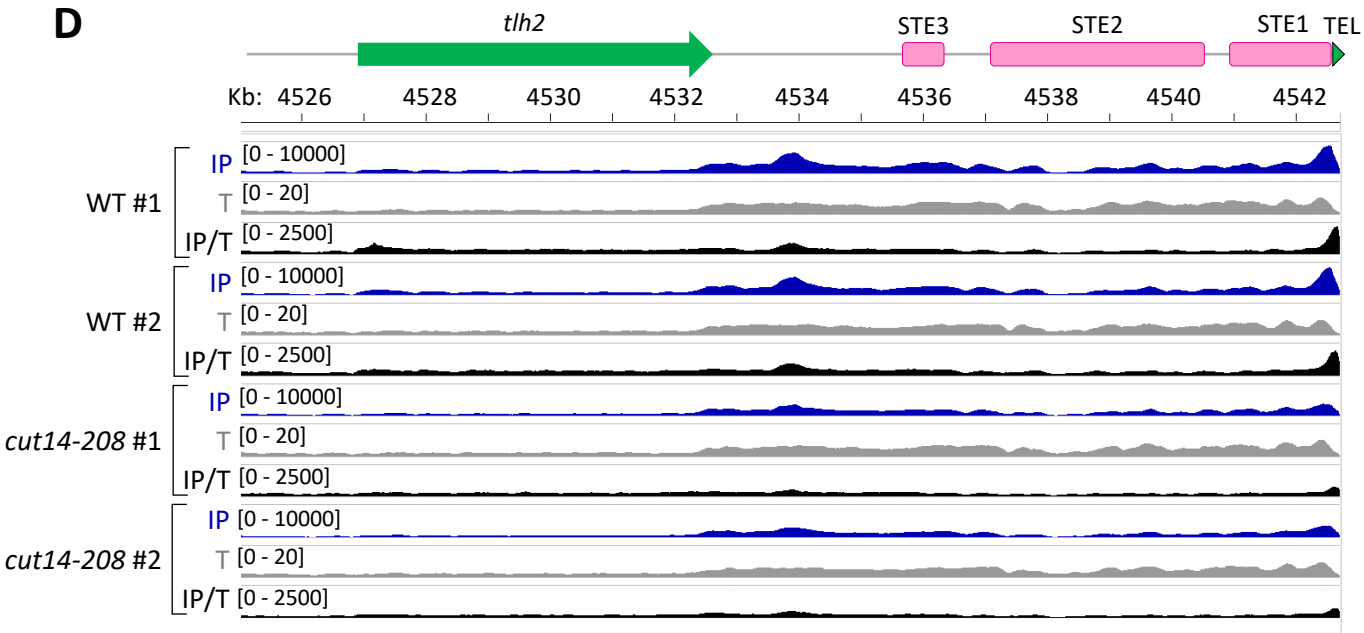
D
tlh2
STE3
STE2
STE1
TEL
Kb: 4526 4528 4530 4532 4534 4536 4538 4540 4542
WT #1
WT #2
cut14-208 #1
cut14-208 #2
IP
T
IP/T
[0 - 10000]
[0 - 20]
[0 - 2500]

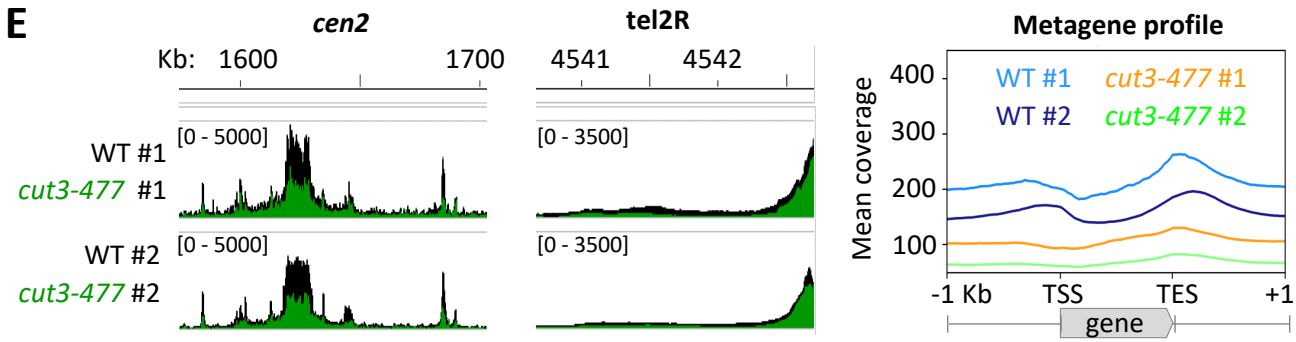
E
cen2
Kb: 1600 1700
tel2R
4541 4542
WT #1
cut3-477 #1
WT #2
cut3-477 #2
[0 - 5000]
[0 - 3500]
Metagene profile
Mean coverage
400
300
200
100
WT #1
WT #2
cut3-477 #1
cut3-477 #2
-1 Kb
TSS
TES
+1
gene

Figure S1

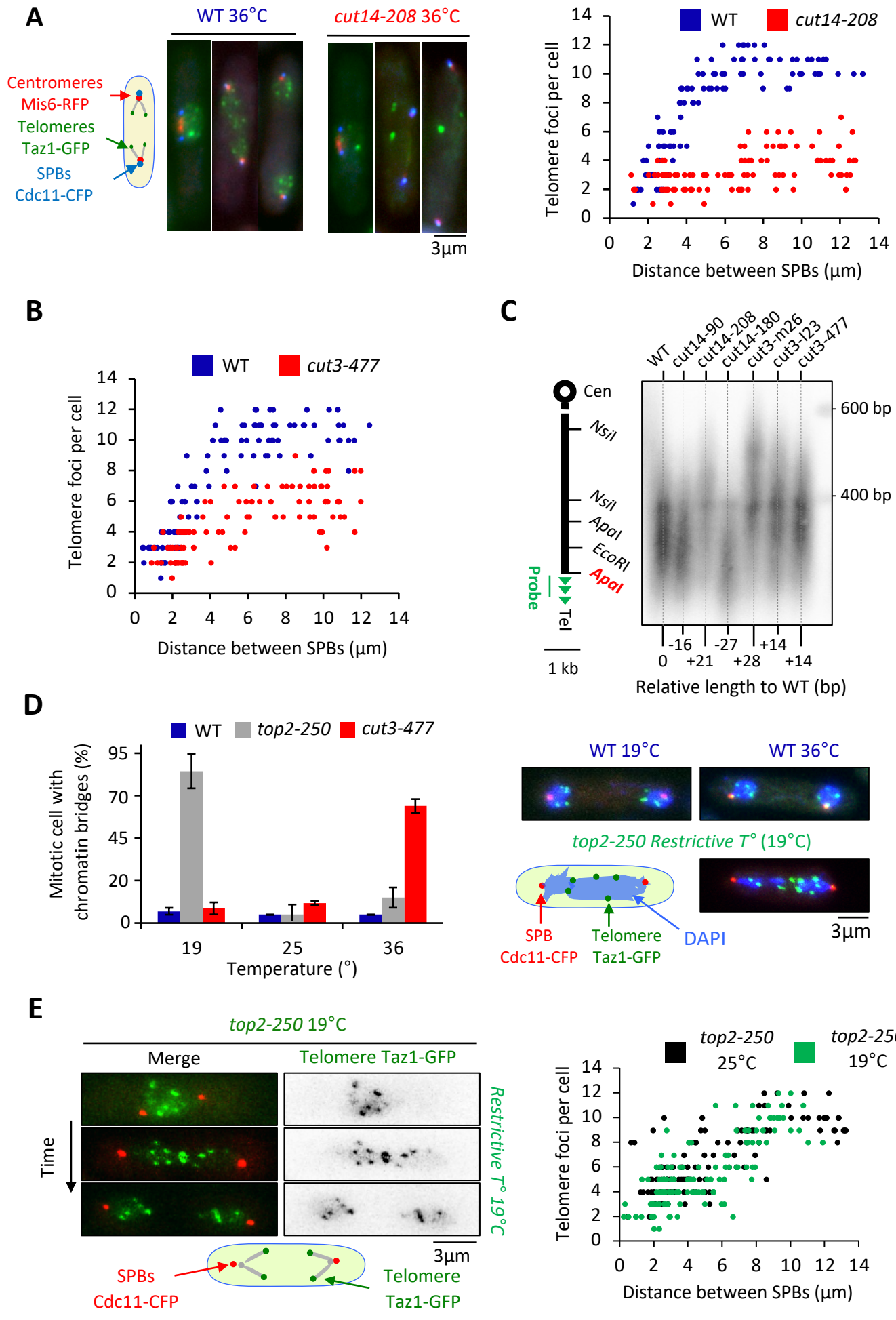
A
WT 36°C
cut14-208 36°C
Centromeres
Mis6-RFP
Telomeres
Taz1-GFP
SPBs
Cdc11-CFP
3µm
WT
cut14-208
Telomere foci per cell
Distance between SPBs (µm)
B
WT
cut3-477
Telomere foci per cell
Distance between SPBs (µm)
C
WT
cut14-90
cut14-208
cut14-180
cut3-m26
cut3-I23
cut3-477
Cen
NsiI
NsiI
ApaI
EcoRI
ApaI
Probe
Tel
1 kb
600 bp
400 bp
-16
-27
+14
0
+21
+28
+14
Relative length to WT (bp)
D
WT
top2-250
cut3-477
Mitotic cell with chromatin bridges (%)
Temperature (°)
WT 19°C
WT 36°C
top2-250 Restrictive T° (19°C)
SPB
Cdc11-CFP
Telomere
Taz1-GFP
DAPI
3µm
E
top2-250 19°C
Merge
Telomere Taz1-GFP
Time
Restrictive T° 19°C
3µm
SPBs
Cdc11-CFP
Telomere
Taz1-GFP
top2-250
25°C
top2-250
19°C
Telomere foci per cell
Distance between SPBs (µm)

Figure 2

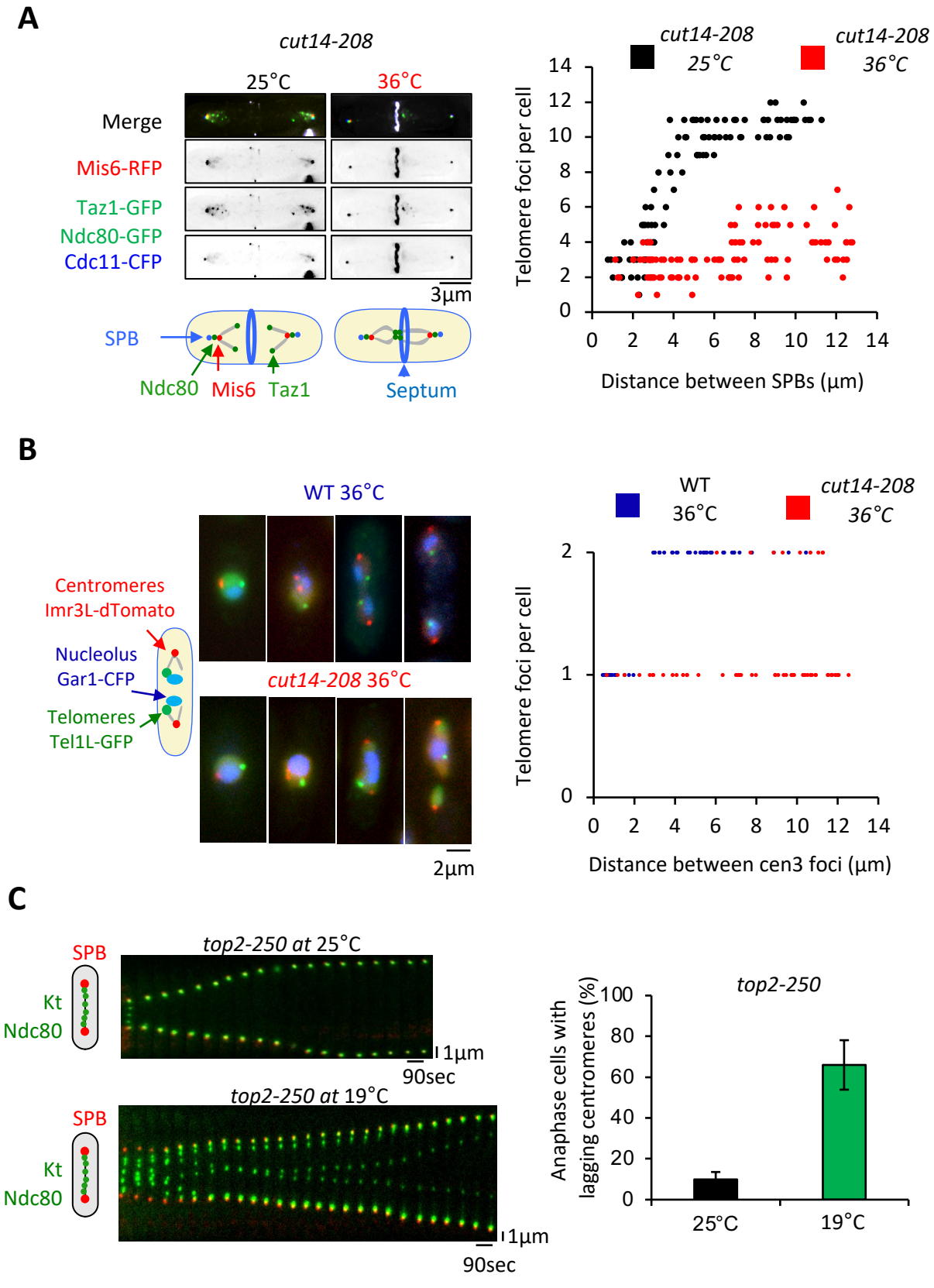
A
cut14-208
25°C
36°C
Merge
Mis6-RFP
Taz1-GFP
Ndc80-GFP
Cdc11-CFP
3μm
SPB
Ndc80
Mis6
Taz1
Septum
cut14-208 25°C
cut14-208 36°C
Telomere foci per cell
Distance between SPBs (μm)
B
WT 36°C
Centromeres
Imr3L-dTomato
Nucleolus
Gar1-CFP
Telomeres
Tel1L-GFP
cut14-208 36°C
2μm
WT 36°C
cut14-208 36°C
Telomere foci per cell
Distance between cen3 foci (μm)
C
top2-250 at 25°C
SPB
Kt
Ndc80
1μm
90sec
top2-250 at 19°C
SPB
Kt
Ndc80
1μm
90sec
top2-250
Anaphase cells with lagging centromeres (%)
25°C
19°C

Fig. S2

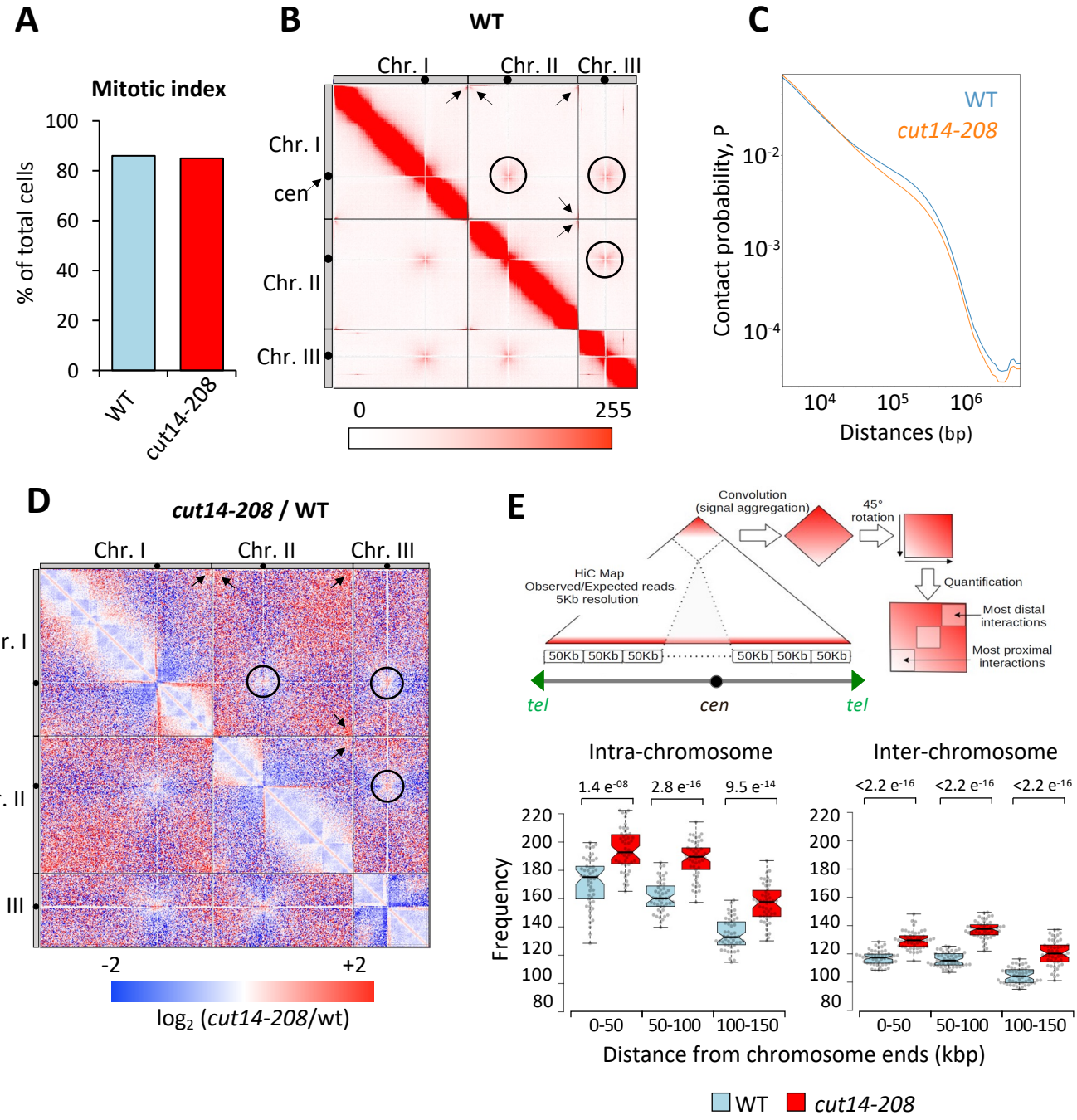
A
Mitotic index
% of total cells
100
80
60
40
20
0
WT
cut14-208
B
WT
Chr. I
Chr. II
Chr. III
cen
0
255
C
WT
cut14-208
Contact probability, P
Distances (bp)
D
cut14-208 / WT
-2
+2
log2 (cut14-208/wt)
E
Convolution (signal aggregation)
45° rotation
Quantification
HiC Map
Observed/Expected reads
5Kb resolution
Most distal interactions
Most proximal interactions
50Kb
tel
cen
Intra-chromosome
Inter-chromosome
1.4 e-08
2.8 e-16
9.5 e-14
<2.2 e-16
Frequency
0-50
50-100
100-150
Distance from chromosome ends (kbp)
WT
cut14-208

Figure 3

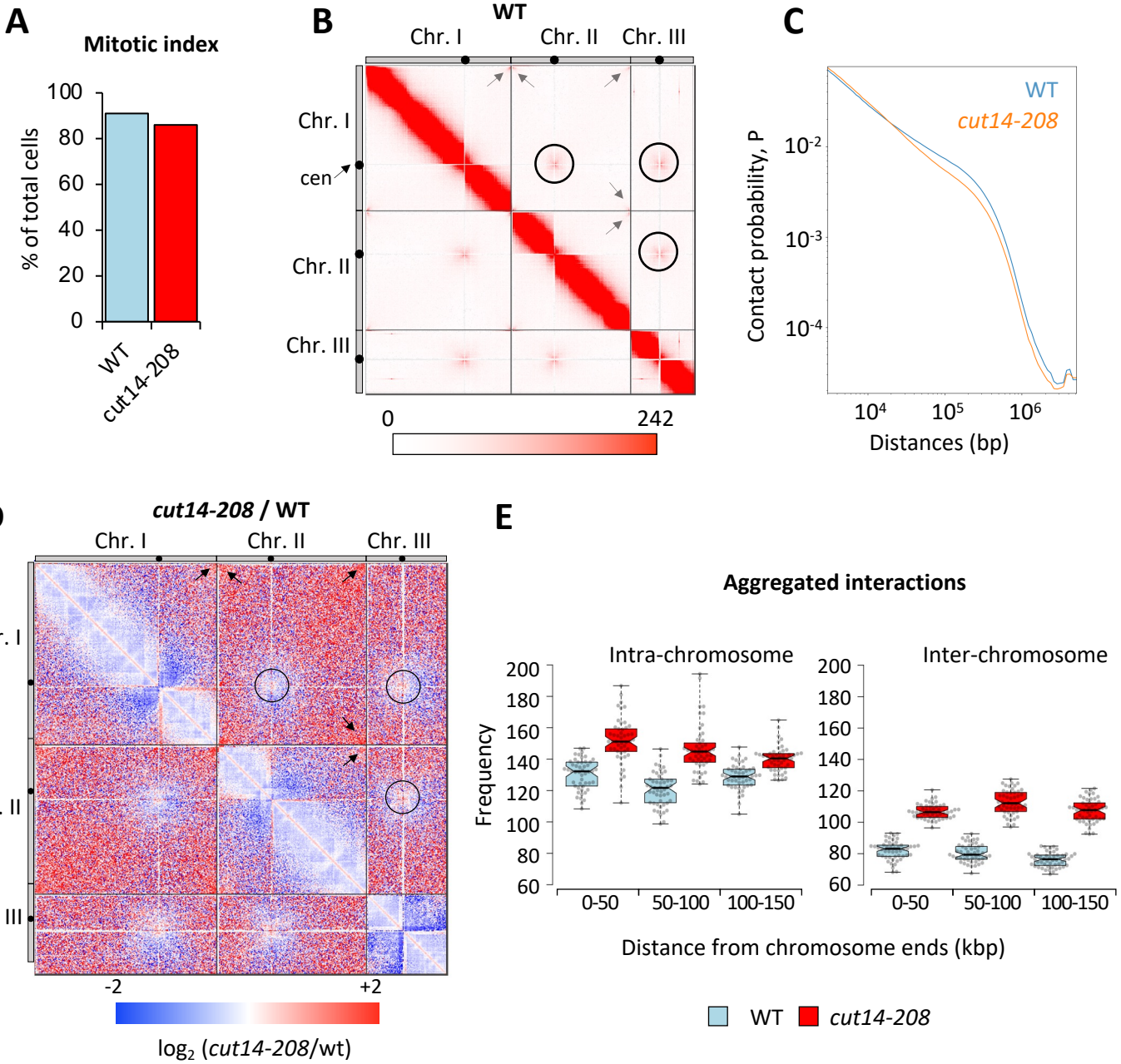
A
Mitotic index
% of total cells
100
80
60
40
20
0
WT
cut14-208
B
WT
Chr. I
Chr. II
Chr. III
cen
0
242
C
WT
cut14-208
Contact probability, P
Distances (bp)
D
cut14-208 / WT
-2
+2
log2 (cut14-208/wt)
E
Aggregated interactions
Intra-chromosome
Inter-chromosome
Frequency
0-50
50-100
100-150
Distance from chromosome ends (kbp)
WT
cut14-208

Figure S3

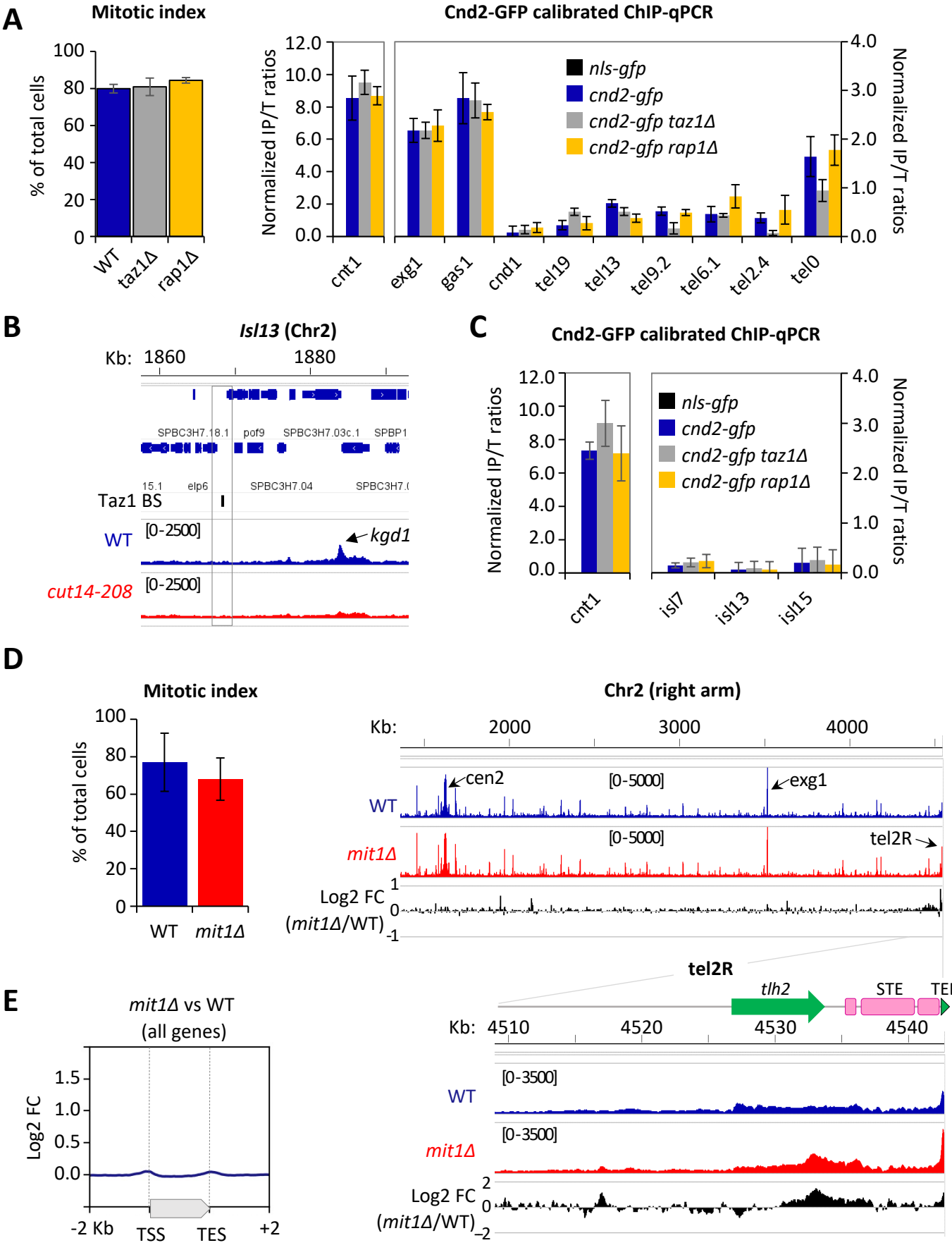
A
Mitotic index
% of total cells
WT
taz1Δ
rap1Δ
Cnd2-GFP calibrated ChIP-qPCR
Normalized IP/T ratios
nls-gfp
cnd2-gfp
cnd2-gfp taz1Δ
cnd2-gfp rap1Δ
cnt1
exg1
gas1
cnd1
tel19
tel13
tel9.2
tel6.1
tel2.4
tel0
B
Isl13 (Chr2)
Kb: 1860
1880
SPBC3H7.18.1
pof9
SPBC3H7.03c.1
SPBP1
SPBC3H7.04
Taz1 BS
WT
[0-2500]
kgd1
cut14-208
C
Cnd2-GFP calibrated ChIP-qPCR
isl7
isl13
isl15
D
Mitotic index
mit1Δ
Chr2 (right arm)
Kb: 2000
3000
4000
cen2
exg1
tel2R
[0-5000]
Log2 FC
(mit1Δ/WT)
E
mit1Δ vs WT
(all genes)
Log2 FC
-2 Kb
TSS
TES
+2
tel2R
tlh2
STE
TEL
Kb: 4510
4520
4530
4540
[0-3500]

Figure 4

A

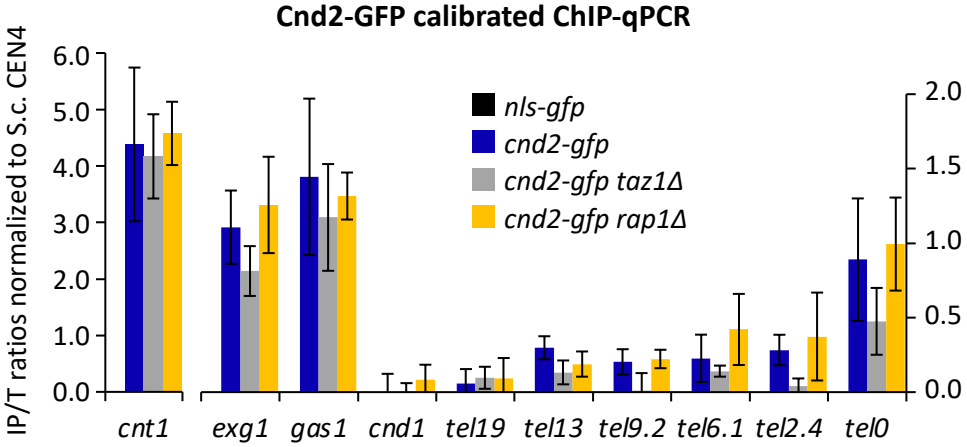

B

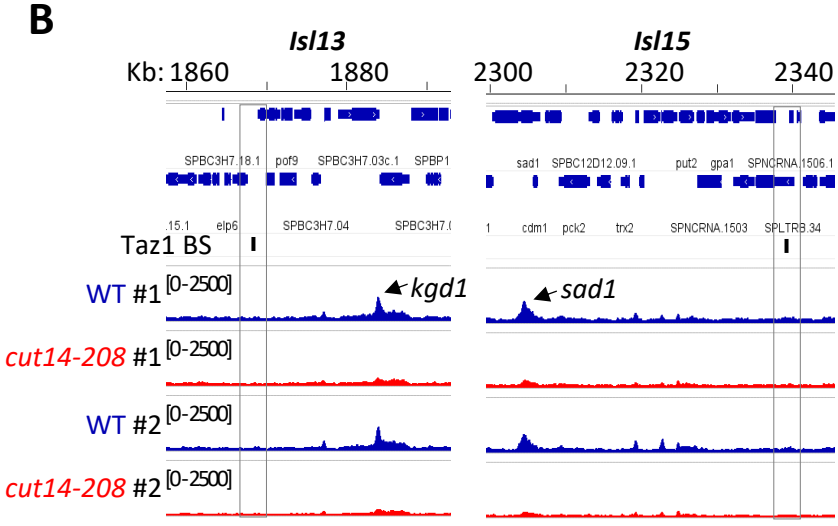

C

Condensin occupancy at internal Taz1 Binding sites

Island	Loci	Taz1 binding	Condensin enrichment
Is3	spac23h3.14	++	-
Is7	spac144.02	++	-
Is13	spbc3h7.08c	+++	-
Is14	eno101	++	-
Is15	spbc26c6.09c	++	-
Is19	spbc1259.02c	+	-

D

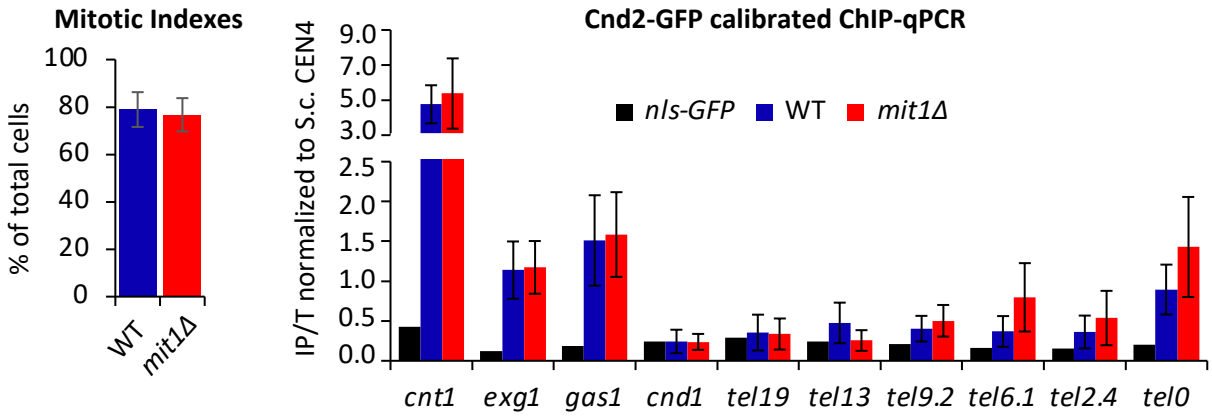

E

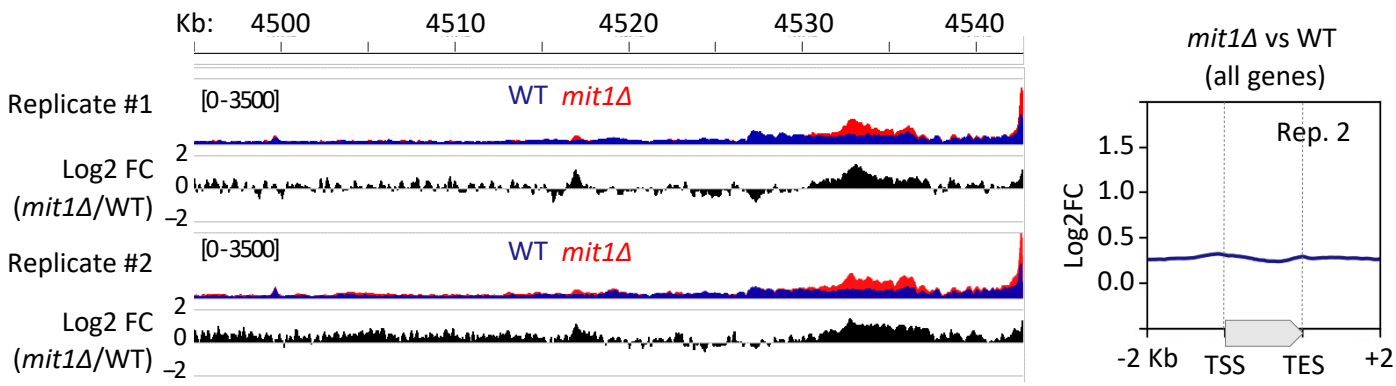

Figure S4

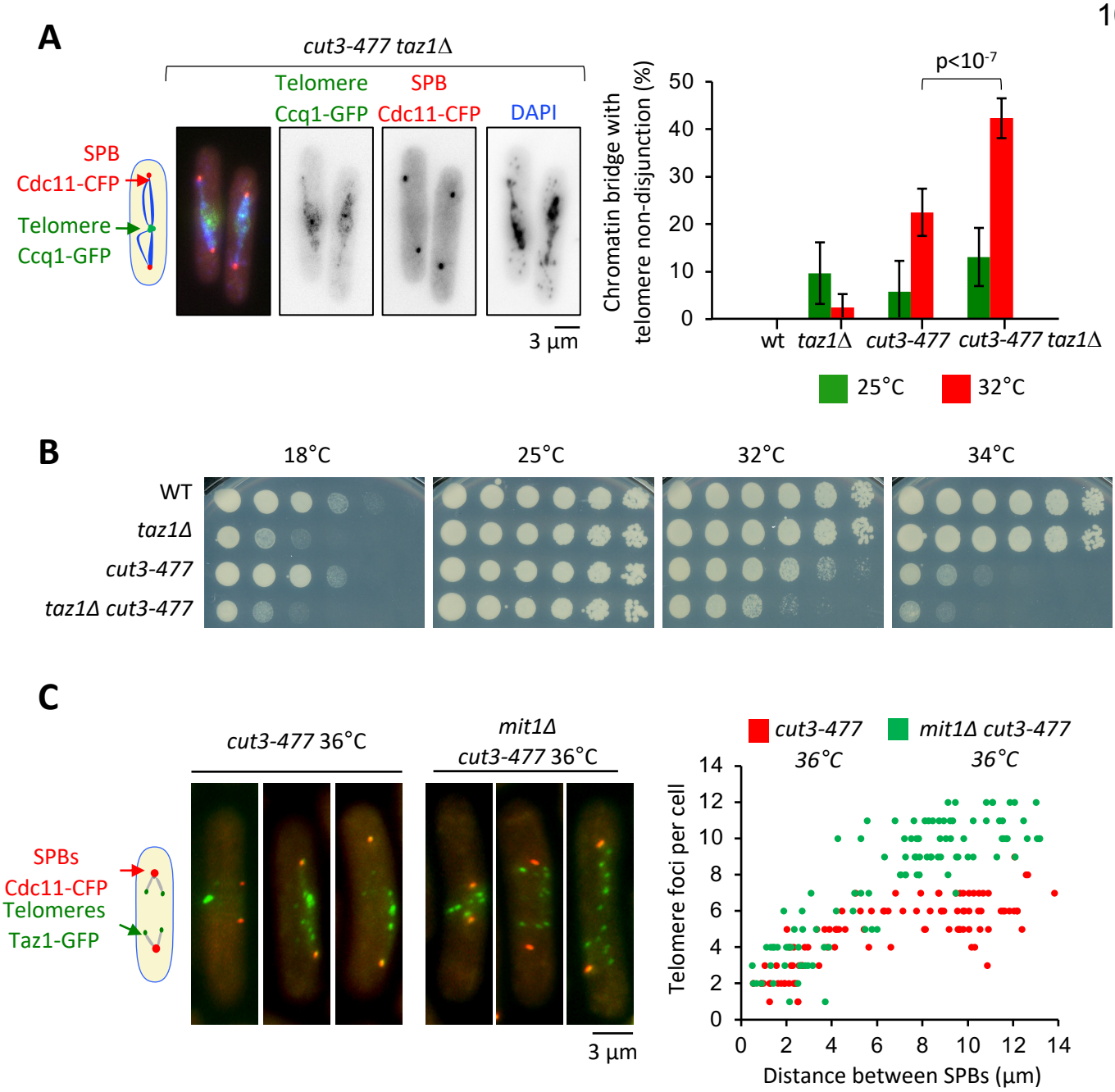
A
cut3-477 taz1Δ
Telomere
Ccq1-GFP
SPB
Cdc11-CFP
DAPI
SPB
Cdc11-CFP
Telomere
Ccq1-GFP
3 µm
Chromatin bridge with telomere non-disjunction (%)
p<10-7
wt
taz1Δ
cut3-477
cut3-477 taz1Δ
25°C
32°C
B
18°C
25°C
32°C
34°C
WT
taz1Δ
cut3-477
taz1Δ cut3-477
C
cut3-477 36°C
mit1Δ cut3-477 36°C
SPBs
Cdc11-CFP
Telomeres
Taz1-GFP
3 µm
cut3-477 36°C
mit1Δ cut3-477 36°C
Telomere foci per cell
Distance between SPBs (µm)

Figure 5

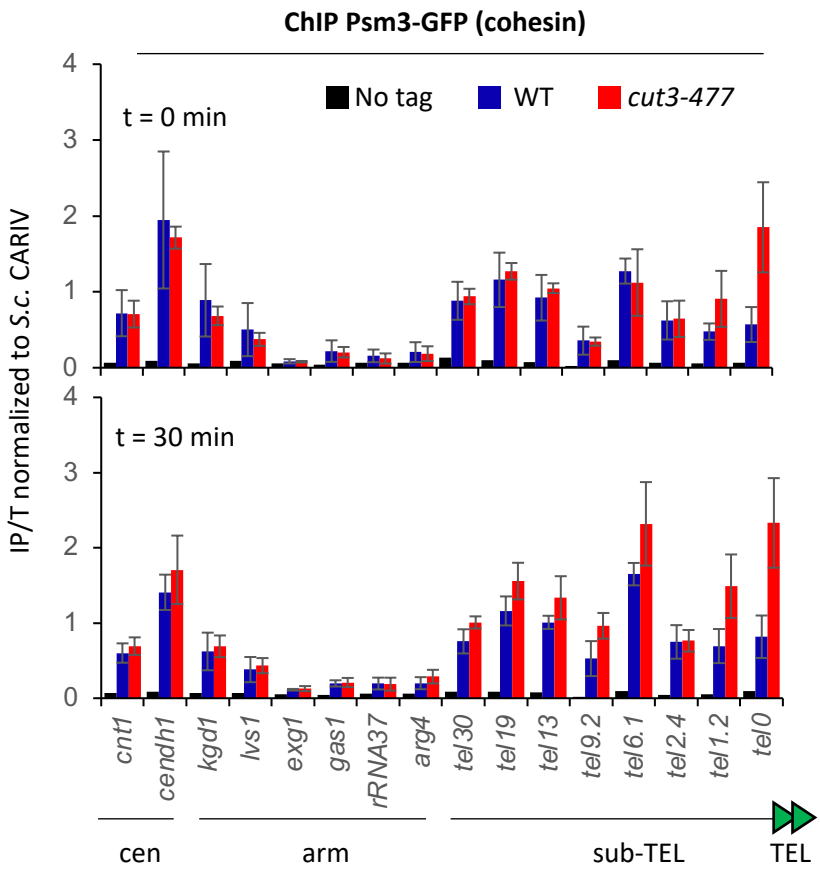
ChIP Psm3-GFP (cohesin)
No tag
WT
cut3-477
t = 0 min
t = 30 min
IP/T normalized to S.c. CARIV
0
1
2
3
4
cnt1
cendh1
kgd1
lvs1
exg1
gas1
rRNA37
arg4
tel30
tel19
tel13
tel9.2
tel6.1
tel2.4
tel1.2
tel0
cen
arm
sub-TEL
TEL

Figure S5

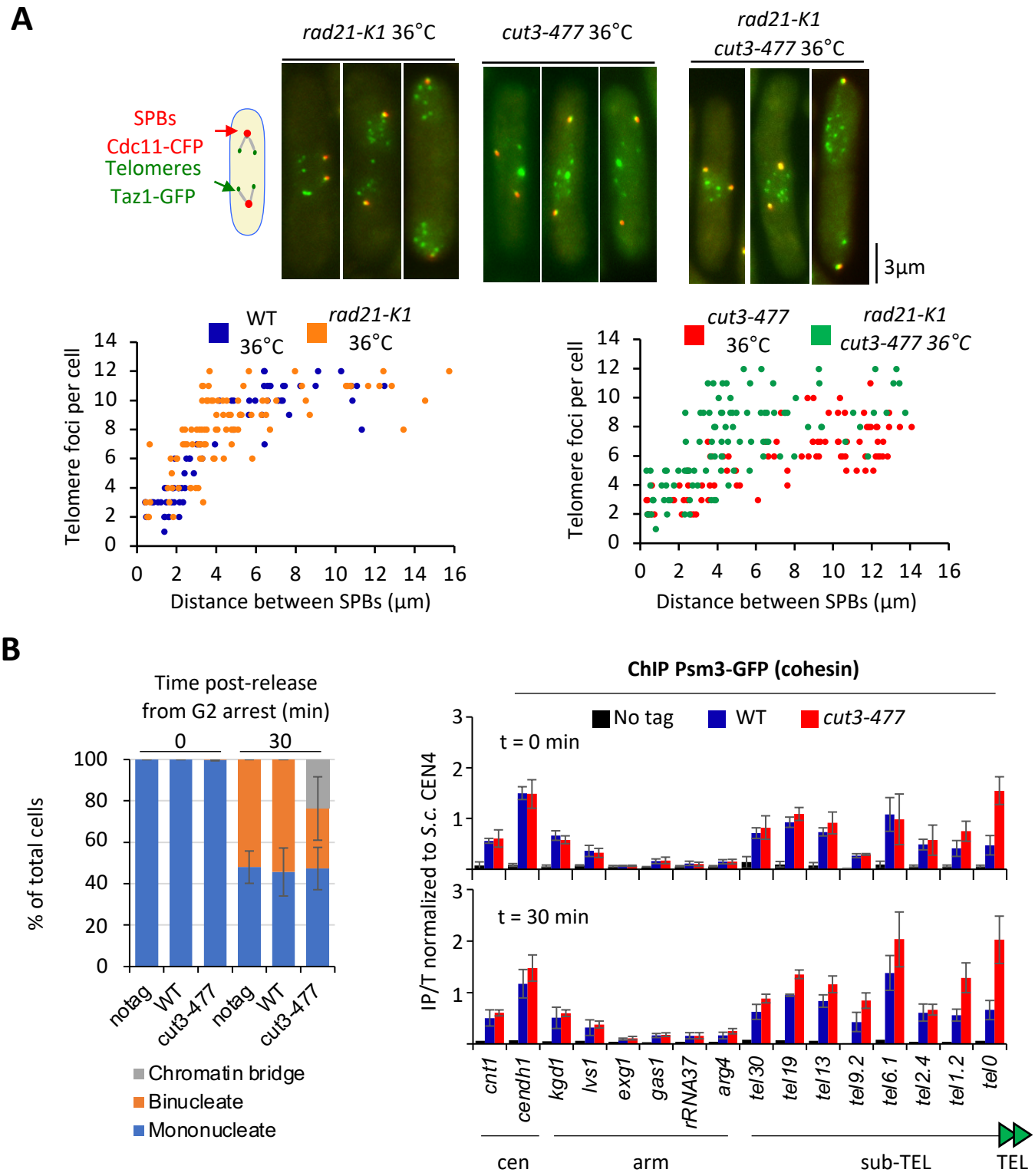
A
rad21-K1 36°C
cut3-477 36°C
rad21-K1
cut3-477 36°C
SPBs
Cdc11-CFP
Telomeres
Taz1-GFP
3µm
WT
36°C
rad21-K1
36°C
Telomere foci per cell
Distance between SPBs (µm)
cut3-477
36°C
rad21-K1
cut3-477 36°C
Telomere foci per cell
Distance between SPBs (µm)
B
Time post-release
from G2 arrest (min)
0
30
% of total cells
notag
WT
cut3-477
notag
WT
cut3-477
Chromatin bridge
Binucleate
Mononucleate
ChIP Psm3-GFP (cohesin)
No tag
WT
cut3-477
t = 0 min
t = 30 min
IP/T normalized to S.c. CEN4
cnt1
cendh1
kgd1
lvs1
exg1
gas1
rRNA37
arg4
tel30
tel19
tel13
tel9.2
tel6.1
tel2.4
tel1.2
tel0
cen
arm
sub-TEL
TEL

Figure 6

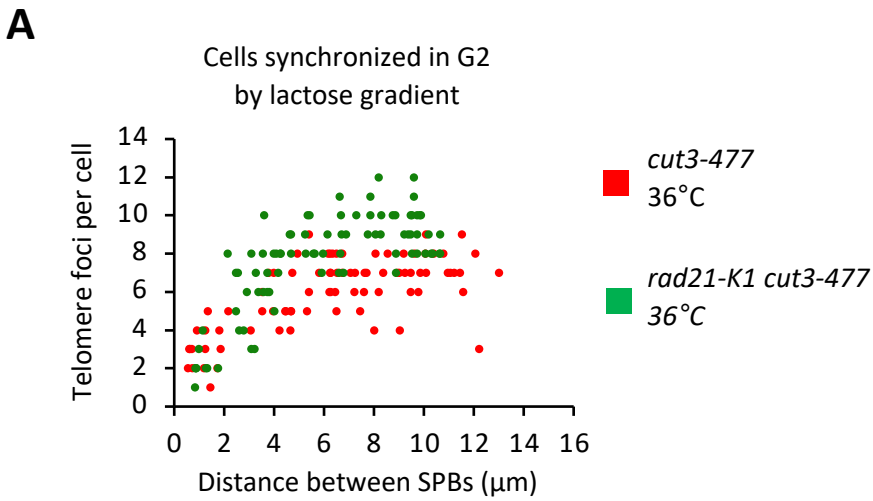
A
Cells synchronized in G2
by lactose gradient
Telomere foci per cell
0
2
4
6
8
10
12
14
0
2
4
6
8
10
12
14
16
Distance between SPBs (µm)
cut3-477
36°C
rad21-K1 cut3-477
36°C

Figure S6

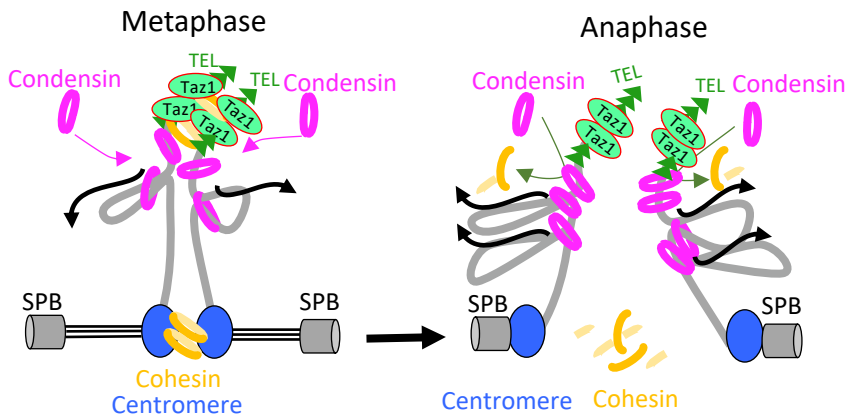
Metaphase
Anaphase
Condensin
TEL
Taz1
Taz1
Taz1
TEL
Condensin
SPB
SPB
Cohesin
Centromere
Condensin
TEL
Taz1
Taz1
TEL
Condensin
Taz1
Taz1
SPB
SPB
Centromere
Cohesin

Figure 7

5.3 Supplementary results to Part 5

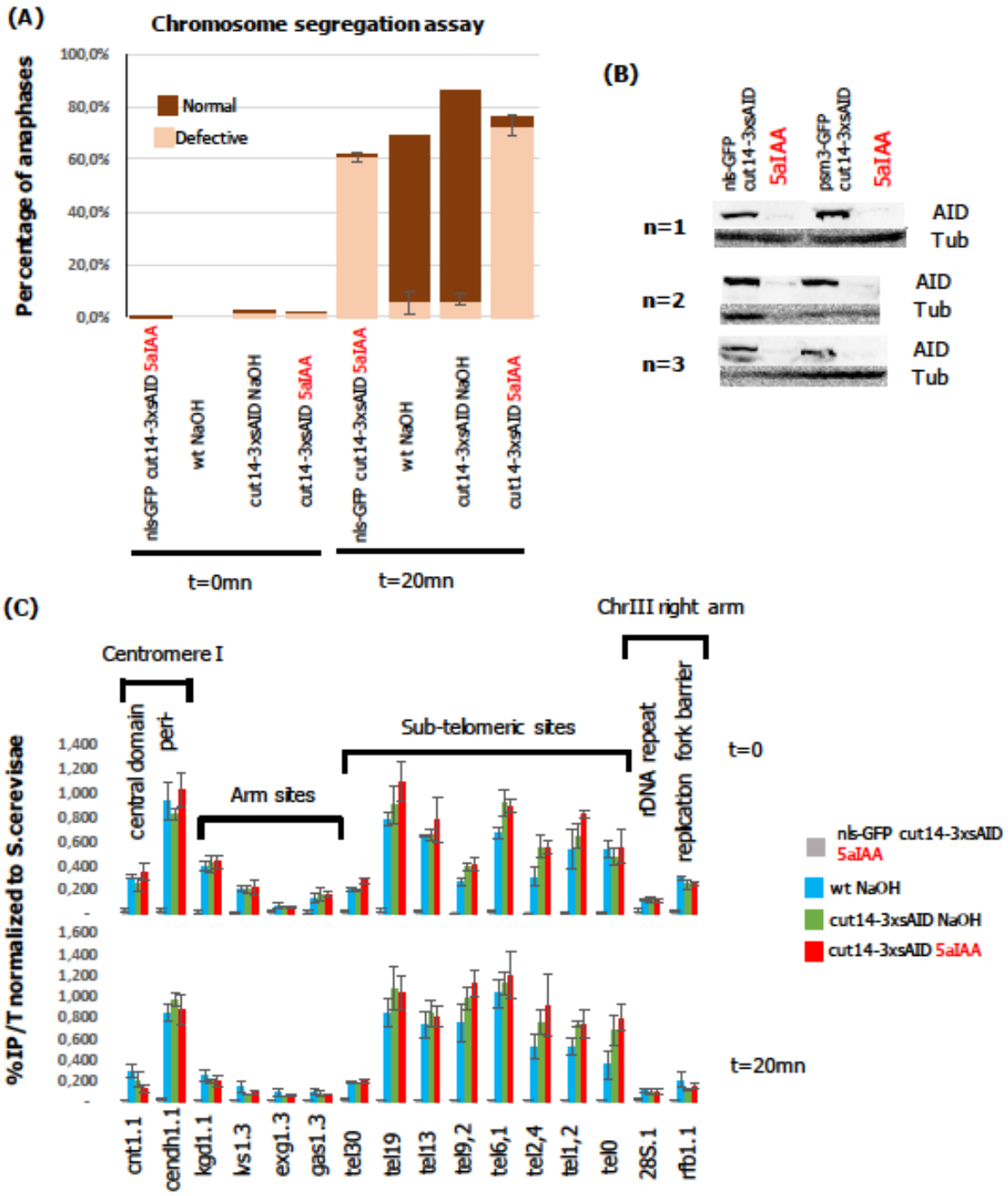

Fig. D1 The impact of controlled depletion of Cut14/SMC2 on cohesin binding at telomeres
(A) Cells were grown at 32°C and exposed for 1h to 3-Brbpp1, then exposed for 2h to 5aIAA or NaOH while arrested in late G2. Cells were then released into media containing 5aIAA or NaOH. Aliquots were collected to assess the efficiency of anaphase progression (two separated DNA masses by DAPI) and the frequency of chromatin bridges at t=0 and t=20mn post release. Values shown are averages and bars standard deviations from three biological replicates. In parallel, samples were collected at the same times for western blotting and fixed for ChIP-qPCR against Psm3-GFP.
(B) Western blotting showing the depletion of Cut14-3xsAID in the experimental conditions of (A) in all three biological replicates.
(C) ChIP-qPCR against nls-GFP or psm3-GFP in the indicated conditions at the indicated genomic loci. Values are %IP/T normalized to a cerevisae site added as spike-in.

I tried to ask whether the increase in cohesin association is dependent on a function of condensin just prior to mitosis, by depleting Cut14 at the G2/M transition using an auxin sensitive *cut14-3xsAID* allele with cohesin tagged *psm3-GFP*. Cells were blocked using the *cdc2asM17* allele sensitive to 3-BrbPP1, Cut14 was depleted in G2 and cells were collected and fixed 20mn after the release from the G2 arrest or just prior to release at 0mn (Fig. D1A). I performed ChIP-qPCR on the indicated conditions using an anti-GFP antibody (A111-22) and assessed the levels of cohesin binding at sub-telomeres and arm sites (Fig. 1DC).

We observe increases at some sites in *cut14-3xsAID* NaOH or 5aIAA conditions relative to wild-type. The telomere proximal tel0 site shows specific increase in anaphase, while other subtelomeric sites such as tel1.2, tel2.4, tel9.2 show increases both in G2 and in anaphase (Fig. D1C). Moreover, the 3xsAID tag itself appears to produce an increase in cohesin association, thus the question of whether condensin plays a role in mitosis at telomeres or has an impact through a prior step of the cell-cycle remains open.

PART 6 – DHP1-RPB1 Project Lebreton & Colin 2024

While I was working on FACT and Jeremy on RNA binding proteins, we both developed tools that we used to address the impact of transcription on condensin in mitosis and led to this collaborative study. Of note, Jeremy performed all the Spt-PALM work and analysis (Fig. 2) and the work on Dhp1 and we analysed the data together.

6.1 Active transcription by RNA polymerase on condensin activity

As mentioned in the introduction, the process of transcription can deeply impact the chromatin template and by extension the chromosome. Many properties of actively transcribed units can be cited as examples : as mentioned in the introduction, elongation factors allow RNA polymerases to bypass the nucleosomal obstacles that impede transcription **(Kujirai et al., 2018)**. Transcriptionally associated chromatin remodelers can retain nucleosomes in the wake of polymerase and reposition them **(Farnung et al., 2021; Filipovski et al., 2022)**. Highly expressed genes can become bulky, polymerase dense regions **(Miller and Beatty, 1969)** and transcription is also a source of positive and negative supercoiling (upstream and downstream of the direction of transcription, respectively).

The establishment of the promoter region for polymerase recruitment involves specific chromatin remodeling activities that position nucleosomes just upstream/downstream of the PIC **(Wang et al., 2023)** and create a NDR region **(Lee et al., 2004)**. Finally, enhancer regions in metazoans can establish contacts with promoter regions and can themselves be transcribed **(Kim et al., 2010)**.

Multiple studies combining in vivo experiments with modelling suggest that cohesin and bacterial SMCs may be stalled by translocating RNA polymerases **(Banigan et al., 2023; Brandão et al., 2019; Busslinger et al., 2017a; Heinz et al., 2018; Jeppsson et al., 2022b; Tran et al., 2017; Wang et al., 2017)**. In budding yeast, cohesin was found associated at tandem repeats of rDNA **(Laloraya et al., 2000)** and eventually, in a chromosome-wide approach at sites of convergent transcription **(Lengronne et al., 2004)**. Furthermore, release from G1 arrest suggests that this association is dynamic and that the cohesin complexes translocate towards these convergent transcription sites **(Lengronne et al., 2004)**. More recent evidence in budding yeast suggests that convergent sites of transcription also accumulate cohesin **(Jeppsson et al., 2022)**. Notably, in human cells when cohesin residence time is increased and CTCF barriers are removed **(Banigan et al., 2023; Busslinger et al., 2017b)** it is found relocated at convergent transcriptional units. Together these evidence suggest that transcription is a conserved positioning device of cohesin SMC. Consistent with this model, shutting down transcription or RNAPII depletion produces loss of cohesin accumulation in the loci where RNAPII was otherwise active **(Busslinger et al., 2017; Jeppsson et al., 2022; Zhang et al., 2023)**. Meanwhile, translocation of cohesin in vitro can be stalled and even pushed by RNA polymerases **(Davidson et al., 2016)** although in this assay cohesin is topologically associated to DNA and is not extruding a loop. When performing loop extrusion, cohesin can bypass a single DNA-bound RNA polymerase II **(Pradhan et al., 2022a)**.

Nonetheless, transcription appears to limit the ability of cohesin to structure larger loops. Inhibition of transcription promotes the formation of long-range contacts (Jeppsson et al., 2022b) and formation of new loops after RNA pol II depletion has been reported in human cells **(S. Zhang et al., 2023)** correlated with loss of cohesin binding at loci where loop anchors are lost.

In comparison, evidence for condensin is less abundant. Condensin is enriched at actively transcribed genes **(Nakazawa et al., 2015; Sutani et al., 2015)** but it has been argued that while reducing

transcription rescues phenotypes caused by condensin mutations, it also leads to dissociation of condensin from chromatin **(Sutani et al., 2015)**. On the other hand, evidence in fission yeast from the hosting lab suggests condensin position is determined by active RNA polymerase, either pol II or pol III at specific loci tested **(Rivosecchi et al., 2021)**.

These conflicting evidence underlie a problem at the center of condensin function in vivo, and appears essential to better understand "mechanistic parallels and conflicts between transcription-driven and condensin-mediated conformational changes of chromatin" **(Hirano, 2016)**. In particular, what is the impact of the the processive, chromatin-associated movement of RNA polymerases **(Kujirai et al., 2018)** on the processive ATP-driven translocation of condensin **(Ganji et al., 2018)** ?

We set out to revisit the role of transcription in condensin function, by degron-tagging two proteins :

- Rpb1, the largest subunit of RNA polymerase II. With Rpb2 it forms the core of the RNAPII catalytic enzyme and holds the active site **(Cramer et al., 2000)**, with additional key functional domains important for the transcription process **(Schier and Taatjes, 2020)**. Depletion of Rpb1 therefore is certain to lead to the abolishment of RNAPII transcription.
- Dhp1/XRN2, the torpedo exoribonuclease which is involved in proper transcription termination by co-transcriptional cleavage **(West et al., 2004)**. In fission yeast depletion of Dhp1 leads to reading-through polymerases beyond the normal 3' TES site **(Larochelle et al., 2018; Nakazawa et al., 2019)**, which also leads to condensin accumulation at two genes tested **(Nakazawa et al., 2019)**.

I attempted, with a pilot experiment described in Fig. D2, to assess whether RNAPII could be re-expressed in mitosis after depletion – to demonstrate a direct effect of RNAPII on condensin localisation and chromosome conformation. Unfortunately, this was not experimentally feasible as RNAPII levels recovered in the extract did not associate to chromatin. This could be explained by several non-mutually exclusive hypotheses, such as 1/ a slow assembly of transcribing RNAPII complexes relative to the recovery of Rpb1 levels, 2/ a mechanism preventing reassociation to chromatin specifically during mitosis, 3/ remaining RNAPII chromatin-bound subunits preventing the reassociation of Rpb1, 4/ loss of chromatin features required for PIC assembly.

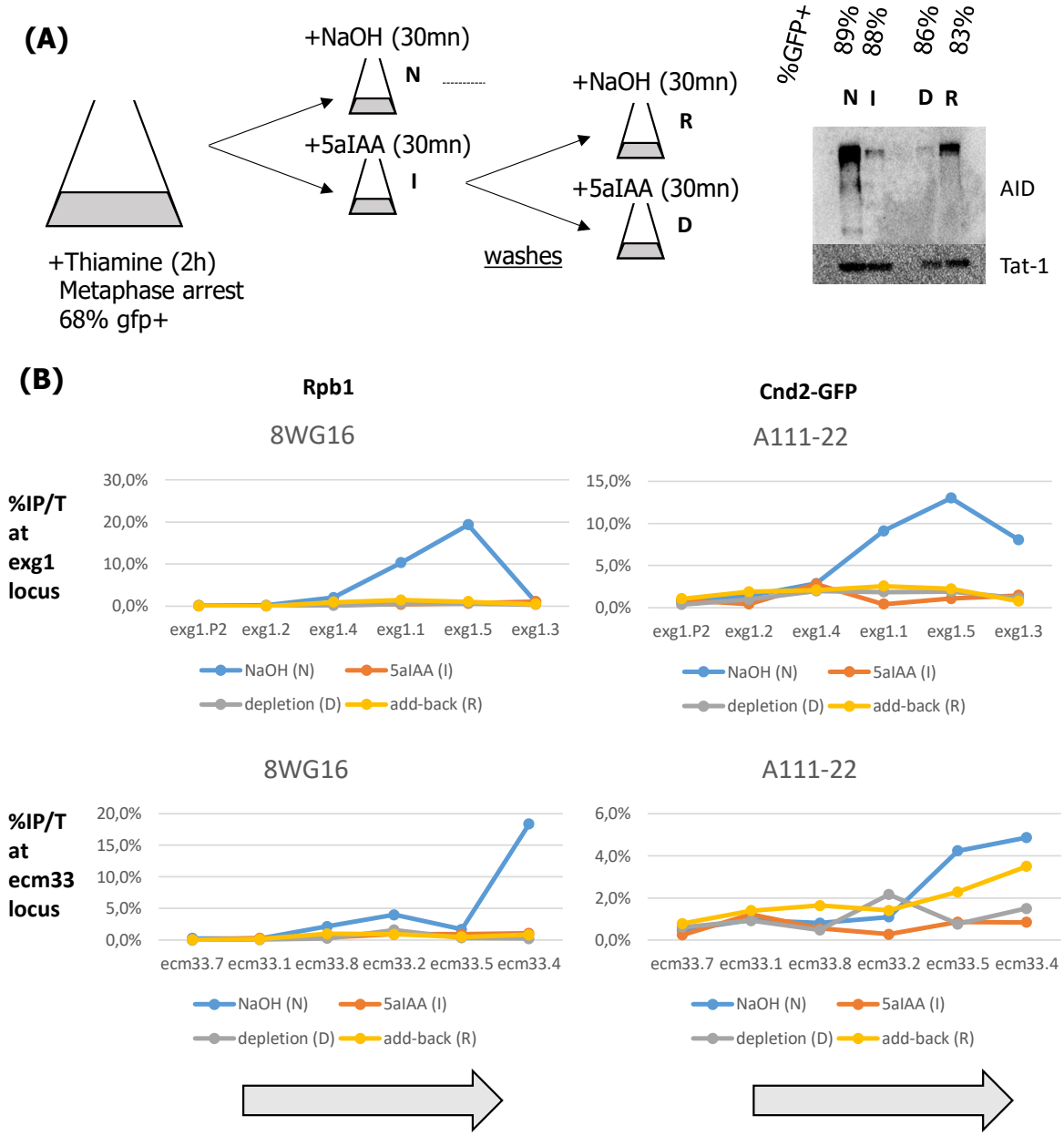

Fig. D2 Rpb1 association is not recovered in mitosis

(A) Left : principle of the Rpb1 recovery experiment in metaphase. rpb1-3xsAID is arrested in metaphase by exposition to Thiamine for 2h. Cells are then split in two and each sample is exposed to NaOH (N) or 5aIAA (I) for 30mn. The (I) sample is then split in two and washed/released into Thiamine containing medium with either 5aIAA, depletion (D) or with NaOH, add-back (R) for 30mn. Cells are then fixed and processed for ChIP-qPCR. Right : Western blot showing levels of Rpb1-3xsAID in the extract with the corresponding mitotic indexes.

(B) ChIP-qPCR against Rpb1 (8WG16) or Cnd2-GFP (A111-22), with the value expressed as the ratio of quantification in the IP relative to the input. Two protein coding genes expressed in M (*exg1* and *ecm33*) were probed along their length by the indicated primers. Despite recovery in the add-back condition of Rpb1-3xsAID as seen in the R sample in (A), chromatin-bound Rpb1 is not recovered.

In this paper we provide evidence that in fission yeast metaphase, active RNA pol II positions condensin genome wide and hinders its ability to establish long range contacts. With a reverse approach we show that efficient transcription termination limits the negative impact of RNA pol II on condensin function in metaphase. We show that transcription in mitosis impacts the physiology of sister chromatid segregation in anaphase without determining steady state levels of condensin association in metaphase.

6.2 RNA Pol II antagonises mitotic chromatin folding and chromosome segregation by condensin. bioRxiv. https://doi.org/10.1101/2023.08.08.552486

bioRxiv preprint doi: https://doi.org/10.1101/2023.08.08.552486; this version posted August 11, 2023. The copyright holder for this preprint (which was not certified by peer review) is the author/funder. All rights reserved. No reuse allowed without permission.

RNA Pol II antagonises mitotic chromatin folding and chromosome segregation by condensin

Jeremy Lebreton[1,4], Léonard Colin[2,4], Elodie Chatre[3] and Pascal Bernard[1,2*]

[1] ENS de Lyon, Univ Lyon, 46 allée d'Italie, F-69007, Lyon, France

[2] CNRS Laboratory of Biology and Modelling of the Cell, UMR 5239, ENS de Lyon, 46 allée d'Italie, F-69007, Lyon, France

[3] Lymic-Platim, Univ Lyon, Université Claude Bernard Lyon 1, ENS de Lyon, CNRS UAR3444, Inserm US8, SFR Biosciences, 50 Avenue Tony Garnier, F-69007 Lyon, France.

[4] Equal contribution

*Corresponding author and lead contact

Abstract

Condensin shapes mitotic chromosomes by folding chromatin into loops but whether it does so by DNA-loop extrusion remains speculative. While loop-extruding cohesin is stalled by transcription, no conclusive evidence has been provided regarding the impact of transcription on condensin despite its conserved enrichment at highly expressed genes. Using degrons of Rpb1 or the torpedo nuclease Dhp1^{XRN2}, we depleted or displaced RNAP2 on chromatin in fission yeast metaphase cells. We show that RNAP2 does not load condensin on DNA but instead retains condensin and hinders its ability to fold mitotic chromatin and to support chromosome segregation, consistent with the stalling of a loop-extruder. Transcription termination by Dhp1 limits such a hindrance. Our results shed a new light on the integrated functioning of condensin and we argue that a tight control of transcription underlies mitotic chromosome assembly by loop-extruding condensin.

Keywords: condensin, SMC complexes, loop-extrusion, mitotic chromosome assembly, transcription, transcription-termination.

bioRxiv preprint doi: https://doi.org/10.1101/2023.08.08.552486; this version posted August 11, 2023. The copyright holder for this preprint (which was not certified by peer review) is the author/funder. All rights reserved. No reuse allowed without permission.

Introduction

During mitosis, chromatin is reshaped into rod-shaped chromosomes in preparation for the accurate segregation of sister chromatids in anaphase. The assembly and maintenance of mitotic chromosomes is driven by the nonhistone protein complex condensin[1], whose deficiency manifests in anaphase by the stereotypical formation of chromatin bridges[2–4]. Condensin has two variants, named condensin I and II, with the latter being lost several times during evolution[1]. Budding and fission yeasts only have a single complex similar to condensin I in term of primary amino acid sequence. Current data indicate that yeasts and vertebrates condensins shape mitotic chromosomes by folding chromatin into loops[5–8], but the underlying mechanisms remain incompletely understood.

Condensins belong to the conserved family of SMC (Structural Maintenance of Chromosomes) genome organizers, which in eukaryotes includes cohesin and SMC5/6[1]. SMC protein complexes are composed at their core of two SMC-ATPases and a kleisin subunit that together form a ring, which associates with additional regulatory subunits[1]. A prevalent model proposes that SMCs drive intrachromosomal 3D contacts by processively extruding loops of DNA[9]. Condensins, cohesin and SMC5/6 have been observed extruding naked DNA into loops in an ATP-dependent manner in *vitro*[10–14]. Hi-C studies have further shown that, in addition to mediating sister-chromatid cohesion, cohesin organises chromatin into loops and intrachromosomal topologically associated domains (TADs) during interphase[15,9], while condensin-mediated loops enlarge during mitosis[5,6,8]. Although loop-extrusion *per se* has not been directly observed *in vivo*, a large body of studies support the idea that loop-extruding cohesin is halted by DNA-bound proteins such as pairs of convergent CTCF or active RNA polymerases in the context of chromatin[9,16–19]. However, similar experimental evidence remains scarce for eukaryotic condensins[20,21]. An alternative non-mutually exclusive model, namely diffusion capture[22], proposes that condensin shapes mitotic chromosomes by stabilizing random 3D contacts between its binding sites, either by capturing two DNA molecules inside its ring or through condensin-to-condensin contacts. Biophysical simulation recapitulates features of budding and fission yeast mitotic chromosomes[22,23], and experimental evidence indicates that condensin-condensin interactions underlie chromosome formation by a loop-extrusion independent mechanism in Xenopus egg extracts[24]. Thus, the mechanism(s) by which condensins fold chromatin into loops during mitosis remain(s) unclear.

bioRxiv preprint doi: https://doi.org/10.1101/2023.08.08.552486; this version posted August 11, 2023. The copyright holder for this preprint (which was not certified by peer review) is the author/funder. All rights reserved. No reuse allowed without permission.

To gain in functional understanding of condensin, we sought to compare its interplays with RNA polymerases with those of cohesin, taking advantage of the fact that transcription remains active during mitosis in fission yeast[25]. Chromatin immunoprecipitation coupled with high throughput sequencing (ChIP-seq) studies performed from yeasts to human have revealed a same broad basal association of condensins along the genome punctuated by peaks of high occupancy at centromeres, telomeres and rDNA repeats, as well as in the vicinity of highly expressed genes of any class along chromosome arms[25–28]. While cis-acting factors localising condensin at rDNA repeats[29,30], centromeres[31,32,30] or telomeres[33] have been identified, the mechanisms underlying the enrichment of condensin at highly expressed genes and its functional consequences remain poorly understood. In fission yeast, condensin accumulates at the 3'ends of genes highly-transcribed during mitosis[25]. Mouse and human condensin II are also enriched at active genes in cycling cells[34]. Even chicken and human condensin I, which bind transcriptionally silent chromatin in mitosis, accumulate in the vicinity of promoters that were active in the previous G2 phase[25,27]. We reported that nucleosome eviction from gene promoters facilitates the loading of fission yeast condensin onto DNA in vivo[35]. It also has been shown in xenopus egg extracts, which lack transcription, that the general transcription factor TFIIH promotes the loading of condensin I and II by competing with nucleosomes[36]. The TATA binding protein Tbp1^{TBP}, as well as sequence-specific DNA binding transcription factors, such as TFIIIC or Ace2, have been involved in the localisation of condensins at their target genes in yeasts and/or mammalian cells, but whether they act as a condensin loaders or positioning devices remains unclear[26,37,38,34]. The functional significance of condensin enrichment at highly expressed genes is further questioned by the finding that, in both chicken and fission yeast cells synchronized in mitosis, those sites exhibit only marginally increased frequencies of chromatin loops as compared to non-enriched loci[6,8]. It has been proposed that fission condensin and human condensin I bind to unwound DNA segments generated by transcription and reduce such structures to promote chromosome segregation during mitosis[25,39]. On the other hand, there is evidence that induction of transcription by either RNAP1 or RNAP2 of the 35S coding region of rDNA repeats antagonises condensin binding[40,41] and we recently suggested that backtracked RNA polymerases constitute a barrier for condensin[21]. Thus, no clear picture emerges as to the functional significance of condensin enrichment in the vicinity of highly expressed genes.

bioRxiv preprint doi: https://doi.org/10.1101/2023.08.08.552486; this version posted August 11, 2023. The copyright holder for this preprint (which was not certified by peer review) is the author/funder. All rights reserved. No reuse allowed without permission.

Here, we used degrons alleles to rapidly deplete or displace RNAP2 on mitotic chromatin in fission yeast cells and assessed the consequences on condensin's localization, chromatin folding in metaphase and accurate chromosome segregation in anaphase. In contrast to a previous study[25], we found that RNAP2 transcription does not recruit fission yeast condensin, but instead retains it in cis. We further show that RNAP2 hinders both condensin-mediated chromatin folding in metaphase and condensin-dependent accurate chromosome segregation in anaphase. We argue that our results are best explained by the stalling of translocating condensin against a transcriptional barrier and provide indirect evidence for condensin shaping mitotic chromosomes by DNA-loop extrusion.

Results

Transcribing RNAP2 causes the accumulation of condensin at the 3'end of class II genes

Fission yeast condensin binds chromatin throughout mitosis and accumulates at mitotically transcribed genes, forming peaks of high occupancy notably at the 3'end of class II genes whose expression is maximal in the M-G1 phases[25]. To revisit the role played by RNAP2 in condensin's localisation, we created an auxin-inducible degron of Rpb1 (Rpb1-sAID), the largest subunit of RNAP2. Fission yeast cells expressing both the kleisin subunit of condensin tagged with GFP (Cnd2-GFP) and Rpb1-sAID were arrested in metaphase, exposed to either auxin (OFF condition) or NaOH (solvent, ON condition) while maintaining the arrest, and chromosomal associations of both Cnd2-GFP and Rpb1-sAID were measured by calibrated-ChIP (cal-ChIP). This type of experimental approach was used for all metaphase arrests. Auxin induced a rapid (30 minutes) and acute depletion of Rpb1 while Cnd2-GFP level and mitotic indexes remained unchanged (Fig. S1A-B). Quantitative (q)PCR analysis of representative mitotically-expressed protein-coding genes confirmed their near-complete loss of Rpb1 upon auxin adjunction (Fig. S1C, upper panel, n = 3 biological replicates). Consistent with a previous report showing that a chemical inhibition of RNA polymerases reduces condensin occupancy[25], Rpb1 depletion from those genes caused a strong reduction of Cnd2-GFP, while it remained unchanged at control, non-RNAP2, condensin binding sites (Fig. S1C, lower panel). These results confirm that RNAP2 impinges upon condensin localisation. However, Cnd2-GFP occupancy remained constantly above background after depletion of Rpb1 (Fig. S1C), suggesting that a fraction of condensin persisted on chromatin.

bioRxiv preprint doi: https://doi.org/10.1101/2023.08.08.552486; this version posted August 11, 2023. The copyright holder for this preprint (which was not certified by peer review) is the author/funder. All rights reserved. No reuse allowed without permission.

To assess the genome wide relevance of these results, cal-ChIP samples were pooled and processed for high throughput sequencing (cal-ChIP-seq). Ranking ChIP-seq signals at protein coding genes by mean normalized Rpb1 signal revealed that Cnd2-GFP association mirrored Rpb1 (Rpb1-ON, Fig. 1A). Auxin-mediated depletion of Rpb1 caused a strong reduction of Cnd2-GFP at the 3'end of most if not all protein-coding and non-coding genes transcribed by RNAP2 (Rpb1-OFF, Fig. 1A-B and Fig. S1D) while a subset of gene promoters retained Cnd2-GFP occupancy (Fig.1B and S1C lower panel). It has been reported that treatment with the RNA polymerase inhibitor 1,10- phenanthroline causes condensin to dissociate from chromatin[25]. In contrast, when we scored the full normalized amounts of Cnd2-GFP reads mapped to the genome, we observed no major difference between the Rpb1-ON and Rpb1-OFF conditions (Fig. 1C), suggesting that Cnd2-GFP did not dissociate from chromatin and might instead translocate away from Rpb1-depleted genes. Cal-ChIP-seq also validated that auxin adjunction reduced the binding of Cnd2-GFP neither at tDNAs (Fig. 1D), nor at rDNA repeats or the kinetochore assembly site of centromere 1 (Fig. S1E,F) where condensin localisation relies respectively on the transcription factor TFIIIC[26,42,34] and monopolin[30]. The enrichment of fission yeast condensin at the 3'end of active class II genes is therefore dependent on Rpb1 in *cis*. Consistently, ~70% of the condensin peaks identified in RPB1-OFF were associated with tDNAs, rDNA genes or long terminal repeats retrotransposons (Fig. S1G) for which specific factors position condensin[26,31,34,43]. The remaining 30% contained no feature previously associated with condensin.

If condensin is positioned by RNAP2 in mitosis, displacing RNAP2 on chromatin should shift condensin positions. To test this, we constructed an auxin inducible degron of Dhp1^{XRN2} (Dhp1-sAID), the torpedo ribonuclease involved in the termination of RNAP2 transcription[44]. Dhp1 loss of function in fission yeast causes active RNAP2 (S2P) to invade DNA sequences downstream of transcription end sites (TES)[44]. We depleted Dph1-sAID from metaphase arrests (Fig. S1A-B) and performed cal-ChIP-seq against Cnd2-GFP. Density heatmaps of read counts revealed an increase of Cnd2-GFP around the TES of a subset of protein-coding genes (Fig. 1E and S1H), but the most prominent phenotype was a shift of Cnd2-GFP peaks downstream the 3'end of genes (Fig. 1F). The shift was particularly obvious at sn(o)-RNA genes (Fig. 1G) and specific to class II genes (Fig. S1E-F). These results strengthen and extend a previous observation by ChIP-qPCR at two mitotically-transcribed protein-coding genes[39]. Larochelle et al. described a similar shift of Rpb1 cal-ChIP-seq signals in Dhp1-depleted fission

bioRxiv preprint doi: https://doi.org/10.1101/2023.08.08.552486; this version posted August 11, 2023. The copyright holder for this preprint (which was not certified by peer review) is the author/funder. All rights reserved. No reuse allowed without permission.

yeast cells[44]. Reanalysing their data showed that the displacements of Cnd2-GFP upon Dph1-depletion mirrored those of Rpb1, both in orientation and in amplitude (Fig. 1F and 1G), arguing that condensin localisation responded to features associated with transcribing RNAP2. Since readthrough transcription can invade downstream genes, we analysed condensin localisation in Dhp1-ON vs OFF cells as a function of gene orientation (Fig. 1H). The shift of Cnd2-GFP signals upon Dhp1 depletion proved independent of gene orientation. However, convergent genes exhibited the highest condensin occupancy in Dhp1-ON and a specific increase of Cnd2-GFP occupancy in their body in Dhp1-OFF (Fig. 1H). This is consistent with our previous work suggesting that condensin is pushed by polymerases[21] as converging reading-through RNAP2 may trap condensin. Thus, transcribing RNAP2 plays a role in *cis* in the accumulation of condensin at the 3'end of active class II genes.

RNAP2 transcription does not recruit condensin onto DNA

Our finding that the steady state level of Cnd2-GFP on chromatin remained largely unchanged upon depletion of Rpb1 (Fig. 1C) appeared inconsistent with a preferential binding of condensin to unwound DNA generated by transcription[25,39]. To further investigate this, we took an orthogonal approach and performed photoactivated localisation microscopy and single particle tracking (SPT-PALM) of condensin in living fission yeast cells. A recent study has shown that SPT-PALM provides accurate measurements of the chromatin association of the related SMC5/6 complex in asynchronous fission yeast cells[45]. Using Cnd2 tagged with mEOS3.2 (Cnd2-mEOS3.2)[45], we first characterized condensin behaviour in an otherwise wild-type (WT) background. Cells were arrested in metaphase, subsets of Cnd2-mEOS3.2 were photoconverted, imaged at a framerate of 33.6 ms, individual tracks were reconstituted and analysed with sptPALM viewer[46]. To identify metaphase cells, we used Cdc11-GFP to fluorescently-label spindle pole bodies (SPBs, the counterpart of centrosomes) and selected cells showing two SPBs separated by 2-3 µm (Fig. 2A). In WT, we observed two main populations of nuclear condensin characterized by their slow or fast molecular movements (Fig. 2B-C). The Cnd2-mEOS3.2 fast fraction showed a diffusion coefficient of around 0.5 $\mu m^2.s^{-1}$, reminiscent of the 0.7 $\mu m^2.s^{-1}$ of nucleosoluble Mcm4 in *S. pombe*[47]. By depleting the $Cut14^{SMC2}$ subunit of condensin to detach Cnd2 from metaphase chromatin (Fig. 2D and S2A), we attributed the slow and fast Cnd2-mEOS3.2 signals to the chromatin-bound and nucleosoluble fractions of condensin, respectively (Fig. 2E). Next, we depleted Rpb1 from

bioRxiv preprint doi: https://doi.org/10.1101/2023.08.08.552486; this version posted August 11, 2023. The copyright holder for this preprint (which was not certified by peer review) is the author/funder. All rights reserved. No reuse allowed without permission.

metaphase-arrested cells (Fig. S2A) and recorded Cnd2-mEOS3.2 movements. The fraction of slow, chromatin-bound, molecules of Cnd2-mEOS3.2 remained unchanged (Fig. 2F and S2B). In contrast, degrading Dhp1 in metaphase (Fig. S2A) slightly increased the steady state level of slow Cnd2-mEOS3 molecules (Fig. 2F and S2C) (see Discussion). Data analyses performed with another software (Spot-ON [48]) provided identical results (Fig. S2D-E). These data confirm that RNAP2 transcription plays no role in the steady-state binding level of condensin to DNA *in vivo*.

Active RNAP2 hinders the folding of chromatin into mitotic chromosomes

In fission yeast, cohesin folds chromatin into TADs of 30-50 kb during interphase[49,50], while condensin shapes larger intrachromosomal domains in mitosis (median size ~ 300-500 kb) by mediating cis contacts over longer distances ranging from ~ 70 kb to ~ 1 Mb[8,38,50]. To determine the consequences of transcribing RNAP2 on condensin activity, we assessed the impact of Rpb1 and Dhp1 on chromatin folding in mitosis, using chromosome conformation capture (Hi-C). We found that depleting Rpb1 from metaphase-arrests increased the frequencies of intrachromosomal contacts between 20 kb and 2 Mb (Fig. 3A, left panel), suggesting enhanced cohesin and/or condensin activity. The average size of chromatin loops can be inferred by studying the slope of the distance law, the maximum value closely matching the average length of loops[51]. Using this metric, we further found that the average size of loops in metaphase was increased upon depletion of Rpb1 (Fig. 3A, right panel). In contrast, depleting Dhp1 decreased the frequencies of intrachromosomal contacts between 100 kb and 1 Mb and reduced the average size of chromatin loops (Fig. 3B). Thus, Rpb1 limits chromatin folding in metaphase while Dhp1 promotes the formation of longer loops in the range of condensin activity. In line with this, comparing Hi-C maps between the ON and OFF conditions revealed that removing Rpb1 erased large TADs (Fig. 3C and S3A) to the benefit of long-range interactions across their borders where both Rpb1 and Cnd2-GFP were strongly reduced (Fig. 3D and S3A). Small TADs appeared reduced as well (Fig. 3C). In contrast, degrading Dhp1 decreased the frequencies of intrachromosomal contacts between large TADs (Fig. 3E and S3B) while increasing Cnd2-GFP and Rpb1 levels at the cognate borders (Fig. 3F). Similar results obtained from a second set of biological replicates are shown in Figure S3C-F. Thus, Rpb1 hinders the folding of chromatin in metaphase while Dhp1, in contrast, promotes condensin-mediated long-range 3D contacts. Since depleting fission yeast condensin is sufficient to erase

bioRxiv preprint doi: https://doi.org/10.1101/2023.08.08.552486; this version posted August 11, 2023. The copyright holder for this preprint (which was not certified by peer review) is the author/funder. All rights reserved. No reuse allowed without permission.

large TADs characteristic of metaphase chromosomes[8], the concurrence between a gain of contacts across a TAD boundary and a local reduction of Cnd2-GFP occupancy (Rpb1-OFF), and vice-versa (Dhp1-OFF), might therefore reflect condensin's accumulation at a RNAP2-dependent barrier to loop formation.

Active RNAP2 creates barriers for chromatin loop formation by condensin

We assessed whether condensin local enrichment correlated with boundaries. Using the insulation score and MACS2, we scanned the genome for any boundary and high-occupancy condensin peak, respectively. We identified 280 boundaries and 290 condensin peaks in RPB1-ON metaphases, 56 of which overlapped (Fig. 4A, red dots). This limited overlap is consistent with previous studies[8,38] and can conceivably be explained, at least in part, by the presence within the data sets of cohesin boundaries, since small TADs formed by the latter persist in mitosis in fission yeast[50]. The insulating strength of a border correlated positively with condensin enrichment, notably when associated with a condensin peak (Fig. 4A). Aggregating Hi-C signals around two adjacent high-occupancy condensin sites confirmed that they define intrachromosomal domains (Fig. 4B). Depleting Rpb1 increased the frequencies of intrachromosomal 3D contacts across those boundaries while the insulation of condensin domains was strengthened in Dhp1-OFF (Fig. 4B), suggesting that condensin boundaries depend on their associated levels of active RNAP2. We next assessed how the changes in insulation compared with condensin occupancy. Of the 280 boundaries identified in Rpb1-ON, 45% were weakened upon depletion of Rpb1, 49% remained stable and 6% appeared strengthened (Fig. 4C). Weakened boundaries showed a high condensin peak in Rpb1-ON which was virtually erased in Rpb1-OFF (Fig. 4D), while stable and strengthened boundaries respectively exhibited unchanged and slightly increased condensin occupancy relative to the surrounding basal signal (Fig. 4D). Conversely, boundaries gaining in insulation (19%) in Dhp1-OFF gained in condensin occupancy, but stable (52%) or weakened (29%) borders exhibited no clear change (Fig. 4C-D). Thus, active RNAP2 creates insulating barriers at highly expressed genes where the accumulation of condensin matches the insulation strength.

Transcription termination limits the strength of RNAP2 barriers to condensin

To understand how Dhp1 controls border strength, we sorted protein coding genes according to the change in condensin binding upon Dhp1 depletion using K-means clustering (Fig. 5A left

bioRxiv preprint doi: https://doi.org/10.1101/2023.08.08.552486; this version posted August 11, 2023. The copyright holder for this preprint (which was not certified by peer review) is the author/funder. All rights reserved. No reuse allowed without permission.

panel) and analysed those genes for specific features. Among five clusters, cluster 1 revealed the strongest increase in condensin level within gene bodies (Fig. 5A, left panel). Strikingly, in Dhp1-ON, these cluster 1 genes exhibited high levels of condensin at their 3' end but, unlike the other clusters, also at their 5' ends (Fig. 5A, right panel). Cluster 1 genes were more frequently in convergent orientation (Fig. 5B) relative to the other clusters. They were also smaller and closer to their neighbouring genes (Fig. S4A-B) and displayed higher levels of active RNAP2 upstream of their 5'end (Fig. S4C). Such biases suggested that cluster 1 genes could be prone to invasion by transcriptional readthroughs.

Cluster 1 genes were the most insulating in Dhp1-ON and showed the strongest gain in insulation in Dhp1-OFF (Fig. 5C), suggesting that the depletion of Dhp1 mostly strengthened pre-existing boundaries. In contrast, the other clusters showed lower insulation in both conditions. Notably, cluster 5, which displayed similar levels of condensin as cluster 1 in Dhp1-ON but only at the 3' end (Fig. 5A), gained neither in condensin occupancy within gene bodies (Fig. 5A) nor in insulation upon depletion of Dhp1 (Fig. 5C). Considering the existing biases in cluster 1 genes which are reversed in cluster 5 (Fig. 5B and S4), we assessed whether transcriptional readthroughs could explain their different sensitivities to Dhp1. To this end, we selected the nearest facing neighbour of each gene of cluster 1 and assessed the condensin and RNAP2 ChIP-seq profiles of every gene pairs (Fig. 5D). This clearly showed that depleting Dhp1 caused transcriptional readthroughs across their common intergenic region and increased RNAP2 occupancy in the body of the less transcribed downstream gene (Fig. 5D, lower panels), a likely consequence of the invasion of the latter by reading-through polymerases. The condensin peak initially proximal to the TES of the upstream gene became higher and larger upon depletion of Dhp1 and was displaced in the direction of the strongest transcription, encroaching on the body of the downstream gene (Fig. 5D, upper panels). The same analysis applied to cluster 5 revealed readthroughs of lower amplitude and no visible invasion of condensin into the downstream gene (Fig. 5E). Thus, these data suggest that Dhp1 dampens the strength of condensin borders by ensuring an efficient termination and removal of RNAP2 from chromatin.

RNAP2 hinders condensin-dependent mitotic chromosome segregation in anaphase

The formation of chromatin bridges in anaphase caused by condensin deficiency conceivably stems from the fact that condensin orientates the activity of Topoisomerase II towards the

bioRxiv preprint doi: https://doi.org/10.1101/2023.08.08.552486; this version posted August 11, 2023. The copyright holder for this preprint (which was not certified by peer review) is the author/funder. All rights reserved. No reuse allowed without permission.

decatenation of chromosomes and sister-chromatids[52,53] and confers to chromosome arms the elasticity to withstand the spindle traction forces[54]. If condensin achieved these tasks by folding chromatin, depleting Rpb1 or Dhp1 was expected to respectively lower or increase the frequency of chromatin bridges caused by a mutation in condensin. We and others previously observed a rescue of accurate chromosome segregation in condensin mutant cells when a component of the transcriptional co-activator Mediator was impaired[55] or upon pharmacological inhibition of transcription[25]. We therefore measured the effect of depleting Rpb1 or Dhp1 on the frequency of chromatin bridges caused by the thermosensitive *cut3-477* mutation in the Cut3^{SMC4} subunit of condensin[2], which reduces condensin binding at the restrictive temperature of 36°C[33]. Consistent with previous reports[2,55], ~80% of *cut3-477* cells in anaphase displayed a chromatin bridge at 36°C (Fig. 6A-B). The frequency sharply dropped to ~ 40% when Rpb1 was depleted in *cut3-477* mutant cells (Fig. 6B). Depleting Dhp1, in contrast, almost doubled the frequency of chromatin bridges caused by the *cut3-477* condensin mutation at the semi-permissive temperature of 32°C (Fig. 6C), as expected. To validate these observations, we next assessed the impact of the DNA-binding transcription factor Fkh2, which together with Ace2 drives the transcription of most of the mitotically expressed protein-coding genes where condensin accumulates in mitosis[38,56]. Consistent with the rescue effect by Rpb1 depletion, deleting *fkh2* restored the growth of *cut3-477* mutant cells at 36°C (Fig. 6D). Thus, these data extend the idea that Rpb1 and Dhp1 respectively antagonises and facilitates the functioning of condensin from metaphase to anaphase by affecting its ability to fold chromatin and by extension to support accurate chromosome segregation.

Discussion

Here we investigated the enrichment of fission yeast condensin at genes highly transcribed by RNAP2, and the functional consequences of such an accumulation on chromatin folding in metaphase and accurate chromosome segregation in anaphase. By rapidly and acutely depleting Rpb1 and Dhp1, we modulated the occupancy and the location of transcribing RNAP2 in metaphase and collected compelling experimental evidence showing that RNAP2 does not control the steady state level of condensin binding but instead creates transcriptional barriers that accumulate condensin and hinder condensin-mediated chromatin folding and chromosome segregation. Our results are in perfect agreement with the stalling of

bioRxiv preprint doi: https://doi.org/10.1101/2023.08.08.552486; this version posted August 11, 2023. The copyright holder for this preprint (which was not certified by peer review) is the author/funder. All rights reserved. No reuse allowed without permission.

translocating bacterial SMCs against transcriptional barriers[57,58], and fully consistent with the way transcription interferes with cohesin localisation and loop-formation activity in various systems[17–19,59,60]. Thus, given the large body of studies supporting loop extrusion by cohesin in vivo[9], and by all eukaryotic SMCs in vitro[10–14], we argue that transcription is a barrier for chromatin folding by condensin in vivo as indirect evidence that condensin folds mitotic chromosomes by loop extrusion (Fig. 6E).

Our finding that the steady state level of chromosomal condensin is not modified by the acute depletion of Rpb1 sheds a new light on the possible molecular determinants of condensin loading sites within chromatin. First, it demonstrates that Rpb1, the core component of RNAP2, is not required for condensin loading. Second, it challenges the idea that unwound or positively supercoiled DNA structures generated by transcription could recruit condensin [39,61] as they are unlikely to survive the depletion of Rpb1[62]. On the other hand, DNA-bound transcription factors and nucleosome-depleted promoters can persist in mitosis despite transcriptional repression[63,64], raising the possibility that they may underly the Rpb1-independent localisation of condensin in the vicinity of some gene promoters. Further study is needed to assess whether or not it could be the case.

Regarding the mechanism by which RNAP2 impinges upon condensin, the most parsimonious hypothesis should explain how RNAP2 positions condensin along the genome while antagonising its chromatin folding activity. The moving barrier model[19,58] fulfils these criteria. Indeed, the stalling of loop extruding condensin molecules upon head-on collision with a transcriptional barrier formed in a Rpb1-dependent manner (Fig. 6E) provides a straightforward explanation to the redistribution of condensin, the gain of long-range intrachromosomal contacts in metaphase and the weakening of condensin boundaries in Rpb1-depleted metaphases. The removal of a transcriptional hindrance to condensin-mediated chromatin folding is also consistent with the rescue of accurate chromosome segregation observed in condensin mutant cells upon depletion of Rpb1. Such a mechanistic model also convincingly explains our experimental observations in Dhp1-depleted cells (Fig. 6 6E, as expected from the control exerted by Dhp1 over Rpb1[44]. The loss of Dhp1 leads to (1) an enlargement of the domains occupied by active RNAP2, (2) a rise in condensin occupancy in cis that positively correlates with boundary strength, particularly at a subset of convergent genes separated by short intergenic regions, (3) reduced frequencies of intrachromosomal contacts and (4) an increased hindrance on condensin-mediated chromosome segregation. A

bioRxiv preprint doi: https://doi.org/10.1101/2023.08.08.552486; this version posted August 11, 2023. The copyright holder for this preprint (which was not certified by peer review) is the author/funder. All rights reserved. No reuse allowed without permission.

similar mechanism likely explained the accumulation of condensin at a subset of tRNA genes that we previously observed when the RNAP3 transcription termination factor Sen1 was deleted[21]. On the other hand, the possibility that Dhp1 and/or Rpb1 could impact condensin-mediated diffusion capture appears less likely. Since high-occupancy condensin binding sites are postulated to mediate diffusion capture[22,23], it is difficult to imagine how the mere redistribution of condensin upon depletion of Rpb1 could benefit the accurate segregation of chromosomes in anaphase in a condensin mutant background, and reciprocally depleting Dhp1 be detrimental to the folding of chromatin by diffusion capture while it increases condensin occupancy at those sites.

It is therefore tempting to speculate that the broad and basal condensin-ChIP-seq signal observed in a wide range of species correspond to translocating condensin complexes caught in the process of loop-extrusion. The slight increase in condensin occupancy in Dhp1-depleted metaphases might stem from an increased residence time of such active condensin complexes trapped in between converging reading-though polymerases, among other possible mechanisms. Along this line, it is unclear why Dhp1-depletion had no apparent impact on the frequencies of contacts in the range size of cohesin in our Hi-C data. This might be due to the fact that our experiments were performed in metaphase and/or to varying sensitivities to Dhp1 loss since condensin and cohesin respond differently to single obstacles in loop-extrusion assays[65].

Although loop-extruding condensin has been observed traversing DNA-bound isolated obstacles of sizes ranging from tens to 200 nm in in-vitro assays[65], it has also been reported that engineered arrays of tightly bound proteins impair in *cis* the activity of condensin in budding yeast[20]. Thus, features associated with tracks of RNAP2, be it proteins, nascent RNA, chromatin modifications, specific DNA structures and/or changes in the local chromatin fiber rigidity are as many possible candidates to stall condensin. Whatever the molecular determinants, the fact that read-through transcripts are produced in wild-type fission yeast cells[66,67] and that condensin accumulation and insulation are found more often at closely spaced convergent genes points towards efficient transcription termination as a key player in the folding of transcribed chromatin by condensin complexes. In that context, the downregulation of transcription taking place upon mitotic entry in metazoans might provide an increase in fitness for the folding of large genomes by loop extruding condensin.

bioRxiv preprint doi: https://doi.org/10.1101/2023.08.08.552486; this version posted August 11, 2023. The copyright holder for this preprint (which was not certified by peer review) is the author/funder. All rights reserved. No reuse allowed without permission.

Figure legends

Figure 1. Active RNAP2 localises condensin in cis

(A) Heatmaps of normalized Rpb1 (8WG16) and Cnd2-GFP (A111-22) cal-ChIPseq signal at protein coding genes ranked by the mean Rpb1 signal, in NaOH (Rpb1-ON) or auxin-treated (Rpb1-OFF) *rpb1-sAID* metaphase arrested degron strains. The values represent the IP/T ratio of *S. pombe* calibrated by the *S. cerevisiae* SMC3-GFP IP (see Materials and Methods).

(B) Mean metagene profile of the normalized Cnd2-GFP ChIPseq signal from (A).

(C) Occupancy ratio (OR) of cal-ChIPseq from (A) in the indicated conditions. The OR is the ratio between the total amount of mapped reads in the IP and the Total of *S. pombe* normalized by the ratio between the amount of reads in the Total and the IP of *S. cerevisiae.*

(D) Normalized Cnd2-GFP (top) and Rpb1 (bottom) cal-ChIPseq at chromosome III (810000-822500) in Rpb1-ON and Rpb1-OFF.

(E) Heatmap of normalized Cnd2-GFP cal-ChIPseq signal at protein coding genes ranked by mean strength, in NaOH (Dhp1-ON) or auxin-treated (Dhp1-OFF) *dhp1-sAID* metaphase arrested degron strains. The values represent the IP/T ratio of *S. pombe* calibrated by the *S. cerevisiae* SMC3-GFP IP.

(F-G) Metagene profile of the mean normalized cal-ChIPseq signal from (E) and the mean normalized RNAP2(S2P) cal-ChIPseq signal in WT or Pnmt41-dhp1-off from ref.44.

(H) Metagene profile of the data in (F) grouped according to gene orientation.

Figure 2. RNAP2 plays no major role in the steady-state level of condensin on chromatin.

(A) Representative images of SPT-PALM acquisition on metaphase arrested fission yeast cells expressing Cnd2-mEOS3.2. Left, stack of Cnd2-mEOS3.2 during a 20 000-time series (27.7 Hz) using a TIRF illumination. Middle, position of the SPBs (spindle poles) labelled by Cdc11-GFP. Right, brightfield acquisition.

(B) Median (+/- SE) mean-square displacement of the two populations of Cnd2-mEOS3.2 identified during metaphase as slow (blue) or fast (red) in WT cells (2670 tracks).

(C) Distribution of the apparent diffusion coefficient ($\mu m^2.s^{-1}$) of 2670 tracks from metaphase arrested WT cells identified from one representative SPT-PALM acquisition. The vertical line represents the optimal $\log_{10}(D_{inst})$ separating the two populations of molecules according to a skewed-Gaussian mixture model (FMSMSN). The fitted gaussians are represented in blue and

bioRxiv preprint doi: https://doi.org/10.1101/2023.08.08.552486; this version posted August 11, 2023. The copyright holder for this preprint (which was not certified by peer review) is the author/funder. All rights reserved. No reuse allowed without permission.

orange for slow and fast populations respectively. The fraction of molecules belonging to each population is indicated on the left of the panel.

(D) ChIP α-Cnd2-GFP after 2 hours of NaOH (ON) or IAA (OFF) treatment on either *cut14-sAID cnd2-GFP* or *NLS-GFP* cells arrested in metaphase. qPCRs were performed on two biologically independent experiments on centromere I (*cnt1)* or the condensin-enriched *exg1* gene. For statistical analysis t.test was used to compare the OFF and ON conditions: * p.value < 0.05.

(E) Same as in (C) but for metaphase arrested Cut14 ON and OFF cells. The same model fitting was applied to both conditions but a single population of molecules was identified in the Cut14-OFF condition. Representative results of at least 2 independent experiments.

(F) The fraction of slow Cnd2-mEOS3.2 molecules identified as described in (B-C) was calculated for WT, *rpb1-sAID* and *dhp1-sAID* metaphase arrested cells. Each point corresponds to a biologically independent experiment and at least two consecutive acquisitions (1000-4000 tracks). t.test was used to compare the OFF and ON conditions: * p.value < 0.05.

Figure 3. Active RNAP2 hinders chromatin folding by condensin in metaphase

(A-B) Hi-C contact probability curve P(s) as a function of distance and its corresponding slope in Rpb1-ON and Rpb1-OFF conditions (A) or in Dhp1-ON and Dhp1-OFF conditions (B). Arrows indicate the estimated size of the maximum in the slope.

(C) Hi-C contact maps of Rpb1-ON and Rpb1-OFF at 10kb resolution on the left arm of chromosome I. Black arrows point to domain borders that disappear in Rpb1-OFF.

(D) log2 differential map of Rpb1-OFF/Rpb1-ON at 10kb resolution on the left arm of chromosome I (Top) and tracks of the cal-ChIPseq of Cnd2-GFP and RNAP2 presented in Fig. 1 on the same region. Black arrows are the same as in (C).

(E-F) Same as in (C) and (D) but for Dhp1-OFF/ Dhp1-ON. Black arrow indicates a border that is strengthened in the Dhp1-OFF condition.

Figure 4. Active RNAP2 creates barriers for chromatin loop formation by condensin

(A) Distribution of the insulation score determined from Hi-C maps as a function of condensin enrichment at peaks identified by MACS2. Condensin peaks were considered overlapping with a border when they were located within the 3kb bin defining the border and are shown in red. The Pearson correlation coefficient r and its associated p.value are plotted in black for all

bioRxiv preprint doi: https://doi.org/10.1101/2023.08.08.552486; this version posted August 11, 2023. The copyright holder for this preprint (which was not certified by peer review) is the author/funder. All rights reserved. No reuse allowed without permission.

peaks, in red for condensin peaks associated with borders. The linear regression for each population is drawn.

(B) Off-diagonal pileup of Hi-C signal at n=110 condensin sites identified in the Rpb1-ON condition separated by a distance range of 100-300kb in Rpb1-ON or Rpb1-OFF and Dhp1-ON or Dhp1-OFF. Signals are shown as a function of the observed/expected log2 ratio.

(C) Domain boundaries were identified with the insulation score and compared between the OFF and ON samples. A border was considered stable if the log2 ratio OFF/ON was between -0.58 and 0.58, and strengthened or weakened otherwise.

(D) Metagene profiles of the mean normalized Cnd2-GFP cal-ChIPseq signal at the border classes shown in (C) in the indicated conditions.

Figure 5. Transcription termination limits the strength of RNAP2 barriers to condensin

(A) Left panel: metagene profile of the mean log2 ratio of Dhp1-OFF/Dhp1-ON normalized Cnd2-GFP cal-ChIPseq signals, grouped after k-means clustering (k=5) at protein coding genes. Right panel: metagene profile of the mean normalized Cnd2-GFP cal-ChIPseq signal in Dhp1-ON using the same clusters.

(B) Frequency of intergenic regions flanked by protein-coding genes in convergent or divergent orientations in clusters I to V defined in (A).

(C) Mean normalized Cnd2-GFP cal-ChIPseq signal at clusters I to V in the indicated conditions and their corresponding mean Hi-C insulation score (bottom). The region shown is 100kb centered on the border.

(D) Metagene profile of mean normalized Cnd2-GFP and RNAP2 (S2P)[44] cal-ChIPseq-signals in Dhp1-ON or OFF samples of cluster I genes. A 6kb window centered on the intergenic region flanked by converging or tandem genes is shown. For convergent gene pairs, the most expressed gene is always on the left.

(E) Same as in (D) for cluster V.

Figure 6. RNAP2 hinders condensin-dependent mitotic chromosome segregation in anaphase

(A) Representative images of normal and defective anaphases in fission yeast cells.

(B-C) Indicated cells were fixed and processed for immunofluorescence against α-tubulin. Anaphase cells showing a mitotic spindle > 5 µm in length were selected and chromosome

bioRxiv preprint doi: https://doi.org/10.1101/2023.08.08.552486; this version posted August 11, 2023. The copyright holder for this preprint (which was not certified by peer review) is the author/funder. All rights reserved. No reuse allowed without permission.

segregation assessed. Shown are frequencies calculated from 2 or 3 replicates with n = 100 anaphases per experiment.

(D) Serial dilution spot assays (5-fold) of the indicated *S. pombe* strains. Images are taken after 60 hours of growth at the indicated temperatures.

(E) Model of condensin activity at highly transcribed genes. In wild-type, loop-extruding condensin accumulates at chromosomal sites densely bound by RNAP2, such as the 3' end of genes near the TES. Condensin can eventually bypass this domain-defining barrier with an indeterminate probability. When $Dhp1^{XRN2}$ is depleted from metaphase cells, RNAP2 transcribes through the TES, pushing condensin complexes further downstream. At gene dense regions, $Dhp1^{XRN2}$ depletion causes reading through RNAP2 to invade downstream genes, creating larger and less permeable barriers that further stall condensin and lowers its ability to extrude beyond this region.

Supplementary Figure 1: Active RNAP2 localises condensin in cis, related to Figure 1

(A) Representative western blots of total protein extracted from *rpb1-sAID* or *dhp1-sAID* metaphase arrests before and after 30 min and 1h of 5-adamantyl-IAA treatment, respectively. Tubulin is shown as a loading control.

(B) Mitotic indexes, calculated as the percentage of mononucleate cells exhibiting high Cnd2-GFP fluorescent signals in their nucleus within the total cell population, used for cal-ChIP-seq in Figure 1.

(C) ChIP-qPCR signal of Rpb1-ChIP (top) and Cnd2-GFP-ChIP (bottom) at two mitotically expressed protein coding genes (*exg1, ecm33*), central domain of centromere I (*cnt1*), at ribosomal DNA from the right arm of chromosome III (rDNA) and a low condensin binding site (*fet4*). Mean values from three biological replicates are shown, with standard deviation.

(D) Metagene profile of the mean normalized Rpb1 and Cnd2-GFP cal-ChIPseq signal at snRNA and snoRNA genes in Rpb1-ON and Rpb1-OFF.

(E-F) Normalized Cnd2-GFP ChIPseq signal at the at the rDNA locus on the right arm of chromosome III (E) or at the central domain of centromere 1 (F) in Rpb1-ON and Rpb1-OFF and Dhp1-ON and Dhp1-OFF conditions.

(G) Distribution of features associated with condensin peaks detected by MACS2 in Rpb1-OFF.

(H) Heatmap of normalized Cnd2-GFP cal-ChIPseq signals at protein coding genes ranked by mean strength, in Dhp1-ON and Dhp1-OFF of the second biological replicate.

bioRxiv preprint doi: https://doi.org/10.1101/2023.08.08.552486; this version posted August 11, 2023. The copyright holder for this preprint (which was not certified by peer review) is the author/funder. All rights reserved. No reuse allowed without permission.

Supplementary Figure S2: RNAP2 does not influence the steady-state level of condensin on chromatin, related to Figure 2.

(A) Western blots showing the depletion of Rpb1-sAID (30 min), Dhp1-sAID (1h) and Cut14-sAID (4h) from cells used for the SPT-PALM experiments.

(B) Distribution of the apparent diffusion coefficient ($\mu m^2.s^{-1}$) for the three independents *rpb1-sAID* experiments shown in Figure 2F. The vertical line represents the optimal $\log_{10}(D_{inst})$ separating the two populations of molecules according to a skewed-Gaussian mixture model (FMSMSN). The fitted gaussians are represented in blue and orange for slow and fast populations respectively. The fraction of molecules belonging to each population is indicated.

(C) Same as in (B) but for *dhp1-sAID* experiments.

(D) Jump distance distribution calculated by spot-ON[48] for the Cut14-sAID ON and OFF conditions. This represents the spatial distance separating two dots from the same tracks separated by Δτ ms (1 dt=33.6ms).

(E) The fraction of slow Cnd2-mEOS3.2 molecules identified by spot-ON with a three-state model (Materials and Methods) quantified for WT, *cut14-sAID*, *rpb1-sAID* and *dhp1-sAID* metaphase arrested cells (same tracks as for Fig. 2F). t.test was used to compare the OFF and ON conditions: * indicates a p.value < 0.05.

Supplementary Figure S3: Active RNAP2 hinders chromatin folding by condensin in metaphase, relative to Figure 3

(A-B) Genome-wide log2 differential maps at 20kb resolution of (A) Rpb1-OFF/Rpb1-ON and (B) Dhp1-OFF/Dhp1-ON.

(C-D) Hi-C contact probability curve P(s) as a function of distance and corresponding slope and genome-wide log2 differential map at 20kb resolution (D) in Rpb1-ON and Rpb1-OFF samples of the second biological replicate.

(E-F) Hi-C contact probability curve P(s) as a function of distance and its corresponding slope and genome-wide log2 differential map at 20kb resolution (F) in Dhp1-ON and Dhp1-OFF samples of the second biological replicate.

bioRxiv preprint doi: https://doi.org/10.1101/2023.08.08.552486; this version posted August 11, 2023. The copyright holder for this preprint (which was not certified by peer review) is the author/funder. All rights reserved. No reuse allowed without permission.

Supplementary Figure S4: Transcription termination limits the strength of RNAP2 barriers to condensin, related to Figure 5

Violin plots of (A) gene lengths, (B) intergenic region lengths and (C) mean RNAP2 (S2P) cal-ChIPseq signals in WT in clusters defined in Figure 5A.

Materials and Methods

Media, growth, maintenance of strains and genetic methods were as described[68]. Standard genetics and PCR-based gene targeting method were used to construct *S. pombe* strains and sanger sequencing was performed to confirm the insertions. Dhp1 and Rpb1 were tagged at their C-terminus with 3x sAID repeats and the degron alleles transferred into *osTIR1-F74A*[69] expressing genetic backgrounds by crossing. The *cnd2-GFP* and degron alleles are expressed under the control of their natural promoter at their native chromosomal location. Strains used in this study are listed in Table S1. For metaphase arrests, cells expressing the APC/C co-activator Slp1 under the control of thiamine-repressible promoter *nmt41* were cultured in synthetic PMG medium at 32°C and arrested in metaphase for 3 hours at 32°C by exposure to 20 µM thiamine. Mitotic indexes were determined by scoring the percentage of cells exhibiting Cnd2-GFP fluorescence in their nucleoplasm[3]. Liquid cultures of cells expressing either Dhp1-sAID or Rpb1-sAID treated with thiamine to induce their metaphase arrest were exposed to 100 nM 5-adamantyl-IAA (or NaOH as control) for 1h or 30 minutes (min), respectively, before the end of the 3h metaphase arrest.

Chromosome segregation assay

Cells were grown to exponential phase in PMG liquid medium at 32°C (for dhp1-sAID) or grown in YES+A liquid medium at 30°C and shifted for 2.5 h at 36°C (for rpb1-sAID). Before collecting cells, liquid cultures were exposed to 100 nM 5-adamantyl-IAA or NaOH as control (1h before collecting for dhp1-sAID or 30 min for rpb1-sAID). 2.10^7 cells were fixed in cold methanol and stored at -20°C. Cells were processed for immunofluorescence by washing three times with PEM (100 mM PIPES, 1mM EGTA, 1mM MgSO4, pH 6.9) with the last wash performed on a wheel at room temperature for 30 mn to rehydrate cells. Cells were digested with 0.4mg of zymoliase 100T (nacalai tesque) in PEMS (PEM + 1.2M Sorbitol) for 30 min at 37°C in a waterbath. Cells were washed twice with cold PEMS, and incubated for ~1-2 min in PEMS + 2% Triton at room-temperature. Cells were pelleted, washed with PEM and resuspended in

bioRxiv preprint doi: https://doi.org/10.1101/2023.08.08.552486; this version posted August 11, 2023. The copyright holder for this preprint (which was not certified by peer review) is the author/funder. All rights reserved. No reuse allowed without permission.

PEMBAL (PEM, 1% BSA, 100mM Lysine-HCl, 0,1% sodium azide) on a wheel at room temperature for 30 min. Cells were resuspended in 100 µl PEMBAL with 1/50 TAT1 antibody and incubated on a wheel overnight at 4°C in the dark. Cells were washed three times with PEMBAL, incubated in 100 µl PEMBAL with 1/400 anti-mouse AlexaFluor488 fluorescent antibody for 2h on a wheel at RT. Cells were washed a final time in PEMBAL and resuspended in PEM+0,5 µg/ml DAPI. 4 µl were placed on a slide, covered by a coverslip and observed with Zeiss Axioscope A.1, objective Apopchromat 63x 1.4NA. Chromatin bridges were scored manually.

Calibrated-ChIP and sequencing

Calibrated ChIP was performed as described previously[33]. Briefly, fission yeast cells expressing either Cnd2-GFP or NLS-PK9-GFP and arrested in metaphase by the depletion of Slp1 were fixed with 1% formaldehyde for 25 min, quenched with glycine 0.125 M final, washed twice with PBS, frozen in liquid nitrogen and stored at -80°C until use. *Saccharomyces cerevisiae* cells expressing Smc3-GFP, used for internal calibration, were grown in Yeast Peptone Dextrose liquid medium at 30°C in log phase and fixed with 2.5% formaldehyde for 25 min. To perform calibrated ChIPseq against Cnd2-GFP or RNAP2, fixed fission yeast and budding yeast cells were mixed at a ratio of 5:1 prior to lysis with Precellys® (Bertin). Anti-GFP and anti-RNAP2 ChIPs were performed using the A111-22 and 8WG16 antibodies, respectively. Libraries were prepared using NEBNext® Ultra™ II DNA Library Prep Kit for Illumina® according to the manufacturer's instructions. DNA libraries were size-selected using Ampure XP Agencourt beads (A63881) and sequenced paired-end 150 bp with Novaseq S6000 (Novogene®). To make ChIP-seq libraries for Rpb1-sAID depletion, IP and Total fractions from three independent biological experiments were pooled.

Hi-C

Fission yeast cells, expressing Cnd2-GFP and arrested in metaphase by the depletion of Slp1 were fixed with 3% formaldehyde for 5 min at 32°C followed by 20 min at 19°C, washed twice with PBS, frozen in liquid nitrogen and stored at -80°C. 2.10^8 cells were lysed in ChIP lysis buffer with Precellys® (Bertin). Lysates were centrifuged 5000 g at 4°C for 5 min and pellets were resuspended once in 1 mL lysis buffer and twice in NEB® 3.1 buffer. SDS was added to reach 0.1% final and samples were incubated for 10 min at 65°C. SDS was quenched on ice with 1%

bioRxiv preprint doi: https://doi.org/10.1101/2023.08.08.552486; this version posted August 11, 2023. The copyright holder for this preprint (which was not certified by peer review) is the author/funder. All rights reserved. No reuse allowed without permission.

Triton X-100 and DNA digested overnight at 37°C with 200 Units of *Dpn*II restriction enzyme. Samples were incubated at 65°C for 20 min to inactivated *Dpn*II. Restricted-DNA fragments were filled-in with 15 nmol each of biotin-14-dATP (cat. 19524016, Thermofisher), dTTP, dCTP and dGTP, and 50 units of DNA Klenow I (cat. M0210M, NEB) for 45 min at 37°C. Samples were diluted in 8 ml of T4 DNA ligase buffer 1X and incubated 8 hours at 16°C with 8000 Units of T4 DNA ligase (NEB). Crosslinks were reversed overnight at 60°C in the presence of proteinase K (0.125 mg / ml final) and SDS 1% final. 1 mg of proteinase K was added again and tubes were further incubated for 2 hours at 60°C. DNA was recovered by phenol-chloroform-isoamyl-alcohol extraction, resuspended in 100 µl TLE (Tris/HCl 10 mM, 0.1 mM EDTA, pH8) and treated with RNAse A (0.1 mg / ml) for 30 min at 37°C. Biotin was removed from unligated ends with 3 nmol dATP, dGTP and 36 Units of T4 DNA polymerase (NEB) for 4 hours at 20°C. Samples were incubated at 75°C for 20 min, washed using Amicon® 30k centrifugal filters and sonicated in 130 µl H_2O using Covaris® S220 (4 min 20°C, duty factor 10%, 175W peak power, 200 burst per cycle). DNA was end-repaired with 37.5 nmol dNTP, 16.2 Units of T4 DNA polymerase, 54 Units of T4 polynucleotide kinase, 5.5 Units of DNA Pol I Klenow fragment for 30 min at 20°C and then incubated for 20 min at 75°C. Ligated junctions were pulled-down with Dynabeads® MyOne™ Streptavidin C1 beads for 15 min at RT and DNA ends were A-tailed with 15 Units of Klenow exo- (cat. M0212L, NEB). Barcoded PerkinElmer adapters (cat. NOVA-514102) were ligated on fragments for 2 hours at 22°C. Libraries were amplified with NextFlex PCR mix (cat. NOVA-5140-08) for 5 cycles, and cleaned up with Ampure XP Agencourt beads (A63881). Hi-C libraries were paired-end sequenced 150bp on Novaseq6000 (Novogene®).

SPT-PALM

Cells were cultured at 30°C in filter-sterilized PMG for 48h and shifted to 25°C, in exponential phase, for 5 hours. 3.5 h before the beginning of the acquisition, thiamine 20 µM was added to the culture to repress transcription of *nmt41-slp1* gene and arrest cells in metaphase. 10 min before the acquisition, 2 mL of culture was taken, centrifuged 15 sec at 10 000 g at room temperature and resuspended to reach 5.10^8cells/mL. Cells were transferred to an agarose pad as described below. Coverslips (Marienfeld 0107052 22x22mm No. 1.5H) were washed 10 min in acetone, two times 5 min in ethanol, 10 min in KOH 1M, five times in Milli Q water and finally dried with a flame. Coverslips showing a defect or a carbon deposit after the drying step were discarded. On a clean glass slide (RS BPB018, frosted end), two pieces of double-sided

bioRxiv preprint doi: https://doi.org/10.1101/2023.08.08.552486; this version posted August 11, 2023. The copyright holder for this preprint (which was not certified by peer review) is the author/funder. All rights reserved. No reuse allowed without permission.

tape were placed to fix the CoverWell imaging chamber (Grace Bio-labs 635021, 25x25mm). 1 mL of PMG 2% Agarose (invitrogen 16500) supplemented with 20 µM thiamine was poured in the CoverWells. 5 µL of fresh cell suspension (5.10^8 cells/mL) were deposited on the pad and covered with a KOH-treated coverslip, sealed with nail varnish and immediately used for acquisition. We depleted Rpb1-sAID for 30 min, Dhp1-sAID for 1h and Cut14-sAID for 4h prior to acquisition. SPT-PALM microscopy was performed with a Zeiss Elyra 7 system, equipped with a TIRF setup and controlled by Zen Black software. An oil immersion 100x objective α Plan-Apochromat 1.46NA, and an EMCCD (iXon EMCCD 897 Ultra, pixel size=16µM) was used for the acquisition. Cnd2-mEOS3.2 acquisition was done in a field with 5-20 living yeast cells, using a TIRF angle around 66° which should correspond to a penetration of 100-150 nm. A 405 nm laser was used for photoconversion of mEOS3.2 with constant activation and low intensity (0.015%, 0.4-1.3 µW as measured by Optical Power Meter 100D, slide S170C with an epifluorescence illumination). Excitation of converted mEOS3.2 by the 561 nm laser was done with an exposure time of 20 ms and 20% power (5.6 mW in epifluorescence). Time Series of 20 000 cycles without interval and with Definite Focus 2 (Zeiss, continuous) were performed. During the acquisition the 405 nm laser power was slightly adjusted to always see enough particles. With these settings, the framerate was 33.6 ms. Once the time series was finished, GFP (Cdc11-GFP, SPB/centrosome) and brightfield acquisitions were done in a z-stack.

SPT-PALM data analysis

Cells showing two separated Cdc11-GFP dots were included in the Region Of Interest (ROI). Trackmate[70] was used on Fiji[71] for segmentation with the LoG detector set at diameter = 1 µm and quality threshold at 100. Track reconstruction was done by the Simple LAP tracker with a Linking max distance and a gap closing distance of 0.8 µm and a gap-closing max frame of 3. Path between 5 and 50 spots were exported and analysed with both spot-ON[48] and sptPALM viewer[46]. The spot-ON parameters were as described in [45] and for sptPALM viewer, on matlab we ran the script, imported the csv and set the maximal distance to 0.8 µm and minimal frame number to 5. Trajectory were further analysed in R as described[46].

Hi-C data analysis

Alignments were performed using *hicstuff* version 3.1.2 with options (-d –D –m iterative –e DpnII) after merging.fq.gz files of the same sample from different sequencing runs. Matrices

bioRxiv preprint doi: https://doi.org/10.1101/2023.08.08.552486; this version posted August 11, 2023. The copyright holder for this preprint (which was not certified by peer review) is the author/funder. All rights reserved. No reuse allowed without permission.

were visualized and compared with *hicstuff view* after subsampling to the same number of contacts. For log2 differential maps, all three chromosomes were represented at 20kb binning. To visualize individual matrices, chrI :100000-3700000 was viewed at 10kb binning. Insulation scores (IS) at protein coding genes were determined using cooltools[72] with a binning of 3kb and a window of 9kb and plotted with R. Border were identified in cooltools in all the conditions with the IS as described above. For each degron, the borders in the ON and OFF conditions were merged and the IS of their bin compared. A border was considered weakened if log2(IS-OFF/IS-ON) > 0.58, strengthened if log2(IS-OFF/IS-ON) < -0.58 and stable otherwise.

ChIP-seq data analysis

Alignments were performed as described previously[33]. Briefly, reads were mapped using an nf-core (https://doi.org/10.1038/s41587-020-0439-x) modified pipeline with TEL2R extended ASM294v2 genome (Omnibus GEO GSE196149) for *Schizosaccharomyces pombe* mapping reads, and sacCER3 release R64-1-1 for calibrating, *Saccharomyces cerevisae* mapping reads. Deeptools2 was used to plot metagene profiles and heatmaps[73], as well as to perform k-means clustering of bigwig data using scale-regions. Peak calling was performed on BAM files using the MACS2 software[74]. For the definition of gene-pairs in Fig. 5D, we considered as neighbours any gene oriented towards a gene of cluster I with a TES closer to 1kb from the TSS or TES of cluster I.

Data availability

Cal-ChIP–seq and Hi-C data were deposited in the Gene Expression Omnibus under accession no. GSE236395.

bioRxiv preprint doi: https://doi.org/10.1101/2023.08.08.552486; this version posted August 11, 2023. The copyright holder for this preprint (which was not certified by peer review) is the author/funder. All rights reserved. No reuse allowed without permission.

References

1. Hirano, T. Condensin-Based Chromosome Organization from Bacteria to Vertebrates. *Cell* **164**, 847–857 (2016).
2. Saka, Y. *et al.* Fission yeast cut3 and cut14, members of a ubiquitous protein family, are required for chromosome condensation and segregation in mitosis. *Embo J* **13**, 4938–52 (1994).
3. Sutani, T. *et al.* Fission yeast condensin complex: essential roles of non-SMC subunits for condensation and Cdc2 phosphorylation of Cut3/SMC4. *Genes Dev* **13**, 2271–83 (1999).
4. Gerlich, D., Hirota, T., Koch, B., Peters, J. M. & Ellenberg, J. Condensin I stabilizes chromosomes mechanically through a dynamic interaction in live cells. *Curr Biol* **16**, 333–44 (2006).
5. Naumova, N. *et al.* Organization of the mitotic chromosome. *Science* **342**, 948–953 (2013).
6. Gibcus, J. H. *et al.* A pathway for mitotic chromosome formation. *Science* **359**, (2018).
7. Schalbetter, S. A. *et al.* SMC complexes differentially compact mitotic chromosomes according to genomic context. *Nat. Cell Biol.* **19**, 1071–1080 (2017).
8. Kakui, Y., Rabinowitz, A., Barry, D. J. & Uhlmann, F. Condensin-mediated remodeling of the mitotic chromatin landscape in fission yeast. *Nat. Genet.* **49**, 1553–1557 (2017).
9. Davidson, I. F. & Peters, J.-M. Genome folding through loop extrusion by SMC complexes. *Nat Rev Mol Cell Biol* **22**, 445–464 (2021).
10. Ganji, M. *et al.* Real-time imaging of DNA loop extrusion by condensin. *Science* **360**, 102–105 (2018).
11. Davidson, I. F. *et al.* DNA loop extrusion by human cohesin. *Science* **366**, 1338–1345 (2019).

bioRxiv preprint doi: https://doi.org/10.1101/2023.08.08.552486; this version posted August 11, 2023. The copyright holder for this preprint (which was not certified by peer review) is the author/funder. All rights reserved. No reuse allowed without permission.

12. Kim, Y., Shi, Z., Zhang, H., Finkelstein, I. J. & Yu, H. Human cohesin compacts DNA by loop extrusion. *Science* **366**, 1345–1349 (2019).
13. Kong, M. *et al.* Human Condensin I and II Drive Extensive ATP-Dependent Compaction of Nucleosome-Bound DNA. *Mol Cell* **79**, 99-114.e9 (2020).
14. Pradhan, B. *et al.* The Smc5/6 complex is a DNA loop-extruding motor. *Nature* **616**, 843–848 (2023).
15. Rao, S. S. P. *et al.* Cohesin Loss Eliminates All Loop Domains. *Cell* **171**, 305-320.e24 (2017).
16. de Wit, E. *et al.* CTCF Binding Polarity Determines Chromatin Looping. *Mol Cell* **60**, 676–684 (2015).
17. Busslinger, G. A. *et al.* Cohesin is positioned in mammalian genomes by transcription, CTCF and Wapl. *Nature* **544**, 503–507 (2017).
18. Jeppsson, K. *et al.* Cohesin-dependent chromosome loop extrusion is limited by transcription and stalled replication forks. *Sci Adv* **8**, eabn7063 (2022).
19. Banigan, E. J. *et al.* Transcription shapes 3D chromatin organization by interacting with loop extrusion. *Proc Natl Acad Sci U S A* **120**, e2210480120 (2023).
20. Guérin, T. M. *et al.* Condensin-Mediated Chromosome Folding and Internal Telomeres Drive Dicentric Severing by Cytokinesis. *Mol. Cell* **75**, 131-144.e3 (2019).
21. Rivosecchi, J. *et al.* RNA polymerase backtracking results in the accumulation of fission yeast condensin at active genes. *Life Sci Alliance* **4**, e202101046 (2021).
22. Gerguri, T. *et al.* Comparison of loop extrusion and diffusion capture as mitotic chromosome formation pathways in fission yeast. *Nucleic Acids Research* **49**, 1294–1312 (2021).

bioRxiv preprint doi: https://doi.org/10.1101/2023.08.08.552486; this version posted August 11, 2023. The copyright holder for this preprint (which was not certified by peer review) is the author/funder. All rights reserved. No reuse allowed without permission.

23. Cheng, T. M. K. *et al.* A simple biophysical model emulates budding yeast chromosome condensation. *Elife* **4**, e05565 (2015).
24. Kinoshita, K. *et al.* A loop extrusion-independent mechanism contributes to condensin I-mediated chromosome shaping. *J Cell Biol* **221**, e202109016 (2022).
25. Sutani, T. *et al.* Condensin targets and reduces unwound DNA structures associated with transcription in mitotic chromosome condensation. *Nat Commun* **6**, 7815 (2015).
26. D'Ambrosio, C. *et al.* Identification of cis-acting sites for condensin loading onto budding yeast chromosomes. *Genes Dev.* **22**, 2215–2227 (2008).
27. Kim, J. H. *et al.* Condensin I associates with structural and gene regulatory regions in vertebrate chromosomes. *Nat Commun* **4**, 2537 (2013).
28. Kranz, A. L. *et al.* Genome-wide analysis of condensin binding in Caenorhabditis elegans. *Genome Biol* **14**, R112 (2013).
29. Johzuka, K. & Horiuchi, T. The cis element and factors required for condensin recruitment to chromosomes. *Mol Cell* **34**, 26–35 (2009).
30. Tada, K., Susumu, H., Sakuno, T. & Watanabe, Y. Condensin association with histone H2A shapes mitotic chromosomes. *Nature* **474**, 477–83 (2011).
31. Nakazawa, N. *et al.* Dissection of the essential steps for condensin accumulation at kinetochores and rDNAs during fission yeast mitosis. *J Cell Biol* **180**, 1115–31 (2008).
32. Verzijlbergen, K. F. *et al.* Shugoshin biases chromosomes for biorientation through condensin recruitment to the pericentromere. *eLife* **3**, e01374 (2014).
33. Colin, L. *et al.* Condensin positioning at telomeres by shelterin proteins drives sister-telomere disjunction in anaphase. *eLife* **12**, (2023).

bioRxiv preprint doi: https://doi.org/10.1101/2023.08.08.552486; this version posted August 11, 2023. The copyright holder for this preprint (which was not certified by peer review) is the author/funder. All rights reserved. No reuse allowed without permission.

34. Yuen, K. C., Slaughter, B. D. & Gerton, J. L. Condensin II is anchored by TFIIIC and H3K4me3 in the mammalian genome and supports the expression of active dense gene clusters. *Sci Adv* **3**, e1700191 (2017).

35. Toselli-Mollereau, E. *et al.* Nucleosome eviction in mitosis assists condensin loading and chromosome condensation. *EMBO J* **35**, 1565–1581 (2016).

36. Haase, J. *et al.* The TFIIH complex is required to establish and maintain mitotic chromosome structure. *eLife* **11**, e75475 (2022).

37. Iwasaki, O. *et al.* Interaction between TBP and Condensin Drives the Organization and Faithful Segregation of Mitotic Chromosomes. *Mol. Cell* **59**, 755–767 (2015).

38. Kim, K.-D., Tanizawa, H., Iwasaki, O. & Noma, K.-I. Transcription factors mediate condensin recruitment and global chromosomal organization in fission yeast. *Nat. Genet.* **48**, 1242–1252 (2016).

39. Nakazawa, N., Arakawa, O. & Yanagida, M. Condensin locates at transcriptional termination sites in mitosis, possibly releasing mitotic transcripts. *Open Biol* **9**, 190125 (2019).

40. Wang, B.-D., Butylin, P. & Strunnikov, A. Condensin function in mitotic nucleolar segregation is regulated by rDNA transcription. *Cell Cycle* **5**, 2260–2267 (2006).

41. Johzuka, K. & Horiuchi, T. RNA polymerase I transcription obstructs condensin association with 35S rRNA coding regions and can cause contraction of long repeat in Saccharomyces cerevisiae. *Genes Cells* **12**, 759–771 (2007).

42. Haeusler, R. A., Pratt-Hyatt, M., Good, P. D., Gipson, T. A. & Engelke, D. R. Clustering of yeast tRNA genes is mediated by specific association of condensin with tRNA gene transcription complexes. *Genes Dev* **22**, 2204–14 (2008).

bioRxiv preprint doi: https://doi.org/10.1101/2023.08.08.552486; this version posted August 11, 2023. The copyright holder for this preprint (which was not certified by peer review) is the author/funder. All rights reserved. No reuse allowed without permission.

43. Tanaka, A. *et al.* Epigenetic regulation of condensin-mediated genome organization during the cell cycle and upon DNA damage through histone H3 lysine 56 acetylation. *Mol Cell* **48**, 532–46 (2012).

44. Larochelle, M. *et al.* Common mechanism of transcription termination at coding and noncoding RNA genes in fission yeast. *Nat Commun* **9**, 4364 (2018).

45. Etheridge, T. J. *et al.* Live-cell single-molecule tracking highlights requirements for stable Smc5/6 chromatin association in vivo. *Elife* **10**, e68579 (2021).

46. Bayle, V. *et al.* Single-particle tracking photoactivated localization microscopy of membrane proteins in living plant tissues. *Nat Protoc* **16**, 1600–1628 (2021).

47. Etheridge, T. J. *et al.* Quantification of DNA-associated proteins inside eukaryotic cells using single-molecule localization microscopy. *Nucleic Acids Res* **42**, e146 (2014).

48. Hansen, A. S. *et al.* Robust model-based analysis of single-particle tracking experiments with Spot-On. *Elife* **7**, e33125 (2018).

49. Mizuguchi, T. *et al.* Cohesin-dependent globules and heterochromatin shape 3D genome architecture in S. pombe. *Nature* **516**, 432–435 (2014).

50. Tanizawa, H., Kim, K.-D., Iwasaki, O. & Noma, K.-I. Architectural alterations of the fission yeast genome during the cell cycle. *Nat Struct Mol Biol* **24**, 965–976 (2017).

51. Gassler, J. *et al.* A mechanism of cohesin-dependent loop extrusion organizes zygotic genome architecture. *The EMBO Journal* **36**, 3600–3618 (2017).

52. Baxter, J. *et al.* Positive supercoiling of mitotic DNA drives decatenation by topoisomerase II in eukaryotes. *Science* **331**, 1328–1332 (2011).

53. Charbin, A., Bouchoux, C. & Uhlmann, F. Condensin aids sister chromatid decatenation by topoisomerase II. *Nucleic Acids Res* **42**, 340–348 (2014).

bioRxiv preprint doi: https://doi.org/10.1101/2023.08.08.552486; this version posted August 11, 2023. The copyright holder for this preprint (which was not certified by peer review) is the author/funder. All rights reserved. No reuse allowed without permission.

54. Renshaw, M. J. *et al.* Condensins promote chromosome recoiling during early anaphase to complete sister chromatid separation. *Dev Cell* **19**, 232–44 (2010).

55. Robellet, X. *et al.* A genetic screen for functional partners of condensin in fission yeast. *G3 (Bethesda)* **4**, 373–81 (2014).

56. Buck, V. *et al.* Fkh2p and Sep1p regulate mitotic gene transcription in fission yeast. *J Cell Sci* **117**, 5623–5632 (2004).

57. Wang, X., Brandão, H. B., Le, T. B. K., Laub, M. T. & Rudner, D. Z. Bacillus subtilis SMC complexes juxtapose chromosome arms as they travel from origin to terminus. *Science* **355**, 524–527 (2017).

58. Brandão, H. B. *et al.* RNA polymerases as moving barriers to condensin loop extrusion. *Proc. Natl. Acad. Sci. U.S.A.* **116**, 20489–20499 (2019).

59. Heinz, S. *et al.* Transcription Elongation Can Affect Genome 3D Structure. *Cell* **174**, 1522-1536.e22 (2018).

60. Zhang, S., Übelmesser, N., Barbieri, M. & Papantonis, A. Enhancer-promoter contact formation requires RNAPII and antagonizes loop extrusion. *Nat Genet* **55**, 832–840 (2023).

61. Kim, E., Gonzalez, A. M., Pradhan, B., van der Torre, J. & Dekker, C. Condensin-driven loop extrusion on supercoiled DNA. *Nat Struct Mol Biol* **29**, 719–727 (2022).

62. Naughton, C. *et al.* Transcription forms and remodels supercoiling domains unfolding large-scale chromatin structures. *Nat Struct Mol Biol* **20**, 387–395 (2013).

63. Hsiung, C. C.-S. *et al.* Genome accessibility is widely preserved and locally modulated during mitosis. *Genome Res.* **25**, 213–225 (2015).

64. Teves, S. S. *et al.* A dynamic mode of mitotic bookmarking by transcription factors. *eLife* **5**, e22280 (2016).

bioRxiv preprint doi: https://doi.org/10.1101/2023.08.08.552486; this version posted August 11, 2023. The copyright holder for this preprint (which was not certified by peer review) is the author/funder. All rights reserved. No reuse allowed without permission.

65. Pradhan, B. *et al.* SMC complexes can traverse physical roadblocks bigger than their ring size. *Cell Reports* **41**, (2022).

66. Gullerova, M. & Proudfoot, N. J. Cohesin complex promotes transcriptional termination between convergent genes in S. pombe. *Cell* **132**, 983–95 (2008).

67. Zofall, M. *et al.* Histone H2A.Z cooperates with RNAi and heterochromatin factors to suppress antisense RNAs. *Nature* **461**, 419–22 (2009).

68. Moreno, S., Klar, A. & Nurse, P. Molecular genetic analysis of fission yeast Schizosaccharomyces pombe. *Methods Enzymol* **194**, 795–823 (1991).

69. Zhang, X.-R. *et al.* An improved auxin-inducible degron system for fission yeast. *G3 (Bethesda)* **12**, jkab393 (2021).

70. Tinevez, J.-Y. *et al.* TrackMate: An open and extensible platform for single-particle tracking. *Methods* **115**, 80–90 (2017).

71. Schindelin, J. *et al.* Fiji: an open-source platform for biological-image analysis. *Nat Methods* **9**, 676–682 (2012).

72. Open2C *et al.* Cooltools: enabling high-resolution Hi-C analysis in Python. 2022.10.31.514564 Preprint at https://doi.org/10.1101/2022.10.31.514564 (2022).

73. Ramírez, F. *et al.* deepTools2: a next generation web server for deep-sequencing data analysis. *Nucleic Acids Res* **44**, W160-165 (2016).

74. Zhang, Y. *et al.* Model-based Analysis of ChIP-Seq (MACS). *Genome Biology* **9**, R137 (2008).

bioRxiv preprint doi: https://doi.org/10.1101/2023.08.08.552486; this version posted August 11, 2023. The copyright holder for this preprint (which was not certified by peer review) is the author/funder. All rights reserved. No reuse allowed without permission.

Acknowledgments

We thank T. Etheridge for the *cnd2-mEOS3.2* strain; J. Brocard for SPT-PALM analyses, F. Beckouët for critical reading of the manuscript and V. Vanoosthuyse and A. Piazza for helpful discussions. J.L. and L.C. are supported by PhD studentships from respectively the Ecole Normale Supérieure and la Ligue Contre le Cancer. This work was funded by the CNRS, ENS-Lyon and grants from the ANR (ANR-22-CE12-0035 condensinchromatin) and la Fondation ARC (PJA 20191209370) to P.B.

Author contributions

Investigation: J.L. and L.C.; Formal Analysis: J.L., L.C. and E.C; Conceptualization, Methodology, Validation, Visualization and Writing original draft: J.L., L.C. and P.B; Supervision, Project Administration and Funding Acquisition: P.B.

Declaration of interests

Authors declare that they have no competing interest.

bioRxiv preprint doi: https://doi.org/10.1101/2023.08.08.552486; this version posted August 11, 2023. The copyright holder for this preprint (which was not certified by peer review) is the author/funder. All rights reserved. No reuse allowed without permission.

Figure 1

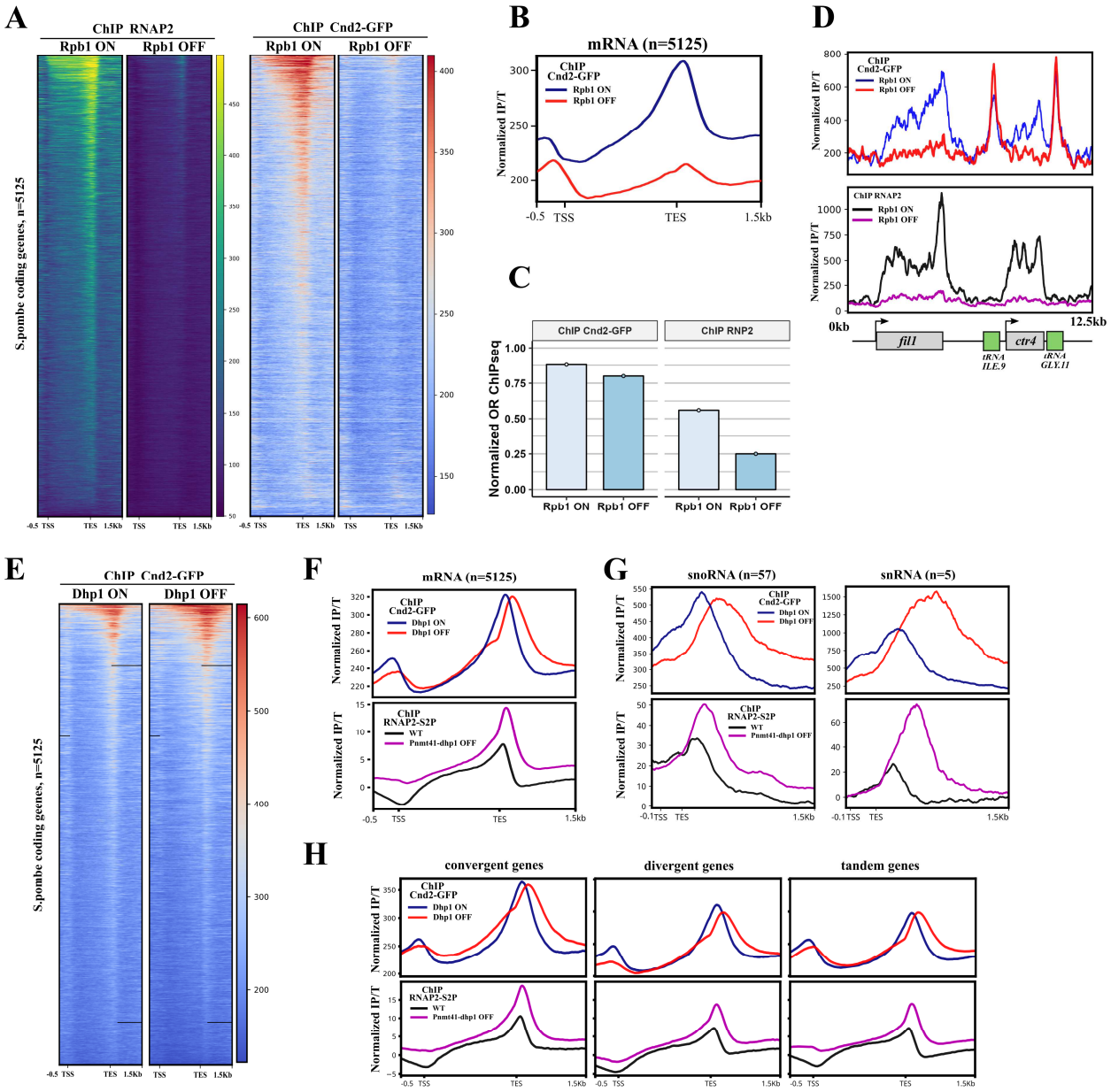

bioRxiv preprint doi: https://doi.org/10.1101/2023.08.08.552486; this version posted August 11, 2023. The copyright holder for this preprint (which was not certified by peer review) is the author/funder. All rights reserved. No reuse allowed without permission.

Figure 2

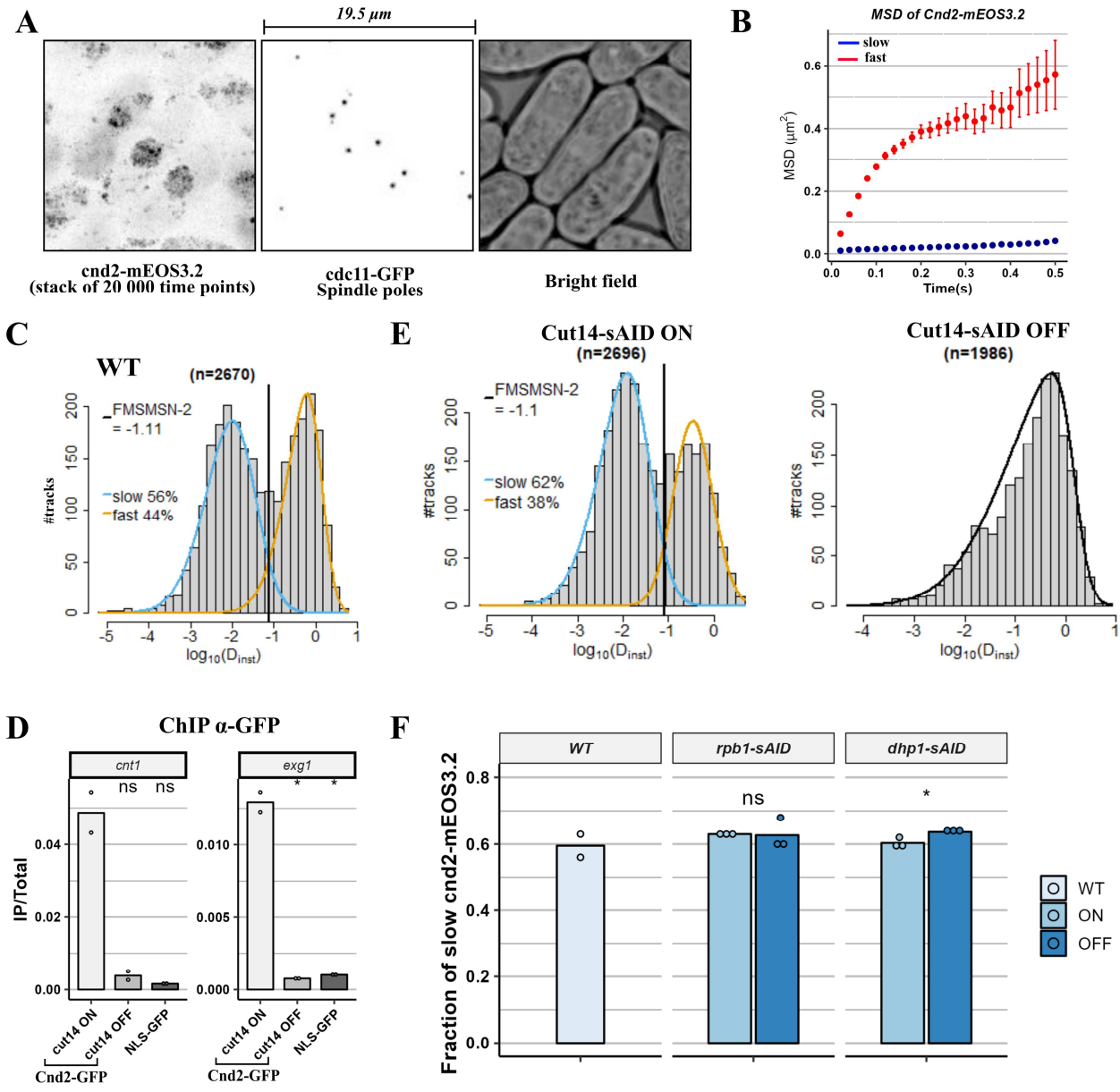

bioRxiv preprint doi: https://doi.org/10.1101/2023.08.08.552486; this version posted August 11, 2023. The copyright holder for this preprint (which was not certified by peer review) is the author/funder. All rights reserved. No reuse allowed without permission.

Figure 3

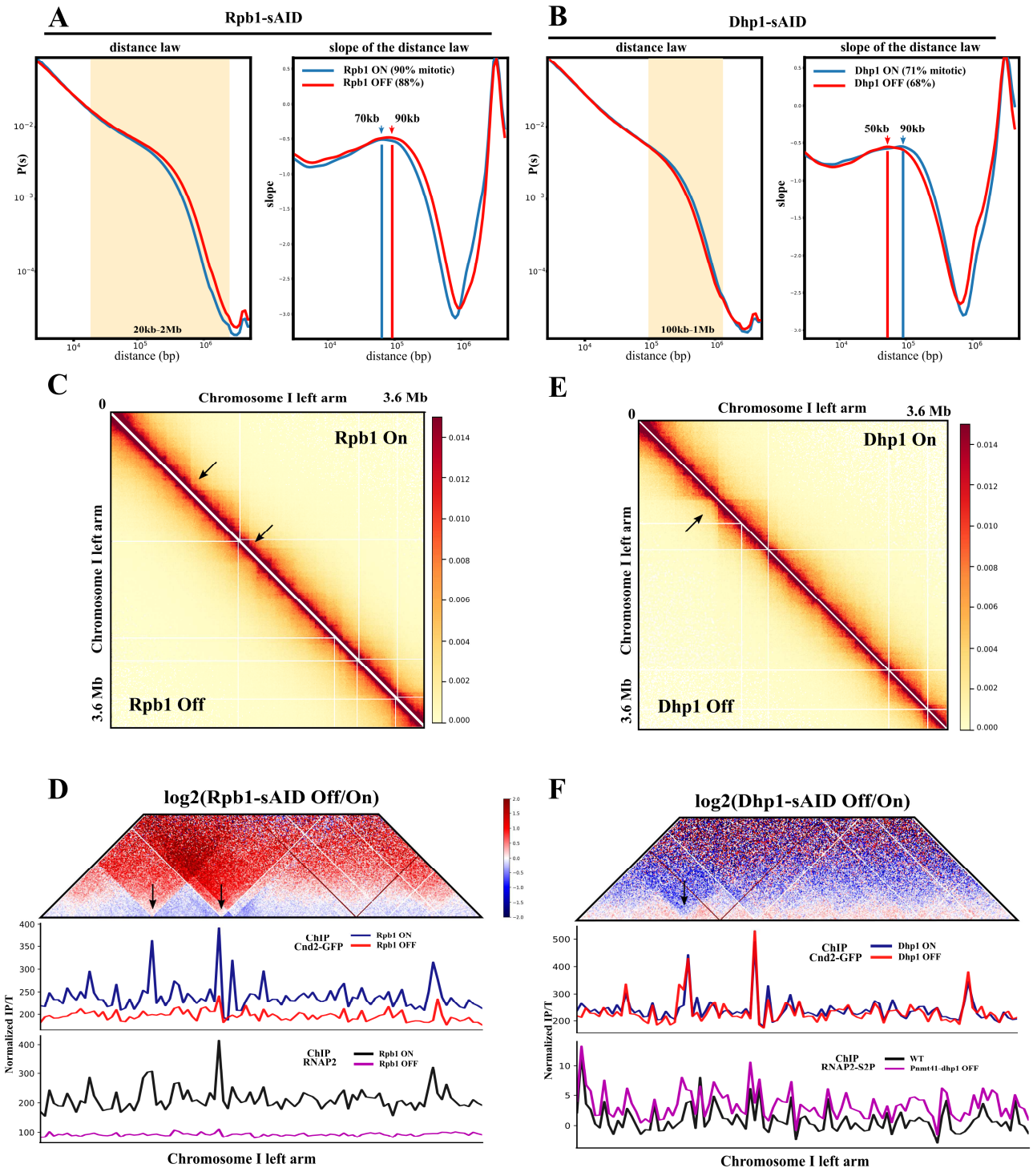

bioRxiv preprint doi: https://doi.org/10.1101/2023.08.08.552486; this version posted August 11, 2023. The copyright holder for this preprint (which was not certified by peer review) is the author/funder. All rights reserved. No reuse allowed without permission.

Figure 4

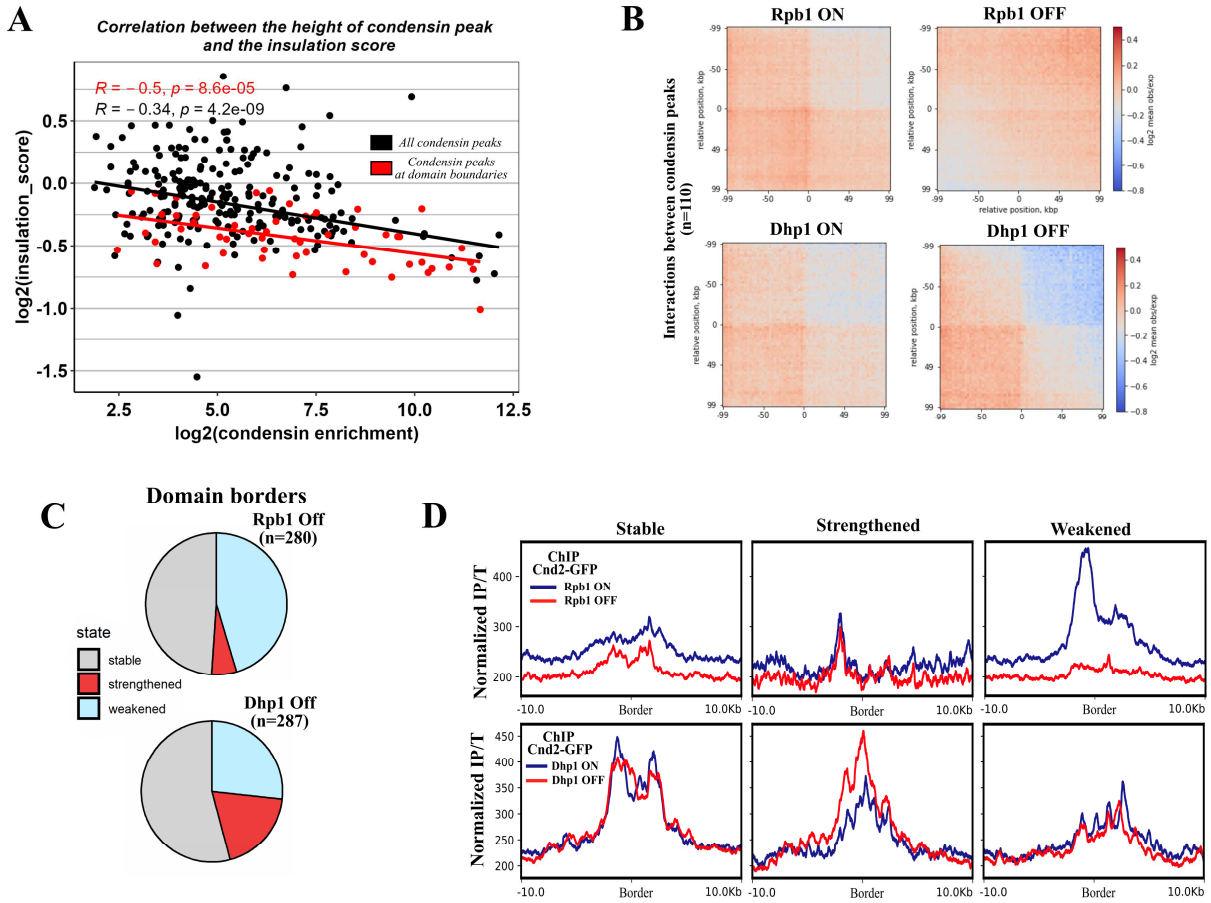

bioRxiv preprint doi: https://doi.org/10.1101/2023.08.08.552486; this version posted August 11, 2023. The copyright holder for this preprint (which was not certified by peer review) is the author/funder. All rights reserved. No reuse allowed without permission.

Figure 5

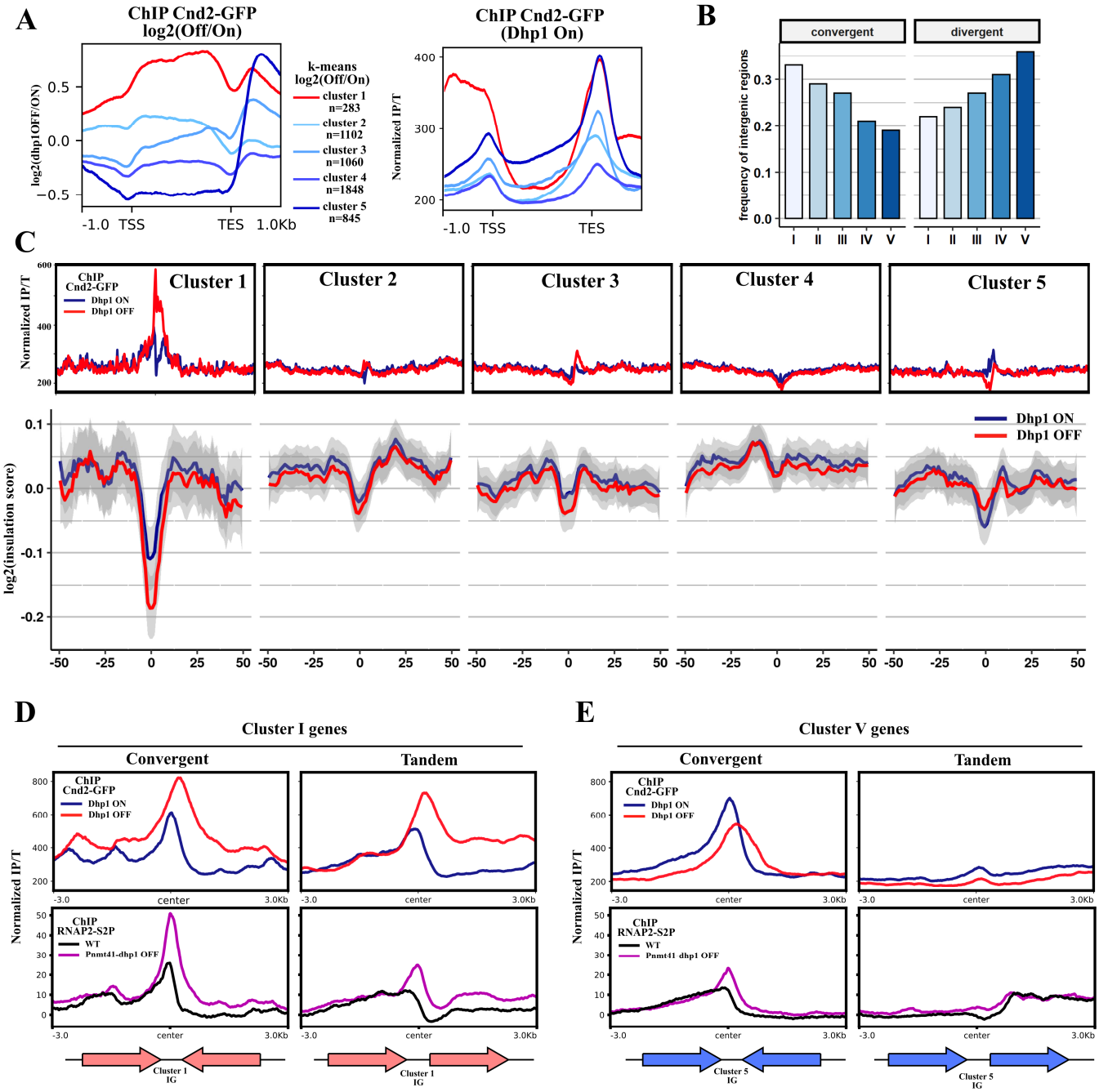

bioRxiv preprint doi: https://doi.org/10.1101/2023.08.08.552486; this version posted August 11, 2023. The copyright holder for this preprint (which was not certified by peer review) is the author/funder. All rights reserved. No reuse allowed without permission.

Figure 6

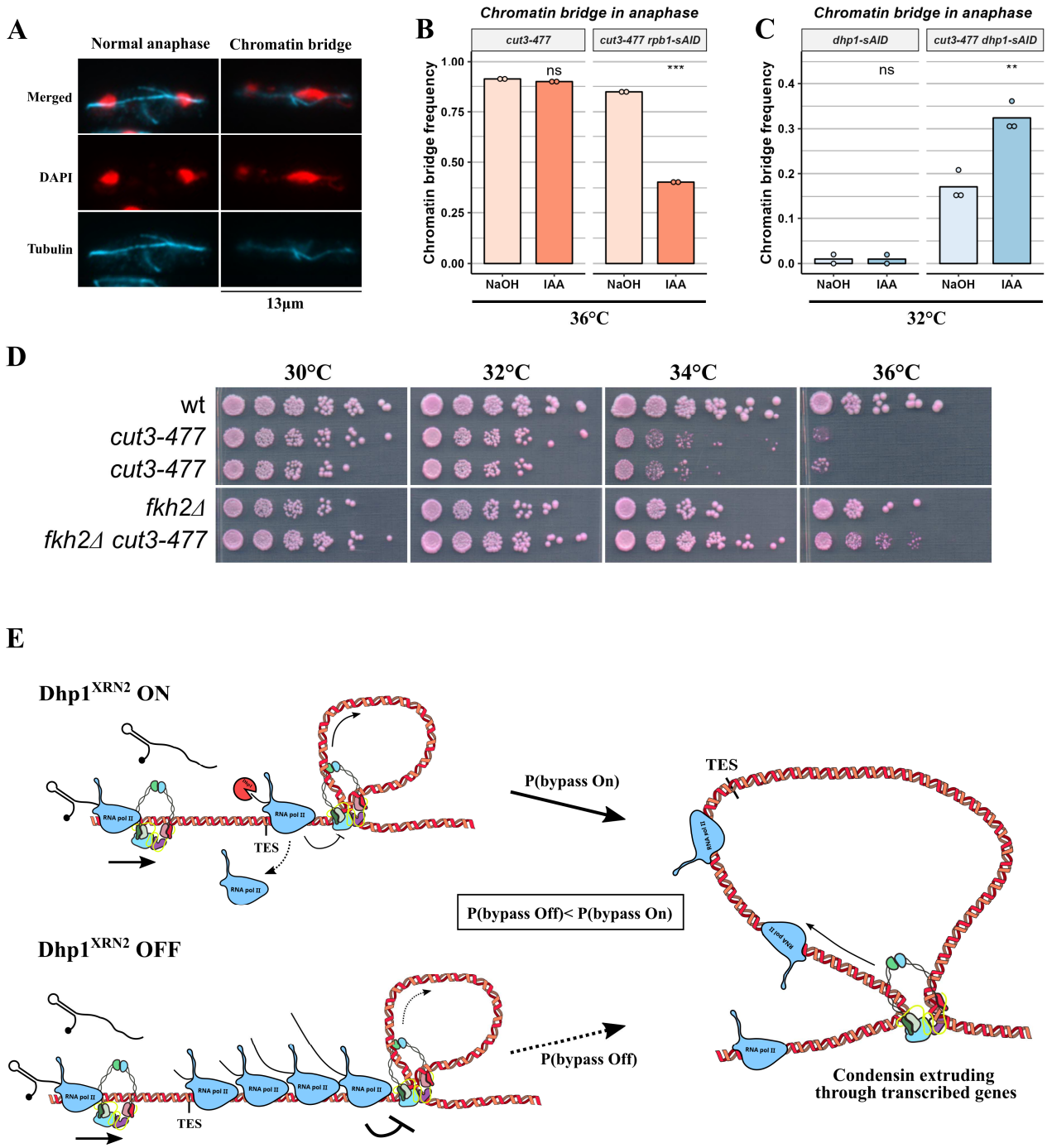

bioRxiv preprint doi: https://doi.org/10.1101/2023.08.08.552486; this version posted August 11, 2023. The copyright holder for this preprint (which was not certified by peer review) is the author/funder. All rights reserved. No reuse allowed without permission.

Figure S1

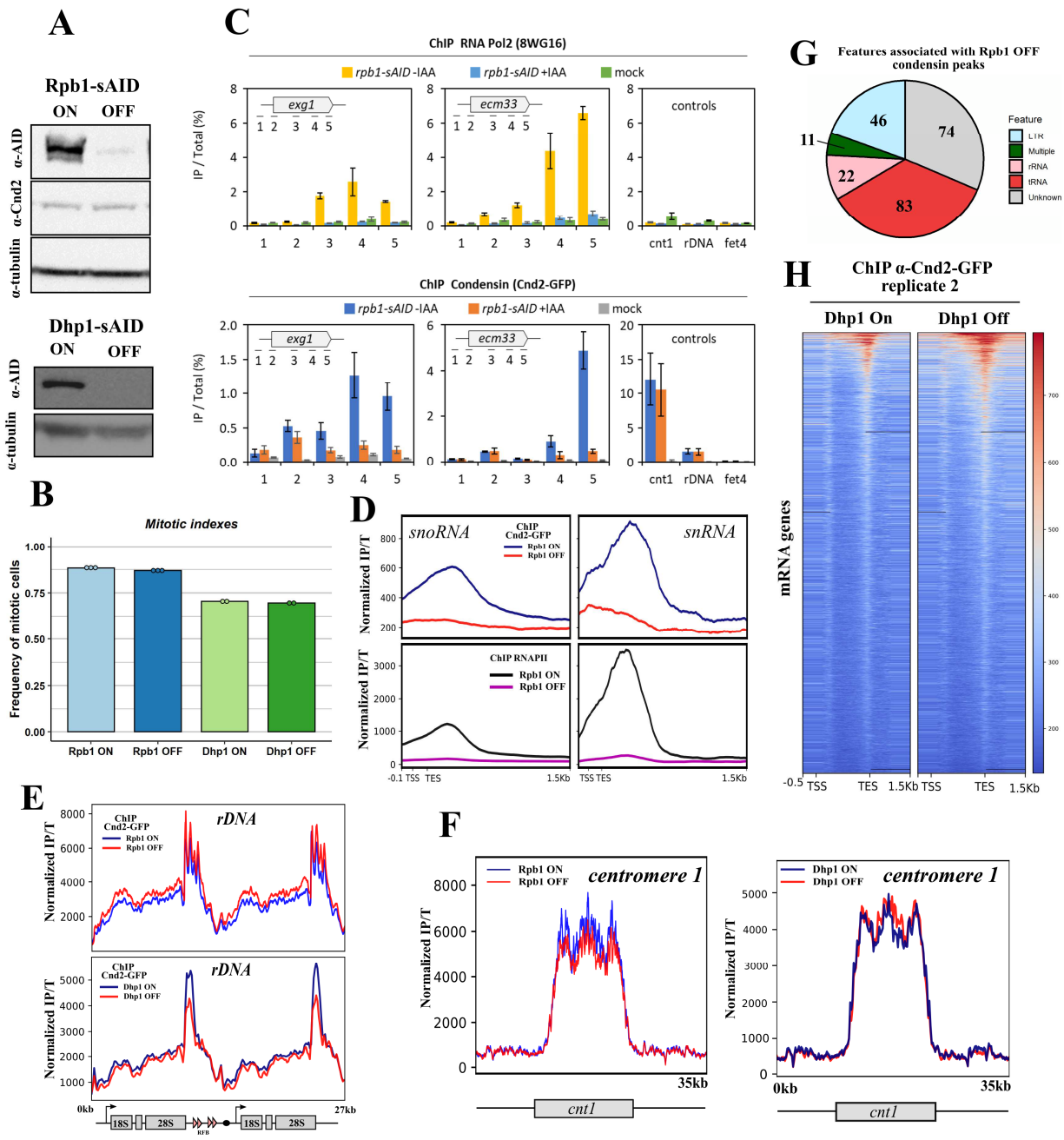

bioRxiv preprint doi: https://doi.org/10.1101/2023.08.08.552486; this version posted August 11, 2023. The copyright holder for this preprint (which was not certified by peer review) is the author/funder. All rights reserved. No reuse allowed without permission.

Figure S2

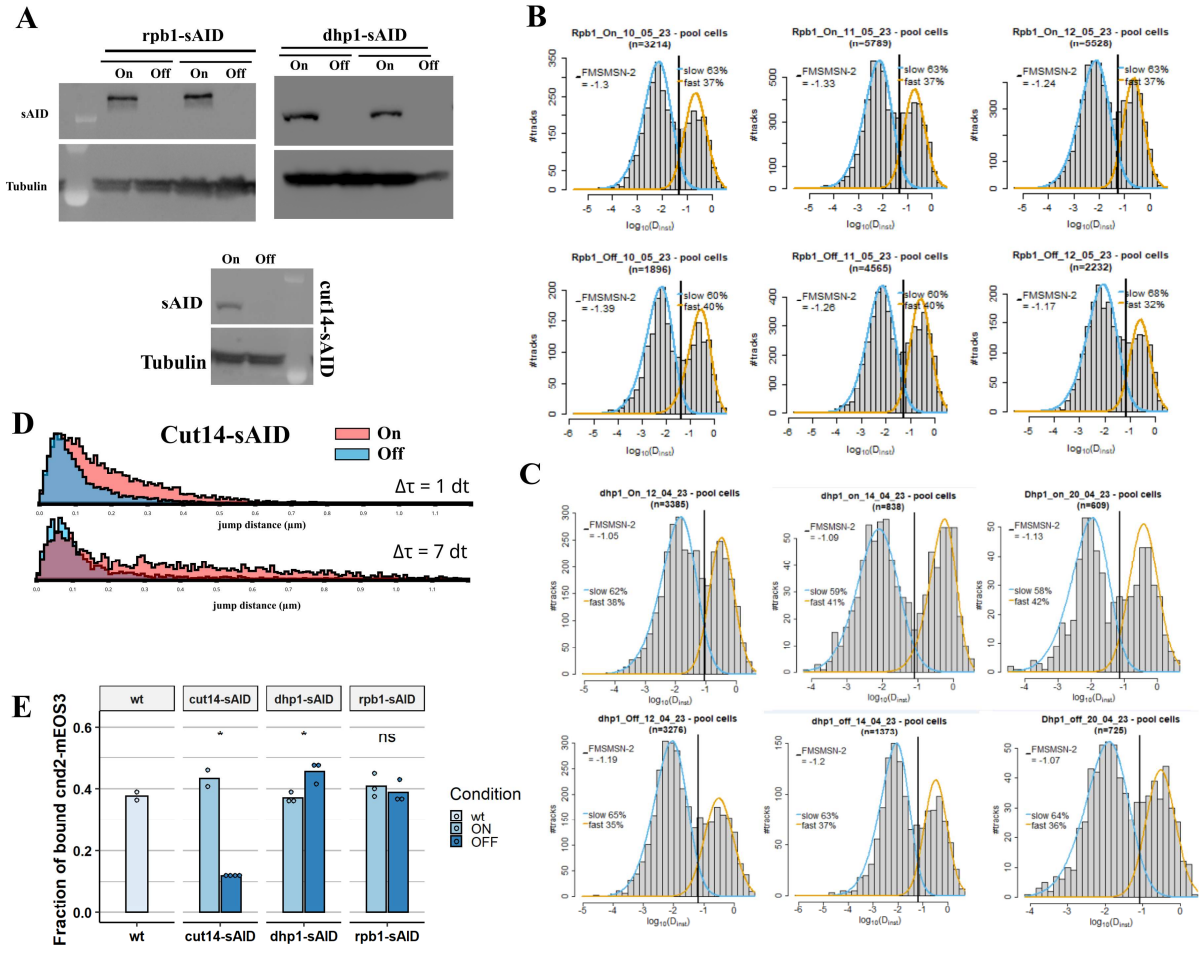

bioRxiv preprint doi: https://doi.org/10.1101/2023.08.08.552486; this version posted August 11, 2023. The copyright holder for this preprint (which was not certified by peer review) is the author/funder. All rights reserved. No reuse allowed without permission.

Figure S3

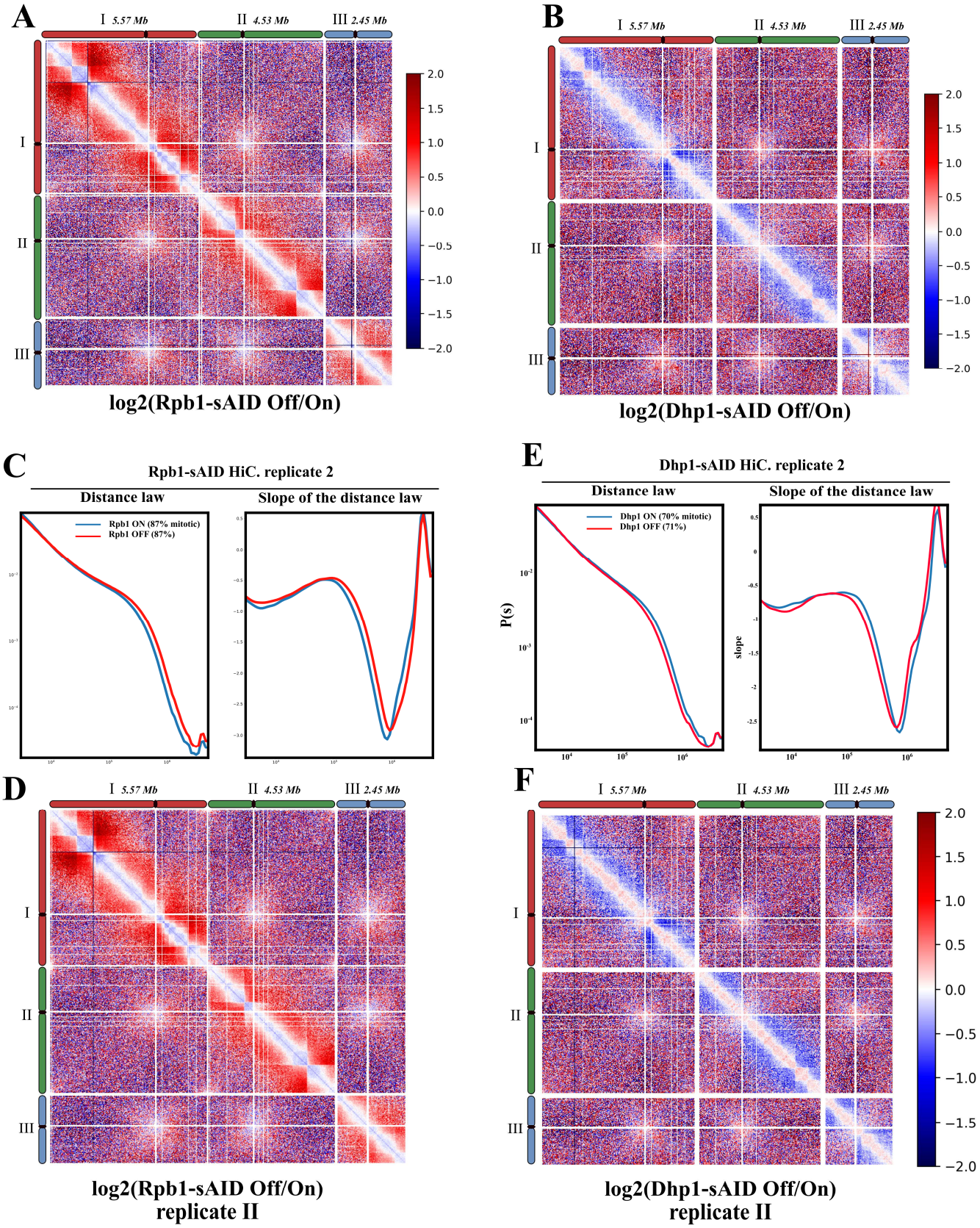

bioRxiv preprint doi: https://doi.org/10.1101/2023.08.08.552486; this version posted August 11, 2023. The copyright holder for this preprint (which was not certified by peer review) is the author/funder. All rights reserved. No reuse allowed without permission.

Figure S4

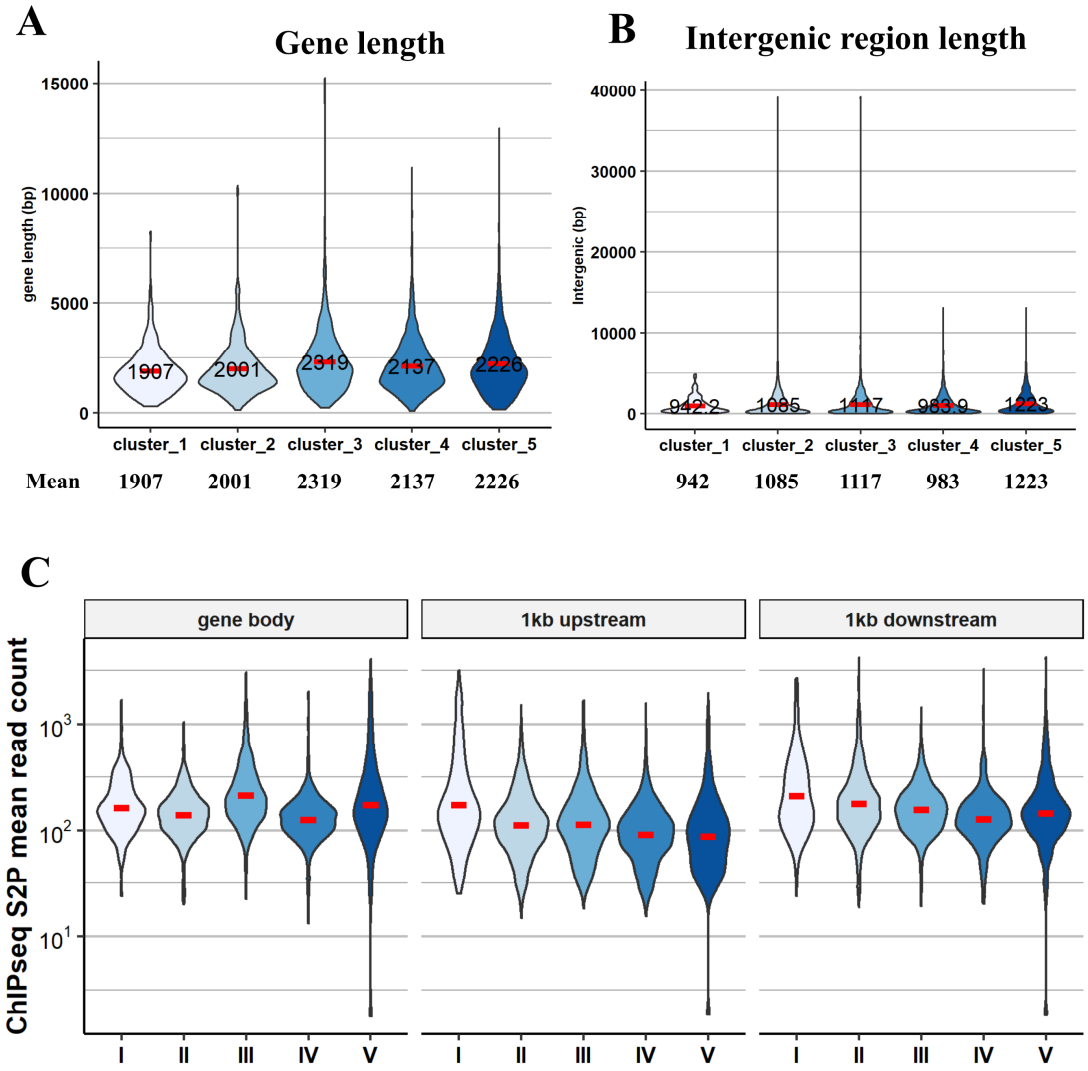

6.3 Supplementary results to Part 6

To investigate potential RNAPII-independent, biologically relevant sites of condensin enrichment we asked whether peaks remaining in Rpb1-OFF conditions may constitute loci of interest. First, I manually verified that the enrichment of condensin at telomeres we visualized (Part 5 – Fig. 1B-C) was independent of RNAPII (Fig. D3A), suggesting that positioning of condensin by Shelterin is independent of Rpb1 at telomeres. The enrichment at Tel2R is comparable to the nearest Rpb1-dependent peak (Fig. D3A) and also ranks 21/5126 relative to all protein coding genes, although this underestimates the potentially high binding level of condensin due to limitations in our ability to confidently estimate enrichment after position 4,542,700 (see Part 5 – Material & Methods). Then, I performed k-means clustering of condensin signal centered on the TSS of protein-coding genes in Rpb1-OFF which sorted the data in four clusters : two large clusters which showed decrease upon Rpb1 depletion and two clusters which showed retained condensin binding. In the top cluster, composed of very few hits (examples of tracks shown in Fig. D3B), the majority of TSS positions of cluster 1 (Fig. D3C) were flanking centromeres. These peaks were also the first major signal increase when moving away from the centromere (Fig. D3B). Some, but not all of them, can be assigned to known annotations of condensin enrichment. The left side of centromere II appears to have 2 peaks. The peak on the right side of chr II is close to a CU-region (low complexity), the peak at the left side of chr I is close to a tRNA and the peak at the left side of chr III appears to be close to a LTR, although none of these peaks seem to clearly overlap with these annotations. To determine the chromatin associated landscape of these peaks we analyzed data (from Part 7 – Fig. 5) to estimate levels of histone binding at these centromeric peaks and found that consistent with their nature of a TSS they show reduced H3 levels (Fig. D3D). Strikingly, the positions of these condensin peaks appear to be insulating in the vicinity of the centromere as seen by the 2D maps (Fig. D3E) suggesting they are not simply artefacts of the ChIP-seq procedure.

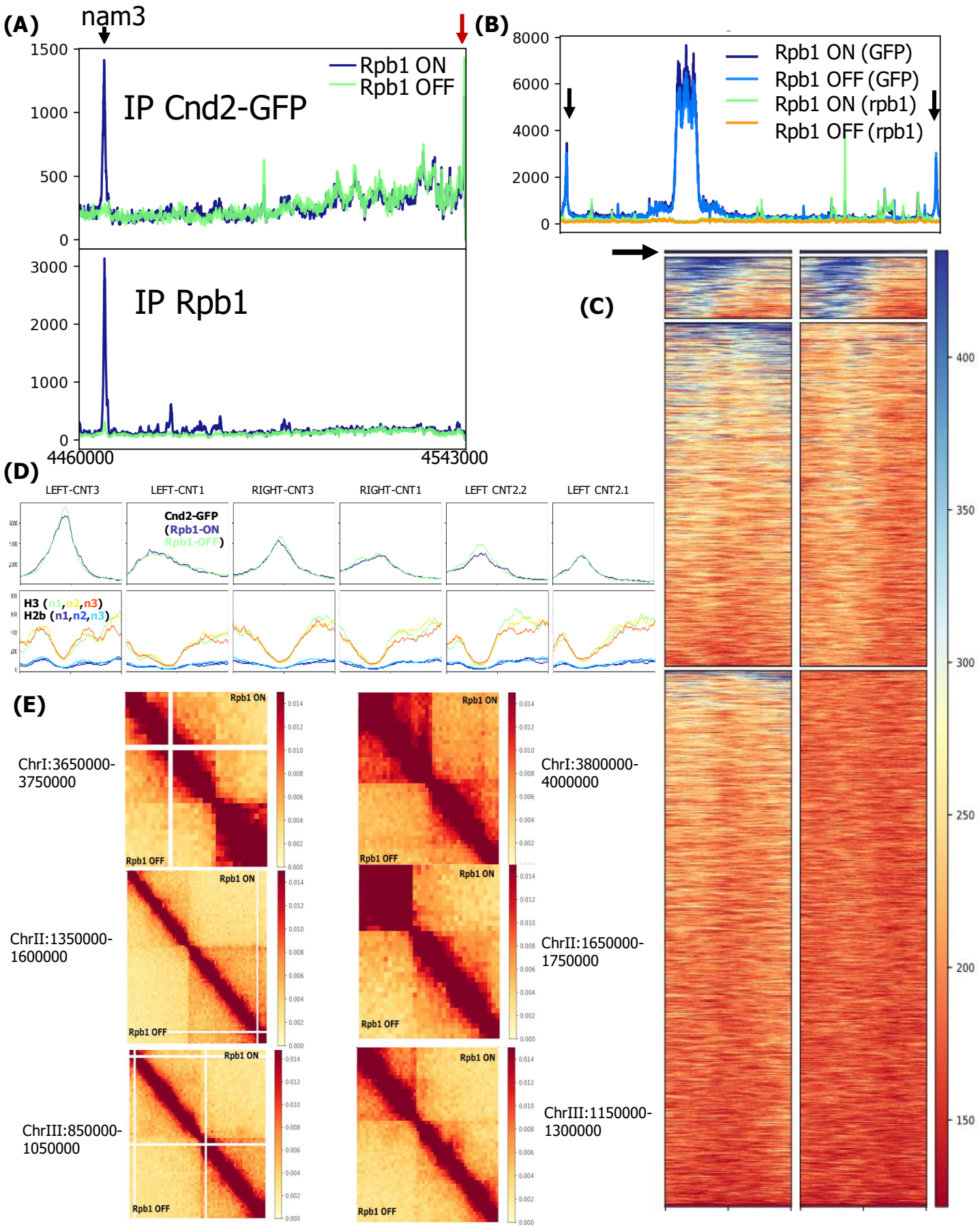

Fig. D3 Condensin peaks flank all fission yeast centromeres in metaphase

Extended right arm of chromosome II (Tel2R) in conditions of Rpb1 depletion. Red arrow indicates the telomeric peak and black arow points to the nam3 locus.

(B) Example of centromere flanking peaks (black arrows) at chromosome I.

(C) Cnd2-GFP calChIPseq signal clustered with k-means = 4 at protein coding genes TSS according to the signal in Rpb1-OFF. Cluster 1 (black arrow) contains 6/7 peaks flanking the centromeres.

(D) Centromere flanking peaks found in cluster 1, with histone calChIPseq signal centered around TSS.

PART 7 – Evidence that nucleosomes hinder condensin in vivo. Colin & Toselli et al., 2024

This project was my main PhD project which I started to work on back during my masters internship. For this project in particular I would like to thank Esther who performed many of the experiments.

7.1 Nucleosomes and their impact on condensin activity

The most abundant DNA-bound proteins in eukaryotes are the histones, which form nucleosomes fiber, the building blocks of chromatin. Few studies in the literature have addressed whether SMC functioning is impacted by nucleosomal arrays and in vitro studies have not yet fully addressed the functioning of SMC complexes relative to properly chromatinized DNA.

An early report suggested that nucleosomes acted as receptors of condensin **(Tada et al., 2011)**. However, the binding of DNA within condensin's safety-belt **(Kschonsak et al., 2017)** which is the anchor chamber for the loop formation process **(Shaltiel et al., 2022)** is sterically incompatible with the presence of a nucleosome. Consistent with this observation of the structure, human condensin does not bind nucleosomal DNA **(Kong et al., 2020)**, histones are not required to assemble mitotic-like structures **(Shintomi et al., 2017)** and condensin binding is anticorrelated with MNase protected signal **(Piazza et al., 2014)**. The hosting lab also provided experimental evidence suggesting that activities evicting nucleosomes (RSC and Gcn5 histone acetyl transferase) facilitated condensin association to chromatin and condensin function **(Toselli-Mollereau et al., 2016)**. Whether chromatin can antagonize or facilitate the rest of the ATP cycle (i.e loop expansion) and whether other chromatin-bound factors participate in condensin activity in vivo remains unclear. As described in the general introduction, the chromatinized template is a dynamic physical entity which can organize the genome into higher-order structures and whether nucleosome arrays can impinge on condensin function is not clear.

The canonical activity of condensin and topo II cannot assemble chromatinized DNA into mitotic chromatids **(Shintomi et al., 2015)** while they can do so on naked DNA **(Shintomi et al., 2017)**. This indirectly suggested that condensin in a minimal system requires additional activities to condense chromosomes. In a minimal system where tailless H2A embryonic histones are used the activity of the FACT histone chaperone is required for condensation **(Shintomi et al., 2015)** although how FACT

mechanistically controls this process, and whether its does so through Topo II or condensin was not clear. In parallel, the hosting lab had performed functional and proteomic screens in fission yeast to identify chromatin-associated activities that might facilitate or antagonize condensin activity. One of the identified partners was FACT **(Orphanides et al., 1998)** consistent with the minimal system **(Shintomi et al., 2015)**. Additionally, FACT was not characterized in mitosis of fission yeast. We therefore set out to understand the function of FACT in mitosis and how it impacted condensin functioning in vivo.

7.2 Evidence that nucleosomes hinder condensin in vivo. Colin & Toselli et al., 2024.

(A)

Proteomics : Cut3-TAP purification and MS analysis

Complex	Gene names	Score	unique peptides	coverage [%]
Condensin	cut3	13,0	147	81,3
	cut14	13,7	131	84,6
	cnd1	12,8	81	63,5
	cnd2	14,4	58	82,5
	cnd3	13,9	70	78,7
Nucleosome	H2A	9,8	3	28,2
	H2B	3,6	6	38,1
	H4	11,0	4	40,8
FACT	pob3	6,4	5	14,1
	spt16	6,6	10	11
ChD1	hrp1	4,9	9	10,9
	hrp3	5,8	12	12
RSC	snf21	5,1	6	7,2
	arp42	4,9	2	6,8

Benoit Gilquin & André Verdel
IAB Grenoble

(B)

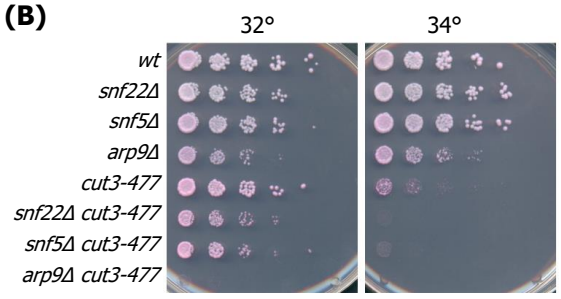

(C)

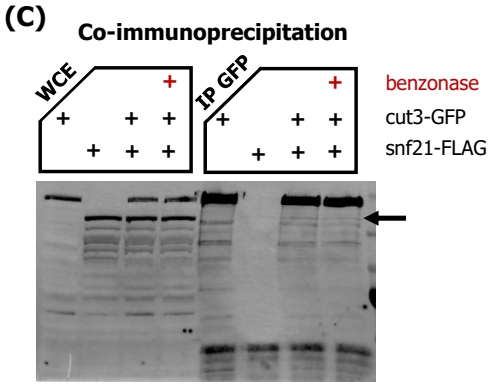

Fig. 1 Chromatin remodelers facilitate condensin function
(A) Candidate physical partners of condensin after Cut3-TAP mass spectrometry.
(B) Spot assay showing genetic interactions between chromatin remodellers SWI/SNF, RSC and condensin.
(C) Immunoprecipitation of cell lysates expressing Cut3-GFP or Snf21-FLAG. Membranes were probed with a mix with a mix of anti-FLAG and anti-GFP antibodies and co-revealed with a Starbright secondary antibody.

Should condensin require chromatin remodeling activities to assist its function in vivo, then mutants of said activities would display genetic interactions with (partial) condensin loss of function. Furthermore,

one might also expect a physical interaction between subunits of the condensin SMC and subunits of such a putative chromatin remodeler.

To answer this question, the hosting lab and collaborators performed genetic and proteomic screens to identify chromatin-based enzymes that might participate in condensin function and/or physically interact with condensin. Using a genetic screen **(Robellet et al., 2014)** the hosting lab identified candidate mutations displaying genetic interactions with a thermosensitive mutation in the SMC4 subunit of condensin, *cut3-477* which reduces condensin association to chromatin (Part 5). Both synthetic sickness and suppressor phenotypes in double mutants. In parallel, mass spectrometry was performed on Cut3-TAP pulldowns mildly digested with benzonase. Multiple candidates were identified with examples shown in (Fig.1A). A notable candidate identified was the RSC complex. Arp9, a subunit common to both SWI/SNF and RSC in fission yeast and required for the binding of RSC to chromatin, showed strong synthetic lethality with *cut3-477*, while other components of SWI/SNF such as *snf22* and *arp5* showed milder synthetic sickness (Fig. 1B). Within the RSC complex, the catalytic subunit of RSC, Snf21, was identified (Fig. 1A) which was described as colethal with *cut3-477* **(Robellet et al., 2014)** and determines binding association of condensin to chromatin **(Toselli-Mollereau et al., 2016)** via reducing histone levels at promoters. To determine whether condensin and RSC interacted, we asked whether Snf21-FLAG could be recovered in lysates of metaphase arrested cells after immunoprecipitating Cut3-GFP. We found a very weak physical interaction between condensin and the ATPase of RSC Snf21 (Fig. 1C) suggesting a potentially relevant physical interplay. Hence, the collective genetic and physical evidence on the RSC complex appears to validate the proteomic screen as a way to identify functional partners of condensin. Both screens underlined a potentially relevant interplay between chromatin remodeling activities and condensin function. Consistent with this, we identified both the histone chaperone FACT, as well as the Chd1 remodeller (Fig. 1A) which also physically interacts with FACT **(Farnung et al., 2021; Simic et al., 2003)** in the context of transcription.

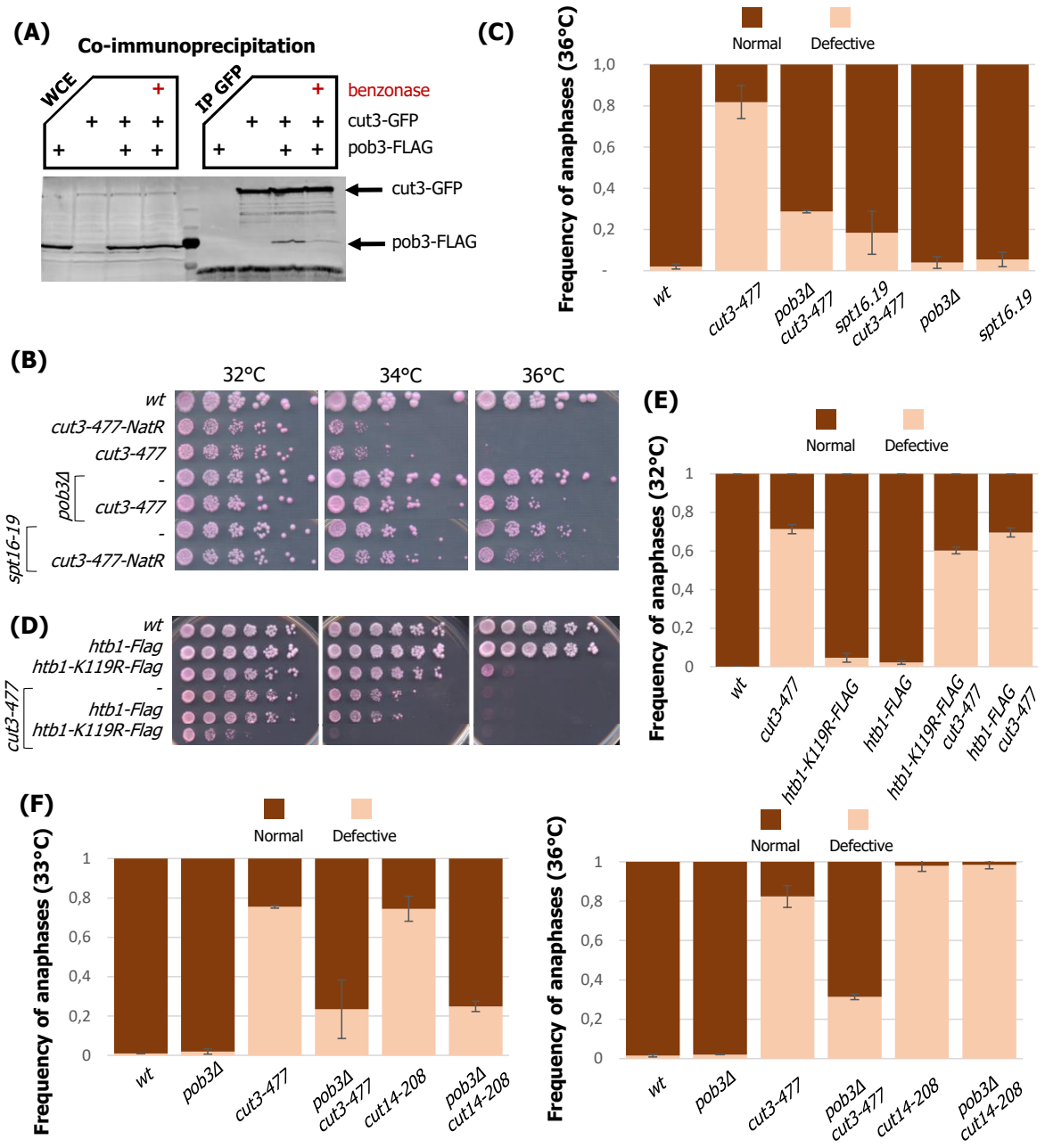

Fig. 2 FACT is a functional antagonist of condensin

(A) Immunoprecipitation of GFP in cell lysates expressing CUT3-GFP and/or POB3-FLAG. Membranes were probed with a mix of anti-FLAG and anti-GFP antibody, and co-revealed with fluorescent starbright antibodies with separate wavelengths.

(B) Spot assay showing the genetic interaction between FACT mutants and cut3-477.

(C) Chromosome segregation assay in cycling cells of the indicated genotype after 2h30mn at 36°C. Values are averages and bars are standard deviation from two biological replicates. χ2 test was used to determine the statistical significance.

(D) Spot assay showing the genetic interaction between *htb1-K119R* and *cut3-477*.

(E) Chromosome segregation assay in cycling cells of the indicated genotype shifted for 2h30mn at 32°C. Values are averages and bars are standard deviation from two biological replicates. χ2 test was used to determine the statistical significance.

(F) Chromosome segregation assay in cycling cells of the indicated genotype shifted for 2h30mn at 36°C (left) or 33°C (right). Values are averages and bars are standard deviation from two biological replicates. χ2 test was used to determine the statistical significance.

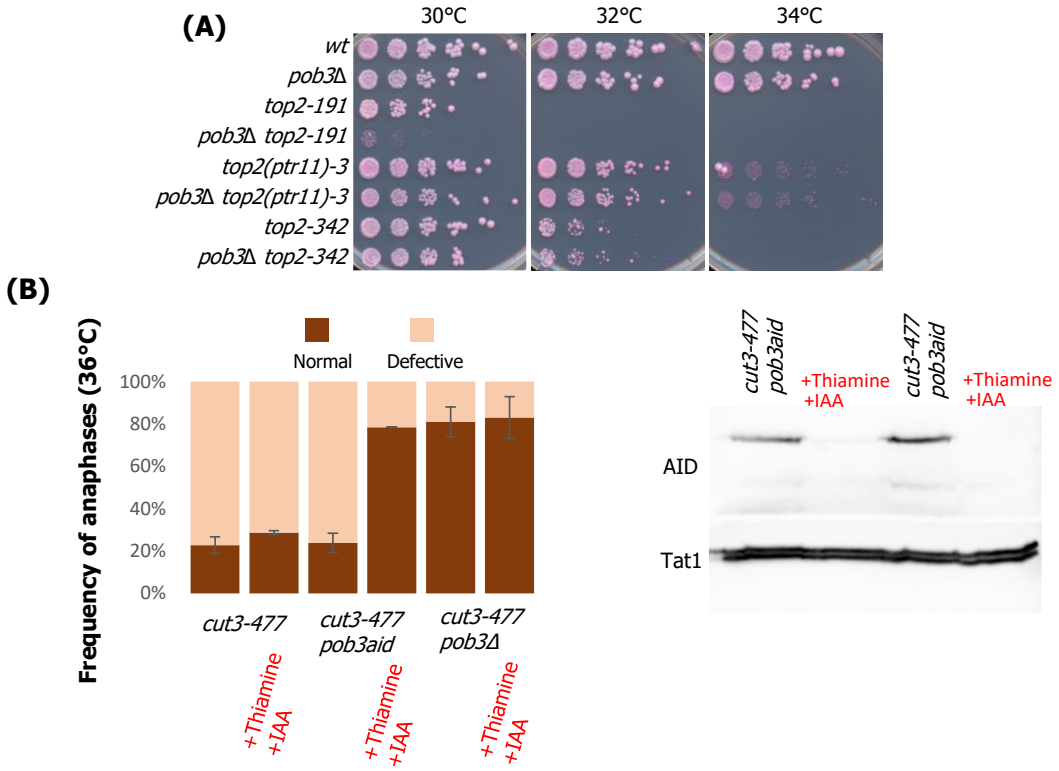

Fig. S2 FACT is a functional antagonist of condensin
(A) Spot assay showing the genetic interaction between topo II mutants and pob3Δ.
(B) Left : Chromosome segregation assay in cycling cells exposed for 2h with Thiamine and IAA at 30°C, then shofted 2h 30mn at 36°C. Values are averages and bars standard deviations from two biological replicates.
Right : western blot showing Pob3-AID depletion after 2h at 30°C with Thiamine and IAA.

The histone chaperone FACT, had already been described as a functional partner of condensin in a cell free chromatinized system **(Shintomi et al., 2015)**. In yeast, the FACT histone chaperone is composed of two subunits, Spt16 (SUPT16H in humans) and Pob3 (SSRP1 in humans) which we found both present in the proteomics screen (Fig. 1A). To validate our proteomics data we immunoprecipitated a GFP tagged Cut3 subunit from mitotically arrested fission yeast cells and asked whether a FLAG-tagged Pob3 subunit co-immunoprecipitated with our bait (Fig. 2A). The Pob3-Flag subunit weakly co-immunoprecipitated with Cut3-GFP and this was highly dependent on the presence of nucleic acids, as benzonase treatment before the IP abolished most of the signal. This data suggest that FACT and condensin are in close proximity on chromatin during mitosis but are not directly physically interacting in a stable manner.

Remarkably a *pob3Δ* background is viable in pombe but this is not the case in budding yeast **(SGD Database)**. One likely explanation is that Spt16 can still bind to chromatin in the absence of Pob3 **(Murawska et al., 2021)** and must provide an essential function to chromatin physiology.

To investigate the functional interplay between FACT and condensin we crossed multiple FACT mutant strains in a *cut3-477* genetic backgrounds including the *pob3Δ* mutation. We found systematically that the partial FACT loss of function rescued growth and viability defects induced by the *cut3-477* mutation (Fig 2B). To determine whether the rescue of growth defects could be caused during chromosome segregation, we analyzed the frequency of chromatin bridge phenotypes in anaphase cells after a shift at high temperatures to trigger a thermosensitive response from the *cut3-477* allele. We observed that *pob3Δ* and *spt16.19* mutations led to significant reductions in the frequency of chromatin bridges in a *cut3-477* backgrounds but no obvious defects in an otherwise *wild-type* background (Fig. 2C). This suggested *cut3-477* induced chromatin bridges were highly dependent on even partial function of FACT (Fig. 2C). These results suggest that FACT negatively regulates condensin function in fission yeast. We assessed the specificity of this interaction by asking whether partial defects in topoisomerase II function showed similar phenotypes. Using a *top2-191* mutation which is deficient in condensation **(Petrova et al., 2013)** we found that *pob3Δ* lowered the semi-permissive temperature of the ts *top2-191* background but had no obvious effect on two other mutations tested (Fig. S2A). This data suggest that the rescue of *cut3-477* associated defects is unlikely to be caused by a facilitation of topoisomerase function. Two caveats however preclude us from making any final interpretations regarding the functional interplay between FACT and Topo II. The first is that we did not assess chromosome segregation in anaphase in those backgrounds (which will be assessed in future experiments). The second is that the synthetic lethality observed in *top2-191 pob3Δ* may reflect a crosstalk in S phase between the roles of both Topo II and FACT during replication, and not during mitotic chromosome assembly.

To try and strengthen our functional data we asked whether the negative relationship between FACT and condensin could be demonstrated in a reverse manner by increasing FACT binding to chromatin. A *h2bk119r* mutation increases FACT binding in vivo in cycling cells **(Murawska et al., 2020)**. We crossed FLAG-tagged *h2bk119r* mutations into a *cut3-477* background and performed a spot assay to determine whether *cut3-477* growth and viability defects would be sensitized by H2BK119R histones (Fig 2D, see 32/33°C). Indeed, H2BK119R lowered the semi-permissive temperature of *cut3-477*, suggesting that increasing the association of FACT to chromatin leads to sensitization to partial condensin deficiency. However, when we assessed the frequency of chromatin bridges after shifting

asynchronously growing cells at 30°C to 32°C for 2h30 we found no increase in the occurrence of chromatin bridges in the double mutants relative to *cut3-477* (Fig 2E). Thus it is unclear whether increasing FACT association to chromatin sensitizes chromosomes to partial condensin loss of function.

Next, we asked whether the functional interplay between FACT and condensin was allele-specific and performed a chromatin bridge assay after shifting *cut3-477* and *cut14-208* mutant cells for 2h30 at either 36°C and 33°C (Fig. 2F). At 33°C we found that loss of Pob3 could rescue both temperature sensitive-allelles demonstrating that the functional conclusion from the previous data can be extended to *cut14-208*. However at 36°C the frequency of chromatin bridges in *cut14-208* became close to 100% and loss of Pob3 did not rescue this phenotype. This data suggest that loss of Pob3 can only rescue condensin defects in the presence of a sufficient threshold of remaining condensin activity in anaphase.

Finally, we asked whether a conditional depletion of Pob3 over multiple generations could phenocopy a constitutive *pob3Δ* mutant. We constructed a degron-tagged Pob3 subunit and began the depletion for 2hrs, then shifted the culture for 2h30 at 36°C (Fig. S2). We found that in regards to the reduction of *cut3-477* induced chromatin bridges, conditional depletion of Pob3 over 2-3 generation times fully reproduced the rescue of a *pob3Δ* mutant. This data suggests that the functional interplay between FACT and condensin is unlikely to be caused by long-term cumulative effects caused by the constitutive lack of Pob3.

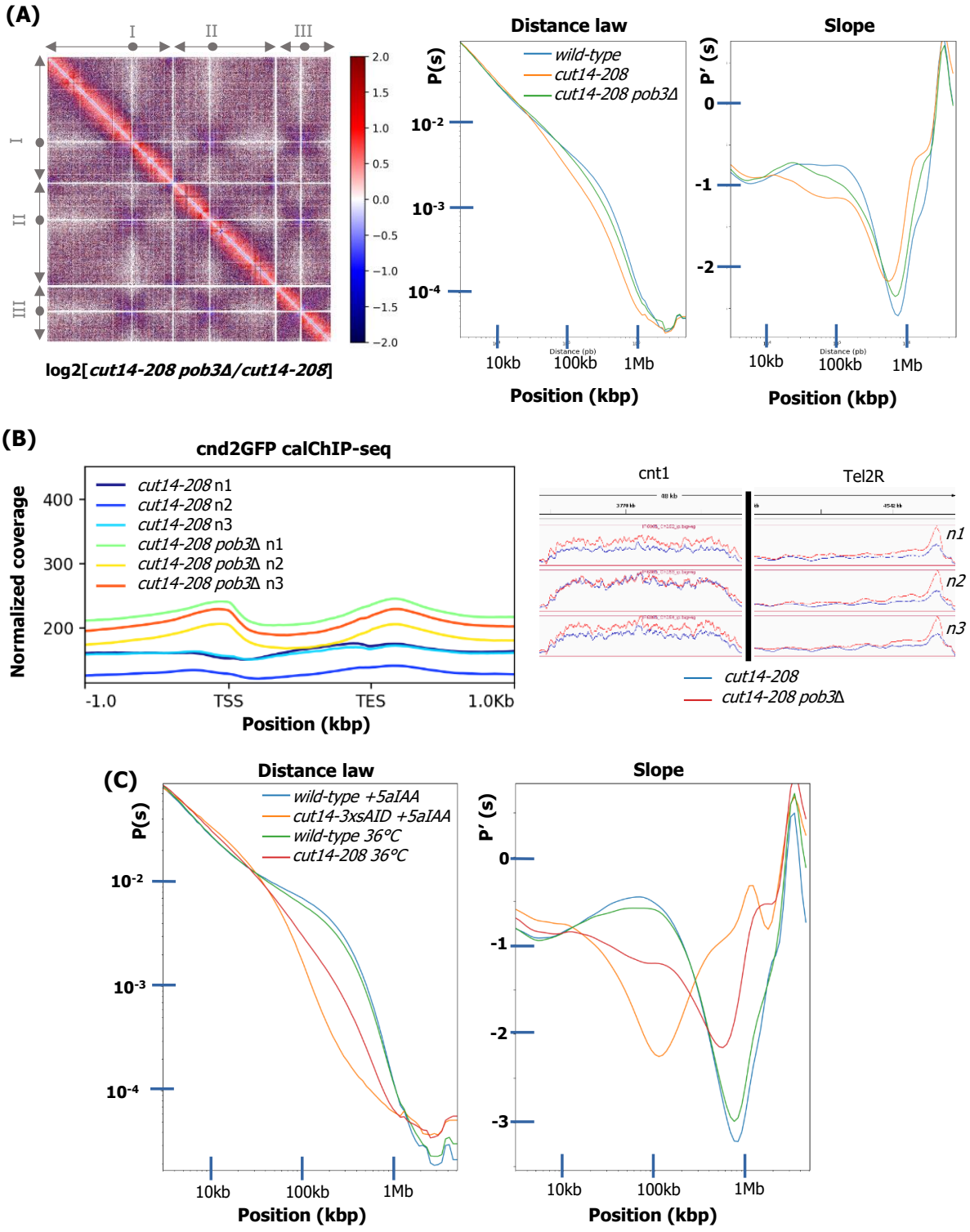

Fig. 3 The constitutive presence of Pob3 prevents condensin association to chromatin
(A) Left : Log2 differential Hi-C contact heatmap of metaphase arrested fission yeast cells *cut14 pob3Δ / cut14-208* after arrest at 36°C. Right : Corresponding Hi-C distance laws and slopes with color coded genotypes.
(B) Left : Average values of calibrated Cnd2-GFP ChIP-seq signal at protein coding genes in *cut14-208* and *cut14-208 pob3Δ* mutant backgrounds after a metaphase arrest at 36°C. Right : IGV profile of calibrated Cnd2-GFP ChIP-seq signal at selected loci in cut14-208 and *cut14-208 pob3Δ.*
(C) Hi-C distance law and its slope of metaphase arrested fission yeast cells color coded as the indicated genotype.

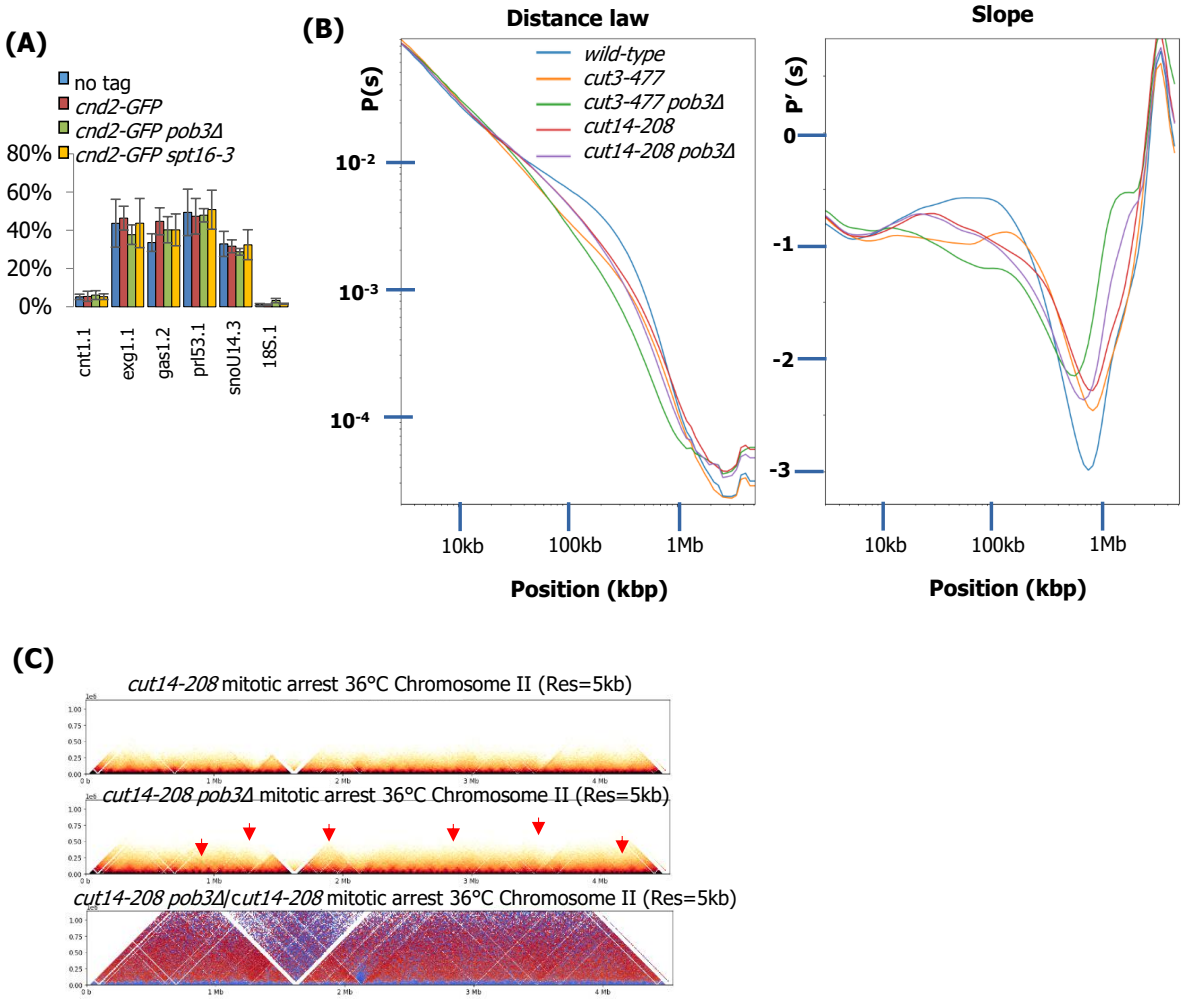

Fig. S3 The constitutive presence of Pob3 prevents the association of condensin to chromatin
(A) Metaphase arrested cells of the indicated genotype were processed for ChIP against RNA pol II S2P. The ratio of quantification obtained in the IP relative to the input (%IP/T) is shown at the indicated loci. Values are averages and bars standard deviation of four biological independent replicates. Cnt1.1 is centromere 1, 18S an rDNA site, and the other sites highly expressed genes.
(B) Hi-C distance law and its slope of metaphase arrested fission yeast cells color coded as the indicated genotype.
(C) Hi-C data from Fig. 3C is shown at chr II at a resolution of 5kb in the indicated conditions, with the ratio at the bottom. Red arrows show gain in contacts in the double mutant.

To investigate how FACT impinges upon condensin dependent chromosome segregation we asked whether levels of RNA polymerase were unchanged in FACT mutants. We immunoprecipitated chromatin with an antibody specific to the Ser2 phosphorylated form of RNA Polymerase II in metaphase arrested wild-type and FACT mutant cells. We observed no apparent difference in levels of RNA pol II at the tested loci by ChIP-qPCR (Fig S3A), suggesting the suppressive effect of FACT mutations on condensin defects cannot be explained by a large scale-reduction of transcription in mitosis.

If the phenotype of rescue of chromosome segregation defects were physiologically relevant and directly tied to condensin function we expect to observe a phenotype on chromosome condensation. We performed Hi-C experiments at 36°C in in metaphase arrested *wild-type, cut14-208, cut3-477, cut3-477 pob3Δ, cut14-208 pob3Δ* strains (Fig. S3B). We found that the *pob3Δ* mutation led to an increase in average contact probability over 20kb-1MB in both condensin mutant backgrounds, and a decrease of contact frequency at shorter range (Fig. 3A, S3B), comforting this hypothesis. This increase appeared condensin specific as we could observe larger scale contacts reappearing when we zoomed in on the 2D Hi-C maps (Fig. S3C red arrows). These results together, suggest that the constitutive loss of Pob3 leads to an improved folding of mitotic chromosomes in backgrounds with partial impairment of condensin activity. We therefore sought to determine the effect of constitutive partial loss of FACT function on the genome-wide binding of condensin. We performed calibrated ChIP-seq against the GFP tagged kleisin subunit of the condensin SMC complex (cnd2-GFP) in *cut14-208* (ts) and *cut14-208 pob3Δ* strains arrested in metaphase. After normalization steps, we visualized the distribution of the signal at fission yeast protein coding genes. We have shown previously that this signal is reduced in a *cut14-208* background relative to *wild-type* (see Part 5, data from the same experiment). In *cut14-208 pob3Δ* compared to *cut14-208* we observed a reproducible (3 replicates) increase of condensin association to chromatin, both at the 3' end and at the 5' end of protein-coding genes (Fig. 3B, left). This increase was also visible at relevant condensin positioning sites such as the extended telomere sequence on the right side of chromosome II (Part 5) and the centromere of chromosome I (Fig 3B, right). Together these data suggested that constitutive lack of Pob3 led to an increase in condensin binding in *cut14-208* backgrounds and a rescue of metaphase chromosome condensation. Strikingly, this phenotype was visible in *cut14-208* backgrounds despite this mutation behaving like a null of function allele in anaphase (Fig. 2F) suggesting that *cut14-208* in metaphase was hypomorphic. To determine if this is the case we performed Hi-C experiments in 3h long metaphase arrests in both *wild-type* and *cut14-208* at 36°C and separately in *wild-type* and *cut14-3xsAID* at 32°C in the presence of 5aIAA for 2hours. While technically in different experimental conditions, the phenotype of the degron was clearly more penetrant than the ts-phenotype of *cut14-208* on mitotic chromosome condensation. Hence, constitutive partial loss of FACT function can facilitate hypomorphic condensation in metaphase but not severe defects in anaphase caused by

cut14-208. This is consistent with reports suggesting partial condensin depletion can lead to individualized chromatids but cause defects in anaphase **(Hirota et al., 2004; Vagnarelli et al., 2006)**.

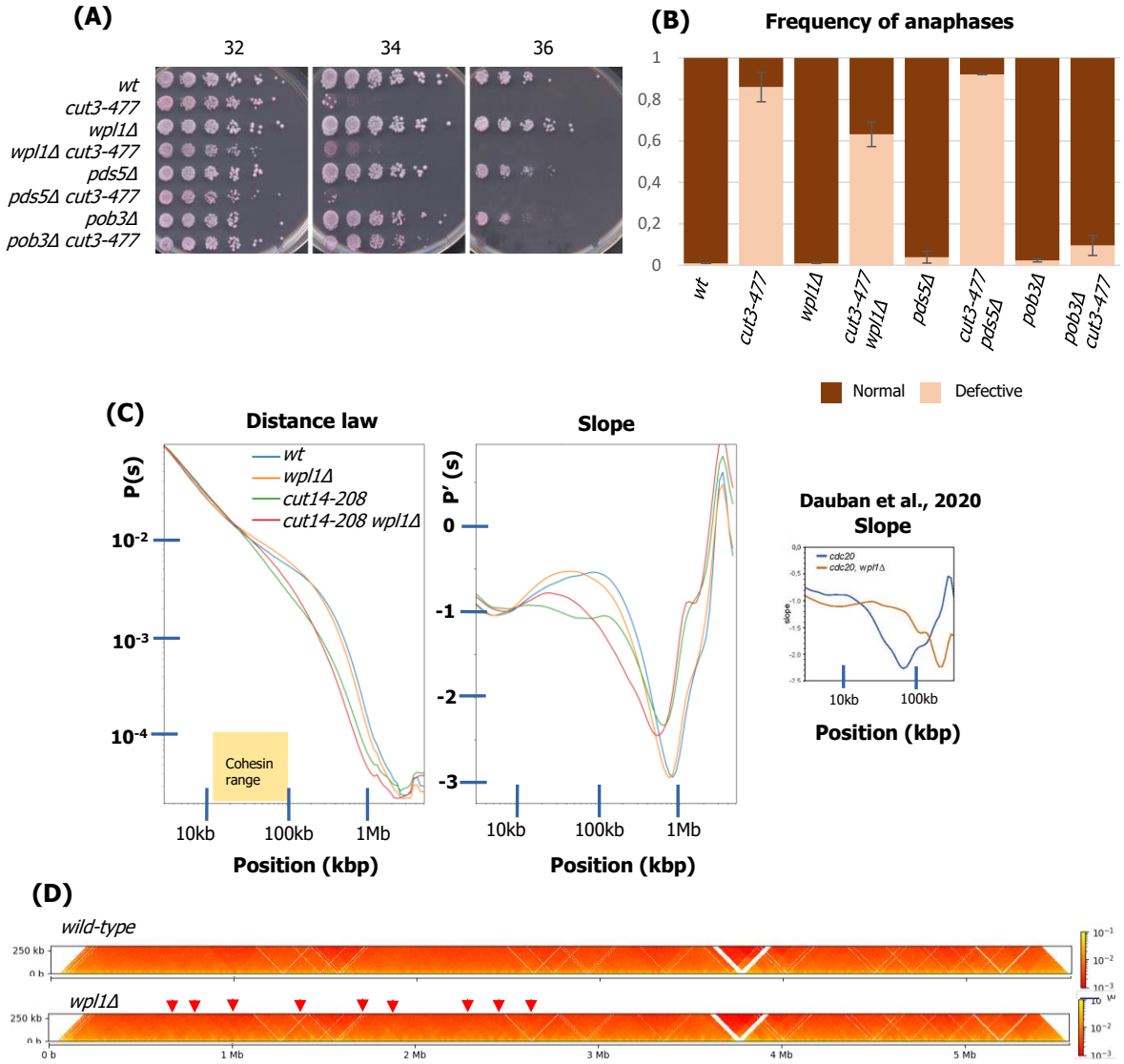

Fig. 4 Cohesin does not antagonize condensin function
(A) Spot assay showing the genetic interaction between *wpl1Δ*, *pds5Δ*, *pob3Δ* and *cut3-477*.
(B) Chromosome segregation assay in cycling cells of the indicated genotype shifted for 2h30mn at 36°C. Values are averages and bars are standard deviation from two biological replicates. χ2 test was used to determine the statistical significance.
(C) Hi-C distance law and its slope for metaphase arrested fission yeast cells color coded as the indicated genotype. Right : Slope of budding yeast Hi-C distance law taken from Dauban et al. (2020), to illustrate the effect of *wpl1Δ* in budding yeast.
(D) Zoom of 2D Hi-C contact map on chromosome I, with red arrow indicating new contacts in the *wpl1Δ* mutant. Resolution is 5kb

FACT has been proposed as a positive activity facilitating cohesin-mediated chromatin folding in budding yeast **(Garcia-Luis et al., 2019)**. Thus, despite the physical interaction between FACT and condensin, our functional data may be illustrating a consequence of an existing interplay between

cohesin and condensin rather than a direct function of FACT on condensin activity. This is particularly relevant in fission yeast as only 5-10% of cohesin is cleaved by separase upon anaphase onset **(Schmidt et al., 2009; Tomonaga et al., 2000)** and removal of cohesin in metaphase is inefficient **(Schmidt et al., 2009)**.

We first asked whether enhancing cohesin loop extrusion could be sufficient to rescue condensin deficiency in mitosis. To do so we assessed the frequency of chromatin bridges in backgrounds where the activity of cohesin is enhanced, by using null mutants of the Wapl (*wpl1Δ*) and Pds5 (*pds5Δ*). Wpl controls cohesin residence time in fission yeast **(Bernard et al., 2008)** while pds5 restricts loop formation by cohesin in budding yeast **(Dauban et al., 2020)**. We found that the *wpl1Δ* background provided a slight rescue of the growth and viability defects of condensin ts mutants (Fig. 4A) and this correlated with a slight rescue of condensin associated defects in anaphase, although not at the level of *pob3Δ* (Fig. 4B). We found no obvious genetic interaction between *pds5Δ* and *cut3-477*. To investigate further the potential rescue of condensin activity by cohesin, we produced Hi-C maps of wild-type and *wpl1Δ* metaphase-arrested populations and found that the contact probability in the distance range where cohesin has been proposed to act is increased **(Mizuguchi et al., 2014; Tanizawa et al., 2017)**. The peak of the slope also appeared more well defined in these arrests, and suggested shorter mean contact distances, but was clearly different from what is observed in cerevisae cells (Fig. 4C, right). We validated the *wpl1Δ* phenotype by observing new contacts in 2D maps reminiscent of those observed in human cells **(Haarhuis et al., 2017)** in these metaphase arrests (Fig. 4D). These data suggest that while increasing the steady state loop size of cohesin by *wpl1Δ* may weakly facilitate condensin activity it cannot recapitulate the full breadth of the rescue phenotype of *pob3Δ* on condensin ts mutants, particularly in anaphase where cells appear more sensitive to partial condensin loss of function. Hence, the effect of *pob3Δ* on condensin is unlikely to rely solely on enhancing cohesin activity. Future experiments will address the effect of cohesin loss of function on condensin associated defects.

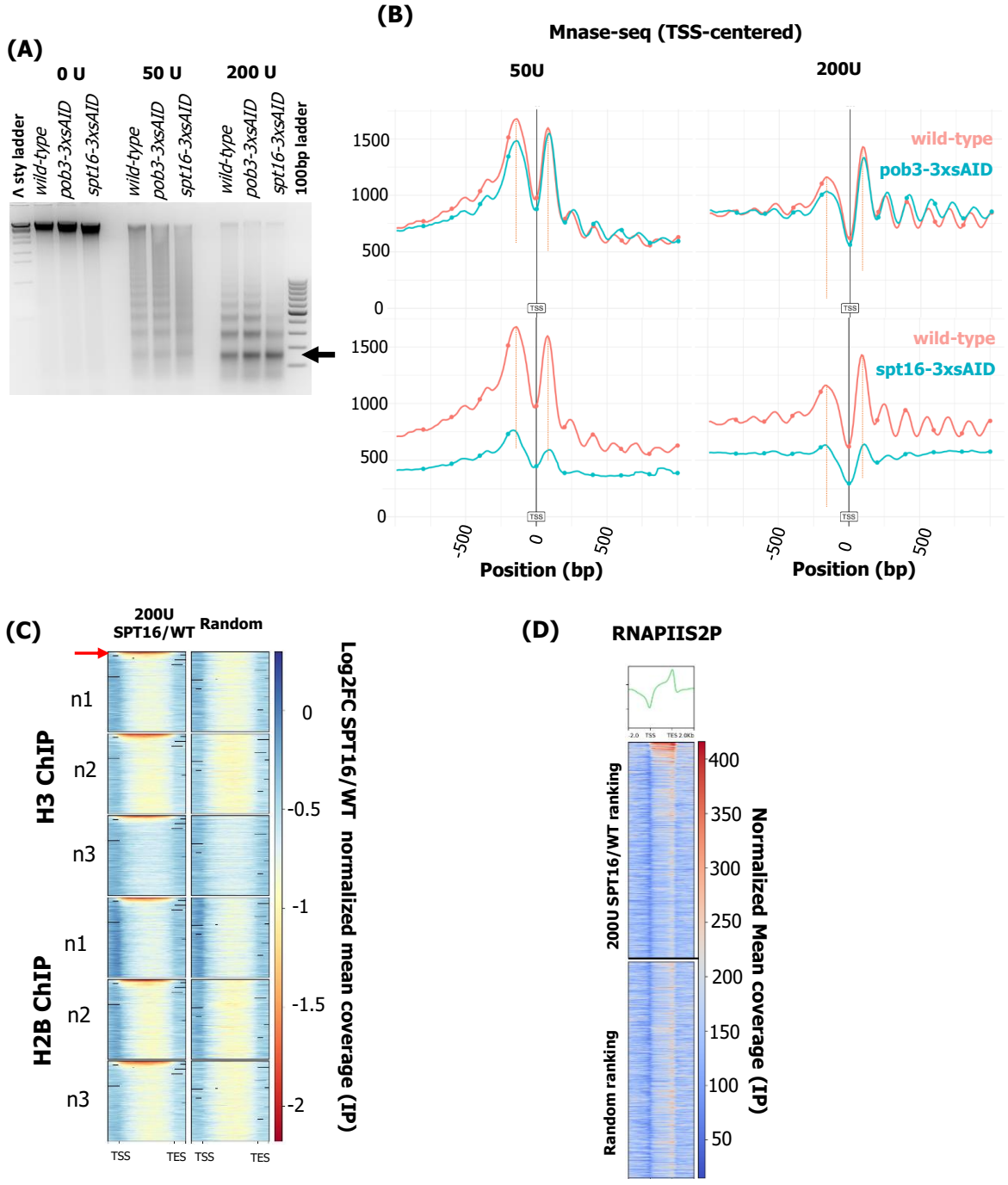

Fig. 5 FACT maintains nucleosome structure in metaphase

(A) Representative Mnase gel after digestion of fixed, metaphase arrested *wild-type, pob3-3xsAID* and *spt16-3xsAID* liquid cultures incubated with 5aIAA. Digestions treated with 0, 50 or 200 units of Mnase were loaded and the bands indicated by the black arrow at 50 and 200U were extracted for library preparation.

(B) Mean coverage of the Mnase-seq signal centered around the TSS of protein coding genes. One biological replicate is shown. Top : *wild-type* vs *pob3-3xsAID*. Bottom : *wild-type* vs *spt16-3xsAID* .

(C) Heatmap of RNAPIIS2P mean calibrated ChIP-seq signal in wild-type. Protein coding genes were ranked decreasingly (top to bottom) starting from the genes showing the greatest loss of signal when comparing *spt16-3xsAID* vs *wild-type* in Mnase digestions at 200U. A random ranking was included as control.

(D) Heatmap of the log2 fold-change (SPT16/WT) of normalized calibrated ChIP-seq against H3 or H2B. Data for the three biological replicates are shown. Protein coding genes were ordered by hypersensitive FACT sites (200U SPT16/WT) or by random ranking.

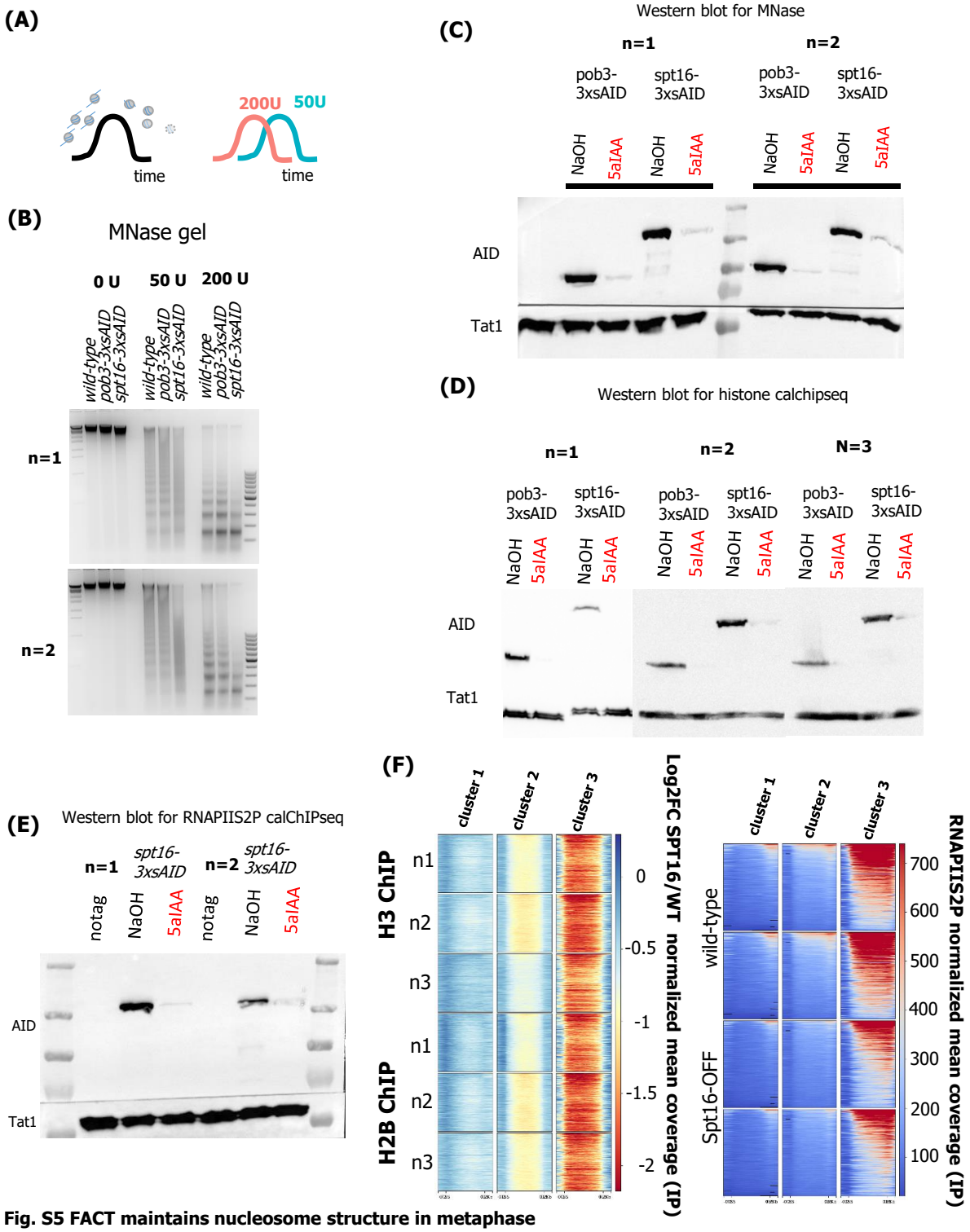

Fig. S5 FACT maintains nucleosome structure in metaphase

(A) In a timecourse experiment, the signal reaches a plateau before Mnase digests the DNA bound to a nucleosome and decreases. Using two different quantities of enzymes for a given duration, one can estimate the stability of a given nucleosome by the relative comparison between the two quantities.

(B) Mnase gels of both biological replicates used for library preparations are shown.

(C-E) Western blots of all biological replicates for the indicated experiments are shown.

(F) Protein coding genes were clustered (k=3) according to the loss in calChIPseq signal in H2B and H3 ChIPs (left). These clusters were used to sort RNAPIIS2P signal in wild-type and Spt16 depleted conditions in the 2 biological replicates (right).

While our data suggest FACT may impinge upon condensin, we do not know whether the effect is direct, i.e takes place in M – or indirect, via alterations of chromatin structure or of transcription during interphase. Moreover, it is not evident whether FACT has a function in M in vivo. To answer these questions we constructed degron tagged strains of the Pob3 and Spt16 subunit of FACT using an improved method **(Zhang et al., 2021)** termed *pob3-3xsAID* and *spt16-3xsAID* which was also used to generate the *cut14-3xsAID* allele. We grew cells to exponential phase and incubated our two degrons with sodium hydroxyde (solvent, NaOH) or 5-adamantyl-IAA 1h after the adjunction of Thiamine for 2h (3h total arrest, Fig. 5A). Thus, we depleted either FACT subunit in metaphase arresting cells and could ask what was the contribution of each subunit of the FACT complex to metaphase nucleosome organization. We performed Mnase-seq experiments in these conditions (Fig. 5A-B, S5 A-B) using two different quantities of MNase to determine the extent of nucleosome fragility **(Chereji et al., 2019)** upon depletion of FACT subunits (Fig. S5C). Strikingly, depletion of Pob3 vs Spt16 performed markedly different gel migration patterns with loss of Spt16 visibly altering chromatin and increasing sensitivity to the Mnase enzyme (Fig. 5A, S5B). We generated sequencing libraries from the mononucleosomal DNA and aligned the reads at the TSS. We observed that depletion of Pob3 led to decrease of the Mnase protected signal at the -1/+1 nucleosomes and increased signal yield at the gene body. We interpret this as an enhancement of the Mnase accessibility (Fig. S5A) and as a more fragile chromatin. We also noted a slight shift in nucleosome positioning, consistent with previous work reporting a phasing defect in a *pob3Δ* mutant background **(Murawska et al., 2020)**. On the other hand, when we aligned reads obtained upon Spt16 depletion we observed drastic loss of Mnase-protected signal at the genes, consistent with the pattern on gel (Fig. 5B). -1/+1 nucleosomes could still be resolved although the peaks were broader, but the positioning defect seen in *pob3Δ* could not be properly observed at the gene body. These results are highly consistent with loss of histones following depletion of Spt16 from metaphase chromosomes. To validate this hypothesis we performed calibrated ChIP-seq against H2B and H3 histone subunits in *wild-type*, *pob3-3xsAID* and *spt16-3xsAID* metaphase arrested backgrounds (Fig. 5C) in the presence of 5aIAA (Fig. S5D). When we ranked protein coding genes from the largest to smallest loss of Mnase signal when comparing Spt16 depletion to wild-type, the most fragile protein coding genes also

showed the strongest loss of histones (Fig. 5C, Fig. S5F), and all genes seemed to universally experience a decrease in histone association upon Spt16 depletion.

As FACT is involved in transcription elongation **(Orphanides et al., 1998)** and we described the importance of RNAPII on condensin distribution and activity (Part 6), we performed calChIPseq in metaphase arrested cells using an antibody against the elongating form of RNAPII in metaphase cells. We ranked the calibrated ChIP-seq signal at protein coding genes from the largest to smallest loss of Mnase signal when comparing Spt16 depletion to wild-type. These FACT-hypersensitive Mnase sites proved to be the most actively transcribed in wild-type in mitosis (Fig. 5D), consistent with known links between active transcription and destabilized nucleosomes in interphase cells and suggesting the role of FACT in mitosis is conserved in fission yeast. We confirmed the most actively transcribed genes were also those that showed the highest histone loss (Fig. S5F, right) by k-means clustering.

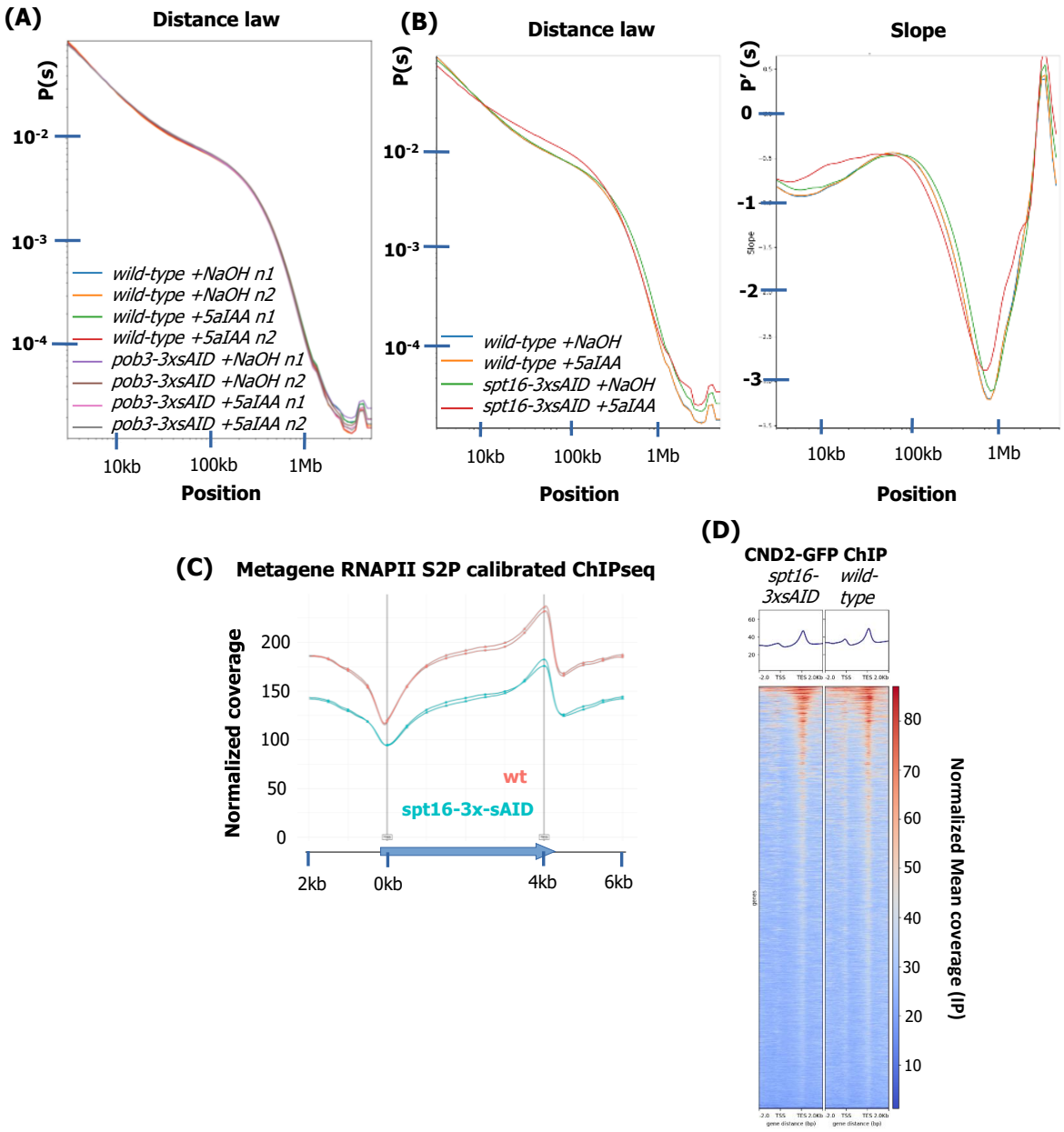

Fig. 6 FACT determines mitotic chromatin folding in metaphase

(A) Hi-C distance law of metaphase arrested fission yeast cells color coded as the indicated genotype, showing the effect of depleting Pob3 in metaphase in two biological replicates.

(B) Hi-C distance law and its slope of metaphase arrested fission yeast cells color coded as the indicated genotype, showing the effect of depleting Spt16 in metaphase. One biological replicate is shown.

(C) Metagene average of the RNAPIIS2P calibrated ChIPseq data at protein coding genes. Two biological replicates shown, in the indicated conditions.

(D) Heatmap of CND2-GFP mean calibrated ChIP-seq signal in *wild-type* an *spt16-3xsAID*. Protein coding genes were ranked decreasingly (top to bottom)

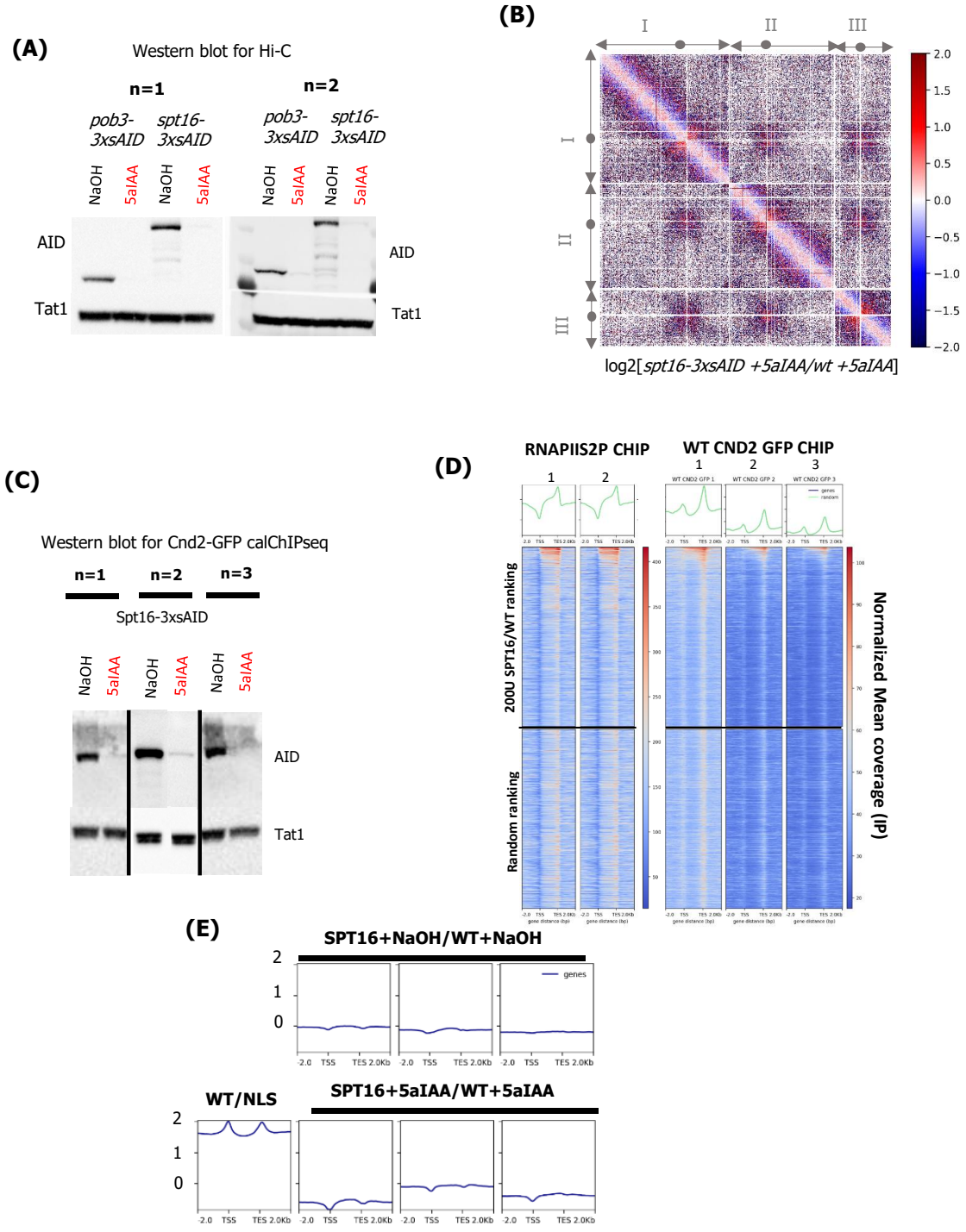

Fig. S6 FACT stabilizes chromatin structure in metaphase
(A) Western blots for the Hi-C experiment showing depletion of Pob3-3xsAID and Spt16-3xsAID.
(B) Log2 differential map of spt16-sAID+5aIAA/wt+5aIAA
(A) Western blots for the calChIPseq experiment showing depletion of Spt16-3xsAID.
(D) Heatmaps at protein coding genes for all biological replicates of the calibrated ChIP-seq experiments in Fig. 6C-D are shown, ranked according to levels of RNAPIIS2P association.
(E) Log2 ratio of the indicated comparisons for Cnd2-GFP calChIPseq normalized mean signal at protein coding genes. The three biological replicates are shown.

Having described the genome-wide function of FACT on chromatin organization, we asked what were the impacts of FACT depletion on the 3D organization of mitotic chromosomes by Hi-C experiments. Strikingly, depletion of Pob3 had no visibe effect on the structure of chromatin (Fig. 6A), implying the effects we previously described (Fig. 3) are not a direct consequence of Pob3 function in mitosis or are caused by insufficient depletion. However, Pob3 depletion was consistently as penetrant, if not slightly more efficient than Spt16 depletion (Fig. S5C-D, S6A) arguing against this hypothesis. Strikingly, depleting Spt16 produced a visible loss of contact probability <20kb and an increase of contact probability in the 20-200kb range (Fig. 6B). This suggested that the effects we observed in *cut14-208* backgrounds (Fig. 3) originate from a role of Pob3 in interphase. When looking at the slopes of contact probability curves it appeared as if the size of average loops of Spt16 depleted cells in mitosis is reduced (Fig. 6B). We also noted that depletion of FACT led to marked loss of insulation at the centromere (Fig. S6B) consistent with evidence suggesting that partial loss of FACT function leads to a loss in hererochromatin integrity caused by reduced occupancy of Swi6/HP1 **(Lejeune et al., 2007)**. As lack of Pob3 does not prevent Spt16 function and binding on chromatin **(Murawska et al., 2020)**, we focused on *spt16-3xsAID* to address the role of FACT in mitosis.

The changes in contact probability observed upon Spt16 depletion appeared as an intermediate phenotype where the contact ranges affected were both in the range of cohesin and condensin. Since we had described RNA pol II as a positioning device of condensin (Part 6) we compared the mean calibrated ChIP-seq signal between wild-type and Spt16 depleted cells and found that depletion of FACT in metaphase led to a reliable, mild reduction (~25% on average) of transcribing RNA pol II (Fig. 6C, Fig. S5F). As FACT hypersensitive sites correlated with highly transcribed genes (Fig. 5D, S5F) we validated that these sites were also associated with high condensin levels as seen by calChIPseq (Fig. S6D). Since our Hi-C maps showed long-range contact changes upon Spt16 depletion, we asked whether Spt16 was important for condensin association to chromatin in metaphase. We performed calibrated ChIP-seq against Cnd2-GFP in wild-type and Spt16 depleted backgrounds. Over three biological replicates, Cnd2-GFP signals were slightly reduced, if not unchanged at protein coding genes (Fig 6D, S6E). This suggests FACT does not significantly determine the distribution of condensin at protein coding genes.

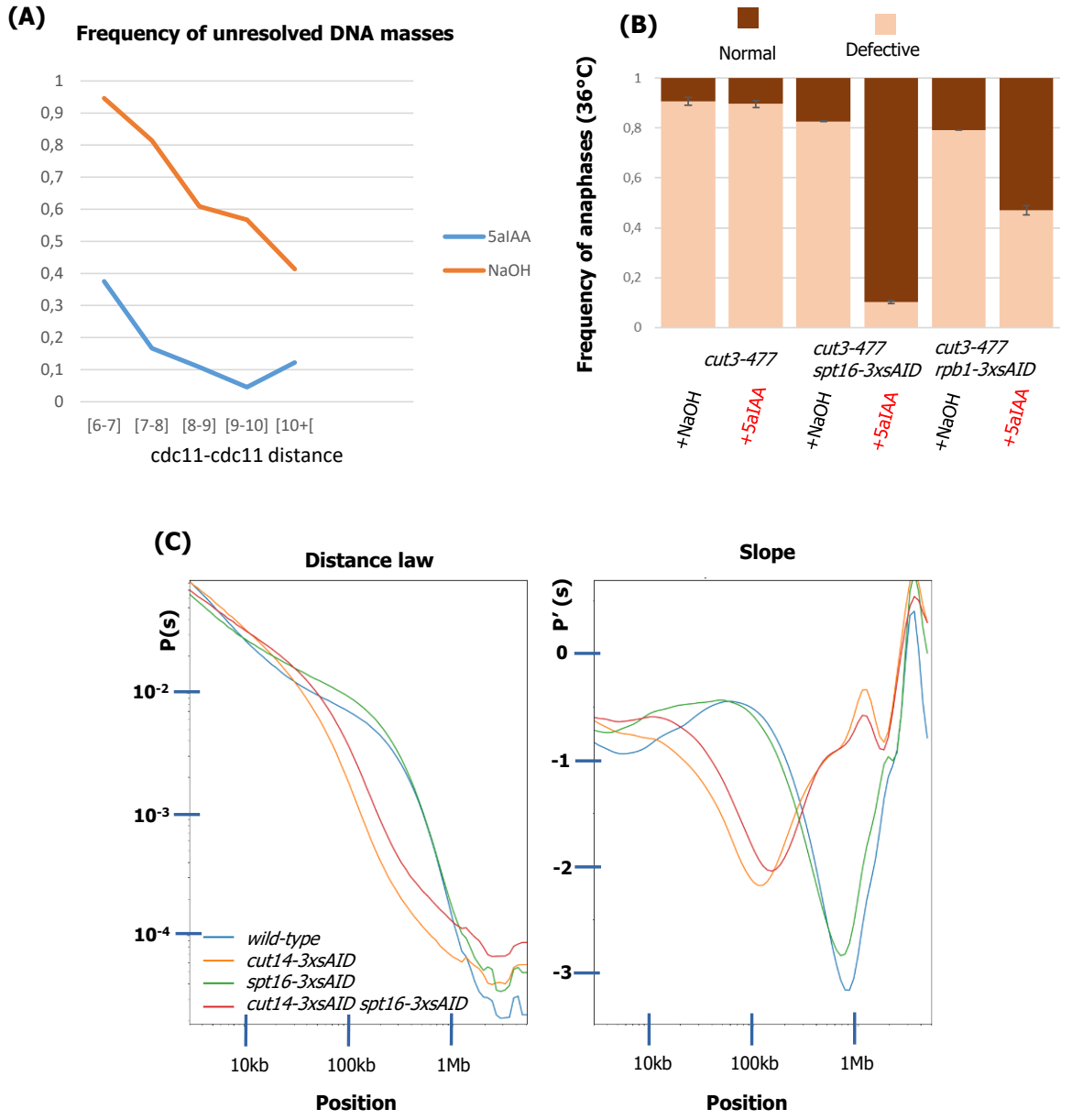

Fig. 7 FACT activity in metaphase appears independent of condensin
(A) cdc2asM17 cells were exposed to 3-Brbpp1 for 1h, then exposed to NaOH or 5aIAA for 2h to deplete Spt16-3xsAID from G2 arrested cells. Cells were released into NaOH or 5aIAA containing media and the frequency of chromatin bridges was determined as a function of the distance between two Spindle Pole Bodies (cdc11-cdc11 distance).
(B) Chromosome segregation assay of cycling cells shifted for 2h 30mn at 36°C. *cut3-477 spt16-3xsAID* was exposed to 5aIAA or NaOH for 2h, 30min into the shift. *cut3-477* and *cut3-477 rpb1-3xsAID* were exposed to NaOH and 5aIAA for 30min, 2h into the shift. Values are averages and bars are standard deviations of two biological replicates.
(C) Hi-C distance law and its slope of metaphase arrested fission yeast cells color coded as the indicated genotype, showing the depletion of Spt16 in both wild-type and condensin depleted backgrounds.. One representative biological replicate is shown.

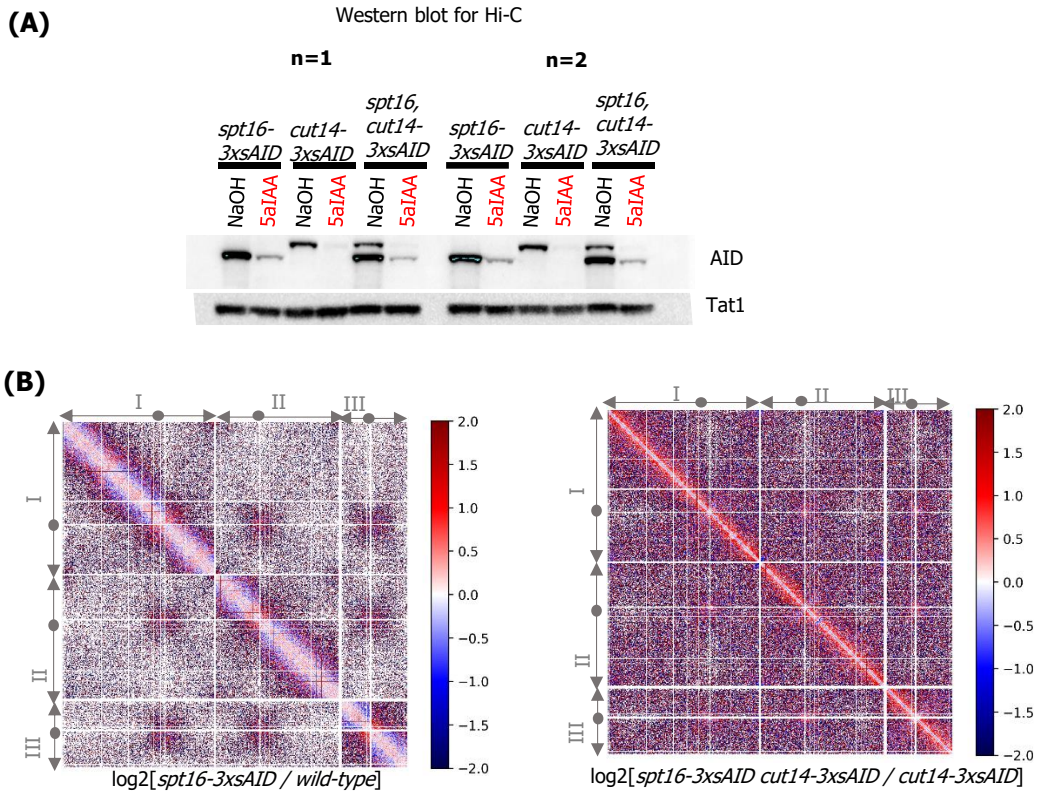

Fig. S7 FACT activity in metaphase appears independent of condensin
(A) Western blot showing the depletion of Spt16-3xsAID and of cut14-3xsAID in the indicated Hi-C experiment.
(B) Log2 differential map of the indicated ratios
(C) Log2 ratio of the indicated comparisons for Cnd2-GFP calChIPseq normalized mean signal at protein coding genes. The three biological replicates are shown.

Since Spt16 appeared to play a role in chromatin structure in metaphase, but not Pob3, we asked whether depletion of Spt16 in just prior to anaphase onset was sufficient to rescue condensin defects. We employed a cdc2asM17 shokat allele **(Aoi et al., 2014)** to block cells in G2/M by addition of 4-Amino-1-tert-butyl-3-(3-bromobenzyl)pyrazolo[3,4-d]pyrimidine (3-BrbPP1) in liquid cultures. Cells were exposed to the cell cycle block for 1h at 30°C before splitting the culture and adding 5aIAA or NaOH and shifting at 33°C to begin depletion of Spt16 in *cut14-208* sensitized backgrounds. After 2 hours of depletion, we washed cells on a nitrocellulose membrane in media without 3-BrbPP1 (but with NaOH or 5aIAA) and released them into anaphase at 33°C. We noticed depletion of Spt16 induced a slower release into anaphase. In practice we collected aliquots to score defects 15mn (NaOH) or 25 mn (5aIAA) after release and quantified the frequency of defects as a function of the length of the anaphase spindle (estimated by the distance between two cdc11-GFP foci). As expected **(Hocquet et al., 2018)**, a high frequency of defects is observed at short spindles that diminishes as cells enter late anaphase. Strikingly, Spt16 depletion showed a marked reduction in the frequency of

unresolved chromatid masses (Fig. 7A). This suggests that the rescue phenotype can be attributed to a function of Spt16 between the time just before entry into M phase and anaphase.

We have shown that condensin localization in fission yeast is biased towards actively transcribed regions (Part 6). Actively transcribed regions also happen to show the largest loss of histones when Spt16 is depleted (Fig. S5F) and a mild reduction in RNAPIIS2P. In that context, it becomes complicated to uncouple transcription and chromatin fragility to understand the rescue phenotype of Spt16 on condensin activity. For instance, part of the suppressive effect on the loss of function of FACT could be explained by a reduction in RNA pol II barriers.

We thus sought to determine whether depletion of Rpb1 could phenocopy FACT depletion. We confirmed that depleting Spt16 on a short timescale was sufficient to reproduce the suppressive effect observed with partial, constitutive loss of function mutants. 2 hours of depletion were sufficient to strongly rescue condensin defects (Fig. 7B) validating that loss of Spt16, like a null mutant of Pob3, facilitates condensin activity in anaphase and consistent with the G2 release experiment (Fig. 7A). Furthermore, the reduction in *cut3-477* associated chromatin bridges was significantly stronger in Spt16 depletion compared to Rpb1 depletion, despite stronger reduction in chromatin bound RNA pol II in Rpb1 depletion (our results in Part 6 vs Fig. 6D).

To better understand whether the changes seen in Hi-C were condensin dependent we created a double *spt16-3xsAID cut14-3xsAID* degron strain (Fig. S7A). If the changes observed in metaphase are independent of condensin, then the phenotype of Spt16 depletion should still be visible in a background where Cut14 is depleted. We performed Hi-C experiments in such backgrounds and found indeed that Spt16 depletion induced a reduction in short range contacts <20kb and an increase at longer ranges whether condensin was present or not. This suggests that mitotic chromosome folding by condensin is largely independent of a function of FACT in metaphase, although we cannot formally rule out a genetic rescue in Cut14-3xsAID depletion with trace amounts of condensin (although not readily visible by Western, Fig. S7A).

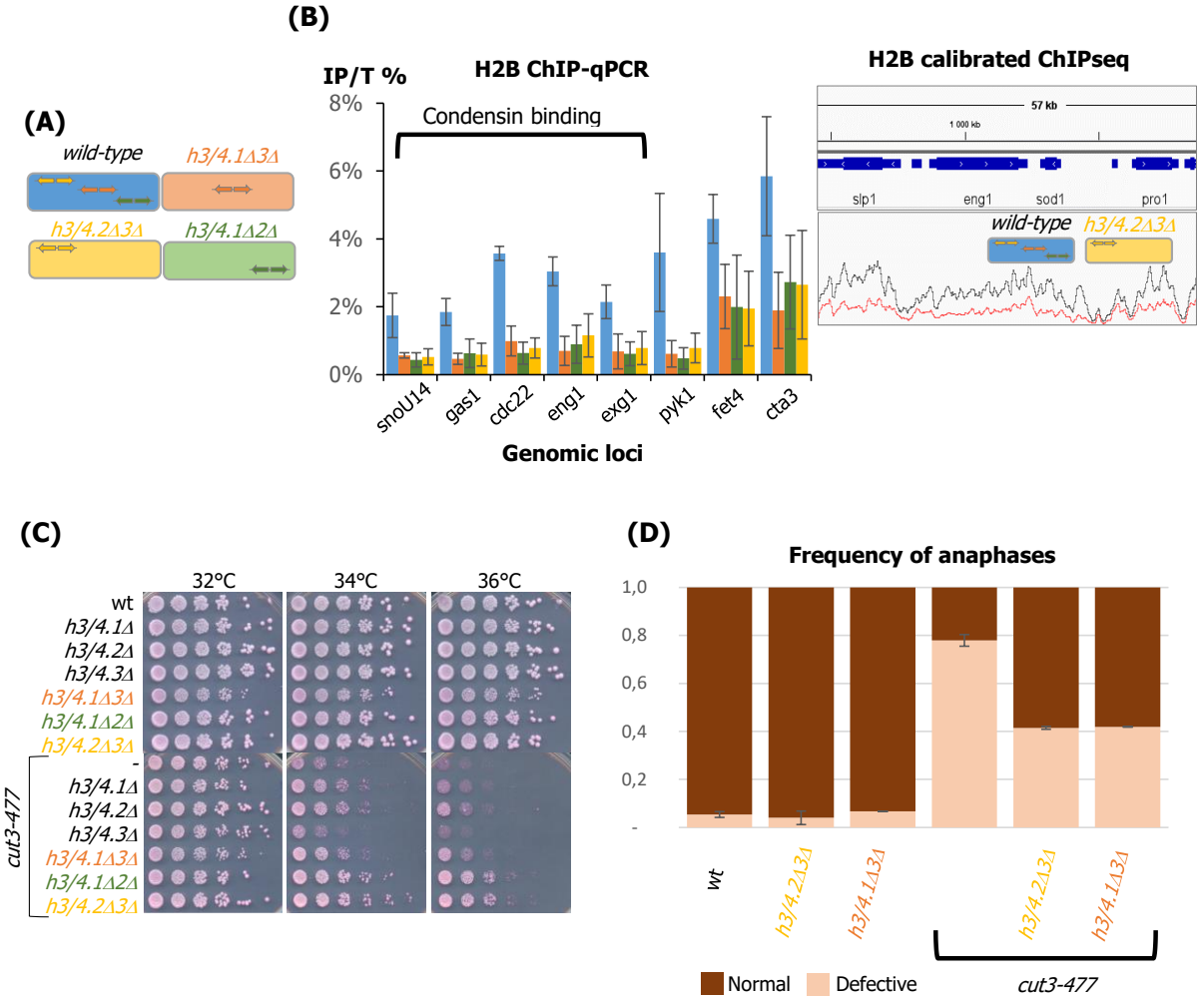

Fig. 8 Nucleosome density antagonizes condensin function.
(A) Pairs of H3/H4 core histone genes in fission yeast. The color of the mutant corresponds to the color code of the remaining histone pair.
(B) Left : IGV profile of calibrated H2B ChIP-seq signal at a selected locus. Right : H2B ChIP qPCR signal expressed as the ratio of DNA signal recovered in the IP over the DNA signal recovered in the input, at the indicated genomic loci. Genotypes used follow the color code in (A)
(C) Spot assay showing the genetic interaction between *cut3-477* and histone copy number mutants in (A).
(D) Chromosome segregation assay in cycling cells of the indicated genotype shifted for 2h30mn at 36°C. Values are averages and bars are standard deviation from two biological replicates. χ^2 test was used to determine the statistical significance.

To assess whether nucleosomes may pose a functional hindrance to condensin we constructed fission yeast strains with altered copy number of core histone genes. Fission yeast encodes three copies of H3 and H4 which are expressed as divergent transcriptional units (Fig. 8A). We produced three combination of mutants leaving only a single of these H3/H4 pairs left in the genome. By ChIP qPCR on asynchronously growing cells we assessed the % of DNA co-immunoprecipitated with the H2B subunit relative to input in wild-type versus these combinations of mutants (Fig. 8B, right). We found similar reductions in H2B binding, suggesting that loss of 2/3 of H3/H4 gene copy number is sufficient to induce a loss of nucleosomes. To validate these results, we performed calibrated H2B-ChIPseq on

asynchronously growing wild-type and one of these mutants. We confirmed by visualizing igv profiles that the histone mutant reduces reproducibly the levels of DNA-bound H2B (Fig. 8B, left). Since we observed reduced levels of H2B in these H3/H4 copy number mutants we can comfortably assume these mutants show a true reduction in nucleosome occupancy.

Due to technical limitations in crossing these H3/H4 copy number mutants in *nmt-slp1* backgrounds we were unable to evaluate levels of histone-bound DNA in metaphase, preventing us from performing relevant genomic experiments with these mutants.

Nonetheless, in a genomic context where levels of nucleosomes are reduced genome-wide, serially diluting *cut3-477* versus *cut3-477* in histone copy number mutants showed an alleviation of condensin induced growth and viability defects across all mutants (Fig. 8C) This suggests that in a *cut3-477* background part of the defect may be caused by histone gene-copy number and potentially nucleosome occupancy. To confirm this observation we analyzed chromatin bridges in asynchronously growing cells in two of these histone copy number mutants, shifted at 36°C for 2h and 30mn. As predicted by the spot assay, loss of H3/H4 gene copy number leads to a partial rescue of the frequency of chromatin bridges (Fig. 8D). Together these results suggest that the density of nucleosomes genome-wide becomes a hindrance to proper chromosome segregation when condensin is partially impaired.

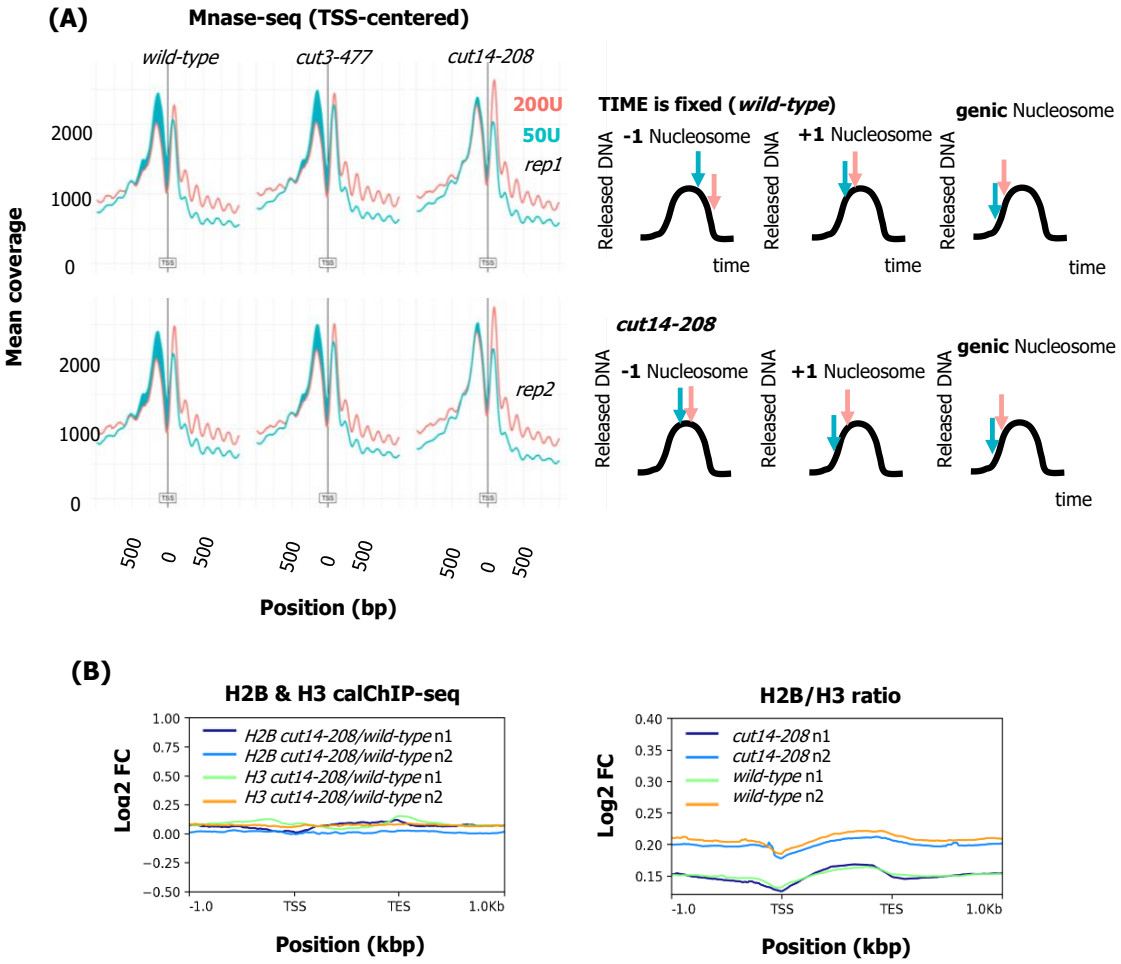

Fig. 9 Condensin does not promote chromatin remodeling
(A) Mnase-seq mean coverage centered around the TSS for each indicated genotype. Chromatin was digested either with 200 (orange) or 50 (turquoise) units of Mnase. Two biological replicates (rep1, rep2) are shown. On the right, interpretation of the data.
(B) Calibrated H2B and H3 ChIP-seq data at protein coding genes. Two biological replicates shown. **Left :** log2 fold change of calibrated ChIP-seq (both H2B and H3) signal expressing the difference in *cut14-208* over *wild-type*. **Right :** log2 fold change of the calibrated ChIP-seq signal ratio H2B/H3 in the indicated genotypes.

As we identified in screens chromatin remodeling activities, and found that backgrounds reducing nucleosome occupancy genome-wide (Fig. 5B-C, Fig. 8B) rescued partial condensin loss of function (Fig. 7A-B, Fig. 8C-D) we asked whether condensin itself drives chromatin remodeling. We performed Mnase digestions of mitotically arrested cells in *wild-type*, *cut3-477* and *cut14-208* backgrounds for different levels of condensin loss of function (Fig. 2F).

We built sequencing libraries out of the mononucleosomal digestion products and aligned the reads to the genome. After plotting the reads centered around the TSS of genes in both digestion conditions (Fig. 9A, left) we found that the position of peaks remained similar between wild-type and condensin mutants. This suggests that condensin does not drive the position of nucleosomes on metaphase

chromosomes. We did observe slight differences in amplitudes of signal between 200 and 50 units (Fig. 9A compare *wild-type* and *cut14-208* and interpretation Fig. 9A right). The difference in coverage at 50 U vs 200 U is reduced in a *cut14-208* compared to *wild-type* at the -1 and +1 nucleosomes. This suggests that condensin deficiency leads to a partial loss of fragility at these nucleosomes. This phenotype is not observed in the less penetrant *cut3-477*. While we do observe higher levels of Mnase signal for the same digestion at gene bodies in mutant backgrounds compared to wild-type (Fig. 9A position 500 bp and further downstream of the TSS), this is difficult to interpret. Indeed, it is hard to tell whether this is due to a bona fide role of condensin in stabilizing chromatin. More Mnase protected signal released from gene-body nucleosomes in *cut3-477* or *cut14-208* might be simply explained by a better accessibility of the Mnase enzyme because condensin is lost from chromatin. In other words, the condensin complex itself might hinder the digestion of DNA by Mnase. It would therefore be difficult to distinguish a biological scenario where condensin stabilizes chromatin from this technical artefact.

To circumvent this issue we performed calibrated ChIPseq against core histones H2B and H3 in metaphase arrests of *wild-type* and *cut14-208* mutants. After normalization we expressed the ratio of Histone-ChIP signal between condensin mutants and wild-type, as well as the ratio of ChIP signal between H2B over H3 in both conditions (Fig. 9B). We found that both : the levels of histone at protein coding genes and the H2B/H3 ratio remained identical between *wild-type* and *cut14-208* strains. This data suggest that condensin does not globally drive a change in occupancy of histones, nor does it determine the stoechiometry of nucleosomes on chromatin.

To summarize, we find that condensin functionally interacts with the FACT histone chaperone, and that this interaction causes defects when condensin is partially impaired. We show that FACT in mitosis controls the density of nucleosomes and their positioning along the chromatin, and that FACT does not appear to impinge upon condensin function in metaphase but does so at least in anaphase. Finally we provide functional evidence that nucleosome density antagonizes condensin function despite condensin itself not being able to remodel nucleosomes.

7.3 Supplementary results to Part 7

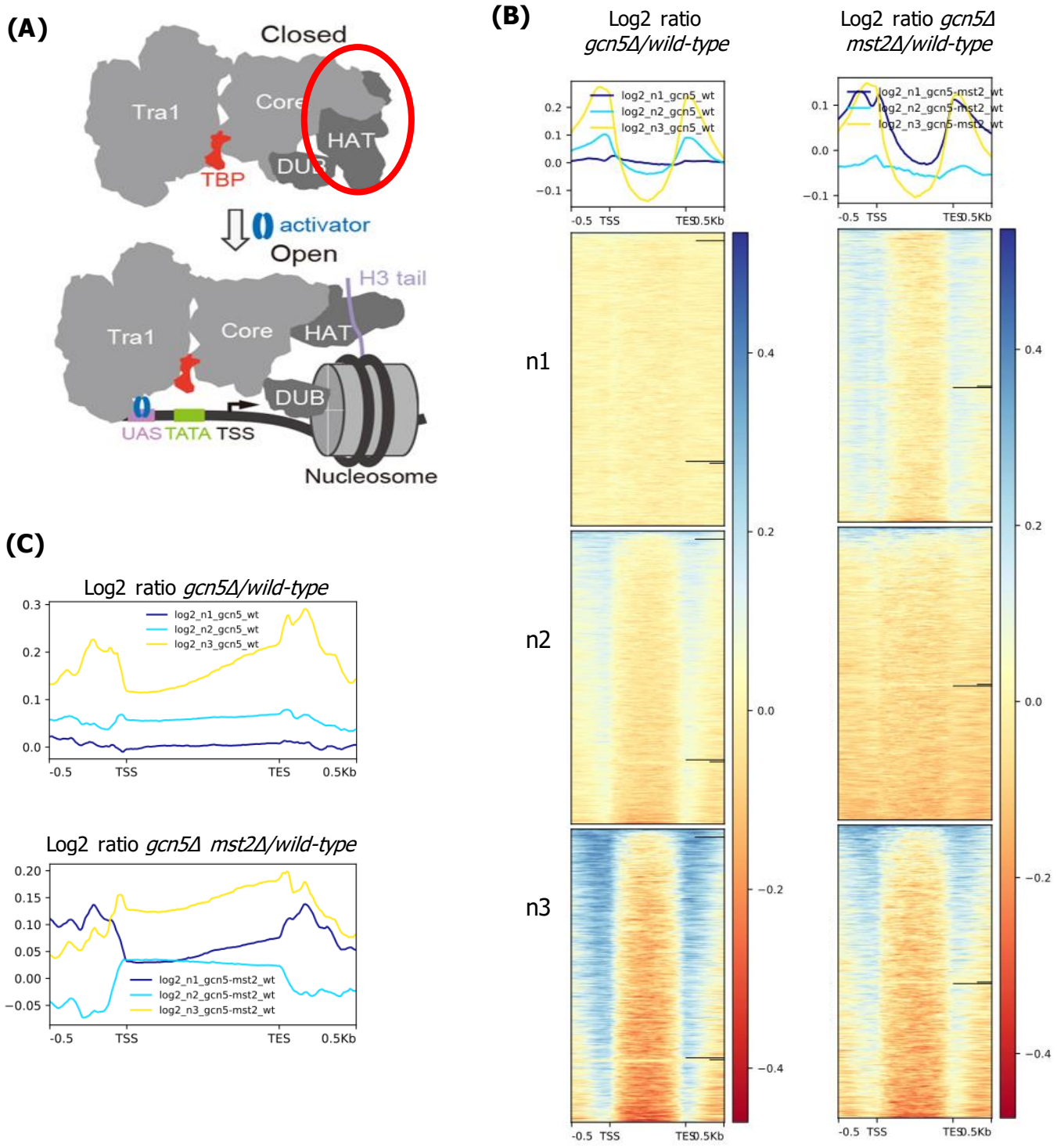

Fig. D4 Mitotic chromatin at tRNA genes.
(A) Figure adapted from (Wang et al. 2020) showing the yeast SAGA complex. Circled in red is the histone acetyl transferase domain containing the Gcn5 subunit.
(B) Mnase data from (Toselli et al., 2016) showing log2 ratios of the indicated comparisons (*gcn5Δ/wild-type* and *gcn5Δ mst2Δ/wild-type)* for all biological replicates separately at tRNA genes.
(C) Metagene averages of Mnase signal at tRNA genes for all biological replicates.

I asked whether The Gcn5 (Fig. D4A) and Mst2 acetyl-transferases, which are reported to control histone eviction at tDNA in interphase through RNAPII **(Yague-Sanz et al., 2023)** would influence in mitosis the chromatin at the level of tDNA. To do this I reanalyzed published data from **(Toselli et al., 2016)** in which I could estimate the change in MNase-protected DNA at tDNA (Fig. D4B-C). Across the three biological replicates, there appeared to be on average no significant difference in the accessibility of DNA by the MNase enzyme caused by the constitutive loss of Gcn5 when cells were arrested in M. Moreover this was not potentialized in the double mutant *gcn5Δ mst2Δ* (Fig. D4B right panel) suggesting this pathway is potentially not implied in the control of histone density specifically at the tDNA during mitosis.

DISCUSSION

The mechanisms behind the *in vivo* function of condensin in the context of chromatinized DNA remain to be elucidated. Condensin is proposed to assemble mitotic chromosomes by loop extrusion or by diffusion capture mechanisms. To what extent each model can recapitulate the activity of SMC complexes and how condensin can function in a crowded chromatin environment is not clear. Below I discuss several aspects of mitotic chromosome biology related to the results gathered during this PhD.

8.1 The architecture of fission yeast mitotic chromosomes

From our Hi-C data and previous datasets **(Kakui et al., 2017)** several key features underline stark morphological contrasts between mitotic chromosome of fission yeast from vertebrates. We do not observe a second diagonal band as opposed to what is seen in vertebrates which can easily be explained by a single condensin variant in fungi, which is condensin II dependent in chicken **(Gibcus et al., 2018)**. Moreover, cohesin domain at short ranges persist in mitosis (our data, **(Tanizawa et al., 2017)**) and are partially sensitive to the presence of Wpl1 (Part 7 – Fig. 4). We provide evidence that these domains depend on the presence of RNAPII (Part 6 – Fig. 3), suggesting that active transcription in mitosis shapes these domains. Removal of RNAPII makes fission yeast chromosomes more similar to vertebrate metaphase chromosomes, in which no obvious triangular domains are visible by Hi-C **(Choppakatla et al., 2021; Gibcus et al., 2018; Naumova et al., 2013)**, consistent with transcriptional downregulation in M of vertebrates **(Palozola et al., 2017)**.

Thus, fission yeast metaphase chromosomes, akin to vertebrates with condensin I and II, form cohesin loops nested by larger condensin-dependent loops. Whether cohesin and condensin engage in functional crosstalks has not been precisely assessed **(Tanizawa et al., 2017)**, and whether there would be interplay between these two SMC complexes to form mitotic domains is unclear. Evidence suggests that cohesive cohesin can antagonize the formation of cohesin loops in budding yeast **(Bastié et al., 2023)** potentially suggesting that cohesive cohesin may also antagonize condensin loops as well. Strikingly, data actually suggest that throughout mitosis very little cohesin is removed from chromatin in fission yeast **(Schmidt et al., 2009)** and only the centromere but not control arm sites lose cohesin binding upon anaphase onset after a *nda3-KM311* arrest **(Schmidt et al., 2009; Tomonaga et al., 2000)**. However, our data suggest that in fission yeast mitosis the effect of Wpl1 is limited and appears independent of condensin (Part 7 – Fig. 4), suggesting that cohesin and condensin act mostly independently from each other and consistent with condensin being the main mitotic folding activity **(Kakui et al., 2017)**. To appreciate the role of cohesin in forming mitotic domains in fission yeast, we would need to establish whether Wpl1 loss has stronger effects in interphase than in metaphase. Nonetheless, such interplays would be relevant to the early prophase stage of mitosis in vertebrates when cohesin is still present on chromosome arms and condensin II is bound. Mild defects in condensin II binding have been reported after loss of Wapl **(Gandhi et al., 2006; Shintomi and Hirano, 2011)** and increased binding of condensin to meiotic chromosomes has been reported after knockdown of Rad21 **(Choi et al., 2022)** but whether these betray : a true antagonism in loop formation, like what can be observed in loop extrusion assays between two condensin complexes competing for slack **(Kim et al., 2020)** ; competition for accessible DNA ; or simply the consequences of a change in mitotic chromosome architecture remains to be determined.

It is hard to gauge from high-resolution microscopy the outline of fission yeast mitotic chromosomes and whether they form straight rods **(Kakui et al., 2022)**. Hypercondensed rod-like fission yeast chromosomes from cryosensitive *nda3-KM311* cells (a β-tubulin mutant) can be individually visualized after a very long arrest, typically 8-12 hours at 19°C **(Hiraoka et al., 1984)**. However in classical metaphase arrests (3 hours at 30°C) using the thiamine-repressible *slp1* allele, individual mitotic chromosomes are not defined. In fact the morphological differences of chromosomes in a *slp1* arrest

versus interphase are not evident under a microscope. It is not evident whether an axis comparable to vertebrates is present in fission yeast metaphase. This raises the question of the control of condensation in fission yeast. The long duration of the *nda3* arrest may naturally lead to hypercondensation and individualization of sister chromatids. Alternatively, *nda3-KM311* cells may bypass a key upregulation of condensin whose binding increases from metaphase to anaphase (Part 5 – Fig. 1B). A physiologically relevant candidate is the presence of the mitotic spindle which has been shown to enable supercoiling in specific backgrounds **(Baxter et al., 2011)** and control condensin redistribution outside of centromeres in budding yeast **(Leonard et al., 2015)**. What is clear is that a rod shaped chromosome in metaphase seems incompatible with condensin-mediated gene clustering through very long range (over a Mb) contacts as reported by ChIA-PET and FISH **(Kyoung-Dong Kim et al., 2016a)** although it is hard to say whether this data was acquired in metaphase cells. Further studies mitotic chromosome employing microscopy may benefit from technical advancements such as expansion approaches **(Hinterndorfer et al., 2022)**.

8.2 Telomeres do not segregate like arms

For both sister chromatid arms to be segregated, cohesin is removed from arms by separase-driven cleavage **(Uhlmann et al., 1999)** or by the prophase dissolution pathway in vertebrates **(Waizenegger et al., 2000)**. Sister chromatids must also be condensed and decatenated by the combined activity of condensin and topoisomerase II so as to disentangle the two sister DNA molecules from S phase. At centromeres cohesin is protected from separase by Shugoshin until anaphase **(Kitajima et al., 2005, 2004)** where it allows bipolar microtubule attachment and dynamic reassociation of sister centromeres until cleavage **(Tanaka et al., 2000)**.

Strikingly, in a condensin mutant a large majority of centromeres can segregate towards the opposite poles of the mitotic spindle but arms and telomeres fail to properly dissociate at anaphase (Part 5 – Fig. 3A-B). More striking even, sister segregation of telomeres and arms can be uncoupled by using a topo II cryosensitive catalytically inactive mutant **(Uemura et al., 1987)** : despite chromatin bridges, telomeres dissociate (Part 5 – Fig.2E), suggesting that the segregation of sister telomeres does not depend on decatenation by topoisomerase II, but it does depend on condensin. While

condensin inactivation will impair sister arm segregation and may, as a consequence, lead to sister telomere non disjunction – our findings that 1/ there is potentially a separation of function between topo II and condensin at telomeres 2/ and that we can adjust the levels of condensin in cis at telomeres and impact either positively or negatively the disjunction of sister telomeres – suggests that condensin plays a direct role at telomeres.

We could imagine that *top2-250*, on top of chromatin bridges has, a delay in resolving entanglements which are resolved after some time. Hence the fact that the sister telomeres in top2-250 could segregate properly over increasing distances between SPBs at 19°C (Part 5 - Fig. 2E) may suggest that the steps to increase SPB-SPB distance simply take longer.

However I believe this is not the case because 1/ *top2-250* shows severe chromatin bridges in anaphase (~80%), on the same order of magnitude as cut3-477. One could expect a similar rationale for condensin mutants, but they fail to segregate sister telomeres in the duration of the experiment (and *cut3-477* induced chromatin bridges can be rescued by other mutations, suggesting some activity remains). 2/ In a similar experimental setup (Part 5 - FIG. S2C) over the course of the entire duration of anaphase there are high frequencies of lagging centromeres in *top2-250*, suggesting chromosome segregation defects despite telomeres segregating seemingly normally 3/ If it were simply a delay, we could expect a change in the behavior of sister telomere separation at shorter distances (say when we begin to see the transition from 6 to 12) which would be later resolved, but this is not what is observed (Part 5 – Fig. 2E).

Additional evidence could consist in scoring the events with separated telomeres within chromatin bridges in fixed cycling cells shifted at 19°C (example Part 5 – Fig. 2D bottom right) unfortunately we do not have that data. If these events are a majority within chromatin bridges then it must imply that topo II is not essential to separate sister telomeres. Unfortunately it is not clear whether the cut phenotype of this *top2-250* mutant is fully penetrant since **(Uemura et al., 1987)** do not provide quantifications. If the cut phenotype is fully penetrant, then it would imply sister telomeres could separate despite these severe chromosome segregation defects at mitotic exit.

Two explanations for this specific role of condensin at telomeres as opposed to topo II can be conjured : the first is that there are no catenations at telomeres, the second is that catenations at telomeres are eliminated even in the absence of topo II because the topology is only constrained from one side, towards the rest of the genome. In that scenario, sister-entanglements could be dissolved without requiring topo II. Determining whether this is the case could be tested experimentally with whole chromosome fusions. Fusing chromosomes at telomere ends leads to a maintenance of the Rabl like organization, suggesting subtelomeric/telomeric chromatin function is maintained at least prior to mitosis **(Kakui et al., 2022)**. In that context determining 1/ the binding pattern of condensin at this synthetic region, 2/ whether Taz1 and Mit1 perform similar functions as in canonical telomeres and 3/ whether topo II defects trigger non-segregation in this locus would be informative as to whether the endedness of chromosomes is important for condensin function and whether it enables sister telomeres to resolve independently of topo II.

Evidence in the literature does suggest pathways are specifically involved in the separation of sister telomeres and points to particular chromatin environments. In human cells, tankyrase-1 (TNKS1) depletion leads to a mitotic arrest and sister telomere non-disjunction **(Dynek and Smith, 2004)**. Tankyrase is a Poly-ADP ribosyltransferase (PARP) which has a conserved binding site that can serve as a platform for multiple protein binding events. When telomeres are non-disjoined in tankyrase depleted cells, knocking out TIN2/Poz1 (subunit of shelterin binding both TRF1 & TRF2 ~ Taz1) leads to TRF1 degradation and also rescues non disjunction of telomeres **(Canudas et al., 2007)**. This suggests that shelterin itself contributes to maintain the cohesion of sister telomeres but whether cohesin itself plays a role is unclear. Despite cohesin being cleaved in TNKS1 KO cells **(Dynek and Smith, 2004)** the presence of SA1 (Stromatin Antigen/STAG) is also required to cause non-disjunction of telomeres in this context **(Bisht et al., 2013; Canudas et al., 2007)**. Importantly, SA1 specifically physically interacts with shelterin (both TRF1/Taz1 and TIN2/Poz1) and overexpressing SA1 specifically is sufficient to drive telomere non-disjunction, but inactivating Rad21 has no impact on the cohesion of sister telomeres **(Bisht et al., 2013)**.

Interestingly, in human cells a physical interaction between TNKS-1 and condensin II appears to be important for proper rDNA segregation **(Daniloski et al., 2019)**. rDNA segregation in budding yeast

relies on condensin **(Sullivan et al., 2004)** but also on topo II, as it is also the case in human **(D'Ambrosio et al., 2008a; Daniloski et al., 2019)** strengthening the idea that the separation of sister telomeres is uniquely independent of topo II.

Whether a functional equivalent for this kind of pathway exists is unclear since TNKS1 is not conserved in yeast **(Citarelli et al., 2010)**. In fact, no PARPs are conserved in unicellular fungi to my knowledge. Cohesin subunit SA1/SA2 variants are not present either. Whether cohesin and shelterin physically interact in fission yeast (by testing physical interactions via both Taz1 and Poz1 ; and whether *taz1Δ* affects cohesin levels at telomeres) are interesting avenues of explorations. Since data in mammalian cells suggest that cohesin itself is not important for sister telomere disjunction **(Bisht et al., 2013; Canudas et al., 2007)** but SA1 is, a physical interaction in yeast between cohesin and shelterin might not be the mechanism responsible for sister-telomere cohesion. On the other hand, evidence in budding yeast does suggest that cleavage by TEV of Scc1/Rad21 is sufficient to segregate telomeres, or at least a locus 30kb upstream **(Sullivan et al., 2004)** suggesting cohesin might take part in sister-telomere cohesion in fungi and failure to dissolve this link might explain non-disjunction. Shelterin is poorly conserved between budding yeast and fission yeast which brings into question whether cohesin would physically interact with shelterin at all in eukaryotes. On the other hand, depletion of cohesin does rescue telomere segregation defects in condensin deficient backgrounds in budding yeast **(Renshaw et al., 2010)** consistent with our data (Part 5 – Fig. 6A).

8.3 Condensin driving telomere segregation

At this stage the exact mechanism to explain sister telomere segregation by condensin is unknown. Resolving sister telomere entanglements appears as a long process relative to the duration of anaphase in wild-type **(Chu et al., 2022)**. It is difficult to imagine how diffusion capture by condensin may facilitate the segregation of sister telomeres, as it might even impinge on resolution by maintaining cohered sister telomeres. On the other hand, average loop sizes on chromosome arms is 80 kb in size in chicken **(Gibcus et al., 2018)**, HeLa cells **(Naumova et al., 2013; Wang et al., 2022)** in our own data in fission yeast (example Part 6 – Fig. 3), and can range from anywhere to 100kb to 1Mb in Xenopus **(Choppakatla et al., 2021).** If now we compare these average loop sizes with average telomere length from different species, which can range from 5 to ~100kb

(Whittemore et al., 2019) and as low as 300-400bp in both budding and fission yeast, the telomere is unlikely to be folded as a loop (at least of average size) in M phase. What we know is that in both scenarios, entanglements following deficiency of condensin are partially rescued by impairing the function of cohesin or worsened by impairing the function of TRF1/Taz1.

Condensin undergoing ATP hydrolysis, may promote the power stroke necessary to resolve the entanglements between sister telomeres. An alternative model is that condensin deficiency leads to a defect at telomeres outside of M, such as DNA damage **(Kakui et al., 2020)** which leads to entanglement. Shortening of telomeres during pre-replicative senescence is correlated with increased telomere cohesion **(Azarm et al., 2020; Yalon et al., 2004)** although penetrant telomere shortening cannot be the cause of the entanglement in condensin mutants (Part 5 – Fig. 2C). Furthermore, inhibiting Aurora B kinase in mitosis, which controls condensin in fission yeast, is sufficient to impair telomere disjunction. These defects are rescued by the phosphomimetic Cnd2-3E mutant **(Reyes et al., 2015)** consistent with a mitotic function of condensin at telomeres. Investigating the possibility of such a mitotic-specific function will require a conditional allele to inactivate condensin just before mitotic entry or anaphase onset to properly assess a direct contribution to the disjunction of telomeres.

The data presented in Fig. D1 is not fully explanatory, however they strengthen the idea that condensin deficiency increase cohesin association with subtelomeres in G2 and the following anaphase (Part 5 - Fig. 6B) and – speculatively - at the telomeres in anaphase. Perhaps direct inhibition by a designed peptide may provide a way to kill condensin activity at specific times of the cell cycle **(Elias et al., 2023)**. We have shown that impairing cohesin function by a *rad21-K1* allele can rescue the telomere separation defects of *cut3-477* cells (Part 5 – Fig. 6A). This is consistent with an increase in cohesin association at telomeres being causal to the non-disjunction defects. Whether loop extruding or cohesive cohesin **(Nagasaka et al., 2023)** at telomeres is responsible for this defect remains unaddressed and could be interesting to address with a ChIP approach using antibodies recognizing the acetylated form of cohesin. One could establish a ratio of cohesin Ac/total cohesin at telomeres, subtelomeres and control arm sites in wild-type and condensin deficient backgrounds. Alternatively, one may inactivate Mis4/SCC2/NIPBL just after S-phase to eliminate loop-forming cohesin and retain

only cohesive cohesin **(Feytout et al., 2011)**. Such an approach suggests cohesive cohesin is enriched close to telomeres **(Feytout et al., 2011)**.

A final point is that our ChIP experiments in anaphase in condensin deficient backgrounds generate increases of cohesin binding at subtelomeres, yet, the reason why these cohesin complexes would not be cleaved by separase is puzzling. Condensin defects may lead to issues in the timing of cohesin cleavage, or at least that this specific pool of cohesin appearing after condensin inactivation is subjected to misregulated cleavage. Alternatively, these sites show abnormal recovery of cohesin after anaphase onset.

8.4 Roadblocks in loop extrusion assays are poor models for *in vivo* chromatin

Loop extrusion assays **(Ganji et al., 2018)** have provided strong in vitro demonstration of the ability of SMC complexes to processively enlarge loops in an ATP-dependent manner. They have also provided key investigations on the nature of an obstacle to SMC translocation. The relevance of this problem is two-fold, and at the center of our understanding of SMC function. First, it will allow us to understand how SMC complexes perform their function in crowded nuclei, and what other activities in cells might take part in this process – of course, with potential biomedical implications, or implications on the interplay between SMC activity and chromatin during evolution. Second, it can give us key insight into how the SMC complex, which is structurally challenging to apprehend, performs conformational changes that enable its molecular activities.

Loop extrusion assays determine response to roadblock size by using DNA-bound factors at low density on a 50kb λDNA molecule. There are two main limitations to this approach. The first is the low density of the obstacles assessed *in vitro*. Taking telomeres as an examples, the repetitive DNA sequence, shelterin binding, presence of a T-loop, and cohesion between sisters in anaphase provide a clearly distinct environment from a linear, tethered dsDNA molecule for condensin to perform loop extrusion. *In vivo* evidence suggest that highly dense obstacles clearly cause local impairments in condensin activity. LacI (~2nm size) bound to its LacO site x200 is sufficient to induce condensin mediated breakages in dicentric chromosomes **(Guérin et al., 2019)**. Interestingly, internal

telomeres of physiological length in budding yeast dicentric chromosomes also cause similar phenotypes **(Guérin et al., 2019)**.

The second is that *in vivo* obstacles to condensin loop extrusion can be dynamic and translocating themselves, and under current conditions loop extrusion assays do not allow simultaneous loop extrusion and, say, transcription by RNAPII **(Davidson et al., 2019, 2016)**. Indeed, translocating RNAPII could be an obstacle to condensin – after all processive complexes can push topologically entrapped cohesin in translocation assays **(Stigler et al., 2016)**. While it seems individual condensin complexes can bypass one another **(Kim et al., 2020)**, other motor activities like polymerases use a processive bp per bp mechanism for motion. These might disturb condensin loop formation in a way that other condensin complexes using a non-topological mechanism **(Pradhan et al., 2022b, 2022a)** with large step sizes **(Ryu et al., 2021b)** do not.

In vitro condensin loop formation is known to stall at low tension forces on naked DNA **(Ganji et al., 2018)**. In similar conditions loading condensin on DNA with more slack is sufficient to see loop formation **(Kong et al., 2020)**. Finally, stalling/blocking at obstacles is more frequent when the end to end length is long (more tension) **(Davidson et al., 2023)** which lends credence to this hypothesis.

To summarize, whether a higher order structure impairing the function of condensin, a specific mechanical property of the fiber such as stiffness, or the accessibility to DNA, perhaps linker DNA, are the key parameters for condensin to function in vivo remain unclear – and key questions to attempt to answer in the future.

8.5 Testing the semi-permeable barrier model genome wide applied to condensin and transcription

Condensin is found enriched in the vicinity of highly transcribed genes **(Kim et al., 2013; Kranz et al., 2013; Sutani et al., 2015)**. Particularly in yeast, condensin is enriched at the 3' end of genes. Despite this co-localization of RNAPII and condensin, reducing transcription facilitates condensin

function in condensin mutant backgrounds as shown previously **(Sutani et al., 2015)** and in our work (Part 6 – Fig. 6B).

We show that the loss of RNAPII leads to a loss of condensin at highly RNAPII-bound genes (Part 6 - Fig. 1A-B) and conversely that Dhp1 depletion leads to an increase of condensin binding at the 3' end of genes (Part 6 - Fig. 1E-H). Finally both of these conditional depletions suggest that in metaphase RNAPII antagonizes the formation of long range contacts. Taken together our data suggest that the peaks of condensin at transcribed genes in fission yeast are not loci of high condensin activity - consistent with previously published results suggesting they are not loci of greater chromatin folding **(Kakui et al., 2017)** - but an accumulation with a negative role in condensin function.

Our data is perfectly consistent with a scenario where SMC high binding peaks represent a local stalling of condensin translocation along DNA, as shown for bacterial SMC **(Brandão et al., 2019; Tran et al., 2017).** Consequently, SMC-dependent juxtaposition of chromosomes is sensitive to the presence of transcriptional units and their orientation **(Tran et al., 2017; Wang et al., 2017)**.

A model where head-on collisions with RNA polymerase stall the translocation of SMC complexes holds strong explanatory power to explain existing data in human, bacteria and yeast, and our work expands this observation to condensin using genome-wide approaches. Of note, fission yeast here appears as a powerful experimental system where the impact of mitotic, transcribing RNA polymerase on condensin can be investigated. Human cells, with downregulation of RNA polymerase in mitosis **(Palozola et al., 2017)** and a different pattern of condensin binding **(Sutani et al., 2015)** (5' vs gene body and 3' end binding) does not properly highlight this evolutionary conserved attribute of condensin especially since evidence shows that RNAPII is cleared from vertebrate mitotic chromatin in early prophase by a wave of transcriptional elongation **(K. Liang et al., 2015)**.

While we show evidence suggesting that RNAPII is a barrier to condensin we have not described whether RNA pol I and III have similar impacts on SMC/condensin function genome-wide.

Levels of condensin binding seem to be anti-correlated with RNA pol I transcription in budding yeast (at least in a background where the condensin positioning factor *fob1* is missing) at the rDNA **(Ide et al., 2010; Wang et al., 2006)**. RNA pol I transcription is downregulated in anaphase by Cdc14 and

this is required for the proper segregation of the rDNA **(Clemente-Blanco et al., 2009; Iacovella et al., 2015).** Cdc14 phosphatase triggers a condensin activity in anaphase that appears independent of the condensation/compaction of the rDNA locus (and is linked to decatenation by topo II) to segregate sister rDNA repeats **(Sullivan et al., 2004)**.

Evidence in the literature appears contradictory regarding the interplay between RNAPIII and condensin. In budding yeast, condensin appears enriched at RNAPIII transcribed genes but its association is reported (not shown) to be independent of transcription by RNAPIII **(D'Ambrosio et al., 2008b)**. A minimal B-box inserted elsewhere on the genome is sufficient to induce TFIIIC, an RNAPIII initiation factor, and condensin binding **(D'Ambrosio et al., 2008b)**. Removal of a TFIIIC binding sequence induces an increase of neighboring condensin peaks **(D'Ambrosio et al., 2008b)** consistent with a barrier stalling the translocation of the complex. On the other hand, physical interactions were reported between condensin and TFIIIC **(Haeusler et al., 2008; Yuen et al., 2017)** and deficiency in TFIIIC leads to a reduction of condensin association to chromosomes **(D'Ambrosio et al., 2008b)** more consistent with the role of a loader. TFIIIC is also shown to colocalize with condensin II at non transcribed binding sites in mouse **(Yuen et al., 2017)** suggesting it can position condensin independently of RNAPIII but whether it does so by being an obstacle or a loader is not known. In our hands, enrichment of condensin at tDNA is difficult to detect by ChIP-qPCR in fission yeast mitosis **(Rivosecchi, 2019)**, despite peaks visible in ChIPseq (Part 6 – Fig. 1D). However, accumulation of RNAPIII with defective termination in a *sen1Δ* background leads to an accumulation of condensin which can be abolished by forcing termination with a super-terminator sequence **(Rivosecchi et al., 2021)**. As the hosting lab had previousy proposed, condensin may be loaded at the promoter **(Robellet et al., 2017).** This points to a conundrum where loading at promoters occurs for condensin but its translocation is hindered by active RNA polymerases (at least for RNAPII and RNAPIII when the size of the RNAPIII domain is enlarged), and in a wild-type scenario RNAPIII genes are poor barriers because they are small.

All three polymerases are the product of evolutionary divergence, particularly concerning the paralogs of their largest subunits (in fission yeast, in order of I to III : Nuc1, Rpb1, Rpc1) and in terms of the factors required for transcription initation **(Girbig et al., 2022)**. I have been unsuccessful in

attempting to tag Rpb5 with a 3xsAID cassette, a common subunit of the three polymerases, or both of the large subunits of Nuc1 and Rpc1, suggesting obtaining degrons to investigate the full breadth of RNA polymerases remains challenging. Producing the degron tagged strain of Rpb1 worked possibly because its CTD which carries the AID tag consists of heptad repeats that facilitate the recruitment of other RNAPII specific factors **(Girbig et al., 2022)** and is not found in the other polymerases. A hypomorphic loss of function of this structural unit might not have impacted RNA pol II activity sufficiently to prevent tagging. Answering this question could be attempted with drugs targeting these RNA polymerases such as phenantroline which should inhibit all three but with potential indirect effects **(Zencir et al., 2022)** and with effects on condensin binding we do not observe compared to Rpb1 depletion, for instance at centromeres (Part 6 – Fig. S1F vs **(Sutani et al., 2015)**). In our hands, fission yeast is resistant to the inhibitor ML-60218 which inhibits RNAPIII **(D'Ambrosio et al., 2008a)**.

Regardless, our data suggest that while transcription occurs in fission yeast mitosis and antagonizes condensin's function, it is present at levels which support assembly of mitotic chromosomes and sister chromatid segregation in anaphase. It would be interesting to explore whether species with transcription in mitosis undergo selective pressure to avoid clusters of highly transcribed genes, akin to those that can be generated upon Dhp1 depletion. In mammals, defects in transcription termination can lead to chromosome segregation defects **(Jiang et al., 2004)**, suggesting human cells may be under similar constraints despite transcriptional downregulation.

A powerful additional experimental verification that could substantiate our data would be to address the impacts of Rpb1 and Dhp1 depletion on the kinetics of condensation using two fluorescently tagged loci (on the same chromosome arm) after release from a G2/M arrest. If RNAPII are barriersto functional, translocating condensin then we expect an acceleration and a slowing down of the distance between two loci in Rpb1 OFF and Dhp1 OFF respectively. If there is no difference then the phenotypes observed in Hi-C are somehow implicated in the maintenance of the mitotic chromosome structure and not its establishment. The caveat with these experimental systems are that fluorescently tagged loci with LacO /TetO repeats can constitute barriers for condensin **(Guérin et al., 2019)**

themselves. Such questions might be better answered with FISH approaches **(K.-D. Kim et al., 2016)**.

Another strong experimental assessment of our results would be to determine a way to either reactivate transcription in metaphase-arrested vertebrate cells, and ask the consequences on chromosome condensation and condensin I/II position. While some genes are activated during M in mammalian cells, a large number are downregulated **(Palozola et al., 2017).** This would allow us to test directly the hypothesis we evoke at the end of the paper – that downregulation of transcription benefits the fitness of vertebrates with larger genomes by facilitating condensin function. Employing a minimal system in Xenopus **(Shintomi et al., 2015)** or an egg extract capable of transcription **(Barrows and Long, 2019)** would also provide excellent assessment of this model. Alternatively, inducing transcription of a reporter gene in fission yeast using an expression system **(Garg, 2020)** just prior to M entry or during M phase and assessing the consequences on condensin binding and chromosome folding would provide parallel evidence.

Finally, a third experimental system to investigate condensin activity in the context of transcription could be meiosis. In prophase of meiosis I, chromosomes form synaptolemal complexes (SC) to attach homologous chromosomes and enable recombination. Chromosomes condense up to pachytene stage and then the SCs are disassembled, accompanied by a decondensation. Chromosomes are then recondensed at the end of prophase concurrently with the disassembly of the synaptolemal complex **(Zickler and Kleckner, 1999)**. Coincidentally these prophase I steps occur with a significant burst in the elongating form of RNAPII at the pachytene/diplotene stage **(Alexander et al., 2023)**. Whether this corresponds precisely to the timing of decondensation observed in images **(Zickler and Kleckner, 1999)** is unclear. Nonetheless, it is tempting to speculate that the decondensation is partially caused by this increase in transcription and, whether a similar scenario exists in somatic mitosis **(K. Liang et al., 2015; Z. Liang et al., 2015)** are interesting questions. Additionally, assuming nucleosomes are an obstacle to condensin (discussed further below), it is tempting to speculate that this brief transcriptional wave may prime chromatin for further binding of condensin during the late stages of prophase I.

8.6 *In vivo* RNAPII barriers suggest condensin loop extrudes in fission yeast

As mentioned in the Introduction several lines of evidence are consistent with a loop extrusion hypothesis, such as the resolution of entanglements, the effect observed when SMC residence time is increased, processive features such as stripes or the in vitro observation of loop extrusion which constitutes strong evidence. Additionally, I would argue the existing evidence of obstacles to translocation, both in vitro and in vivo, with consequences on Hi-C maps, constitute strong evidence for this model.

If condensin were to follow a diffusion capture model it would need both to capture long range sites in trans but also to translocate and respond to obstacles. An additional difficulty would be to determine by biophysical considerations what parameters should establish the frequency and distance of contact between two sites. In the most recent version of this model **(Gerguri et al., 2021)** this is inferred based on estimations of densities of condensin and distances between peaks. Some modelling approaches with fit from bacterial data have argued that loop extruding factors subjected to multivalent interactions cannot explain complex Hi-C patterns **(Brandão et al., 2021)**. Loop extrusion and diffusion capture should be reinvestigated thoroughly by a proper combination of modelling and experiments.

We argue that loop extrusion is the most parsimonious mechanism explaining the response of condensin to RNAPII barriers in fission yeast metaphase, which we uncover by depleting Rpb1 to remove them and Dhp1 to reinforce them (Part 6 – Fig. 1,3). Our observations are consistent with stalling of the translocating SMC complex at RNA pol II enriched sites and the increased (resp. decreased) long range contacts when Rpb1 (resp. Dhp1) is depleted. Since change in Hi-C contacts are expressed as a frequency of the total interactions it is not possible to strictly determine whether a gain in long range contact is caused by a true loss of short range contacts or, the other way around, whether a true gain in long range contacts causes a loss of short range contacts. However our functional data, effects at condensin peaks, and the fact that the fraction of chromatin bound condensin remains the same in Rpb1-OFF are consistent with semi-permissive barriers to translocation. This is also consistent with Hi-C data suggesting that condensin high binding sites do not determine loci of significantly higher contact frequencies **(Kakui et al., 2017)**. On the other

hand, models of diffusion capture **(Gerguri et al., 2021)** cannot explain why abolishing peaks of high condensin occupancy rescues chromosome segregation defects in anaphase while generating larger peaks worsens the *cut3-477* induced phenotype. While the complementary approach using fkh2 null mutants, with negative interaction between cut3 and fkh2, is consistent with a reduction in transcription of actively upregulated genes in M and a subsequent rescue phenotype, the scope of this result remains limited. We have not checked the penetrance on chromatin bridges, nor do we know the behaviour of these mutants regarding the binding of condensin to chromatin in cis or even altered expression of upstream regulators of condensin.

One main weakness of diffusion capture is that in theory if condensin were to grab DNA in trans it could also establish contacts between sister chromatids and therefore impair individualization of metaphase chromosomes. In that case, one would need to imagine that these trans-contacts would be disfavored in some fashion in mitosis either by a dedicated mechanism or by diffusion capture being minor relative to a coexisting loop extrusion activity. Perhaps in the vein of what is implied in certain model drawings **(Shintomi and Hirano, 2021 - see Fig. 6),** diffusion capture is a late event enabling crosslinking between linearly distant regions after loop extrusion has occurred. On that same point, it is difficult to imagine how condensin, if it were a simple loop extruder as visualized in schemes, that is stalled by very low tension **(Ganji et al., 2018; Golfier et al., 2020)**, could contribute to the stiffness of mitotic chromosomes **(Renshaw et al., 2010; Sun et al., 2018)** without providing some form of crosslinking, whatever the mechanism involved.

Our data do not rule out the existence of diffusion capture for several reasons, listed approximatively with increasing strength. First, a loop extrusion-only mitotic scenario, if spacing of condensin are similar, would lead to the same effective loop size independently of the chromosome arm. However, this is not the case between species or within the same species as longer arms tend to be wider by microscopy **(Kakui et al., 2022)**. Second, in a loop extrusion only mechanism, very long range condensin stripes seen by ChIA-PET **(Kyoung-Dong Kim et al., 2016b)** or large domains existing in our data, would imply a single complex is responsible for the processive extrusion of a large loop on a mitotic chromosome arm at the scale of a Mb or beyond which is conceptually hard to understand especially in the context of chromatin and for a fission yeast chromosome which is at most 5Mb long.

Third, convincing evidence in Xenopus egg extracts points towards a separation of function, likely involving condensin-condensin interactions, that would participate in the assembly of the axis in competition with loop extrusion **(Kinoshita et al., 2022, 2015)**. Such a physical interaction could provide a mechanism to bridge distal sites similar to a diffusion capture mechanism **(Gerguri et al., 2021)** or to aid in formation of a Z-loop **(Kim et al., 2020)**. Fourth, provided we assume the CAP-G subunit drives loop-extrusion **(Kinoshita et al., 2022)** as the anchor chamber **(Shaltiel et al., 2022)** - which is not necessarily the case in all species or depends on salt conditions – it is hard to imagine how CAP-G less condensin I and condensin II can associate to chromatin, form axes and individualize metaphase chromosomes **(Kinoshita et al., 2015; Yoshida et al., 2022**) or how CAP-G2 is dispensable for condensin II function in certain species **(Hoencamp et al., 2021)** if loop extrusion is the only mechanism. Whether the assembly of an axis can be relevant for all mitotic scenarios is unclear but these last two arguments hold for vertebrates.

Our data also cannot rule out diffusion capture by condensin in specific contexts. For instance, condensin presumably in interphase is important for the clustering of tRNA genes in budding yeast **(Haeusler et al., 2008)**.

One prediction of the multimerization of condensin complexes is that condensin association to chromatin should be synergistic with itself if clusters are formed by condensin-condensin interactions, akin to what is observed for cohesin **(Ryu et al., 2021a)**. Hence, association of condensin to chromatin should follow some kind of exponent with increasing input of condensin I concentrations (vs a random control protein forming no clusters) and this behavior should be abolished or reduced in a KG-loop mutant or W-loop/KG-loop double mutant **(Kinoshita et al., 2022)**. Furthermore, one may determine if this synergistic association to chromatin is enhanced when the balance of functions is favored towards the activity of CAP-D2 at the expense of CAP-G as proposed for the formation of an axis **(Kinoshita et al., 2015)**. Unfortunately this was not attempted by the Hirano lab when they altered the ratios of condensin I/II **(Shintomi and Hirano, 2011)** but should be testable in Xenopus egg extracts.

8.7 Roadblocks and asymmetry of condensin loop extrusion

On the basis of *in vitro* loop extrusion assays it has been argued that single obstacles, irrespective of their size, do not prevent translocation of the complex on DNA, suggesting a non-topological mechanism for loop formation **(Pradhan et al., 2022b, 2022a)**.

However the data also show that for budding yeast condensin purified from cycling cells, the frequency of blockage when encountering a nanoparticle increases as a function of the size of the molecule but plateaus at ~50% blocking events. This may be specific to condensin as human cohesin shows similar frequencies of 40-50% blocking independently of the roadblock size **(Pradhan et al., 2022a)** which has been argued to be possibly blocking due to the random orientation of the cas9 construct **(H. Zhang et al., 2023)**. If that hypothesis is correct, the frequency of incorporation of large, 200nm gold particles with dcas9 constructs should be close to 100% for cohesin if oriented properly. This brings into question why condensin loop formation is partially responsive to single roadblock size. Some yet-unknown feature of the yeast condensin structure might be intrinsically sensitive to roadblocks during loop formation, contrary to cohesin, or some yet undescribed mitotic PTM of condensin is required to phenocopy the properties of cohesin loop extrusion.

If an SMC complex with the ability to form loops in both directions were to stall/block at an obstacle, it would still be able to extrude in the other direction. Cohesin is bidirectional in vitro when extruding a loop **(Davidson et al., 2019)** but condensin is biased towards asymmetrical loop expansion **(Ganji et al., 2018; Golfier et al., 2020)**. A pool of fully symmetric loop extruders, or a mixture of stable symmetric and asymmetric loop extruders must be used to reproduce experimental data **(Banigan and Mirny, 2020)**. These theoretical considerations applied to a context where roadblocks are absent. Adding roadblocks to such a model should make a chromosome with only asymmetric loop extrusion even more inefficient in linear compaction for the same loading and residence times. In the context of a chromatinized substrate, the requirement for a symmetrical loop extrusion might be heightened. The shape of fission yeast mitotic domains from our high condensin sites (Part 6 – Fig. 4B) is consistent with modelling approaches forming TADs symmetrically **(Banigan and Mirny, 2020)**. There is no evidence from roadblock assay that loop-forming condensins see an increased

frequency in reversal upon encounter with an obstacle **(Kong et al., 2020; Pradhan et al., 2022a)** but there is evidence for this model in the case of cohesin and CTCF **(Davidson et al., 2023)**.

A multimer of condensin complexes could provide a partial explanation for the symmetrical loop formation observed for condensin I **(Kong et al., 2020)**, but it cannot explain the 50% of symmetrical events observed for single complexes of condensin I & II. Either the extrusion assay used (U shape vs linear, salt concentrations…), or the intrinsic functioning of the complex could explain the difference in bias of loop extrusion direction between yeast and human. In physiologically relevant cell-free egg extracts (with large depletion of histones), loop formation by condensin is mainly asymmetrical **(Golfier et al., 2020)** suggesting that either a relevant mitotic PTM of condensin in yeast enables symmetrical compaction, or a chromatin bound-activity provides this symmetry.

One mechanism which could provide symmetrical loop formation is the encounter of two condensin complexes and the formation of Z-loops with a condensin dimer at the base **(Kim et al., 2020)**. This was tested recently in simulations proposing that asymmetric loop extrusion could reproduce linear compaction if Z-loops and nested loops could form **(Dey et al., 2023)**. Alternatively, condensin-condensin interactions may more simply provide this property to extruding condensin **(Kinoshita et al., 2022)**.

It would be interesting to use a bidirectional condensin mutant **(Shaltiel et al., 2022)** and determine whether the response to roadblock size of condensin **(Pradhan et al., 2022a)** remains in loop extrusion assays. Furthermore, whether this mutant could produce stronger mitotic domains and longer-range contacts if extended to an in vivo system, and whether the gain in condensation/long-range contact formation is less dependent on the presence of chromatin bound roadblocks (say, Rpb1 depletion or histone density) would be interesting problems to tackle. Technically this is challenging because the ΔCAP-G condensin complex leading to symmetrical loop extrusion with *Chaetomnium thermophilum* subunits **(Shaltiel et al., 2022)** prevents loop extrusion with vertebrate subunits **(Kinoshita et al., 2022)** and renders condensin highly salt sensitive in yeast **(Martínez-García et al., 2022)**. One may attempt to use *Chaetomnium thermophilum* with conditional depletion of Ycg1/CAP-G and look at the distribution of condensin and chromatin folding by 3C in the presence of

transcriptional inhibition (or not). Alternatively, one may attempt to immunodeplete condensin from Xenopus egg extracts and add-back reconstituted ΔYcg1 or wild-type *Chaetomnium thermophilum* complexes.

8.8 Transcription independent positioning of condensin

Before engaging in a salt-resistant association to DNA, condensin associates electrostatically to DNA and must engage some loading reaction before proceeding to enlarge loops in an ATP-driven manner **(Eeftens et al., 2017)**. The details of such an initial loading reaction are unclear, and whether the initial loading reaction involves the safety-belt is not known.

The density of genes in fission yeast makes transcription likely a major positioning device for condensin peaks in ChIP-seq data. Thus, the experimental depletion of Rpb1 provides the opportunity of characterizing novel regions driving condensin peaks, either as stalling barriers or, akin to the scenario at telomeres, as peaks of enrichment with positive function. Furthermore, if transcription were to be a major barrier of condensin, it is tempting to speculate that an environment without transcription would be amenable to reveal preferential loading sites of condensin, which are otherwise masked by active RNAPII. Additionally, one might expect, if condensin were loop extruding on chromatin, to capture by ChIP-seq DNA fragments at both the anchored safety-belt and the mobile loop extruding chamber I **(Shaltiel et al., 2022)** and that the safety-belt bound DNA fragment should be in theory overrepresented in ChIP-seq data. However this remains technically challenging to determine. Condensin I is estimated to have a residence time of up to 5mn on chromatin in human cells **(Gerlich et al., 2006a)** and is potentially shorter in yeast **(Robellet et al., 2015; Thadani et al., 2018)**. In our experimental system, removal of a protein by degron such as Rpb1 or Spt16 occurs over multiples of this type of half-life, which implies condensin would unload and reload several times and potentially reach a new distribution by the combination of its new processivity and external positioning and displacing activities. In this context identifying both safety belt-enriched sites and initial loading sites remains extremely challenging. Moreover, condensin in vivo could be subject to events of anchor slippage **(Shaltiel et al., 2022)** even in Rpb1-depleted conditions which would make identification of loading-sites even more challenging.

Releasing cells synchronized in late G2 into M at cold temperatures in control (and potentially Rpb1-depleted conditions) may allow identification of early loading sites of SMC complexes as was previously done **(Lengronne et al., 2004)** but our preliminary attempts at this stage have not yielded anything other than a linear increase over a short time course in cells released from a G2/M block at candidate genes (not shown). To properly capture initial loading events in vivo one would need a release from a G2/M block with a fixation method for ChIP fast enough relative to the initial loading and ATPase cycle of the condensin complex, to capture binding events **(Poorey et al., 2013)**, which for now remains technically difficult.

Despite these caveats, from our ChIP-seq data (Part 6 – Fig. 1A) we can identify peaks which resist RNAPII depletion in metaphase and might constitute functionally relevant loci of condensin enrichment. While these peaks may be a *trompe-l'oeil* the fact that they are close to the centromeres, repeated in all three chromosomes and evoke a symmetric structure suggests there may be a potentially biologically relevant explanation for these loci of enrichment. Condensin is enriched on a region spanning 40kb away from the centromere in budding yeast **(D'Ambrosio et al., 2008b)** but in *S. pombe*, the heterochromatin region flanking the central domain for kinetochore assembly appears poor in condensin. By design the clustering approach identified these sites from the signal at TSS, and these peaks appear positioned at a NDR region (Fig. D3D). While remaining signal in clusters 1 and 2 could be explained by traces of RNAPII following depletion, these peaks cannot reflect incomplete depletion because they are not overlapping with Rpb1 ChIP peaks (see example in Fig. D3C). They therefore reflect high binding of condensin at a NDR of protein coding TSS genes flanking the centromere. Whether they represent sites of stalling by a chromatin bound factor such as a transcription factor is unclear but unlikely, since transcription factors would be present at low density at a promoter, and should not prevent loop extrusion **(Pradhan et al., 2022a)**. Whether they are unknown sites of condensin accumulation (negative) or sites representing positive functional binding of condensin is unclear and will be explored by future work, and whether similar promoters can be identified in cluster 2 as well. Remarkably, similar peaks were observed by the Marston lab when describing the association of cohesin flanking centromeres, although in their case the binding was at convergent genes **(Paldi et al., 2020)**. In their work, they propose that cohesin association at this

convergent region plays a role in kinetochore biorientation. Whether condensin would provide a similar function here remains to be investigated.

8.9 Nucleosomes and the density of factors on DNA during the enzymatic cycle of condensin *in vivo*

Our data on the impact of RNAPII on condensin-mediated loops, suggest that despite a single, non-transcribing RNAPII is readily incorporated into a loop by condensin in vitro **(Pradhan et al., 2022a)** a densely bound region of RNAPII can stall condensin and prevent its ability to translocate. With similar data showing hindrance of condensin by dense LacI or Rap1 bound regions **(Guérin et al., 2019)** it becomes tempting to argue that the density of DNA-bound factors is a key parameter determining whether DNA-bound factors are obstacles to condensin loop formation.

Half of the weight of a chromosome is estimated to be composed of nucleosomes, which are among the most densely DNA-bound protein complexes. As such, nucleosomes have been an immediate candidate for experiments using in-vitro loop extrusion assays. Low-density isolated nucleosomes have been shown to enhance the processivity of loop forming condensin II by 1.5 fold in vitro **(Kong et al., 2020)**. Models for cohesin diffusion have also suggested that nucleosomes can facilitate loop formation. However this is true only when the average linker length reaches the average size of a nucleosomal array or smaller **(Maji et al., 2020)** and would not apply in these condensin loop formation assays with ~4 nucleosomes on 50kb of DNA **(Kong et al., 2020)**.

Multiple studies have shown that single nucleosomes are unable to prevent both SMC translocation and incorporation into loops **(Davidson et al., 2016; Kim et al., 2019; Kong et al., 2020; Pradhan et al., 2022a; Stigler et al., 2016)**. Note that the data also show these isolated nucleosomes reliably across studies induce weak stalling of the SMC complex on the order of 10%. This stalling has been proposed to slow ATP-independent cohesin diffusion on, nucleosome-packed chromatin in vivo, and experimental evidence demonstrates that DNA with 10-50 nucleosomes is not a good substrate for this cohesin diffusion, although whether this is due to a higher order structure is not clear **(Stigler et al., 2016)**. Low frequency stalling events at obstacles happen on timescales which are much larger than individual condensin steps (seconds vs 20ms or less) **(Ryu et al.,**

2021b). Whether the obstacle somehow temporarily impairs the binding of ATPase heads or whether the complex still performs hydrolysis but is unable to incorporate the roadblock into the loop is not clear.

8.10 Shelterin components hint at the negative impact of nucleosomes on condensin function

Evidence in budding yeast demonstrates that in a dicentric chromosome, internal telomeric or repeated Rap1 binding sites are hotspots of breakage, a process likely driven by condensin dependent DNA cutting by the cytokinetic ring. Spacing Rap1 repeats by ~35bp is sufficient to prevent breakage at these Rap1-bound insertions **(Guérin et al., 2019)** likely because translocation of condensin, and/or proper decatenation at this regions is prevented by the lack of available linker DNA. Coincidentally 35bp linkers are sufficient to enable condensin binding **(Kong et al., 2020)** on nucleosomal DNA. Whether this length is the minimal required length is not clear. In our work we do not observe visible changes in condensin association to telomeres in a *rap1Δ* background with the caveat that shelterin structure of mammals and fission yeast is not well conserved in budding yeast **(Armstrong and Tomita, 2017)**. Alternatively, we have suggested that arrays of Taz1 bound to repeated motifs at telomeres constitute a barrier where condensin accumulate. However, since Taz1 is limiting for sister-telomere disjunction when condensin is mutated, Taz1 acts as a positive barrier.

The absence of Mit1 leads to a local increase of condensin at subtelomeric & telomeric loci on the right arm of chromosome II (Part 5 – Fig. 4E, S4E). However, loss of Mit1 leads to mild increases in transcription at telomeres **(Creamer et al., 2014)** which could explain increased condensin binding seen by ChIP at telomeres consistent with our data (Part 5 – Fig. 1), although whether this would be telomere specific is unclear. Since telomere non-disjunction is rescued in *mit1Δ cut3-477* we interpreted the increase in association in *mit1Δ* as reflecting a positive binding of condensin leading to enhanced function, and resolution of sister chromatids, but we did not measure levels of condensin association at telomeres in the double mutant *mit1Δ cut3-477*. Note however, that telomeric condensin appears at least insensitive to Rpb1 depletion (Fig. D3A) suggesting RNAPII does not position condensin in cis at telomeres.

In theory, the chromatin remodeling activity of Mit1 at subtelomeres could counter the nucleosome-destabilizing activity of AT-rich tracts, and this was confirmed experimentally at least at the mating-type locus but not at TEL2R **(Creamer et al., 2014)**. The fact that condensin preferentially binds at AT-rich regions in vitro **(Terakawa et al., 2017)** also supports the idea that condensin association at telomeres might reflect an enrichment with a positive function supporting sister telomere disjunction, rather than a stalling as we propose for RNAPII (Part 6). Additionally, we show that conditional depletion of Spt16 leads to a large, global histone loss but does not increase condensin association (Part 7 – Fig. 5-6) despite strongly rescuing chromatin bridges (Part 7 - Fig. 7A-B). This might suggest that the telomeric context is particular in regards to condensin association and/or activity. In that context, employing histone copy number mutants (Part 7 – Fig. 8A-B) may allow us to answer whether the binding of condensin is correlated negatively with histone density at telomeres. Additionally, one could delete subtelomeric sequences **(Tashiro et al., 2017)** and ask whether *cut3-477* induced non-disjunction of sister-telomeres can still be rescued by loss of Mit1, to determine whether the phenotypes can be explained by a cis mechanism from the neighboring subtelomere region or by the direct presence of Mit1 at telomeres.

EM analysis of reconstituted telomeric chromatin suggests telomeric repeats are heterogeneously packed by nucleosomes but also form highly compacted columnar structures with short NRL **(Soman et al., 2022)** which might antagonize binding of the condensin complex through steric hindrance **(Kschonsak et al., 2017)**. This columnar structure interestingly shows alignment of DNA minor/major grooves perpendicularly to the direction of nucleosome wrapping and full accessibility of the DNA helix, potentially making it susceptible to remodeling and/or a hub for capping by TRF1 (functional equivalent of Taz1) **(Soman et al., 2022)**. Strikingly, a recent publication shows that TRF1/Taz1 changes the angle of DNA at entry/exit sites via Myb domains **(Hu et al., 2023)** and thus may enable the access of condensin to linker DNA within this columnar structure.

8.11 Nucleosomes and transcription-associated chromatin remodeling interplay with condensin

Our current and previous work, as well as evidence in the literature suggest interplays between condensin and chromatin associated activities play a part in mitotic chromosome assembly. We show

that shelterin components (Part 5) can both facilitate condensin function (Taz1) or impair it (Mit1) for sister telomere disjunction in anaphase. Additionally, we (the hosting lab) have shown that histone acetyl transferase Gcn5 and the RSC complex evicting histones at promoters **(Toselli-Mollereau et al., 2016)** play a part in condensin binding and condensation of mitotic chromosomes. We identify a weak physical interaction with RSC (Part 7 – Fig. 1) supporting our previous data and drawing a parallel with evidence of interplays between RSC and cohesin **(Muñoz et al., 2022, 2019)** suggesting conserved interplays between SMC activity and chromatin remodeling. In Xenopus egg extracts, the PIC subunit TFIIH is essential for mitotic chromosome condensation **(Haase et al., 2022)** while we have described genetic interactions between Mediator and condensin **(Robellet et al., 2014)**. In a minimal system the FACT histone chaperone is required for the folding of chromosomes on chromatinized DNA into a mitotic chromosome by condensin I and topo II **(Shintomi et al., 2015).** We identify FACT as a physical and functional partner of condensin in fission yeast (Part 7 – Fig. 2). These accumulating evidence suggest that condensin and RNAPII may share similar chromatin remodeling activities to operate in the context of chromatin – despite the process of transcription itself stalling condensin (Part 6).

A recent report **(Yague-Sanz et al., 2023)** argues that RNAPII elongation promotes chromatin remodeling at tDNA to evict nucleosomes. Consequently, a defect in elongation in RNAPII leads to a reduction in RNAPIII association. If this is the case we should expect a loss of Rpb1-associated chromatin remodeling activities at the tDNA loci and the non-eviction of histones when we deplete Rpb1 in mitotic cells. Additionally, the Gcn5 and Mst2 acetyl-transferase activities, which setup histone levels at high-condensin binding sites in mitosis **(Toselli-Mollereau et al., 2016)** also control histone levels at tDNA loci in cycling cells **(Yague-Sanz et al., 2023)**. However, re-exploration of our previously published MNase-seq data set (Fig. D4B-C) suggests that constitutive loss of Gcn5 & Mst2 does not induce significant Mnase-resistant signals at tDNA loci in mitotic cells, although a calibrated histone ChIP-seq or MNase digestion with two units would have been more appropriate to re-explore this question. Additionally, we never see a decrease in condensin binding at the tDNA upon Rpb1 depletion but rather a weak increase of condensin association (Part 6 – Fig. 1B). This data suggests that in mitosis active RNAPII transcription does not significantly contribute to condensin binding at tDNA.

We have not checked the integrity of chromatin by MNase in mitotic cells with Rpb1 depletion. We can expect a stabilization of nucleosomes from the literature but this would need to be validated. Importantly, the phenotype of RNAPIII reduction when RNAPII elongation is impaired is visible in log but not stationary phase **(Yague-Sanz et al., 2023)**. Whether mitotic and interphase chromatin follow a similar paradigm to stationary and log phase chromatin is unclear.

8.12 Condensin does not affect nucleosomal arrays *in vivo*

If nucleosomes and chromatin in general are barriers to condensin, then it stands to reason that chromatin remodeling activities in cells would alleviate this barrier, as suggested by our genetic evidence (Part 7 – Fig. 8). Importantly, we show that partial loss of condensin function does not impart visible defects to nucleosome phasing or to the stability of nucleosomes as seen by Mnase and cal-ChIPseq (Part 7 – Fig. 9), with one caveat being we did not use a degron system and are susceptible to remaining activity of chromatin-bound condensin in metaphase. However, our data argue that condensin does not appreciably destabilize the primary structure of nucleosomes, suggesting condensin itself is not a chromatin remodeler.

It was previously speculated that an interplay may exist between condensin and nucleosomes to fold the genome **(Hirano, 2014)** based on the ability of condensin to introduce positive supercoils into DNA **(Bazett-Jones et al., 2002; Kimura and Hirano, 1997)**. Whether the (+)-supercoiling by condensin would contribute to compaction of genomes is unclear **(Hirano, 2014)** and whether condensin in general contributes to compaction (3D volume) of chromosomes is also unclear **(Gerguri et al., 2021; Piskadlo et al., 2017; Samejima et al., 2018; Schneider et al., 2022; Swygert et al., 2019)**.

This may be particularly relevant at the 3' end of genes in transcribed chromatin. For instance, RNA polymerases could generate positive supercoiling driving the recruitment of additional condensin complexes **(Kim et al., 2022)**. But this positive role of RNA polymerase would be obfuscated by the barrier effect of RNA pol II on condensin barriers (Part 6). Moreover, the removal of RNA pol II should reduce the steady state level of (+)-supercoiling, yet condensin is not found particularly diminished globally (Part 6 – Fig. 2F), suggesting that (+)-supercoiling by transcription may not be sufficient to

recruit condensin. If this (+)-supercoiling recruiting chromatin were functionally relevant it is also difficult to square with the observation that abolishing transcription rescues *cut3-477* induced chromatin bridges.

Perhaps the ability of condensin to introduce positive supercoiling plays a role in compaction rather than the assembly of mitotic chromosomes and individualization of chromatids, or that (+)-supercoiling is a consequence of a chromatin folding activity of condensin. We may be blind to more subtle torsion related changes of metaphase chromatin with our MNase and histone calChIPseq experiments and could attempt to investigate the supercoiling state of mitotic chromatin in the presence of functional condensin or in its absence using psoralen crosslinking **(Achar et al., 2020)** or GapR-based ChIP-seq **(Guo et al., 2021)**.

In quiescent budding yeast cells where chromatin compaction is condensin dependent **(Swygert et al., 2019)** Micro-C data suggest short range n+1 nucleosome interactions are reduced in favor of n+2 and higher interactions suggesting potentially an increased stacking **(Swygert et al., 2021)**. Whether condensin could introduce supercoiling sufficient to disturb higher-order stacking of nucleosomes or introduce supercoiling that would be buffered by the fiber and drive higher order stacking **(Kaczmarczyk et al., 2020)** is unclear. It is likely that the forces induced by single or multiple condensin complexes on the chromatin fiber must be on the low scale. Indeed, loop extrusion is easily stalled **(Ganji et al., 2018; Kong et al., 2020)**, condensin complexes can compete with each other for DNA slack during loop formation **(Kim et al., 2020)** and condensin does not generate a positive supercoiling on DNA outside of it's bound domain **(Martínez-García et al., 2022)**. Stabilization of positive supercoils occurs at high concentration of condensins **(Martínez-García et al., 2022)** suggesting that the activity first identified in **(Kimura and Hirano, 1997)** may well occur at high condensin binding site. Supercoiling of DNA by single condensin complexes was however described in early in vitro single molecule **(Bazett-Jones et al., 2002)** suggesting the significance of condensin on the topology of DNA is unclear and may result as a side effect of loop formation on topologically constrained DNA molecules. Experimental evidence using Xenopus egg extracts suggests that interphase and metaphase nucleosomes show a majority of (-)-crosslinked DNA **(Arimura et al.,**

2021) bringing into question the validity of positive supercoiling in metaphase chromosomes, or that this supercoiling is resolved by compensatory negative supercoiling.

Despite our finding that condensin does not induce changes to the chromatin fiber, condensin is functionally associated with several chromatin remodeling activities shre with RNAPII previously mentioned. This implies these chromatin remodelers exert their function independently of condensin. Thus it is tempting to speculate that condensin benefits from transcription associated chromatin remodeling to access DNA in an opportunistic fashion. However if this were the case, it would imply condensin must rely on the presence of actively remodeled genes. It is certainly unrealistic to imagine that condensin would function only at highly transcribed, actively remodeled genes which are a minority in fission yeast mitosis. Transposed to vertebrates with larger genomes and lower gene density, it is also difficult to imagine that condensin would function solely in an opportunistic manner, benefitting from the few highly expressed genes **(Palozola et al., 2017)**. As FACT **(Jenness et al., 2018)** and SWI/SNF/RSC **(Zhu et al., 2023)** are retained on mitotic chromosomes, they appear as interesting molecular candidates for remodeling activities independent of transcription to benefit condensin.

8.13 The cryptic role of FACT during mitotic chromosome assembly *in vivo*

The histone chaperone FACT is a good candidate to scan the chromosome in a genome-wide fashion for condensin function. In yeast it is present in comparable amounts to the number of nucleosomes **(Jeronimo and Robert, 2022)** and is abundant on mitotic chromosomes in vertebrates despite transcription being downregulated **(Djeghloul et al., 2020; Jenness et al., 2018)**. We show that depletion of fission yeast FACT in metaphase leads to nucleosome loss which correlates with the levels of active transcription, but importantly is seen at virtually all protein-coding genes of fission yeast (Part 7 – Fig. 5).

More puzzling is the difference in functional role between FACT and condensin in our hands in fission yeast, where FACT loss in mitosis suppresses condensin partial loss of function induced defects in anaphase (Part 7A-B) versus in a minimal cell free system where FACT is required for condensin to assemble mitotic chromatids from chromatinized DNA **(Shintomi et al., 2015)**. Moreover, FACT is

not essential in all cell types **(Jeronimo and Robert, 2022)** suggesting the observations made both by us and the Hirano lab underlie specific contexts where FACT has significant impacts on condensin function. Indeed, FACT activity itself is not directed towards maintenance of chromatin structure – it is context dependent. While FACT destabilizes nucleosomes in optical trap pulling assays, it enables the reassembly of said nucleosomes when the fiber is subjected to multiple cycles of stretching and relaxation **(McCauley et al., 2022)**.

In the minimal system that revealed the positive role of FACT in mitotic chromosome assembly, Shintomi and colleagues used Nap1, Npm1 and histones to remove protamines and assemble chromatin along with condensin and topo II to form mitotic chromatids. In that context, FACT is necessary and sufficient for mitotic chromatid assembly only if histone H2A is replaced by embryonic variants H2AX-F, and furthermore this variant is Nter deleted to remove the histone tail. This variant is capable of assembling into nucleosomes that yield wild-type like Mnase profile. Crucially when FACT is added to chromosomes chromatinized by classical vegetative histones, the mitotic chromosome assembly fails **(Shintomi et al., 2015)** which is perfectly consistent with the inability of FACT to bind intact nucleosomes **(Valieva et al., 2017)** and with our finding that condensin does not appear to destabilize nucleosomes (Part 7 – Fig. 9). Thus, this suggests that the minimal system fails to capture an additional activity which destabilizes nucleosomes (which is neither condensin or topo II) and enables condensin to convert chromatinized DNA into mitotic chromosomes. Consequently, a nucleosome destabilizing activity present in fission yeast but not in the minimal system, be it transcription **(Singh et al., 2021)**, or another undetermined activity, may explain the apparently negative impact of FACT on condensin, because it maintains nucleosomes *in vivo* in fission yeast mitosis.

However, while we propose that chromatin bridges in anaphase caused by partial condensin loss of function can be rescued both by FACT depletion in mitosis, leading to reduced nucleosome density (Part 7 – Fig. 7A-B), and by direct reduction of nucleosome density by histone gene copy number reduction (Part 7 – Fig. 9), we cannot attribute this rescue to increased condensin accessibility to DNA in metaphase by calChIP-seq (Part 7 - Fig. 6D, S6E). Moreover, FACT influence on folding metaphase chromosomes seen by Hi-C appears independent on the presence of condensin (Part 7 – Fig. 7C).

Although we cannot exclude insufficient depletion by degron approaches which prevents us from formally concluding, this raises the possibility that FACT may impinge on loop formation by impacting the chromatin fiber itself or its biophysical properties.

How does FACT loss of function rescue partially deficient condensin activity in anaphase ? The possibility that it may be due to enhanced cohesin activity appears unlikely given the moderate effect of Wpl1 loss of function (Part 7 – Fig. 4), suggesting that enhancing cohesin driven loop extrusion hardly rescues condensin defects in anaphase. As cohesin function has been reported to rely partially on the activity of FACT **(Garcia-Luis et al., 2019)** we cannot exclude that loss of FACT function may facilitate condensin activity via a loss in cohesin binding to chromosomes. We are currently investigating more precisely the contribution of cohesin loss of function towards condensin activity in metaphase and anaphase. Additionally, one of the known consequences on chromatin structure upon FACT loss of function is incorporation of H2A.Z outside of its restricted TSS association **(Jeronimo et al., 2015)**. The H2A.Z histone variant promotes the unwinding of DNA around it **(Lewis et al., 2021; Li et al., 2022)**. Strikingly, in fission yeast, null mutants for H2A.Z^{pht1} show chromatin bridges and reduction in condensin association in anaphase **(Kim et al., 2009; Tada et al., 2011)**. Whether the rescue phenotype of FACT depletion depends on the presence of H2A.Z (using a *pht1Δ* background) would be interesting to address. Finally, while we have also observed that FACT loss of function is synthetically lethal with partial topo II loss of function (Part 7 - Fig. S2A) suggesting FACT is needed for topo II activity, we are also investigating whether this could be the case in anaphase. While FACT is essential, it is not clear from our observations what causes cell death when Spt16 is depleted, because we observed no gross defects observed in mitosis. The synthetic sickness observed on plates between Spt16 and topo II might be a reflection of a function of both these proteins in S phase rather than in mitosis, where topo II is known to be required for decatenation **(Baxter and Diffley, 2008)**.

One possible explanation of our data so far is that FACT and the density of nucleosomes is not important for condensation of mitotic chromosomes in fission yeast, it might be particularly important for a step in decatenation rather than loop formation, similarly to what has been proposed for the rDNA locus **(D'Ambrosio et al., 2008a; Sullivan et al., 2004)**. Since both condensin and topo II

are present in the minimal Xenopus system it is not clear for which activity FACT is important for **(Shintomi et al., 2015)**.

8.14 Testing the properties of the chromatin fiber on condensin function

As mentioned previously, multiple chromatin-associated activities are linked with condensin either physically or functionally : Gcn5 HAT and RSC in fission yeast **(Toselli-Mollereau et al., 2016)**, TFIIIC in yeast **(D'Ambrosio et al., 2008b; Haeusler et al., 2008)** and in mouse with condensin II at both transcribed and non transcribed loci **(Yuen et al., 2017)** consistent with TFIIIC being retained in mitotic chromosomes in vertebrates **(Fairley et al., 2003)**, TFIIH in Xenopus egg extracts, which sets up NDR at promoters as part of the PIC, is essential for condensation **(Haase et al., 2022)** while FACT is required to form mitotic chromatids from a chromatinized minimal template **(Shintomi et al., 2015)** and to spread cohesin outside of the centromeres in yeast **(Garcia-Luis et al., 2019)**. TBP is retained on mitotic chromosomes **(Chen et al., 2002; Fairley et al., 2003)** and has been implicated in fission yeast in condensin association **(Iwasaki et al., 2015)**. Fission yeast specific transcription factors have also been linked to condensin function (Kyoung-Dong Kim et al., 2016b)**.** While many of these factors are involved in some promoter related functions, no clear mechanistic model has elucidated the role of these activities in condensin function, bar the possibility that they provide NDR for condensin binding **(Robellet et al., 2017)**, which is consistent with an increase in condensin association in quiescent budding yeast cells at divergent promoters with low levels of H3 **(Swygert et al., 2019).**

Many transcription factors are now thought to be retained on chromatin in mitosis **(Palozola et al., 2019)**, which might provide a context for condensin to bind at promoters without requiring a specific physical interaction. However while this model provides an explanation for condensin binding at promoters particularly in vertebrates, it does not provide an explanation on the mechanism by which condensin will fold the rest of the chromatinized template. Moreover, mitotic chromosome structure is still composed of contact domains **(Nozaki et al., 2017)**, accessibility to DNA genome-wide is similar to interphase **(Djeghloul et al., 2020)** and individual nucleosomes have similar organization **(Arimura et al., 2021).** Whether these factors would have a specific role in mitotic chromatin outside of promoter regions is unclear. They may remodel chromatin at a basal level genome-wide in

a similar manner to interphase, and this is sufficient for condensin function. We provide evidence that the density of nucleosomes and the FACT histone chaperone may antagonize condensin activity (Part 7) although we never show this in a direct manner by increased condensin association, making this hypothesis difficult to answer currently.

The persistence length of DNA is estimated to be ~45 nm for a random sequence **(Bednar et al., 1995)** which is very similar to the length of the coiled-coil heterodimer in SMC proteins. Strong experimental and phylogenetic evidence suggests that the SMC coiled-coil length is under selective pressure and must respect a certain distribution of length to support viability and translocation on DNA **(Bürmann et al., 2017)**. It is attractive to speculate that the loop forming activity of SMC protein relies on the ability of SMC complexes to perform steps (20-40nm) on a range of distances compatible with the SMC coiled-coil length and the persistence length of DNA **(Ryu et al., 2021b)**. It is not clear yet whether successive steps can accommodate only a single obstacle, regardless of size as suggested by **(Pradhan et al., 2022a)** or multiple. This problem is especially relevant in the case of the chromatin fiber, composed of multiple nucleosomes separated by short stretches of linker DNA.

Theoretically, another key piece of data that can be derived from the interplay between condensin and nucleosome fibers is the mechanism by which condensin folds mitotic chromosomes – that of loop extrusion or crosslinking by diffusion capture. One can attempt to make intuitive predictions regarding the different sensitivities to the density of nucleosomes each mechanism should have. A processive mechanism such as a translocating loop extruder must successively contend with obstacles. With current estimates of step size **(Ryu et al., 2021b)**, ATP-driven translocation would encounter anywhere from 1 to 3 NRL per step. If nucleosomes were significant obstacles, the speed or processivity of metaphase chromosome assembly at constant condensin concentrations should be increased when the template is less densely bound. On the other hand, diffusion capture based mechanisms and/or condensin-condensin based interactions should mostly ignore this dependence to density of nucleosomes, as forming a loop would require only a single "step", - provided we are studying a condensin complex which is already bound to chromatin.

Our data in the case of FACT is puzzling as we do not observe significant changes in condensin binding, despite stark loss of nucleosomes. However, loss of RNAPII association and binding of other chromatin factors may confound our interpretation. Evidence in budding yeast shows that H4 basic tail mutants mimicking acetylation enhance the formation of condensin dependent domains during quiescence **(Swygert et al., 2021)**. Consistent with this data, reformation of cohesin loops after depletion by degron is faster at regions bearing H4K16 acetylation marks **(Rao et al., 2017a)**. On the other hand, inhibiting deacetylation in mitosis leads to only weak chromatin bridge defects **(Cimini et al., 2003)**. Thus higher order association between nucleosomes may impair the ability of condensin to form loops. A reverse experiment to TSA treatment in vertebrates **(Cimini et al., 2003; Schneider et al., 2022)** may provide key insight onto the ability of condensin to assemble mitotic chromosomes in vertebrates and whether higher order structures of chromatin impair on a loop extrusion process.

Other data have suggested that histones may facilitate condensin function. A proposed model of loop extrusion on chromatin fiber, suggest that nucleosomes prevent the slippage of extruded loops and stabilize their compacting activity **(Sun et al., 2023)**. Linker H1 depletion reduced metaphase chromosome compaction more strongly than Asf1 which promotes nucleosome assembly by H3-H4 deposition **(Sun et al., 2023)** implying that chromatosomes may help the compacting activity of condensin. Interestingly, while this is not consistent with increased binding of condensin and topo II **(Choppakatla et al., 2021)**, the striking defects observed in anaphase in H1 depleted egg extracts that have undergone replication **(Maresca et al., 2005)** may underlie a partial loss of function of condensin or topo II, or an imbalance in their respective activities. The role of linker histone relative to condensin must be further investigated as it is a prime candidate to regulate DNA accessibility on an already chromatinized template. Nonetheless, it is challenging to imagine how condensin can access DNA on chromatin in fission yeast when the linker length is on average less than 10bp with no linker H1.

A simple model of 1D translocation of a loop extruder on chromatin suggests the formation of a loop is accelerated by linker lengths shorter than the nucleosome size **(Maji et al., 2020)**. Testing the effects of linker length variation on condensin loop formation is certainly a key question. One such

candidate could prove to be CHD1/Hrp1 (with the additional Hrp3 version in fission yeast) that has a phasing activity **(Hennig et al., 2012; Oberbeckmann et al., 2021)**, shows a suppressive effect in ts- condensin mutant in our hands (not shown) and when overexpressed causes cut phenotypes **(Yoo et al., 2000)**. Loss of Chd1 is reported to increase the median distance between nucleosomes by 10bp in *S. pombe* **(Hennig et al., 2012)**, but full Chd1 loss of function appears to lead to strong phasing defects of nucleosomes beyond the +1, similar to Spt16 depletion (Part 7). This is consistent with FACT and Chd1 working in a same pathway **(Jeronimo et al., 2021)**. The nature of these phasing defects imply that in the population average of mitotic cells, nucleosomes are present but are not found at statistically defined positions. Thus, determining the exact contribution of linker length variation to condensin activitiy (and contribution of chromatin to condensin in general) is challenging and may require an ex-cellulo system with more controllable parameters and tractable chromatin fibers – but that can still assemble physiologically relevant nucleosome arrays compared to current loop extrusion assays. Finally, linker H1 may function through the bending of DNA. Testing whether the bending of DNA by HMG proteins **(Mallik et al., 2018; McCauley et al., 2022, 2019)** can impact the activity of condensin in such assays could also provide important information regarding the impact of the mechanical property of the condensin substrate to its function.

MATERIAL & METHODS

I / Genetics, spot assays, cytological assays

a/ Strain construction

Strains of interest were obtained by crossing freshly thawed parental strains on sporulating agar plates. Mature crosses were resuspended in milliq H20 and digested with cytohelicase overnight at 32°C. Spores were spread on either selective or non selective plates depending on the markers of interest. On rich media (YES+A) 500 to 1000 spores were spread, or 2000 to 4000 spores when selecting a marker. Segregation frequencies were checked against mendelian ratios. When performing crosses to obtain *ura4-pnmt41-slp1* strains spores were spread on PMG+Ura plates at densities

ranging from 20K to 40K spores. Mendelian ratios were not checked due to the low viability and bias caused by *ura4-pnmt41-slp1* alleles. Colonies growing on PMG-Ura were replicated on selective plates and on YES+A to select only strains dying on this media. In our experience many URA+ strains descending from these crosses are also insensitive to thiamine. We hypothesize the *ura4-pnmt41-slp1* allele may have meiotic phenotypes leading to this incongruency.

After selecting isolated colonies, strains were restreaked as patches and subjected to a second round of replication. In case of conflictsof markers, strains were also PCR checked or checked under the fluorescent microscope if applicable. The mating type of the colonies was then checked by crossing with *h+* or *h-* strains on SPA and staining with Iode. Isolated colonies were restreaked, left to grow for 2-3 days and the colonies growing on plates were resuspendended in YES+A (or PMG if thiamine sensitive alleles) + 40% Glycerol and stored at -80°C.

b/ Degron construction

To tag genes of interest with 3x-sAID alleles (Zhang et al., 2022), pDB4581 plasmids were subjected to PCR with Bahler-For (cggatccccgggttaattaa)/Bahler-Rev (gaattcgagctcgtttaaac) primers. Overlapping PCR was performed on this ~2kb product with 200-250 nt PCR products with 20nt homology to the 3xsAID-KanMX6 cassette and 180-230nt homology to the 3' end of the protein coding gene of interest. Exponentially growing wild-type LY113 or *ura4::padh1-osTir1-F74A-NatMX6* LY7141 strains were transformed by Lithium Acetate/DMSO procedure (CSH protocol doi:10.1101/pdb.prot090969), plated on YES+A and replicated ~24h later on YES+A+G418. If the tagged gene was essential, positive colonies were replicated on YES+A+phloxine and YES+A+phloxine+ 5-adamantyl-indole-3-acetic acidAA (5aIAA). Positive transformants were also PCR screened to check the integration of the *3xsAID-KanMX6* cassette. Selected clones were grown to exponential phase at 32°C in YES+A and exposed for 2h to 5aIAA 100nM in liquid culture to validate the strain expressed an auxin-sensitive protein by western blotting.

c/ Strain list for PART VII

LY6281	Mata ade2-1 his3-11 his3-15 ura3 leu2-3 trp1-1 can1-100 SMC3-GFP-KanR	

LY5480	h? leu1-32 ura4D-18 ade6-21? ura4-Pnmt41-slp1+ aur1::pad421-NLS-GFP-9PK::aur1R	
LY4483	h- leu1-32 ura4D-18 ura4-Pnmt41-slp1+ cnd2-GFP-LEU2	
LY6304	h+ leu1-32 ura4D cut3-477 ura4-Pnmt41-slp1+ cnd2-GFP-LEU2	
LY6305	h- leu1-32 ura4D cut14-208 ura4-Pnmt41-slp1+ cnd2-GFP-LEU2	
LY113	h- leu1-32 ura4D18 ade6-210	
LY4012	h- leu1-32 ura4D18 ade6-210 pob3D::KanR	
LY1069	h- leu1-32 ura4D18 cut3-477	
LY4013	h+ leu1-32 ura4D18 cut3-477 pob3D::KanR	
LY659	h+ leu1-32 ura4D18 ade6-210 cut14-208	
LY6481	h- leu1-32 ura4- ade6-210 cut14-208 pob3D::KanR	
LY1000	h+ leu1-32 ura4D? ade6-210 cut3-477-NatR	
LY1289	h- ade6-216 htb1-K119R-Flag-KanR (ts36°C)	
LY1290	h- ade6-216 htb1-Flag-KanR	
LY1313	h- ade6-216 cut3-477-NatR htb1-K119R-Flag-KanR	
LY1315	h+ ade6-210? cut3-477-NatR htb1-Flag-KanR	
LY6337	h- leu1-32 ura4D18 cut3-477 KanR-nmt81-pob3-HA2-IAA17 ura4+ ade6+_skp1-Os(At)TIR1-NatR	
LY5168	h+ leu1-32 ura4- ade6-210 cut3-477-NatR spt16.19-KanR	
LY5166	h- leu1-32 ura4- ade6-210 spt16.19-KanR	
LY3959	h- leu1-32 top2-191	
LY5402	h? leu1-32 ura4D18 ade6-210 top2-191ts pob3D::KanR	
LY5430	h- leu1-32 ura4D18 ade6-210 ptr11-3ts	
LY5431	h- leu1-32 ura4D18 ade6-210 ptr11-3ts pob3D::KanR	
LY5425	h- leu1-32 ura4D18 ade6-210 arg3D4 top2-342ts	
LY5427	h- leu1-32 ura4D18 ade6-210 arg3? top2-342ts	

LY4485	h+ leu1-32 ura4D ade6-21? leu1-Pnmt41-slp1+ cut3-GFP-ura4+	
LY7092	h? ade6? leu1-Pnmt41-slp1+ pob3-flag-NatR	
LY7093	h? ade6? leu1-Pnmt41-slp1+ pob3-flag-NatR cut3-GFP-ura4+	
LY6307	h-? leu1-32 ura4D cut3-477 ura4-Pnmt41-slp1+ pob3D::KanR cnd2-GFP-LEU2	
LY6861	h+ leu1-32 ura4D18 cut14-208 ura4-Pnmt41-slp1+ pob3D::KanR cnd2-GFP-LEU2	
LY6889	h- leu1-32 ura4D18 cut3-477 wpl1D::KanR	
LY6891	h- leu1-32 ura4D18 cut3-477 pds5D::ura4+	
LY662	h+ leu1-32 ura4D18 wpl1::KanR	
LY663	h+ leu1-32 ura4D18 ade6-210 pds5::ura4+	
LY7248	h+ leu1-32 ura4D18 ade6-216 ura4-Pnmt41-slp1+ cnd2-GFP-LEU2 ura4+::NatR_padh1-OsTIR1-F74A	
LY7226	h+ leu1-32 ura4-Pnmt41-slp1+ cnd2-GFP-LEU2 pob3-sAID3-KanR ura4+::NatR_padh1-OsTIR1-F74A	
LY7230	h+? leu1-32 ura4-Pnmt41-slp1+ cnd2-GFP-LEU2 spt16-sAID3-KanR ura4+::NatR_padh1-OsTIR1-F74A	
LY7232	h-? leu1-32 cut3-477 ura4-Pnmt41-slp1+ cnd2-GFP-LEU2 spt16-sAID3-KanR ura4+::NatR_padh1-OsTIR1-F74A	
LY4484	h+ leu1-32 ura4D ura4-Pnmt41-slp1+ cnd2-GFP-LEU2	
LY7065	h- leu1-32 ura4D18 ura4-Pnmt41-slp1+ wpl1D::KanR cnd2-GFP-LEU2	
LY7067	h- leu1-32 ura4D18 cut14-208 ura4-Pnmt41-slp1+ wpl1D::KanR cnd2-GFP-LEU2	
LY7176	h+ leu1-32 cut3-477 ura4+::NatR_padh1-OsTIR1-F74A	
LY7205	h- leu1-32 cut3-477 spt16-sAID3-KanR ura4+::NatR_padh1-OsTIR1-F74A	
LY7452	h- leu1- ade? Lys? cut3-477 rpb1-sAID3-KanR ura4+::NatR_padh1-OsTIR1-F74A	

LY7357	h- leu1-32 ura4-Pnmt41-slp1+ cnd2-GFP-LEU2 cut14-sAID3-HygroR ura4+::NatR_padh1-OsTIR1-F74A	
LY7368	h+ leu1-32 ade? lys? ura4-Pnmt41-slp1+ cnd2-GFP-LEU2 spt16-sAID3-KanR cut14-sAID3-HygroR ura4+::NatR_padh1-OsTIR1-F74A	
LY7494	h+ leu1-32 ura4D cut14-208 cdc2asM17 cdc11-GFP-NatR spt16-sAID3-KanR ura4+::NatR_padh1-OsTIR1-F74A	
LY7285	h+ leu1-32 ura4D ade6- cdc2asM17 cdc11-GFP-NatR	
LY6206	h- leu1-32 ura4-D18 H3.2/H4.2D::HygroR H3.3/H4.3D::NatR	
LY6272	h- leu1-32 ura4D18 H3.1/H4.1D::KanR H3.3/H4.3D::NatR	
LY6204	h- leu1-32 ura4-D18 cut3-477 H3.2/H4.2D::HygroR H3.3/H4.3D::NatR	
LY6273	h- leu1-32 ura4D18 cut3-477 H3.1/H4.1D::KanR H3.3/H4.3D::NatR	
LY6159	h- leu1-32 ura4-D18 H3.2/H4.2D::HygroR H3.3/H4.3D::NatR	
LY5639	h+ leu1-32 ura4D ade6-216 his3D1 arg3D4 H3.1/H4.1D::his3+ H3.3/H4.3D::arg3+	
LY6153	h- leu1-32 ura4-D18 H3.1/H4.1D::KanR H3.2/H4.2D::HygroR	

d/ Spot assays

Freshly thawed strains were resuspended in mq H20, counted on a Toma cell and diluted to a density of 10^6. Five serial dilutions of up to 8 strains were performed in 96 well plates by a factor 5. Drops were deposited on phloxine-stained plates with a flame-sterilized 48 pin replicator (VP407AH), and plates were then transferred at the indicated temperatures (generally ranging from 30°C to 36°C) for 3 to 5 days.

e/ Cytological assays

Cells were grown in the indicated media at 30°C to a final concentration of ~ 10^6 and fixed in 10 volumes of cold MetOH (tubes were incubated at -80°C before fixation). Cells were processed for IF by spinning down, washed once with 20ml PEM. Cells were then washed 3x in 1ml PEM after transferring in 1.5mL Eppendorf tubes with double spin centrifugations (15s x2, 13000rpm, RT

benchtop centrifuge Eppendorf Minispin). For the final wash, cells were left in PEM on a wheel at RT for 30mn.

2.10^7 cells were used for IF, cells were pelleted, supernatant was removed and cells were vortexed gently to be resuspended in the residual volume, then were incubated in 1ml PEMS 0,4mg/mL zymoliase 100T (07665-55 Nacalai tesque) in a 37°C waterbath. Cell lysis was confirmed with 1% SDS final and quenched in an icebath. Cells were pelleted in a cold centrifuge (Sorvall Legend Micro 21R) 13000rpm 4°C 15s x2 and washed twice with cold PEMS. Cells were gently resuspended with low-speed vortexes.

Cells were pelleted at RT benchtop centrifuge and resupended in 1ml PEMS 2% Triton and incubated between 30s to 90s (no more than 3mn). Cells were pelleted and washed 1x with 1ml PEM, washed 1x with 300ul PEMBAL with a 30mn incubation on wheel at RT (with aluminium foil cover). Cells were then pelleted, resuspended in 100ul PEMBAL 1/50 TAT-1 antibody (serum) and left to incubate on a wheel at 4°C o/N in the dark.

Cells were washed the next day 3x with 100ul PEMBAL and incubated with PEMBAL 1/400 Alexa-488 anti-mouse for 2h on a wheel at RT (with aluminium foil cover). Cells were washed 1x with 100ul PEMBAL and resuspended in 30ul PEM+DAPI 0,5 ug/mL final. Defective anaphase phenotypes were scored by manual counting, selecting anaphase cells when microtubules displayed a characteristic linear shape (at least 100 anaphase for each condition) without nucleation marking telophase onset.

For block and release experiments in G2 arrests, cells were grown exponentially in YES+A and exposed to 4-Amino-1-tert-butyl-3-(3-bromobenzyl)pyrazolo[3,4-d]pyrimidine (3-BrbPP1, Toronto Research Chemicals) at 2uM for a total of 3 hours at the indicated temperature. For filtering, 2.10^8 cells were placed on a 45uM filter membrane prewashed with culture media without 3-BrbPP1 (and/or without IAA if required). Cells were then washed 3x with ~20ml of culture media without 3-BrbPP1 (and/or without IAA if required) using a vacuum pump. The media was at the appropriate temperature for the release. Filters containing adsorbed cells were then folded with tweezers and introduced in erlenmeyers containing culture media at the appropriate temperature in rotating water baths.

f/ Mitotic indexes (for Part 7)

To assess the mitotc index, the fraction of cells with a green nucleus (GFP tagged condensin subunit) over the total population was estimated to represent the percentage of metaphase-arrrested cells. An aliquot of culture ~400ul was recovered, supernatant was removed and fixed in ~100ul cold EtOH 70%. 10ul of the resuspension was spread on a glass slide, air-dried for a couple of minutes. 5ul of PEM/DAPI was added to the dried cells, coverslip was added and cells were inspected under an epifluorescent microsocope. %gfp was estimated by counting 100 to 200 cells.

Fig. 1

co-IP

cut3-GFP 87% *snf21-FLAG* / *cut3-GFP snf21-FLAG* 84%

Fig. 2

co-IP

cut3-GFP 81% *pob3-FLAG* / *cut3-GFP pob3-FLAG* 68%

Fig. 3

Hi-C, 2 biological replicates

wild-type 79% +/-8% *cut3-477* 78% +/-10% *cut14-208* 81% +/-6% *cut3-477 pob3Δ* 61% +/-4% *cut14-208 pob3Δ* 70% +/-1%

Cnd2-GFP calChIPseq, 3 biological replicates

cut14-208 63% +/-3% *cut14-208 pob3Δ* 66+/-6%

Fig. 4

Wpl1 Hi-C, 2 biological replicates

wild-type 75% +/-6% *wpl1Δ* 80% +/-5% *cut14-208* 77% +/-4% *cut14-208 wpl1Δ* 81% +/4%

Fig. 5

Mnase-seq, 2 biological replicates

wild-type 94% +/-1% *pob3-3xsAID* 86% +/-5% *spt16-3xsAID* 83% +/-1% 5aIAA

H2B/H3 calChIPseq, 3 biological replicates

wild-type 92% +/-1% *pob3-3xsAID* 90%+/-1% *spt16-3xsAID* 84%+/-6% 5aIAA

Fig. 6

Hi-C, 2 biological replicates

wild-type 93% +/-0% *pob3-3xsAID* 90%+/-3% *spt16-3xsAID* 88%+/-3% NaOH

wild-type 93% +/-1% *pob3-3xsAID* 92%+/-0% *spt16-3xsAID* 89%+/-2% 5aIAA

RNAPIIS2P calChIPseq, 2 biological replicates

wild-type 94% +/-1% *spt16-3xsAID* 85% +/- 5% 5aIAA

Cnd2-GFP calChIPseq, 3 biological replicates

wild-type 92% +/-1% *spt16-3xsAID* 84%+/-6% NaOH

wild-type 94% +/-1% *spt16-3xsAID* 84%+/-2% 5aIAA

Fig. 7

Hi-C, 2 biological replicates

wild-type 88% +/-1% *spt16-3xsAID* 88% +/-1% *cut14-3xsAID* 84%+/-1% *spt16-3xsAID cut14-3xsAID* 82%+/-4% 5aIAA

Fig. 8

N/A

Fig. 9

Mnase-seq

wild-type 78% +/-1% *cut3-477* 76% +/-1% *cut14-208* 76%+/-6%

H2B/H3 calChIPseq

wild-type 76% +/-1% *cut14-208* 73% +/-7%

II/ Molecular biology

a/ Western blotting

2.10^7-5.10^7 cells were pelleted, washed 2x with cold milliq water and snap frozen before storage at -80°C. Proteins were TCA extracted by resuspending cells in TCA 20% and beating in a Precellys 24 (Bertin technologies) with 4 cycles of 12s each at 6800 rpm with acid-glass washed beads. Pellets were left on ice for 1mn between each cycle. Tubes were pierced at the bottom with a hot needle and added on to 5ml polypropylene tubes and centrifuged briefly by reaching 2500rpm to collect the

lysate. Lysate was resuspended, transferred to an Eppendorf tube and centrifuged at 4°C 14.8krpm for 5mn (Sorvall Legend Micro 21R). The supernatant was discarded and the pellet was resuspended in Laemmli buffer 2X with B-mercapto (equilibrated with Tris pH 9.5), and samples were boiled 5mn at 98°C. Samples were centrifuged at 4°C 14.8krpm for 5mn and supernatants were collected and used immediately, or stored at -20°C or -80°C and boiled another 3mn at 98° before use.

7.5% acrylamide gels were loaded with 1/20 volume of recovered samples and migrated at 180V for 1h in 1X Running Buffer. The gel was then transferred using a semi-dry system in 1x Transfer Buffer with 6 whatmann papers total (3/side) and 1x nitrocellulose membrane. The transfer used an amperage of (dimensions in cm x 0.8 mA) which tended to be 31mA. Proteins were transferred on the membrane for 1h30 and membrane was removed, washed in ddH20 and stained with x% Ponceau acetic acid to validate protein transfer. Ponceau was washed 2-3x with ddH20 and membranes were blocked in PBS-Tween 0.1% milk 5% for 30mn – 1h at RT shaking horizontally at ~30rpm. Membranes were incubated with primary antibodies for 1h at RT in PBS-T 5% milk or overnight in a cold room shaking horizontally at ~30rpm. For antibodies, anti-FLAG 1/2000 (F1804) and anti-GFP 1/2000 (JL8) were used. Membranes were washed 2x with PBS-T with no incubation, 1x with PBS-T with 5mn incubation and another time with PBS-T for 10mn. Membranes were incubated with secondary antibody for 30mn in PBS-T 5% milk, and then 2x washes with no incubation, 1x for 5mn and 1x for 10mn were done with PBS-T. Membranes were then generally incubated on saran wrap with 1/1 mix SuperSignal West Femto (Thermo Scientific 34096) for 5mn RT and revealed using electrochemiluminescence machine (Bio-Rad ChemiDoc).

b/ coImmunoprecipitation

2.10^8 cells were pelleted, washed in cold H20q then snap frozen in liquid nitrogen and stored at -80°C. Pellets were weighed on a precision scale and resuspended to reach equal densities. Cells were lysed with glass beads in ChIP lysis buffer 4x12s 6800rpm and left to rest 1mn on ice between each cycle. Tubes were pierced with a hot needle, lysate was recovered with a quick centrifugation and lysates were resuspended to 300ul and 30ul was recovered to check for DNA digestion pre-benzonase. Lysates were treated by adding 15ul of MgCl2 50mM, 500U Benzonase and 0.2mg of RNAse A and leaving 30mn on ice after a low speed vortex. 30ul of the lysate was recovered for post-benzonase

DNA digestion check and lysates were then centrifuged at 1000g at 4°C for 5mn. Supernatant was recovered, recentrifuged for 3mn using double spin technique.

30ul of the supernatant was kept as input (on ice) while the rest was incubated on wheel at 4°C for 1-2h with an antibody+bead mix (typically A111-22 with pA dynabeads)

IPs were then recovered, magnetized and washed 3x with 200ul of cold Lysis buffer. All traces of buffer were removed and then beads were incubated with 25ul of Laemmli Buffer 1x+Bmercaptoethanol and boiled for 5mn at 98°C. Tubes were centrifuged, magnetized and 20ul of supernatant was recovered to load on gel. Inputs received 10ul of Laemmli Buffer 4X with Bmercaptoethanol, boiled 5mn at 98°C and loaded on gels (typically 5ul of Input and 10 to 20ul of IPs). To reveal the signal after the final washes (see previous western blotting steps) membranes incubated with a secondary fluorescent antibody (Alexa fluor) were kept in PBS-T and revealed on a plastic sheet using the appropriate wavelength in the ECL machine (Bio-Rad ChemiDoc)

III/ Genomics

a/ ChIP-seq

Cells were fixed in 1% Formaldehyde final for 5mn at growth temperature (experiment-dependent) and 20mn at 19°C. Formaldehyde was quenched with 125mM Glycine final for 5mn at 19° before transferring the culture to cold 50ml Falcon tubes. Cells pellets were washed 2x with cold PBS 2mn 3000rpm 4° and 2.10^8 cells (for cnd2-GFP ChIP) or 1.10^8 cells (for histone ChIP) were aliquoted in Sarstedt tubes, centrifuged for 1mn 4°C 14,8krpm and supernant was removed. Traces of supernatant were eliminated by double spin. Pellets were snap frozen in liquid nitrogen and stored at -80°.

Cell pellets were resuspended in a mix of lysis buffer + SMC3-GFP s. cerevisae cells (LY6281). S. Cerevisae cells were fixed extemporaneously at either 1% (for RNAPIIS2P ChIP or histones) or 2.5% (psm3-GFP ChIP) in 10^8 pellets. 1/5 ratio of cerevisae to pombe cells was applied (i.e 2.10^7 cerevisae cells were added to 10^8 pombe cells). Fixed cells were lysed with Precellys 4x12s 6800rpm and left on ice with 1mn breaks. Lysates were recovered by piercing the bottom of the tube with a hot needle and centrifugating briefly in 5ml polypropylene tubes. Lysate was resuspended to 1ml and cells were sonicated with Covaris S220 with 140W, 200burst per cycle, Duty factor 5% ~7°C temperature for

either 18 or 15mn depending on the experiment. The lysates were then transferred to cold Costar tubes, clarified once by a 10mn 10krpm 4° centrifugation, the supernatant was transferred to a new Costar tube and clarified once more for 5mn 10krpm 4°. Supernatant was brought to 1mL final with lysis buffer and split into input/total sample and IP sample.

Protein A dynabeads (cat. 10002D, Invitrogen) and antibody at specific concentration. For cnd2-GFP we used 16ug A111-22 for 600ul chromatin of 2.10^8 pombe + 4.10^7 cerevisae. For histone ChIPs : 8ul (H2b) 39237 for 300ul of chromatin and 12ug (H3) ab1791 for 300ul of chromatin of 10^8 pombe + 2.10^7 cerevisae. For RNAPIIS2P, 8ug ab5095 (RNAPIIS2P) with 100ul M-280 sheep anti rabbit beads (Invitrogen 11203D) were incubated with 600ul chromatin of 2.10^8 pombe + 4.10^7 cerevisae. Bead/antibody mixes were incubated on a wheel at RT for ~1h before being split into IP samples. IPs were incubated on a wheel in a cold room (~5°C) and inputs in the cold room on a tube rack. The remaining chromatin was incubated with elution buffer (Tris, EDTA, protK) at 65°C overnight to control shearing.

The next morning (typically 14-17hrs) IPs were washed 3x with consecutive washing buffers I, II and III with 5mn incubation on a wheel at RT. IPs were then washed twice with TE pH8 with no incubation time, supernatant was completely removed and beads were incubated in elution buffer (SDS, Tris, EDTA) and inputs were brought to the same concentration of SDS/Tris/EDTA. Tubes were incubated at 65°C for 15mn at 1100 rpm on a eppimixer, supernatants were transferred to new Costar tubes and inputs were also transferred to new tubes.

Eluted complexes were then incubated 1h at 37° 1100rpm with 10ul of RNAseA, then received 20ul of protK for 5h at 1100rpm. DNA was recovered using Qiagen Quiackick PCR recovery kit (Ref 28106). In earlier versions of the ChIPseq protocol, DNA was recovered using Chelex resin. While we managed to perform qPCRs, quantify the DNA and produce libraries the sequencing tended to be extremely inefficient.

Antibodies

A111-22 (anti-GFP) ; RNAPIIS2P (ab 5095) ; H2B (ab 39237) ; H3 (ab 1791) ; IgGRabbit (I6006 Sigma)

b/ Hi-C

To perform Hi-C, cells were fixed with 3% formaldehyde for 5mn at growth temperature (experiment dependent) and 20mn at 19°C. Formaldehyde was quenched with 125mM Glycine for 5mn at 19°C and cells were transferred to cold Falcon 50ml tubes. Fixation at 1% or 0.5% were tested but produced noisy Hi-C libraries. Cell pellets were collected at 2.10^8 as for calChIPseq.

To process cells for Hi-C, pellets were first thawed on ice and resuspended in 200ul of Lysis Buffer. Cells were lysed by Precellys bead beating 4 x 12s at 6800 rpm with breaks of 1mn on ice. Lysates were collected in 5ml polypropylene tubes and transferred to Eppendorf DNA LoBind safelock tubes. Pellets were centrifuged 5mn 5000g 4°C and washed once in ~1ml of Lysis buffer and twice in ~1ml of NEB 3.1 1X buffer (NEB 3.1 or NEB r3.1 were used interchangeably with no obvious difference). Pellets were then resuspended in NEB r3.1 1X and the volume was adjusted to reach 360 ul (start by adding ~320ul then adjust if needed). 18ul were recovered as an input and 38ul of SDS 1% were added to the Hi-C tubes to reach .1% final. Tubes were gently homogenized with pipette and incubated 10mn at 65°C. Hi-C tubes were transferred to ice and SDS was quenched by adding 43ul of TX-100 10% and homogenized gently with pipette. 9.5 ul of NEB r3.1 10X (B6003S) was added to the Hi-C tubes, along with 4ul of 50U/ul DpnII enzyme (R0543M). Tubes were homogenized gently and overnight digestion was performed on an eppimixer 37°C at 400rpm for 30s every 4mn.

After digestion the next morning, 20ul were recovered as a DpnII control and replaced with 20ul of NEB r3.1 1X. DpnII was inactivated for 20mn at 65°C. Restriction sites were filled-in with biotinylated dATP and dNTP. 15 nmol of each dNTP and of biotin-14-dATP were added to the reaction with 50U of Klenow DNA Polymerase I (M0210M) and enough NEB r3.1 10X to bring the reaction to 1X (6ul). Fill-in was performed for 45mn at 900 rpm for 10s every 4mn, and tubes were inverted every 15mn. Biotin-14-dATP was provided by either Invitrogen (19524016) or JENA Biosciences (NU-835-BIO14-L). Both were tested and yielded similar outputs, although we underline that JENA is commercially much more competitive with better pricing and purity.

Hi-C reactions were then ligated. Earlier versions of our protocol used diluted conditions : in 8ml of T4 DNA Ligase 1x buffer, 20ul of T4 DNA Ligase (M0202L) at 16°C for 8hrs in a cold room, inverting tubes every 2hrs. We then switched to a different protocol, where ligation was performed in 1ml, with

5ul of T4 DNA ligase at 25°C for 4hrs (tubes inverted every hour). The switch from diluted to 'in-situ' Hi-C showed little difference on the output.

In both cases, Hi-C reactions were then decrosslinked with .125 mg/mL proteinase K and SDS ~1% final for 2hrs at 65°C. The same amount of proteinase K was added again and tubes were left overnight at 65°C. In diluted conditions, Hi-C ligation and decrosslink were performed in Falcon tubes 50 mL.

The next morning, samples were cooled to RT. For diluted conditions, 8ml of phenyl-chloroform-isoamyl alcohol were added and Falcon tubes were shaken by hand for 3-4 min after covering caps with parafilm. Tubes were centrifuged in X3R centrifuge at 1500g for 5mn, 8ml of the aqueous phase was recovered and another round of PCI with 8ml was performed. After this second round, 7ml of the aqueous phase was recovered, added to 10 ml 2-propanol 2.6ml H20q 400ul NaCL5M and 5ul glycogen. The tube was homogenized and left at -20°C to precipitate for 2hrs. Falcon tubes were centrifuged 30mn 4°C 13000rpm X3R rotor. Supernatant was removed, another 15mn centrifuged was performed to remove traces of 2-propanol and pellet was carefully resuspended in 1.5 mL H2Oq. The resuspended pellet was transferred to a 15mL Falcon tube and a final round of PCI was performed. Aqueous phase was split in 2x 700 ul in DNA LoBind Eppendorf tubes and received 700ul 2-propanol and 70 ul NaOAC pH 5.2. Tubes were homogenized and left at -20°C for 2hrs or overnight. Tubes were then centrifuged at 4°C for 30 mn 14.8k rpm, supernatant was removed, pellets were washed with 1mL EtOH 70%, recentrifuged 10mn at 4°C and EtOH was completely removed, and pellets left to air dry at 37°C. Pellets were resuspended in 500ul TLE and pooled in an Amicon column 30K. Columns were washed three times with TLE using RT benchtop centrifuged and the remaining volume in Amicon columns was eluted by inverting on a collecting tube and transferred to an Eppendorf DNA LoBind safelock tube.

For non-diluted conditions, Phase Lock Heavy 2 ml tubes (QuantaBio 2302830) were spun down for 30s at max speed on a benchtop centrifuge. Hi-C reactions were split 2x500ul in PLG tubes and received an equal volume of PCI. Tubes where shaken by hand for 2mn, centrifuged 14krpm 10mn under the hood and 450ul of aqueous phase were recovered, pooled in 2mL DNA LoBind Safelock ependorf tubes containing 1ml 2-propanol, 60ul H2Oq and 40 ul NaCl 5M. Tubes were homogenized

and left at -20°C for 2hrs or overnight. Tubes were centrifuged 14.8krpm 30mn at 4°C, washed with 1ml EtOH 70%, centrifuged another 10mn at 4°C and EtOH was completely removed and pellets were left to air dry at 37°C. Pellets were carefully resuspended in 500ul TLE, transferred to an Amicon 30K column and washed three times with TLE with benchtop centrifuged. The remaining volume in the column was eluted ina collecting tube and transferred to an Eppendorf DNA LoBind safelock tube.

Hi-C reactions were adjusted to 100ul of volume and treated with 1ul of RNAse A 10mg/ml (EN0531) for 30mn 37°C.

Biotin was removed from unligated ends with 1X NEB 2.1 final 3nmol dATP & dGTP, 36U T4 DNA polymerase (NEB M0203L) for 4hrs at 20°C on a PCR block and inactivated for 20mn at 75°C. DNA was cleaned 2x with mq H2O on an Amicon column 30K (UFC 503096) and libraries were sonicated in a covaris micro tube either 4mn 20°C Df 10% 175W 200bpc or 80s 20°C Df 10% 200 bpc 175W. Later on the protocol was changed to generate larger fragment size (relative to sequencing conditions of 150bp PE) :

End repair was performed in 1X T4 DNA ligation buffer with 37.5 nmol dNTPs 16.2U T4 DNA polymerase 54U T4 polynucleotide kinase 5.5 U (M0201L) DNA polymerase Klenow I (M0210L) in a PCR block for 30mn at 20°C and inactivated for 20mn at 75°C.

Reactions were adjusted with Binding Buffer 1X final and incubated with 10ul of Streptavidin MyOne C1 Beads (Invitrogen 65001). Beads + Hi-C reactions were incubated for 15mn at RT on a rotating wheel. Beads were magnetized for 1mn, washed 1x with 1X Binding Buffer and transferred to new Costar Low binding tubes. Beads were magnetized and washed twice with TLE and transferred to new Costar tubes. Beads were resuspended in 41ul final and transferred to new Costar tubes. Ends were A-tailed with 10nmol dATP, 1X NEB 2.1X final and 15U Klenow 3'->5' exo- (M0212L) in a PCR block for 30mn at 37°C and inactivated at 65°C for 20mn. Hi-C were transferred to Costar tubes and washed in 1X ligation buffer (Invitrogen 46300018), magnetized, resuspended in 40 ul of 1X ligation buffer. Adapters were ligated in 1X T4 ligation buffer with 3ul of 25uM adapters (Nextflex NOVA-5141012) and 3U of T4 DNA ligase (Invitrogen 15224017).

Ligation was performed in a costar tube at 22°C 300rpm. A low-speed vortex was performed after 1h to resuspend the beads and reaction was left 2hrs total. Beads were magnetized, and washed twice with Tween Wash Buffer on a rotating wheel for 5mn at RT. Magnetized, resuspended in 1X 200 ul Binding Buffer and transferred to a new Costar tube. Beads were washed twice with 200 ul TLE, transferred to a new Costar and resuspended in 10ul TLE. To each Hi-C reaction, 110 H2OQ, 6.7ul primers and 40ul 2X mastermix (Nextflex NOVA-5140-08) were added. Reactions were homogenized and split in 4x PCR tubes and subjected to amplification for 5 cycles.

PCR reactions were pooled and adjusted to 200ul TLE final. 220 ul Ampure XP beads (Beckman Coulter A63881) was added to the reactions. Beads were vortexed and incubated for 10mn at RT, magnetized for 5mn. Supernatant was removed, washed 2x with fresh 1ml EtOH70% and air dried 10mn at RT. Beads were resuspended in 200ul of TLE at 65°C, vortexed and another 220 ul AMpure XP were added, incubated 10mn at RT, 5mn on magnet. Beads were washed 2x with 1ml EtOH 70% air dried ~10mn RT and eluted with ~45ul TLE 65°C. Supernatant was recovered and stored in Eppendorf DNA LoBind Safelock tubes (Eppendorf 022431021).

c/ MNase

Cells were fixed with 0.5% formaldehyde final 5mn at growth temperature and 20mn at 19°C, then quenched for 5mn with Glycine 125mM. Cells were recovered in cold Falcon tubes 50 mL, washed twice with cold H2Oq. Cell pellets of 10^9 were aliquoted and snap frozen in liquid nitrogen.

Cells were thawed on ice and incubated in 30°C warm Pre-incubation buffer supplemented with Bmercaptoethanol and left for 10mn in a shaking water bath 30°C 200rpm. Cells were pelleted at RT 2mn 3000rpm X3R centrifuge and supernatant was removed. Cells were resuspended in 30°C warm SORB/TRIS buffer, received 3.5ul of Bmercaptoethanol and resuspended in Sorb/Tris buffer with 5mg Zymoliase 100T (Nacalai Tesque) per sample. Cells were cheked for lysis at t=18mn and digestion was quenched on ice for 2/3mn. Tubes were centrifuged 2500 rpm 2mn at 4°C. Supernatant was removed and cells were washed with cold SORB/TRIS buffer without Bmercaptoethanol by low-speed vortexing. Cells were centrifuged at 2500 rpm for 2mn at 4°C. Supernatant was removed and cells were resuspended in cold 1.75 ml of NP-Buffer with betamercaptoethanol and split in 3 x 500 ul

fractions in prepared MNase tubes, containing NP-buffer with 0, 50 or 200U of MNase. Tubes were incubated 5mn at 37°C and quenched by adding 125ul of STOP buffer and moving to ice for 5mn.

16ul of RNAse A .8mg/ml was added, mixed gently by pipetting and incubated 30mn at 37°C, 60ul of proteinase K 10mg/ml were added and incubated overnight at 65°C.

The next day, 330ul of NH4-acetate were added, tubes were vortexed and received 1ml of PCI, vortexed for 20s and centrifuged 14krpm 10mn RT. 750ul of aqueous phase was recovered, 2ul of glycogen was added. Tubes were reversed 10 times, incubated 30mn at -80°C and centrifuged 30mn 4°C 14,8krpm. Supernatant was removed, pellet was washed twice with 1ml ETOH 70%, centrifuged and traces of ethanol were removed before air-drying 5mn at 37°C. DNA was resuspended in 30ul TE buffer with 1ul RNAse A 10mg/ml and incubated 30mn at 37°C with shaking to dissolve DNA and remove all RNA.

MNase digestions were run on a large gels 2h 120V and mononucleosome bands and 0 digest bands were cut out with a sterile razor blade. DNA was extracted from the gel using Biorad Freeze and squeeze. A gel slice was placed in a column, columns were placed 5mn at -20°C and centrifuged 3mn at RT 13000rpm. The liquid was resupended to 500ul Tris 1M pH8 and DNA was passed through an Amicon column 10K, and washed once with 500 ul Tris 1M pH8. Remaining volume was inverted onto a collecting tube and transferred to a new DNA Lobind tube.

d/ Library prep

ChIPseq libraries and MNase-seq libraries were prepared using NEB Ultra DNA Prep II Library Kit (E7645S) with associated barcodes (E6609S). Typically for histones 8 cycles were used, for cnd2-GFP ChIP 11-12 cycles were used.

Hi-C libraries were prepared in house with separate reagents, barcodes used were Nextflex DNA Barcodes and amplification was performed with Nextflex PCR Master Mix (see Hi-C section)

e/Sequencing

For all genomic libraries Novogene performed the sequencing. Sequencing was performed on Novaseq6000 using 150 PE. For Hi-C 12G of data, for ChIPseq, 6G for IPs and 3G for Inputs, for Mnase 6G of data were ordered. 20ul library samples were sent at a concentration >0.5ng/ul.

f/ Data analysis

For calibrated ChIP-seq and MNase-seq reads were processed through a nf-core derived pipeline (Part 6) to normalize the calChIPseq data, while MNase-seq does not need normalization. To produce views of genomic loci, we used Integrative Genomics Viewer (igv). To produce metagene plots and heatmaps from calChIPseq data we used deepTools **(Ramírez et al., 2016)**. For Hi-C data analysis we used hicstuff **(Matthey-Doret et al., 2020)** to produce matrices and contact probabilities. To visualize specific genomic segments we used cooltools **(Open2C et al., 2022)** or hicstuff.

IV/ Buffer solutions & reagent references

a/ Growth Media

b/ Buffers used

TE 8

10mM Tris-HCl 1mM EDTA

TLE 8

10mM Tris-HCl, 0,1mM EDTA

Lysis buffer (cal-ChIPseq, coIP)

50 mM Hepes-KOH pH 7,5 ; 140 mM NaCl, 1 mM EDTA, 1% (v/v) Triton X-100, 0,1 % (w/v) sodium deoxycholate. 1mM PMSF and 1 tablet proteinase free cat.11836170001, Roche per 20 ml of buffer, both added just prior to the lysis.

Wash buffer I, II, III (cal-ChIPseq)

WI (Tris-HCl pH8 20 mM, NaCl 150 mM, EDTA 2 mM, Triton X-100 1%, SDS 0.1%)

WII (Tris-HCl pH8 20 mM, NaCl 500 mM, EDTA 2 mM, Triton X-100 1%, SDS 0.1%)

WIII (Tris-HCl pH8 10 mM, sodium deoxycholate 0.5%, EDTA 1 mM, Igepal 1%, LiCl 250 mM)

Tween Wash Buffer (Hi-C)

5 mM Tris-HCl (pH=8.0), 0.5mM EDTA, 1M NaCl, 0.05% Tween

Binding Buffer (Hi-C)

For 2X BB buffer : 10 mM Tris-HCl (pH=8.0), 1mM EDTA, 2M NaCl

Elution buffer (calCHIP-seq shearing)

For 2X elution buffer shearing : Tris HCl pH 8 40 mM, EDTA 20 mM, SDS 2%

Elution buffer (calChIPseq IP/Input)

For IP : 50mM Tris, 10mM EDTA, 1% SDS

For Input : 50mM Tris, 10mM EDTA, 10% SDS

Sorb/Tris buffer (MNase)

1M sorbitol, 50 mM Tris/HCl pH7.4. Sterilize 110°C/30 min. Store at RT.

Pre-Incubation buffer (MNase)

20 mM citric acid, 20 mM Na_2HPO_4, 40 mM EDTA pH 8. Sterilize 110°C/30 min. Store at RT. Add extemporaneously β-mercaptoethanol 30 mM final concentration (stock solution 14 M, SIGMA M3148).

NP-buffer (MNase)

1M sorbitol, 50 mM NaCl, 10 mM Tris/HCl pH7.4, 5 mM $MgCl_2$, 1 mM $CaCl_2$, 0.75% (v/v) IGEPAL. Store at -20°C. Add freshly before use 1 mM β-mercaptoethanol [and 0.5 mM spermidine (Sigma S0266)].

STOP buffer (MNase)

5% SDS, 100 mM EDTA pH8.

Part 9 – FINAL REMARKS & CONCLUSIONS

References

Abramo K, Valton A-L, Venev SV, Ozadam H, Fox AN, Dekker J. 2019. A chromosome folding intermediate at the condensin-to-cohesin transition during telophase. *Nat Cell Biol* **21**:1393–1402. doi:10.1038/s41556-019-0406-2

Achar YJ, Adhil M, Choudhary R, Gilbert N, Foiani M. 2020. Negative supercoil at gene boundaries modulates gene topology. *Nature* **577**:701–705. doi:10.1038/s41586-020-1934-4

Akai Y, Kurokawa Y, Nakazawa N, Tonami-Murakami Y, Suzuki Y, Yoshimura SH, Iwasaki H, Shiroiwa Y, Nakamura T, Shibata E, Yanagida M. 2011. Opposing role of condensin hinge against replication protein A in mitosis and interphase through promoting DNA annealing. *Open Biol* **1**:110023. doi:10.1098/rsob.110023

Alexander AK, Rice EJ, Lujic J, Simon LE, Tanis S, Barshad G, Zhu L, Lama J, Cohen PE, Danko CG. 2023. A-MYB and BRDT-dependent RNA Polymerase II pause release orchestrates transcriptional regulation in mammalian meiosis. *Nat Commun* **14**:1753. doi:10.1038/s41467-023-37408-w

Allan J, Harborne N, Rau DC, Gould H. 1982. Participation of core histone "tails" in the stabilization of the chromatin solenoid. *J Cell Biol* **93**:285–297. doi:10.1083/jcb.93.2.285

Allshire RC, Madhani HD. 2018. Ten principles of heterochromatin formation and function. *Nat Rev Mol Cell Biol* **19**:229–244. doi:10.1038/nrm.2017.119

Alonso-Gil D, Losada A. 2023. NIPBL and cohesin: new take on a classic tale. *Trends Cell Biol* S0962-8924(23)00047–8. doi:10.1016/j.tcb.2023.03.006

Ammar R, Torti D, Tsui K, Gebbia M, Durbic T, Bader GD, Giaever G, Nislow C. 2012. Chromatin is an ancient innovation conserved between Archaea and Eukarya. *eLife* **1**:e00078. doi:10.7554/eLife.00078

Aoi Y, Kawashima SA, Simanis V, Yamamoto M, Sato M. 2014. Optimization of the analogue-sensitive Cdc2/Cdk1 mutant by in vivo selection eliminates physiological limitations to its use in cell cycle analysis. *Open Biol* **4**:140063. doi:10.1098/rsob.140063

Aono N, Sutani T, Tomonaga T, Mochida S, Yanagida M. 2002. Cnd2 has dual roles in mitotic condensation and interphase. *Nature* **417**:197–202. doi:10.1038/417197a

Arimura Y, Shih RM, Froom R, Funabiki H. 2021. Structural features of nucleosomes in interphase and metaphase chromosomes. *Mol Cell* **81**:4377-4397.e12. doi:10.1016/j.molcel.2021.08.010

Arimura Y, Tachiwana H, Oda T, Sato M, Kurumizaka H. 2012. Structural analysis of the hexasome, lacking one histone H2A/H2B dimer from the conventional nucleosome. *Biochemistry* **51**:3302–3309. doi:10.1021/bi300129b

Armstrong CA, Tomita K. 2017. Fundamental mechanisms of telomerase action in yeasts and mammals: understanding telomeres and telomerase in cancer cells. *Open Biology* **7**:160338. doi:10.1098/rsob.160338

Azarm K, Bhardwaj A, Kim E, Smith S. 2020. Persistent telomere cohesion protects aged cells from premature senescence. *Nat Commun* **11**:3321. doi:10.1038/s41467-020-17133-4

Bailey MLP, Surovtsev I, Williams JF, Yan H, Yuan T, Li K, Duseau K, Mochrie SGJ, King MC. 2023. Loops and the activity of loop extrusion factors constrain chromatin dynamics. *MBoC* **34**:ar78. doi:10.1091/mbc.E23-04-0119

Bancaud A, Conde e Silva N, Barbi M, Wagner G, Allemand J-F, Mozziconacci J, Lavelle C, Croquette V, Victor J-M, Prunell A, Viovy J-L. 2006. Structural plasticity of single chromatin fibers revealed by torsional manipulation. *Nature Structural & Molecular Biology* **13**:444–450. doi:10.1038/nsmb1087

Banigan EJ, Mirny LA. 2020. The interplay between asymmetric and symmetric DNA loop extrusion. *eLife* **9**:e63528. doi:10.7554/eLife.63528

Banigan EJ, Tang W, van den Berg AA, Stocsits RR, Wutz G, Brandão HB, Busslinger GA, Peters J-M, Mirny LA. 2023. Transcription shapes 3D chromatin organization by interacting with loop extrusion. *Proc Natl Acad Sci U S A* **120**:e2210480120. doi:10.1073/pnas.2210480120

Bannister AJ, Zegerman P, Partridge JF, Miska EA, Thomas JO, Allshire RC, Kouzarides T. 2001. Selective recognition of methylated lysine 9 on histone H3 by the HP1 chromo domain. *Nature* **410**:120–124. doi:10.1038/35065138

Barrows JK, Long DT. 2019. Cell-free transcription in Xenopus egg extract. *J Biol Chem* **294**:19645–19654. doi:10.1074/jbc.RA119.011350

Bastié N, Chapard C, Nejmi S, Mboumba H, Thierry A, Beckouët F, Koszul R. 2023. Sister chromatid cohesion halts DNA loop expansion. doi:10.1101/2023.07.31.551217

Basu A, Bobrovnikov DG, Qureshi Z, Kayikcioglu T, Ngo TTM, Ranjan A, Eustermann S, Cieza B, Morgan MT, Hejna M, Rube HT, Hopfner K-P, Wolberger C, Song JS, Ha T. 2021. Measuring DNA mechanics on the genome scale. *Nature* **589**:462–467. doi:10.1038/s41586-020-03052-3

Batty P, Langer CC, Takács Z, Tang W, Blaukopf C, Peters J-M, Gerlich DW. 2023. Cohesin-mediated DNA loop extrusion resolves sister chromatids in G2 phase. *EMBO J* e113475. doi:10.15252/embj.2023113475

Bauer BW, Davidson IF, Canena D, Wutz G, Tang W, Litos G, Horn S, Hinterdorfer P, Peters J-M. 2021. Cohesin mediates DNA loop extrusion by a "swing and clamp" mechanism. *Cell* **184**:5448-5464.e22. doi:10.1016/j.cell.2021.09.016

Bauer CR, Hartl TA, Bosco G. 2012. Condensin II Promotes the Formation of Chromosome Territories by Inducing Axial Compaction of Polyploid Interphase Chromosomes. *PLoS Genet* **8**:e1002873. doi:10.1371/journal.pgen.1002873

Baxter J, Diffley JFX. 2008. Topoisomerase II Inactivation Prevents the Completion of DNA Replication in Budding Yeast. *Molecular Cell* **30**:790–802. doi:10.1016/j.molcel.2008.04.019

Baxter J, Sen N, Martínez VL, De Carandini MEM, Schvartzman JB, Diffley JFX, Aragón L. 2011. Positive supercoiling of mitotic DNA drives decatenation by topoisomerase II in eukaryotes. *Science* **331**:1328–1332. doi:10.1126/science.1201538

Bazett-Jones DP, Kimura K, Hirano T. 2002. Efficient supercoiling of DNA by a single condensin complex as revealed by electron spectroscopic imaging. *Mol Cell* **9**:1183–1190.

Bednar J, Furrer P, Katritch V, Stasiak Alicja, Dubochet J, Stasiak Andrzej. 1995. Determination of DNA Persistence Length by Cryo-electron Microscopy. Separation of the Static and Dynamic Contributions to the Apparent Persistence Length of DNA. *Journal of Molecular Biology* **254**:579–594. doi:10.1006/jmbi.1995.0640

Beel AJ, Azubel M, Matteï P-J, Kornberg RD. 2021. Structure of Mitotic Chromosomes. *Mol Cell* **81**:4369-4376.e3. doi:10.1016/j.molcel.2021.08.020

Belotserkovskaya R, Oh S, Bondarenko VA, Orphanides G, Studitsky VM, Reinberg D. 2003. FACT facilitates transcription-dependent nucleosome alteration. *Science* **301**:1090–1093. doi:10.1126/science.1085703

Bernard P, Schmidt CK, Vaur S, Dheur S, Drogat J, Genier S, Ekwall K, Uhlmann F, Javerzat J-P. 2008. Cell-cycle regulation of cohesin stability along fission yeast chromosomes. *EMBO J* **27**:111–121. doi:10.1038/sj.emboj.7601955

Bhalla N, Biggins S, Murray AW. 2002. Mutation of YCS4, a Budding Yeast Condensin Subunit, Affects Mitotic and Nonmitotic Chromosome Behavior. *Mol Biol Cell* **13**:632–645. doi:10.1091/mbc.01-05-0264

Biggs R, Liu PZ, Stephens AD, Marko JF. 2019. Effects of altering histone posttranslational modifications on mitotic chromosome structure and mechanics. *MBoC* **30**:820–827. doi:10.1091/mbc.E18-09-0592

Bilokapic S, Strauss M, Halic M. 2018. Histone octamer rearranges to adapt to DNA unwrapping. *Nat Struct Mol Biol* **25**:101–108. doi:10.1038/s41594-017-0005-5

Bintu B, Mateo LJ, Su J-H, Sinnott-Armstrong NA, Parker M, Kinrot S, Yamaya K, Boettiger AN, Zhuang X. 2018. Super-resolution chromatin tracing reveals domains and cooperative interactions in single cells. *Science* **362**:eaau1783. doi:10.1126/science.aau1783

Bisht KK, Daniloski Z, Smith S. 2013. SA1 binds directly to DNA through its unique AT-hook to promote sister chromatid cohesion at telomeres. *J Cell Sci* **126**:3493–3503. doi:10.1242/jcs.130872

Boeger H, Griesenbeck J, Strattan JS, Kornberg RD. 2003. Nucleosomes Unfold Completely at a Transcriptionally Active Promoter. *Molecular Cell* **11**:1587–1598. doi:10.1016/S1097-2765(03)00231-4

Booth DG, Beckett AJ, Molina O, Samejima I, Masumoto H, Kouprina N, Larionov V, Prior IA, Earnshaw WC. 2016. 3D-CLEM Reveals that a Major Portion of Mitotic Chromosomes Is Not Chromatin. *Molecular Cell* **64**:790–802. doi:10.1016/j.molcel.2016.10.009

Brahmachari S, Marko JF. 2019. Chromosome disentanglement driven via optimal compaction of loop-extruded brush structures. *Proceedings of the National Academy of Sciences* **116**:24956–24965. doi:10.1073/pnas.1906355116

Branco MR, Pombo A. 2006. Intermingling of chromosome territories in interphase suggests role in translocations and transcription-dependent associations. *PLoS Biol* **4**:e138. doi:10.1371/journal.pbio.0040138

Brandão HB, Paul P, van den Berg AA, Rudner DZ, Wang X, Mirny LA. 2019. RNA polymerases as moving barriers to condensin loop extrusion. *Proc Natl Acad Sci U S A* **116**:20489–20499. doi:10.1073/pnas.1907009116

Brandão HB, Ren Z, Karaboja X, Mirny LA, Wang X. 2021. DNA-loop-extruding SMC complexes can traverse one another in vivo. *Nat Struct Mol Biol* **28**:642–651. doi:10.1038/s41594-021-00626-1

Bürmann F, Basfeld A, Vazquez Nunez R, Diebold-Durand M-L, Wilhelm L, Gruber S. 2017. Tuned SMC Arms Drive Chromosomal Loading of Prokaryotic Condensin. *Mol Cell* **65**:861-872.e9. doi:10.1016/j.molcel.2017.01.026

Bürmann F, Funke LFH, Chin JW, Löwe J. 2021. Cryo-EM structure of MukBEF reveals DNA loop entrapment at chromosomal unloading sites. *Mol Cell* **81**:4891-4906.e8. doi:10.1016/j.molcel.2021.10.011

Burns KH, Viveiros MM, Ren Y, Wang P, DeMayo FJ, Frail DE, Eppig JJ, Matzuk MM. 2003. Roles of NPM2 in chromatin and nucleolar organization in oocytes and embryos. *Science* **300**:633–636. doi:10.1126/science.1081813

Busslinger GA, Stocsits RR, van der Lelij P, Axelsson E, Tedeschi A, Galjart N, Peters J-M. 2017a. Cohesin is positioned in mammalian genomes by transcription, CTCF and Wapl. *Nature* **544**:503–507. doi:10.1038/nature22063

Busslinger GA, Stocsits RR, van der Lelij P, Axelsson E, Tedeschi A, Galjart N, Peters J-M. 2017b. Cohesin is positioned in mammalian genomes by transcription, CTCF and Wapl. *Nature* **544**:503–507. doi:10.1038/nature22063

Cai S, Böck D, Pilhofer M, Gan L. 2018a. The in situ structures of mono-, di-, and trinucleosomes in human heterochromatin. *Mol Biol Cell* **29**:2450–2457. doi:10.1091/mbc.E18-05-0331

Cai S, Chen C, Tan ZY, Huang Y, Shi J, Gan L. 2018b. Cryo-ET reveals the macromolecular reorganization of S. pombe mitotic chromosomes in vivo. *Proc Natl Acad Sci U S A* **115**:10977–10982. doi:10.1073/pnas.1720476115

Canudas S, Houghtaling BR, Kim JY, Dynek JN, Chang WG, Smith S. 2007. Protein requirements for sister telomere association in human cells. *EMBO J* **26**:4867–4878. doi:10.1038/sj.emboj.7601903

Carrozza MJ, Li B, Florens L, Suganuma T, Swanson SK, Lee KK, Shia W-J, Anderson S, Yates J, Washburn MP, Workman JL. 2005. Histone H3 methylation by Set2 directs deacetylation of coding regions by Rpd3S to suppress spurious intragenic transcription. *Cell* **123**:581–592. doi:10.1016/j.cell.2005.10.023

Chan FL, Marshall OJ, Saffery R, Won Kim B, Earle E, Choo KHA, Wong LH. 2012. Active transcription and essential role of RNA polymerase II at the centromere during mitosis. *Proceedings of the National Academy of Sciences* **109**:1979–1984. doi:10.1073/pnas.1108705109

Charbin A, Bouchoux C, Uhlmann F. 2014. Condensin aids sister chromatid decatenation by topoisomerase II. *Nucleic Acids Res* **42**:340–348. doi:10.1093/nar/gkt882

Chen CCL, Goyal P, Karimi MM, Abildgaard MH, Kimura H, Lorincz MC. 2018. H3S10ph broadly marks early-replicating domains in interphase ESCs and shows reciprocal antagonism with H3K9me2. *Genome Res* **28**:37–51. doi:10.1101/gr.224717.117

Chen D, Hinkley CS, Henry RW, Huang S. 2002. TBP dynamics in living human cells: constitutive association of TBP with mitotic chromosomes. *Mol Biol Cell* **13**:276–284. doi:10.1091/mbc.01-10-0523

Chen Y, Tokuda JM, Topping T, Meisburger SP, Pabit SA, Gloss LM, Pollack L. 2017. Asymmetric unwrapping of nucleosomal DNA propagates asymmetric opening and dissociation of the histone core. *Proceedings of the National Academy of Sciences* **114**:334–339. doi:10.1073/pnas.1611118114

Cheng TMK, Heeger S, Chaleil RAG, Matthews N, Stewart A, Wright J, Lim C, Bates PA, Uhlmann F. 2015. A simple biophysical model emulates budding yeast chromosome condensation. *Elife* **4**:e05565. doi:10.7554/eLife.05565

Chereji RV, Bryson TD, Henikoff S. 2019. Quantitative MNase-seq accurately maps nucleosome occupancy levels. *Genome Biology* **20**:198. doi:10.1186/s13059-019-1815-z

Choi E-H, Yoon S, Koh YE, Hong TK, Do JT, Lee B-K, Hahn Y, Kim KP. 2022. Meiosis-specific cohesin complexes display essential and distinct roles in mitotic embryonic stem cell chromosomes. *Genome Biol* **23**:70. doi:10.1186/s13059-022-02632-y

Choppakatla P, Dekker B, Cutts EE, Vannini A, Dekker J, Funabiki H. 2021. Linker histone H1.8 inhibits chromatin binding of condensins and DNA topoisomerase II to tune chromosome length and individualization. *Elife* **10**:e68918. doi:10.7554/eLife.68918

Chu L, Liang Z, Mukhina M, Fisher J, Vincenten N, Zhang Z, Hutchinson J, Zickler D, Kleckner N. 2020a. The 3D Topography of Mitotic Chromosomes. *Mol Cell* **79**:902-916.e6. doi:10.1016/j.molcel.2020.07.002

Chu L, Liang Z, Mukhina MV, Fisher JK, Hutchinson JW, Kleckner NE. 2020b. One-dimensional spatial patterning along mitotic chromosomes: A mechanical basis for macroscopic morphogenesis. *Proc Natl Acad Sci U S A* **117**:26749–26755. doi:10.1073/pnas.2013709117

Chu L, Zhang Z, Mukhina M, Zickler D, Kleckner N. 2022. Sister chromatids separate during anaphase in a three-stage program as directed by interaxis bridges. *Proc Natl Acad Sci U S A* **119**:e2123363119. doi:10.1073/pnas.2123363119

Cimini D, Mattiuzzo M, Torosantucci L, Degrassi F. 2003. Histone hyperacetylation in mitosis prevents sister chromatid separation and produces chromosome segregation defects. *Mol Biol Cell* **14**:3821–3833. doi:10.1091/mbc.e03-01-0860

Citarelli M, Teotia S, Lamb RS. 2010. Evolutionary history of the poly(ADP-ribose) polymerase gene family in eukaryotes. *BMC Evolutionary Biology* **10**:308. doi:10.1186/1471-2148-10-308

Clapier CR, Iwasa J, Cairns BR, Peterson CL. 2017. Mechanisms of action and regulation of ATP-dependent chromatin-remodelling complexes. *Nat Rev Mol Cell Biol* **18**:407–422. doi:10.1038/nrm.2017.26

Clemente-Blanco A, Mayán-Santo M, Schneider DA, Machín F, Jarmuz A, Tschochner H, Aragón L. 2009. Cdc14 inhibits transcription by RNA polymerase I during anaphase. *Nature* **458**:219–222. doi:10.1038/nature07652

Cockram C, Thierry A, Gorlas A, Lestini R, Koszul R. 2021. Euryarchaeal genomes are folded into SMC-dependent loops and domains, but lack transcription-mediated compartmentalization. *Molecular Cell* **81**:459-472.e10. doi:10.1016/j.molcel.2020.12.013

Costantino L, Hsieh T-HS, Lamothe R, Darzacq X, Koshland D. 2020. Cohesin residency determines chromatin loop patterns. *eLife* **9**:e59889. doi:10.7554/eLife.59889

Cramer P, Bushnell DA, Fu J, Gnatt AL, Maier-Davis B, Thompson NE, Burgess RR, Edwards AM, David PR, Kornberg RD. 2000. Architecture of RNA polymerase II and implications for the transcription mechanism. *Science* **288**:640–649. doi:10.1126/science.288.5466.640

Creamer KM, Job G, Shanker S, Neale GA, Lin Y, Bartholomew B, Partridge JF. 2014. The Mi-2 Homolog Mit1 Actively Positions Nucleosomes within Heterochromatin To Suppress Transcription. *Mol Cell Biol* **34**:2046–2061. doi:10.1128/MCB.01609-13

Croft JA, Bridger JM, Boyle S, Perry P, Teague P, Bickmore WA. 1999. Differences in the Localization and Morphology of Chromosomes in the Human Nucleus. *J Cell Biol* **145**:1119–1131.

Csankovszki G, Collette K, Spahl K, Carey J, Snyder M, Petty E, Patel U, Tabuchi T, Liu H, McLeod I, Thompson J, Sarkeshik A, Yates J, Meyer BJ, Hagstrom K. 2009. Three distinct condensin complexes control C. elegans chromosome dynamics. *Curr Biol* **19**:9–19. doi:10.1016/j.cub.2008.12.006

Cuvier O, Hirano T. 2003. A role of topoisomerase II in linking DNA replication to chromosome condensation. *J Cell Biol* **160**:645–655. doi:10.1083/jcb.200209023

Cuylen S, Blaukopf C, Politi AZ, Müller-Reichert T, Neumann B, Poser I, Ellenberg J, Hyman AA, Gerlich DW. 2016. Ki-67 acts as a biological surfactant to disperse mitotic chromosomes. *Nature* **535**:308–312. doi:10.1038/nature18610

Cuylen S, Metz J, Haering CH. 2011. Condensin structures chromosomal DNA through topological links. *Nat Struct Mol Biol* **18**:894–901. doi:10.1038/nsmb.2087

Cuylen S, Metz J, Hruby A, Haering CH. 2013. Entrapment of Chromosomes by Condensin Rings Prevents Their Breakage during Cytokinesis. *Developmental Cell* **27**:469–478. doi:10.1016/j.devcel.2013.10.018

D'Ambrosio C, Kelly G, Shirahige K, Uhlmann F. 2008a. Condensin-Dependent rDNA Decatenation Introduces a Temporal Pattern to Chromosome Segregation. *Current Biology* **18**:1084–1089. doi:10.1016/j.cub.2008.06.058

D'Ambrosio C, Schmidt CK, Katou Y, Kelly G, Itoh T, Shirahige K, Uhlmann F. 2008b. Identification of cis-acting sites for condensin loading onto budding yeast chromosomes. *Genes Dev* **22**:2215–2227. doi:10.1101/gad.1675708

Daniloski Z, Bisht KK, McStay B, Smith S. 2019. Resolution of human ribosomal DNA occurs in anaphase, dependent on tankyrase 1, condensin II, and topoisomerase IIα. *Genes Dev* **33**:276–281. doi:10.1101/gad.321836.118

Dauban L, Montagne R, Thierry A, Lazar-Stefanita L, Bastié N, Gadal O, Cournac A, Koszul R, Beckouët F. 2020. Regulation of Cohesin-Mediated Chromosome Folding by Eco1 and Other Partners. *Mol Cell* **77**:1279-1293.e4. doi:10.1016/j.molcel.2020.01.019

Davey CA, Sargent DF, Luger K, Maeder AW, Richmond TJ. 2002. Solvent Mediated Interactions in the Structure of the Nucleosome Core Particle at 1.9Å Resolution††We dedicate this paper to the memory of Max Perutz who was particularly inspirational and supportive to T.J.R. in the early stages of this study. *Journal of Molecular Biology* **319**:1097–1113. doi:10.1016/S0022-2836(02)00386-8

Davidson IF, Barth R, Zaczek M, van der Torre J, Tang W, Nagasaka K, Janissen R, Kerssemakers J, Wutz G, Dekker C, Peters J-M. 2023. CTCF is a DNA-tension-dependent barrier to cohesin-mediated loop extrusion. *Nature* **616**:822–827. doi:10.1038/s41586-023-05961-5

Davidson IF, Bauer B, Goetz D, Tang W, Wutz G, Peters J-M. 2019. DNA loop extrusion by human cohesin. *Science* **366**:1338–1345. doi:10.1126/science.aaz3418

Davidson IF, Goetz D, Zaczek MP, Molodtsov MI, Huis In 't Veld PJ, Weissmann F, Litos G, Cisneros DA, Ocampo-Hafalla M, Ladurner R, Uhlmann F, Vaziri A, Peters J-M. 2016. Rapid movement and transcriptional re-localization of human cohesin on DNA. *EMBO J* **35**:2671–2685. doi:10.15252/embj.201695402

de la Tour EB, Laemmli UK. 1988. The metaphase scaffold is helically folded: Sister chromatids have predominantly opposite helical handedness. *Cell* **55**:937–944. doi:10.1016/0092-8674(88)90239-5

de Wit E, Vos ESM, Holwerda SJB, Valdes-Quezada C, Verstegen MJAM, Teunissen H, Splinter E, Wijchers PJ, Krijger PHL, de Laat W. 2015. CTCF Binding Polarity Determines Chromatin Looping. *Molecular Cell* **60**:676–684. doi:10.1016/j.molcel.2015.09.023

Deep A, Gu Y, Gao Y-Q, Ego KM, Herzik MA, Zhou H, Corbett KD. 2022. The SMC-family Wadjet complex protects bacteria from plasmid transformation by recognition and cleavage of closed-circular DNA. *Mol Cell* **82**:4145-4159.e7. doi:10.1016/j.molcel.2022.09.008

Delamarre A, Barthe A, Saint-André C de la R, Luciano P, Forey R, Padioleau I, Skrzypczak M, Ginalski K, Géli V, Pasero P, Lengronne A. 2020. MRX Increases Chromatin Accessibility at Stalled Replication Forks to Promote Nascent DNA Resection and Cohesin Loading. *Molecular Cell* **77**:395-410.e3. doi:10.1016/j.molcel.2019.10.029

Demeret C, Vassetzky Y, Méchali M. 2001. Chromatin remodelling and DNA replication: from nucleosomes to loop domains. *Oncogene* **20**:3086–3093. doi:10.1038/sj.onc.1204333

Dey A, Shi G, Takaki R, Thirumalai D. 2023. Structural changes in chromosomes driven by multiple condensin motors during mitosis. *Cell Reports* **42**:112348. doi:10.1016/j.celrep.2023.112348

Dixon JR, Selvaraj S, Yue F, Kim A, Li Y, Shen Y, Hu M, Liu JS, Ren B. 2012. Topological Domains in Mammalian Genomes Identified by Analysis of Chromatin Interactions. *Nature* **485**:376–380. doi:10.1038/nature11082

Djeghloul D, Patel B, Kramer H, Dimond A, Whilding C, Brown K, Kohler A-C, Feytout A, Veland N, Elliott J, Bharat TAM, Tarafder AK, Löwe J, Ng BL, Guo Y, Guy J, Huseyin MK, Klose RJ, Merkenschlager M, Fisher AG. 2020. Identifying proteins bound to native mitotic ESC chromosomes reveals chromatin repressors are important for compaction. *Nat Commun* **11**:4118. doi:10.1038/s41467-020-17823-z

Dorigo B, Schalch T, Bystricky K, Richmond TJ. 2003. Chromatin Fiber Folding: Requirement for the Histone H4 N-terminal Tail. *Journal of Molecular Biology* **327**:85–96. doi:10.1016/S0022-2836(03)00025-1

Dorigo B, Schalch T, Kulangara A, Duda S, Schroeder RR, Richmond TJ. 2004. Nucleosome Arrays Reveal the Two-Start Organization of the Chromatin Fiber. *Science* **306**:1571–1573. doi:10.1126/science.1103124

Doron S, Melamed S, Ofir G, Leavitt A, Lopatina A, Keren M, Amitai G, Sorek R. 2018. Systematic discovery of antiphage defense systems in the microbial pangenome. *Science* **359**:eaar4120. doi:10.1126/science.aar4120

Dynek JN, Smith S. 2004. Resolution of Sister Telomere Association Is Required for Progression Through Mitosis. *Science* **304**:97–100. doi:10.1126/science.1094754

Earnshaw WC, Halligan B, Cooke CA, Heck MM, Liu LF. 1985. Topoisomerase II is a structural component of mitotic chromosome scaffolds. *Journal of Cell Biology* **100**:1706–1715. doi:10.1083/jcb.100.5.1706

Earnshaw WC, Laemmli UK. 1983. Architecture of metaphase chromosomes and chromosome scaffolds. *J Cell Biol* **96**:84–93. doi:10.1083/jcb.96.1.84

Eeftens JM, Bisht S, Kerssemakers J, Kschonsak M, Haering CH, Dekker C. 2017. Real-time detection of condensin-driven DNA compaction reveals a multistep binding mechanism. *EMBO J* **36**:3448–3457. doi:10.15252/embj.201797596

Eeftens JM, Katan AJ, Kschonsak M, Hassler M, de Wilde L, Dief EM, Haering CH, Dekker C. 2016. Condensin Smc2-Smc4 Dimers Are Flexible and Dynamic. *Cell Rep* **14**:1813–1818. doi:10.1016/j.celrep.2016.01.063

Ehara H, Kujirai T, Fujino Y, Shirouzu M, Kurumizaka H, Sekine S-I. 2019. Structural insight into nucleosome transcription by RNA polymerase II with elongation factors. *Science* **363**:744–747. doi:10.1126/science.aav8912

Elbatsh AMO, Kim E, Eeftens JM, Raaijmakers JA, van der Weide RH, García-Nieto A, Bravo S, Ganji M, Uit de Bos J, Teunissen H, Medema RH, de Wit E, Haering CH, Dekker C, Rowland BD. 2019. Distinct Roles for Condensin's Two ATPase Sites in Chromosome Condensation. *Mol Cell* **76**:724-737.e5. doi:10.1016/j.molcel.2019.09.020

Elias M, Gani S, Lerner Y, Yamin K, Tor C, Patel A, Matityahu A, Dessau M, Qvit N, Onn I. 2023. Developing a peptide to disrupt cohesin head domain interactions. *iScience* **26**:107498. doi:10.1016/j.isci.2023.107498

Eltsov M, MacLellan KM, Maeshima K, Frangakis AS, Dubochet J. 2008. Analysis of cryo-electron microscopy images does not support the existence of 30-nm chromatin fibers in mitotic chromosomes in situ. *Proceedings of the National Academy of Sciences* **105**:19732–19737. doi:10.1073/pnas.0810057105

Emerson DJ, Zhao PA, Cook AL, Barnett RJ, Klein KN, Saulebekova D, Ge C, Zhou L, Simandi Z, Minsk MK, Titus KR, Wang W, Gong W, Zhang D, Yang L, Venev SV, Gibcus JH, Yang H, Sasaki T, Kanemaki MT, Yue F, Dekker J, Chen C-L, Gilbert DM, Phillips-Cremins JE. 2022. Cohesin-mediated loop anchors confine the locations of human replication origins. *Nature* **606**:812–819. doi:10.1038/s41586-022-04803-0

English CM, Adkins MW, Carson JJ, Churchill MEA, Tyler JK. 2006. Structural Basis for the Histone Chaperone Activity of Asf1. *Cell* **127**:495–508. doi:10.1016/j.cell.2006.08.047

English CM, Maluf NK, Tripet B, Churchill MEA, Tyler JK. 2005. ASF1 Binds to a Heterodimer of Histones H3 and H4: A Two-Step Mechanism for the Assembly of the H3–H4 Heterotetramer on DNA. *Biochemistry* **44**:13673. doi:10.1021/bi051333h

Erdel F, Rademacher A, Vlijm R, Tünnermann J, Frank L, Weinmann R, Schweigert E, Yserentant K, Hummert J, Bauer C, Schumacher S, Al Alwash A, Normand C, Herten D-P, Engelhardt J, Rippe K. 2020. Mouse Heterochromatin Adopts Digital Compaction States without Showing Hallmarks of HP1-Driven Liquid-Liquid Phase Separation. *Mol Cell* **78**:236-249.e7. doi:10.1016/j.molcel.2020.02.005

Faast R, Thonglairoam V, Schulz TC, Beall J, Wells JR, Taylor H, Matthaei K, Rathjen PD, Tremethick DJ, Lyons I. 2001. Histone variant H2A.Z is required for early mammalian development. *Curr Biol* **11**:1183–1187. doi:10.1016/s0960-9822(01)00329-3

Fachinetti D, Folco HD, Nechemia-Arbely Y, Valente LP, Nguyen K, Wong AJ, Zhu Q, Holland AJ, Desai A, Jansen LET, Cleveland DW. 2013. A two-step mechanism for epigenetic specification of centromere identity and function. *Nature cell biology* **15**:1056. doi:10.1038/ncb2805

Fairley JA, Scott PH, White RJ. 2003. TFIIIB is phosphorylated, disrupted and selectively released from tRNA promoters during mitosis in vivo. *EMBO J* **22**:5841–5850. doi:10.1093/emboj/cdg544

Falbo L, Raspelli E, Romeo F, Fiorani S, Pezzimenti F, Casagrande F, Costa I, Parazzoli D, Costanzo V. 2020. SSRP1-mediated histone H1 eviction promotes replication origin assembly and accelerated development. *Nat Commun* **11**:1345. doi:10.1038/s41467-020-15180-5

Fan JY, Rangasamy D, Luger K, Tremethick DJ. 2004. H2A.Z Alters the Nucleosome Surface to Promote HP1α-Mediated Chromatin Fiber Folding. *Molecular Cell* **16**:655–661. doi:10.1016/j.molcel.2004.10.023

Farnung L, Ochmann M, Engeholm M, Cramer P. 2021. Structural basis of nucleosome transcription mediated by Chd1 and FACT. *Nat Struct Mol Biol* **28**:382–387. doi:10.1038/s41594-021-00578-6

Feytout A, Vaur S, Genier S, Vazquez S, Javerzat J-P. 2011. Psm3 Acetylation on Conserved Lysine Residues Is Dispensable for Viability in Fission Yeast but Contributes to Eso1-Mediated Sister Chromatid Cohesion by Antagonizing Wpl1. *Molecular and Cellular Biology* **31**:1771–1786. doi:10.1128/MCB.01284-10

Filipovski M, Soffers JHM, Vos SM, Farnung L. 2022. Structural basis of nucleosome retention during transcription elongation. *Science* **376**:1313–1316. doi:10.1126/science.abo3851

Finch JT, Klug A. 1976. Solenoidal model for superstructure in chromatin. *Proc Natl Acad Sci U S A* **73**:1897–1901. doi:10.1073/pnas.73.6.1897

Fischle W, Tseng BS, Dormann HL, Ueberheide BM, Garcia BA, Shabanowitz J, Hunt DF, Funabiki H, Allis CD. 2005. Regulation of HP1–chromatin binding by histone H3 methylation and phosphorylation. *Nature* **438**:1116–1122. doi:10.1038/nature04219

Foltz DR, Jansen LET, Bailey AO, Yates JR, Bassett EA, Wood S, Black BE, Cleveland DW. 2009. Centromere-specific assembly of CENP-a nucleosomes is mediated by HJURP. *Cell* **137**:472–484. doi:10.1016/j.cell.2009.02.039

Formosa T, Eriksson P, Wittmeyer J, Ginn J, Yu Y, Stillman DJ. 2001. Spt16-Pob3 and the HMG protein Nhp6 combine to form the nucleosome-binding factor SPN. *EMBO J* **20**:3506–3517. doi:10.1093/emboj/20.13.3506

Fousteri MI, Lehmann AR. 2000. A novel SMC protein complex in Schizosaccharomyces pombe contains the Rad18 DNA repair protein. *EMBO J* **19**:1691–1702. doi:10.1093/emboj/19.7.1691

Fujiwara T, Tanaka K, Kuroiwa T, Hirano T. 2013. Spatiotemporal dynamics of condensins I and II: evolutionary insights from the primitive red alga Cyanidioschyzon merolae. *MBoC* **24**:2515–2527. doi:10.1091/mbc.e13-04-0208

Funabiki H, Jenness C, Zierhut C. 2017. Nucleosome-Dependent Pathways That Control Mitotic Progression. *Cold Spring Harb Symp Quant Biol* **82**:173–185. doi:10.1101/sqb.2017.82.034512

Furuyama T, Codomo CA, Henikoff S. 2013. Reconstitution of hemisomes on budding yeast centromeric DNA. *Nucleic Acids Res* **41**:5769–5783. doi:10.1093/nar/gkt314

Gandhi R, Gillespie PJ, Hirano T. 2006. Human Wapl is a cohesin-binding protein that promotes sister-chromatid resolution in mitotic prophase. *Curr Biol* **16**:2406–2417. doi:10.1016/j.cub.2006.10.061

Ganji M, Shaltiel IA, Bisht S, Kim E, Kalichava A, Haering CH, Dekker C. 2018. Real-time imaging of DNA loop extrusion by condensin. *Science* **360**:102–105. doi:10.1126/science.aar7831

Garcia-Luis J, Lazar-Stefanita L, Gutierrez-Escribano P, Thierry A, Cournac A, García A, González S, Sánchez M, Jarmuz A, Montoya A, Dore M, Kramer H, Karimi MM, Antequera F, Koszul R, Aragon L. 2019. FACT mediates cohesin function on chromatin. *Nat Struct Mol Biol* **26**:970–979. doi:10.1038/s41594-019-0307-x

Garg A. 2020. A lncRNA-regulated gene expression system with rapid induction kinetics in the fission yeast Schizosaccharomyces pombe. *RNA* **26**:1743–1752. doi:10.1261/rna.076000.120

Gebara MM, Sayre MH, Corden JL. 1997. Phosphorylation of the carboxy-terminal repeat domain in RNA polymerase II by cyclin-dependent kinases is sufficient to inhibit transcription. *J Cell Biochem* **64**:390–402.

Gelléri M, Chen S-Y, Hübner B, Neumann J, Kröger O, Sadlo F, Imhoff J, Hendzel MJ, Cremer M, Cremer T, Strickfaden H, Cremer C. 2023. True-to-scale DNA-density maps correlate with major accessibility differences between active and inactive chromatin. *Cell Reports* **42**:112567. doi:10.1016/j.celrep.2023.112567

Gerguri T, Fu X, Kakui Y, Khatri BS, Barrington C, Bates PA, Uhlmann F. 2021. Comparison of loop extrusion and diffusion capture as mitotic chromosome formation pathways in fission yeast. *Nucleic Acids Research* **49**:1294–1312. doi:10.1093/nar/gkaa1270

Gerlich D, Hirota T, Koch B, Peters J-M, Ellenberg J. 2006a. Condensin I stabilizes chromosomes mechanically through a dynamic interaction in live cells. *Curr Biol* **16**:333–344. doi:10.1016/j.cub.2005.12.040

Gerlich D, Koch B, Dupeux F, Peters J-M, Ellenberg J. 2006b. Live-cell imaging reveals a stable cohesin-chromatin interaction after but not before DNA replication. *Curr Biol* **16**:1571–1578. doi:10.1016/j.cub.2006.06.068

Gibcus JH, Samejima K, Goloborodko A, Samejima I, Naumova N, Nuebler J, Kanemaki MT, Xie L, Paulson JR, Earnshaw WC, Mirny LA, Dekker J. 2018. A pathway for mitotic chromosome formation. *Science* eaao6135. doi:10.1126/science.aao6135

Gibson BA, Blaukopf C, Lou T, Chen L, Doolittle LK, Finkelstein I, Narlikar GJ, Gerlich DW, Rosen MK. 2023. In diverse conditions, intrinsic chromatin condensates have liquid-like material properties. *Proc Natl Acad Sci U S A* **120**:e2218085120. doi:10.1073/pnas.2218085120

Gibson BA, Doolittle LK, Schneider MWG, Jensen LE, Gamarra N, Henry L, Gerlich DW, Redding S, Rosen MK. 2019. Organization of Chromatin by Intrinsic and Regulated Phase Separation. *Cell* **179**:470-484.e21. doi:10.1016/j.cell.2019.08.037

Gillespie PJ, Hirano T. 2004. Scc2 couples replication licensing to sister chromatid cohesion in Xenopus egg extracts. *Curr Biol* **14**:1598–1603. doi:10.1016/j.cub.2004.07.053

Girbig M, Misiaszek AD, Müller CW. 2022. Structural insights into nuclear transcription by eukaryotic DNA-dependent RNA polymerases. *Nat Rev Mol Cell Biol* **23**:603–622. doi:10.1038/s41580-022-00476-9

Golfier S, Quail T, Kimura H, Brugués J. 2020. Cohesin and condensin extrude DNA loops in a cell cycle-dependent manner. *eLife* **9**:e53885. doi:10.7554/eLife.53885

Guacci V, Koshland D, Strunnikov A. 1997. A Direct Link between Sister Chromatid Cohesion and Chromosome Condensation Revealed through the Analysis of MCD1 in S. cerevisiae. *Cell* **91**:47–57.

Guérin TM, Barrington C, Pobegalov G, Molodtsov MI, Uhlmann F. 2023. Cohesin chromatin loop formation by an extrinsic motor. doi:10.1101/2023.11.30.569410

Guérin TM, Béneut C, Barinova N, López V, Lazar-Stefanita L, Deshayes A, Thierry A, Koszul R, Dubrana K, Marcand S. 2019. Condensin-Mediated Chromosome Folding and Internal

Telomeres Drive Dicentric Severing by Cytokinesis. *Molecular Cell* **75**:131-144.e3. doi:10.1016/j.molcel.2019.05.021

Guo MS, Kawamura R, Littlehale ML, Marko JF, Laub MT. 2021. High-resolution, genome-wide mapping of positive supercoiling in chromosomes. *eLife* **10**:e67236. doi:10.7554/eLife.67236

Gurzau AD, Blewitt ME, Czabotar PE, Murphy JM, Birkinshaw RW. 2020. Relating SMCHD1 structure to its function in epigenetic silencing. *Biochem Soc Trans* **48**:1751–1763. doi:10.1042/BST20200242

Gutierrez-Escribano P, Hormeño S, Madariaga-Marcos J, Solé-Soler R, O'Reilly FJ, Morris K, Aicart-Ramos C, Aramayo R, Montoya A, Kramer H, Rappsilber J, Torres-Rosell J, Moreno-Herrero F, Aragon L. 2020. Purified Smc5/6 Complex Exhibits DNA Substrate Recognition and Compaction. *Mol Cell* **80**:1039-1054.e6. doi:10.1016/j.molcel.2020.11.012

Haarhuis JHI, van der Weide RH, Blomen VA, Flach KD, Teunissen H, Willems L, Brummelkamp TR, Rowland BD, de Wit E. 2022. A Mediator-cohesin axis controls heterochromatin domain formation. *Nat Commun* **13**:754. doi:10.1038/s41467-022-28377-7

Haarhuis JHI, van der Weide RH, Blomen VA, Yáñez-Cuna JO, Amendola M, van Ruiten MS, Krijger PHL, Teunissen H, Medema RH, van Steensel B, Brummelkamp TR, de Wit E, Rowland BD. 2017. The Cohesin Release Factor WAPL Restricts Chromatin Loop Extension. *Cell* **169**:693-707.e14. doi:10.1016/j.cell.2017.04.013

Haase J, Chen R, Parker WM, Bonner MK, Jenkins LM, Kelly AE. 2022. The TFIIH complex is required to establish and maintain mitotic chromosome structure. *Elife* **11**:e75475. doi:10.7554/eLife.75475

Haering CH, Farcas A-M, Arumugam P, Metson J, Nasmyth K. 2008. The cohesin ring concatenates sister DNA molecules. *Nature* **454**:297–301. doi:10.1038/nature07098

Haeusler RA, Pratt-Hyatt M, Good PD, Gipson TA, Engelke DR. 2008. Clustering of yeast tRNA genes is mediated by specific association of condensin with tRNA gene transcription complexes. *Genes Dev* **22**:2204–2214. doi:10.1101/gad.1675908

Harris HL, Gu H, Olshansky M, Wang A, Farabella I, Eliaz Y, Kalluchi A, Krishna A, Jacobs M, Cauer G, Pham M, Rao SSP, Dudchenko O, Omer A, Mohajeri K, Kim S, Nichols MH, Davis ES, Gkountaroulis D, Udupa D, Aiden AP, Corces VG, Phanstiel DH, Noble WS, Nir G, Di Pierro M, Seo J-S, Talkowski ME, Aiden EL, Rowley MJ. 2023. Chromatin alternates between A and B compartments at kilobase scale for subgenic organization. *Nat Commun* **14**:3303. doi:10.1038/s41467-023-38429-1

Hassan A, Araguas Rodriguez P, Heidmann SK, Walmsley EL, Aughey GN, Southall TD. 2020. Condensin I subunit Cap-G is essential for proper gene expression during the maturation of post-mitotic neurons. *Elife* **9**:e55159. doi:10.7554/eLife.55159

Hassler M, Shaltiel IA, Kschonsak M, Simon B, Merkel F, Thärichen L, Bailey HJ, Macošek J, Bravo S, Metz J, Hennig J, Haering CH. 2019. Structural Basis of an Asymmetric Condensin ATPase Cycle. *Mol Cell* **74**:1175-1188.e9. doi:10.1016/j.molcel.2019.03.037

Heinz S, Texari L, Hayes MGB, Urbanowski M, Chang MW, Givarkes N, Rialdi A, White KM, Albrecht RA, Pache L, Marazzi I, García-Sastre A, Shaw ML, Benner C. 2018. Transcription Elongation Can Affect Genome 3D Structure. *Cell* **174**:1522-1536.e22. doi:10.1016/j.cell.2018.07.047

Henneman B, van Emmerik C, van Ingen H, Dame RT. 2018. Structure and function of archaeal histones. *PLoS Genet* **14**:e1007582. doi:10.1371/journal.pgen.1007582

Hennig BP, Bendrin K, Zhou Y, Fischer T. 2012. Chd1 chromatin remodelers maintain nucleosome organization and repress cryptic transcription. *EMBO Rep* **13**:997–1003. doi:10.1038/embor.2012.146

Higashi TL, Eickhoff P, Sousa JS, Locke J, Nans A, Flynn HR, Snijders AP, Papageorgiou G, O'Reilly N, Chen ZA, O'Reilly FJ, Rappsilber J, Costa A, Uhlmann F. 2020. A Structure-Based Mechanism for DNA Entry into the Cohesin Ring. *Mol Cell* **79**:917-933.e9. doi:10.1016/j.molcel.2020.07.013

Hill L, Ebert A, Jaritz M, Wutz G, Nagasaka K, Tagoh H, Kostanova-Poliakova D, Schindler K, Sun Q, Bönelt P, Fischer M, Peters J-M, Busslinger M. 2020. Wapl repression by Pax5 promotes V

gene recombination by Igh loop extrusion. *Nature* **584**:142–147. doi:10.1038/s41586-020-2454-y

Hintermair C, Voß K, Forné I, Heidemann M, Flatley A, Kremmer E, Imhof A, Eick D. 2016. Specific threonine-4 phosphorylation and function of RNA polymerase II CTD during M phase progression. *Sci Rep* **6**:27401. doi:10.1038/srep27401

Hinterndorfer K, Laporte MH, Mikus F, Tafur L, Bourgoint C, Prouteau M, Dey G, Loewith R, Guichard P, Hamel V. 2022. Ultrastructure expansion microscopy reveals the cellular architecture of budding and fission yeast. *Journal of Cell Science* **135**:jcs260240. doi:10.1242/jcs.260240

Hirano M, Hirano T. 2004. Positive and negative regulation of SMC-DNA interactions by ATP and accessory proteins. *EMBO J* **23**:2664–2673. doi:10.1038/sj.emboj.7600264

Hirano M, Hirano T. 2002. Hinge-mediated dimerization of SMC protein is essential for its dynamic interaction with DNA. *EMBO J* **21**:5733–5744. doi:10.1093/emboj/cdf575

Hirano T. 2016. Condensin-Based Chromosome Organization from Bacteria to Vertebrates. *Cell* **164**:847–857. doi:10.1016/j.cell.2016.01.033

Hirano T. 2014. Condensins and the evolution of torsion-mediated genome organization. *Trends Cell Biol* **24**:727–733. doi:10.1016/j.tcb.2014.06.007

Hirano T, Funahashi S, Uemura T, Yanagida M. 1986. Isolation and characterization of Schizosaccharomyces pombe cutmutants that block nuclear division but not cytokinesis. *EMBO J* **5**:2973–2979.

Hirano T, Kobayashi R, Hirano M. 1997. Condensins, chromosome condensation protein complexes containing XCAP-C, XCAP-E and a Xenopus homolog of the Drosophila Barren protein. *Cell* **89**:511–521.

Hirano T, Mitchison TJ. 1994. A heterodimeric coiled-coil protein required for mitotic chromosome condensation in vitro. *Cell* **79**:449–458. doi:10.1016/0092-8674(94)90254-2

Hirano T, Mitchison TJ. 1993. Topoisomerase II does not play a scaffolding role in the organization of mitotic chromosomes assembled in Xenopus egg extracts. *J Cell Biol* **120**:601–612. doi:10.1083/jcb.120.3.601

Hiraoka Y, Toda T, Yanagida M. 1984. The NDA3 gene of fission yeast encodes beta-tubulin: a cold-sensitive nda3 mutation reversibly blocks spindle formation and chromosome movement in mitosis. *Cell* **39**:349–358.

Hirota T, Gerlich D, Koch B, Ellenberg J, Peters J-M. 2004. Distinct functions of condensin I and II in mitotic chromosome assembly. *Journal of Cell Science* **117**:6435–6445. doi:10.1242/jcs.01604

Hirota T, Lipp JJ, Toh B-H, Peters J-M. 2005. Histone H3 serine 10 phosphorylation by Aurora B causes HP1 dissociation from heterochromatin. *Nature* **438**:1176–1180. doi:10.1038/nature04254

Hocquet C, Robellet X, Modolo L, Sun X-M, Burny C, Cuylen-Haering S, Toselli E, Clauder-Münster S, Steinmetz L, Haering CH, Marguerat S, Bernard P. 2018. Condensin controls cellular RNA levels through the accurate segregation of chromosomes instead of directly regulating transcription. *Elife* **7**:e38517. doi:10.7554/eLife.38517

Hoencamp C, Dudchenko O, Elbatsh AMO, Brahmachari S, Raaijmakers JA, van Schaik T, Sedeño Cacciatore Á, Contessoto VG, van Heesbeen RGHP, van den Broek B, Mhaskar AN, Teunissen H, St Hilaire BG, Weisz D, Omer AD, Pham M, Colaric Z, Yang Z, Rao SSP, Mitra N, Lui C, Yao W, Khan R, Moroz LL, Kohn A, St Leger J, Mena A, Holcroft K, Gambetta MC, Lim F, Farley E, Stein N, Haddad A, Chauss D, Mutlu AS, Wang MC, Young ND, Hildebrandt E, Cheng HH, Knight CJ, Burnham TLU, Hovel KA, Beel AJ, Mattei P-J, Kornberg RD, Warren WC, Cary G, Gómez-Skarmeta JL, Hinman V, Lindblad-Toh K, Di Palma F, Maeshima K, Multani AS, Pathak S, Nel-Themaat L, Behringer RR, Kaur P, Medema RH, van Steensel B, de Wit E, Onuchic JN, Di Pierro M, Lieberman Aiden E, Rowland BD. 2021. 3D genomics across the tree of life reveals condensin II as a determinant of architecture type. *Science* **372**:984–989. doi:10.1126/science.abe2218

Hoencamp C, Rowland BD. 2023. Genome control by SMC complexes. *Nat Rev Mol Cell Biol*. doi:10.1038/s41580-023-00609-8

Hoffmann S, Dumont M, Barra V, Ly P, Nechemia-Arbely Y, McMahon MA, Hervé S, Cleveland DW, Fachinetti D. 2016. CENP-A Is Dispensable for Mitotic Centromere Function after Initial Centromere/Kinetochore Assembly. *Cell Rep* **17**:2394–2404. doi:10.1016/j.celrep.2016.10.084

Houlard M, Cutts EE, Shamim MS, Godwin J, Weisz D, Presser Aiden A, Lieberman Aiden E, Schermelleh L, Vannini A, Nasmyth K. 2021. MCPH1 inhibits Condensin II during interphase by regulating its SMC2-Kleisin interface. *eLife* **10**:e73348. doi:10.7554/eLife.73348

Hsiung CC-S, Bartman CR, Huang P, Ginart P, Stonestrom AJ, Keller CA, Face C, Jahn KS, Evans P, Sankaranarayanan L, Giardine B, Hardison RC, Raj A, Blobel GA. 2016. A hyperactive transcriptional state marks genome reactivation at the mitosis–G1 transition. *Genes Dev* **30**:1423–1439. doi:10.1101/gad.280859.116

Hsiung CC-S, Morrissey CS, Udugama M, Frank CL, Keller CA, Baek S, Giardine B, Crawford GE, Sung M-H, Hardison RC, Blobel GA. 2015. Genome accessibility is widely preserved and locally modulated during mitosis. *Genome Res* **25**:213–225. doi:10.1101/gr.180646.114

Hsu JY, Sun ZW, Li X, Reuben M, Tatchell K, Bishop DK, Grushcow JM, Brame CJ, Caldwell JA, Hunt DF, Lin R, Smith MM, Allis CD. 2000. Mitotic phosphorylation of histone H3 is governed by Ipl1/aurora kinase and Glc7/PP1 phosphatase in budding yeast and nematodes. *Cell* **102**:279–291. doi:10.1016/s0092-8674(00)00034-9

Hu H, van Roon A-MM, Ghanim GE, Ahsan B, Oluwole AO, Peak-Chew S-Y, Robinson CV, Nguyen THD. 2023. Structural basis of telomeric nucleosome recognition by shelterin factor TRF1. *Science Advances* **9**:eadi4148. doi:10.1126/sciadv.adi4148

Huang J, Hsu J-M, Laurent BC. 2004. The RSC nucleosome-remodeling complex is required for Cohesin's association with chromosome arms. *Mol Cell* **13**:739–750. doi:10.1016/s1097-2765(04)00103-0

Iacovella MG, Golfieri C, Massari LF, Busnelli S, Pagliuca C, Dal Maschio M, Infantino V, Visintin R, Mechtler K, Ferreira-Cerca S, De Wulf P. 2015. Rio1 promotes rDNA stability and downregulates RNA polymerase I to ensure rDNA segregation. *Nat Commun* **6**:6643. doi:10.1038/ncomms7643

Ibarra-Morales D, Rauer M, Quarato P, Rabbani L, Zenk F, Schulte-Sasse M, Cardamone F, Gomez-Auli A, Cecere G, Iovino N. 2021. Histone variant H2A.Z regulates zygotic genome activation. *Nat Commun* **12**:7002. doi:10.1038/s41467-021-27125-7

Ide S, Miyazaki T, Maki H, Kobayashi T. 2010. Abundance of ribosomal RNA gene copies maintains genome integrity. *Science* **327**:693–696. doi:10.1126/science.1179044

Ishiguro K. 2019. The cohesin complex in mammalian meiosis. *Genes Cells* **24**:6–30. doi:10.1111/gtc.12652

Ivanov D, Schleiffer A, Eisenhaber F, Mechtler K, Haering CH, Nasmyth K. 2002. Eco1 is a novel acetyltransferase that can acetylate proteins involved in cohesion. *Curr Biol* **12**:323–328. doi:10.1016/s0960-9822(02)00681-4

Ivanova AV, Bonaduce MJ, Ivanov SV, Klar AJ. 1998. The chromo and SET domains of the Clr4 protein are essential for silencing in fission yeast. *Nat Genet* **19**:192–195. doi:10.1038/566

Iwasaki O, Tanizawa H, Kim K-D, Yokoyama Y, Corcoran CJ, Tanaka A, Skordalakes E, Showe LC, Noma K. 2015. Interaction between TBP and Condensin Drives the Organization and Faithful Segregation of Mitotic Chromosomes. *Molecular Cell* **59**:755–767. doi:10.1016/j.molcel.2015.07.007

Jamai A, Puglisi A, Strubin M. 2009. Histone chaperone spt16 promotes redeposition of the original h3-h4 histones evicted by elongating RNA polymerase. *Mol Cell* **35**:377–383. doi:10.1016/j.molcel.2009.07.001

Jenness C, Giunta S, Müller MM, Kimura H, Muir TW, Funabiki H. 2018. HELLS and CDCA7 comprise a bipartite nucleosome remodeling complex defective in ICF syndrome. *Proc Natl Acad Sci U S A* **115**:E876–E885. doi:10.1073/pnas.1717509115

Jeppsson K, Sakata T, Nakato R, Milanova S, Shirahige K, Björkegren C. 2022a. Cohesin-dependent chromosome loop extrusion is limited by transcription and stalled replication forks. *Sci Adv* **8**:eabn7063. doi:10.1126/sciadv.abn7063

Jeppsson K, Sakata T, Nakato R, Milanova S, Shirahige K, Björkegren C. 2022b. Cohesin-dependent chromosome loop extrusion is limited by transcription and stalled replication forks. *Sci Adv* **8**:eabn7063. doi:10.1126/sciadv.abn7063

Jeronimo C, Angel A, Nguyen VQ, Kim JM, Poitras C, Lambert E, Collin P, Mellor J, Wu C, Robert F. 2021. FACT is recruited to the +1 nucleosome of transcribed genes and spreads in a Chd1-dependent manner. *Mol Cell* **81**:3542-3559.e11. doi:10.1016/j.molcel.2021.07.010

Jeronimo C, Robert F. 2022. The histone chaperone FACT: a guardian of chromatin structure integrity. *Transcription* **13**:16–38. doi:10.1080/21541264.2022.2069995

Jeronimo C, Watanabe S, Kaplan CD, Peterson CL, Robert F. 2015. The Histone Chaperones FACT and Spt6 Restrict H2A.Z from Intragenic Locations. *Mol Cell* **58**:1113–1123. doi:10.1016/j.molcel.2015.03.030

Jiang Y, Liu M, Spencer CA, Price DH. 2004. Involvement of transcription termination factor 2 in mitotic repression of transcription elongation. *Mol Cell* **14**:375–385. doi:10.1016/s1097-2765(04)00234-5

Johzuka K, Horiuchi T. 2007. RNA polymerase I transcription obstructs condensin association with 35S rRNA coding regions and can cause contraction of long repeat in Saccharomyces cerevisiae. *Genes to Cells* **12**:759–771. doi:10.1111/j.1365-2443.2007.01085.x

Kaczmarczyk A, Meng H, Ordu O, Noort J van, Dekker NH. 2020. Chromatin fibers stabilize nucleosomes under torsional stress. *Nat Commun* **11**:126. doi:10.1038/s41467-019-13891-y

Kakui Y, Barrington C, Barry DJ, Gerguri T, Fu X, Bates PA, Khatri BS, Uhlmann F. 2020. Fission yeast condensin contributes to interphase chromatin organization and prevents transcription-coupled DNA damage. *Genome Biol* **21**:272. doi:10.1186/s13059-020-02183-0

Kakui Y, Barrington C, Kusano Y, Thadani R, Fallesen T, Hirota T, Uhlmann F. 2022. Chromosome arm length, and a species-specific determinant, define chromosome arm width. *Cell Reports* **41**:111753. doi:10.1016/j.celrep.2022.111753

Kakui Y, Rabinowitz A, Barry DJ, Uhlmann F. 2017. Condensin-mediated remodeling of the mitotic chromatin landscape in fission yeast. *Nat Genet* **49**:1553–1557. doi:10.1038/ng.3938

Kato D, Osakabe A, Arimura Y, Mizukami Y, Horikoshi N, Saikusa K, Akashi S, Nishimura Y, Park S-Y, Nogami J, Maehara K, Ohkawa Y, Matsumoto A, Kono H, Inoue R, Sugiyama M, Kurumizaka H. 2017. Crystal structure of the overlapping dinucleosome composed of hexasome and octasome. *Science* **356**:205–208. doi:10.1126/science.aak9867

Kelly AE, Ghenoiu C, Xue JZ, Zierhut C, Kimura H, Funabiki H. 2010. Survivin Reads Phosphorylated Histone H3 Threonine 3 to Activate the Mitotic Kinase Aurora B. *Science* **330**:235–239. doi:10.1126/science.1189505

Kemble DJ, McCullough LL, Whitby FG, Formosa T, Hill CP. 2015. FACT disrupts nucleosome structure by binding H2A-H2B with conserved peptide motifs. *Mol Cell* **60**:294–306. doi:10.1016/j.molcel.2015.09.008

Kemble DJ, Whitby FG, Robinson H, McCullough LL, Formosa T, Hill CP. 2013. Structure of the Spt16 Middle Domain Reveals Functional Features of the Histone Chaperone FACT. *J Biol Chem* **288**:10188–10194. doi:10.1074/jbc.C113.451369

Keogh M-C, Kurdistani SK, Morris SA, Ahn SH, Podolny V, Collins SR, Schuldiner M, Chin K, Punna T, Thompson NJ, Boone C, Emili A, Weissman JS, Hughes TR, Strahl BD, Grunstein M, Greenblatt JF, Buratowski S, Krogan NJ. 2005. Cotranscriptional set2 methylation of histone H3 lysine 36 recruits a repressive Rpd3 complex. *Cell* **123**:593–605. doi:10.1016/j.cell.2005.10.025

Kim E, Gonzalez AM, Pradhan B, van der Torre J, Dekker C. 2022. Condensin-driven loop extrusion on supercoiled DNA. *Nat Struct Mol Biol* **29**:719–727. doi:10.1038/s41594-022-00802-x

Kim E, Kerssemakers J, Shaltiel IA, Haering CH, Dekker C. 2020. DNA-loop extruding condensin complexes can traverse one another. *Nature* **579**:438–442. doi:10.1038/s41586-020-2067-5

Kim H, Loparo JJ. 2016. Multistep assembly of DNA condensation clusters by SMC. *Nat Commun* **7**:10200. doi:10.1038/ncomms10200

Kim H-S, Vanoosthuyse V, Fillingham J, Roguev A, Watt S, Kislinger T, Treyer A, Carpenter LR, Bennett CS, Emili A, Greenblatt JF, Hardwick KG, Krogan NJ, Bähler J, Keogh M-C. 2009. An acetylated form of histone H2A.Z regulates chromosome architecture in Schizosaccharomyces pombe. *Nat Struct Mol Biol* **16**:1286–1293. doi:10.1038/nsmb.1688

Kim JH, Zhang T, Wong NC, Davidson N, Maksimovic J, Oshlack A, Earnshaw WC, Kalitsis P, Hudson DF. 2013. Condensin I associates with structural and gene regulatory regions in vertebrate chromosomes. *Nat Commun* **4**:2537. doi:10.1038/ncomms3537

Kim K.-D., Iwasaki O, Noma K. 2016. An IF-FISH Approach for Covisualization of Gene Loci and Nuclear Architecture in Fission Yeast. *Methods Enzymol* **574**:167–180. doi:10.1016/bs.mie.2016.04.003

Kim Kyoung-Dong, Tanizawa H, Iwasaki O, Noma K. 2016a. Transcription factors mediate condensin recruitment and global chromosomal organization in fission yeast. *Nat Genet* **48**:1242–1252. doi:10.1038/ng.3647

Kim Kyoung-Dong, Tanizawa H, Iwasaki O, Noma K. 2016b. Transcription factors mediate condensin recruitment and global chromosomal organization in fission yeast. *Nat Genet* **48**:1242–1252. doi:10.1038/ng.3647

Kim T-K, Hemberg M, Gray JM, Costa AM, Bear DM, Wu J, Harmin DA, Laptewicz M, Barbara-Haley K, Kuersten S, Markenscoff-Papadimitriou E, Kuhl D, Bito H, Worley PF, Kreiman G, Greenberg ME. 2010. Widespread transcription at neuronal activity-regulated enhancers. *Nature* **465**:182–187. doi:10.1038/nature09033

Kim Y, Shi Z, Zhang H, Finkelstein IJ, Yu H. 2019. Human cohesin compacts DNA by loop extrusion. *Science* **366**:1345–1349. doi:10.1126/science.aaz4475

Kimura K, Hirano M, Kobayashi R, Hirano T. 1998. Phosphorylation and activation of 13S condensin by Cdc2 in vitro. *Science* **282**:487–490. doi:10.1126/science.282.5388.487

Kimura K, Hirano T. 2000. Dual roles of the 11S regulatory subcomplex in condensin functions. *Proc Natl Acad Sci U S A* **97**:11972–11977. doi:10.1073/pnas.220326097

Kimura K, Hirano T. 1997. ATP-dependent positive supercoiling of DNA by 13S condensin: a biochemical implication for chromosome condensation. *Cell* **90**:625–634.

Kimura K, Rybenkov VV, Crisona NJ, Hirano T, Cozzarelli NR. 1999. 13S condensin actively reconfigures DNA by introducing global positive writhe: implications for chromosome condensation. *Cell* **98**:239–248. doi:10.1016/s0092-8674(00)81018-1

Kinoshita E, van der Linden E, Sanchez H, Wyman C. 2009. RAD50, an SMC family member with multiple roles in DNA break repair: how does ATP affect function? *Chromosome Res* **17**:277–288. doi:10.1007/s10577-008-9018-6

Kinoshita K, Kobayashi TJ, Hirano T. 2015. Balancing Acts of Two HEAT Subunits of Condensin I Support Dynamic Assembly of Chromosome Axes. *Developmental Cell* **33**:94–106. doi:10.1016/j.devcel.2015.01.034

Kinoshita K, Tsubota Y, Tane S, Aizawa Y, Sakata R, Takeuchi K, Shintomi K, Nishiyama T, Hirano T. 2022. A loop extrusion-independent mechanism contributes to condensin I-mediated chromosome shaping. *J Cell Biol* **221**:e202109016. doi:10.1083/jcb.202109016

Kireeva ML, Walter W, Tchernajenko V, Bondarenko V, Kashlev M, Studitsky VM. 2002. Nucleosome Remodeling Induced by RNA Polymerase II: Loss of the H2A/H2B Dimer during Transcription. *Molecular Cell* **9**:541–552. doi:10.1016/S1097-2765(02)00472-0

Kireeva N, Lakonishok M, Kireev I, Hirano T, Belmont AS. 2004. Visualization of early chromosome condensation: a hierarchical folding, axial glue model of chromosome structure. *J Cell Biol* **166**:775–785. doi:10.1083/jcb.200406049

Kitajima TS, Hauf S, Ohsugi M, Yamamoto T, Watanabe Y. 2005. Human Bub1 Defines the Persistent Cohesion Site along the Mitotic Chromosome by Affecting Shugoshin Localization. *Current Biology* **15**:353–359. doi:10.1016/j.cub.2004.12.044

Kitajima TS, Kawashima SA, Watanabe Y. 2004. The conserved kinetochore protein shugoshin protects centromeric cohesion during meiosis. *Nature* **427**:510–517. doi:10.1038/nature02312

Kojic A, Cuadrado A, De Koninck M, Giménez-Llorente D, Rodríguez-Corsino M, Gómez-López G, Le Dily F, Marti-Renom MA, Losada A. 2018. Distinct roles of cohesin-SA1 and cohesin-SA2 in 3D chromosome organization. *Nat Struct Mol Biol* **25**:496–504. doi:10.1038/s41594-018-0070-4

Kong M, Cutts EE, Pan D, Beuron F, Kaliyappan T, Xue C, Morris EP, Musacchio A, Vannini A, Greene EC. 2020. Human Condensin I and II Drive Extensive ATP-Dependent Compaction of Nucleosome-Bound DNA. *Mol Cell* **79**:99-114.e9. doi:10.1016/j.molcel.2020.04.026

Kornberg RD, Thomas JO. 1974. Chromatin Structure: Oligomers of the Histones. *Science* **184**:865–868.

Kranz A-L, Jiao C-Y, Winterkorn LH, Albritton SE, Kramer M, Ercan S. 2013. Genome-wide analysis of condensin binding in Caenorhabditis elegans. *Genome Biol* **14**:R112. doi:10.1186/gb-2013-14-10-r112

Kruitwagen T, Denoth-Lippuner A, Wilkins BJ, Neumann H, Barral Y. 2015. Axial contraction and short-range compaction of chromatin synergistically promote mitotic chromosome condensation. *eLife* **4**:e10396. doi:10.7554/eLife.10396

Kschonsak M, Merkel F, Bisht S, Metz J, Rybin V, Hassler M, Haering CH. 2017. Structural Basis for a Safety-Belt Mechanism That Anchors Condensin to Chromosomes. *Cell* **171**:588-600.e24. doi:10.1016/j.cell.2017.09.008

Kubalová I, Câmara AS, Cápal P, Beseda T, Rouillard J-M, Krause GM, Holušová K, Toegelová H, Himmelbach A, Stein N, Houben A, Doležel J, Mascher M, Šimková H, Schubert V. 2023. Helical coiling of metaphase chromatids. *Nucleic Acids Research* **51**:2641–2654. doi:10.1093/nar/gkad028

Kujirai T, Ehara H, Fujino Y, Shirouzu M, Sekine S-I, Kurumizaka H. 2018. Structural basis of the nucleosome transition during RNA polymerase II passage. *Science* **362**:595–598. doi:10.1126/science.aau9904

Kurat CF, Yeeles JTP, Patel H, Early A, Diffley JFX. 2017. Chromatin Controls DNA Replication Origin Selection, Lagging-Strand Synthesis, and Replication Fork Rates. *Mol Cell* **65**:117–130. doi:10.1016/j.molcel.2016.11.016

Laloraya S, Guacci V, Koshland D. 2000. Chromosomal Addresses of the Cohesin Component Mcd1p. *J Cell Biol* **151**:1047–1056.

Lantermann AB, Straub T, Strålfors A, Yuan G-C, Ekwall K, Korber P. 2010. Schizosaccharomyces pombe genome-wide nucleosome mapping reveals positioning mechanisms distinct from those of Saccharomyces cerevisiae. *Nat Struct Mol Biol* **17**:251–257. doi:10.1038/nsmb.1741

Larochelle M, Robert M-A, Hébert J-N, Liu X, Matteau D, Rodrigue S, Tian B, Jacques P-É, Bachand F. 2018. Common mechanism of transcription termination at coding and noncoding RNA genes in fission yeast. *Nat Commun* **9**:4364. doi:10.1038/s41467-018-06546-x

Lee B-G, Merkel F, Allegretti M, Hassler M, Cawood C, Lecomte L, O'Reilly FJ, Sinn LR, Gutierrez-Escribano P, Kschonsak M, Bravo S, Nakane T, Rappsilber J, Aragon L, Beck M, Löwe J, Haering CH. 2020. Cryo-EM structures of holo condensin reveal a subunit flip-flop mechanism. *Nat Struct Mol Biol* **27**:743–751. doi:10.1038/s41594-020-0457-x

Lee B-G, Rhodes J, Löwe J. 2022. Clamping of DNA shuts the condensin neck gate. *Proc Natl Acad Sci U S A* **119**:e2120006119. doi:10.1073/pnas.2120006119

Lee C-K, Shibata Y, Rao B, Strahl BD, Lieb JD. 2004. Evidence for nucleosome depletion at active regulatory regions genome-wide. *Nat Genet* **36**:900–905. doi:10.1038/ng1400

Lejeune E, Bortfeld M, White SA, Pidoux AL, Ekwall K, Allshire RC, Ladurner AG. 2007. The Chromatin-Remodeling Factor FACT Contributes to Centromeric Heterochromatin Independently from RNAi. *Curr Biol* **17**:1219–24. doi:10.1016/j.cub.2007.06.028

Lengronne A, Katou Y, Mori S, Yokobayashi S, Kelly GP, Itoh T, Watanabe Y, Shirahige K, Uhlmann F. 2004. Cohesin relocation from sites of chromosomal loading to places of convergent transcription. *Nature* **430**:573–578. doi:10.1038/nature02742

Leonard J, Sen N, Torres R, Sutani T, Jarmuz A, Shirahige K, Aragón L. 2015. Condensin Relocalization from Centromeres to Chromosome Arms Promotes Top2 Recruitment during Anaphase. *Cell Rep* **13**:2336–2344. doi:10.1016/j.celrep.2015.11.041

Leresche A, Wolf VJ, Gottesfeld JM. 1996. Repression of RNA polymerase II and III transcription during M phase of the cell cycle. *Exp Cell Res* **229**:282–288. doi:10.1006/excr.1996.0373

Levy A, Noll M. 1981. Chromatin fine structure of active and repressed genes. *Nature* **289**:198–203. doi:10.1038/289198a0

Lewis CD, Laemmli UK. 1982. Higher order metaphase chromosome structure: evidence for metalloprotein interactions. *Cell* **29**:171–181. doi:10.1016/0092-8674(82)90101-5

Lewis TS, Sokolova V, Jung H, Ng H, Tan D. 2021. Structural basis of chromatin regulation by histone variant H2A.Z. *Nucleic Acids Res* **49**:11379–11391. doi:10.1093/nar/gkab907

Li B, Jackson J, Simon MD, Fleharty B, Gogol M, Seidel C, Workman JL, Shilatifard A. 2009. Histone H3 lysine 36 dimethylation (H3K36me2) is sufficient to recruit the Rpd3s histone deacetylase complex and to repress spurious transcription. *J Biol Chem* **284**:7970–7976. doi:10.1074/jbc.M808220200

Li G, Widom J. 2004. Nucleosomes facilitate their own invasion. *Nat Struct Mol Biol* **11**:763–769. doi:10.1038/nsmb801

Li S, Wei T, Panchenko AR. 2022. Histone variant H2A.Z modulates nucleosome dynamics to promote DNA accessibility. doi:10.1101/2022.08.29.505317

Li Y, Haarhuis JHI, Sedeño Cacciatore Á, Oldenkamp R, van Ruiten MS, Willems L, Teunissen H, Muir KW, de Wit E, Rowland BD, Panne D. 2020. The structural basis for cohesin-CTCF-anchored loops. *Nature* **578**:472–476. doi:10.1038/s41586-019-1910-z

Li Y, Zhang H, Li X, Wu W, Zhu P. 2023. Cryo-ET study from in vitro to in vivo revealed a general folding mode of chromatin with two-start helical architecture. *Cell Reports* **42**:113134. doi:10.1016/j.celrep.2023.113134

Liang K, Woodfin AR, Slaughter BD, Unruh JR, Box AC, Rickels RA, Gao X, Haug JS, Jaspersen SL, Shilatifard A. 2015. Mitotic Transcriptional Activation: Clearance of Actively Engaged Pol II via Transcriptional Elongation Control in Mitosis. *Mol Cell* **60**:435–445. doi:10.1016/j.molcel.2015.09.021

Liang Z, Zickler D, Prentiss M, Chang FS, Witz G, Maeshima K, Kleckner N. 2015. Chromosomes Progress to Metaphase in Multiple Discrete Steps via Global Compaction/Expansion Cycles. *Cell* **161**:1124–1137. doi:10.1016/j.cell.2015.04.030

Lieberman-Aiden E, van Berkum NL, Williams L, Imakaev M, Ragoczy T, Telling A, Amit I, Lajoie BR, Sabo PJ, Dorschner MO, Sandstrom R, Bernstein B, Bender MA, Groudine M, Gnirke A, Stamatoyannopoulos J, Mirny LA, Lander ES, Dekker J. 2009. Comprehensive mapping of long range interactions reveals folding principles of the human genome. *Science* **326**:289–293. doi:10.1126/science.1181369

Lin C-J, Koh FM, Wong P, Conti M, Ramalho-Santos M. 2014. Hira-Mediated H3.3 Incorporation Is Required for DNA Replication and Ribosomal RNA Transcription in the Mouse Zygote. *Developmental Cell* **30**:268–279. doi:10.1016/j.devcel.2014.06.022

Lioy VS, Cournac A, Marbouty M, Duigou S, Mozziconacci J, Espéli O, Boccard F, Koszul R. 2018. Multiscale Structuring of the E. coli Chromosome by Nucleoid-Associated and Condensin Proteins. *Cell* **172**:771-783.e18. doi:10.1016/j.cell.2017.12.027

Liu HW, Roisné-Hamelin F, Beckert B, Li Y, Myasnikov A, Gruber S. 2022. DNA-measuring Wadjet SMC ATPases restrict smaller circular plasmids by DNA cleavage. *Mol Cell* **82**:4727-4740.e6. doi:10.1016/j.molcel.2022.11.015

Liu Y, Dekker J. 2022. CTCF-CTCF loops and intra-TAD interactions show differential dependence on cohesin ring integrity. *Nat Cell Biol* **24**:1516–1527. doi:10.1038/s41556-022-00992-y

Liu Y, Zhou K, Zhang N, Wei H, Tan YZ, Zhang Z, Carragher B, Potter CS, D'Arcy S, Luger K. 2020. FACT caught in the act of manipulating the nucleosome. *Nature* **577**:426–431. doi:10.1038/s41586-019-1820-0

Losada A, Hirano M, Hirano T. 1998. Identification of Xenopus SMC protein complexes required for sister chromatid cohesion. *Genes Dev* **12**:1986–1997.

Luger K, Mäder AW, Richmond RK, Sargent DF, Richmond TJ. 1997. Crystal structure of the nucleosome core particle at 2.8 A resolution. *Nature* **389**:251–260. doi:10.1038/38444

MacCallum DE, Losada A, Kobayashi R, Hirano T. 2002. ISWI remodeling complexes in Xenopus egg extracts: identification as major chromosomal components that are regulated by INCENP-aurora B. *Mol Biol Cell* **13**:25–39. doi:10.1091/mbc.01-09-0441

Maeshima K, Hihara S, Eltsov M. 2010. Chromatin structure: does the 30-nm fibre exist in vivo? *Current Opinion in Cell Biology*, Nucleus and gene expression **22**:291–297. doi:10.1016/j.ceb.2010.03.001

Maeshima K, Laemmli UK. 2003. A Two-Step Scaffolding Model for Mitotic Chromosome Assembly. *Developmental Cell* **4**:467–480. doi:10.1016/S1534-5807(03)00092-3

Maeshima K, Rogge R, Tamura S, Joti Y, Hikima T, Szerlong H, Krause C, Herman J, Seidel E, DeLuca J, Ishikawa T, Hansen JC. 2016. Nucleosomal arrays self-assemble into supramolecular globular structures lacking 30-nm fibers. *EMBO J* **35**:1115–1132. doi:10.15252/embj.201592660

Maji A, Padinhateeri R, Mitra MK. 2020. The Accidental Ally: Nucleosome Barriers Can Accelerate Cohesin-Mediated Loop Formation in Chromatin. *Biophys J* **119**:2316–2325. doi:10.1016/j.bpj.2020.10.014

Mallik R, Kundu A, Chaudhuri S. 2018. High mobility group proteins: the multifaceted regulators of chromatin dynamics. *Nucleus* **61**:213–226. doi:10.1007/s13237-018-0257-4

Maresca TJ, Freedman BS, Heald R. 2005. Histone H1 is essential for mitotic chromosome architecture and segregation in Xenopus laevis egg extracts. *J Cell Biol* **169**:859–869. doi:10.1083/jcb.200503031

Martínez-García B, Dyson S, Segura J, Ayats A, Cutts EE, Gutierrez-Escribano P, Aragón L, Roca J. 2022. Condensin pinches a short negatively supercoiled DNA loop during each round of ATP usage. *EMBO J* **42**:e111913. doi:10.15252/embj.2022111913

Maruyama H, Prieto EI, Nambu T, Mashimo C, Kashiwagi K, Okinaga T, Atomi H, Takeyasu K. 2020. Different Proteins Mediate Step-Wise Chromosome Architectures in Thermoplasma acidophilum and Pyrobaculum calidifontis. *Frontiers in Microbiology* **11**.

Matthey-Doret C, baudrly, Amaury, axelcournac, Remi-Montagne, Guiglielmoni N, Foutel-Rodier T, Scolari VF. 2020. koszullab/hicstuff: Use miniconda layer for docker and improved P(s) normalisation. doi:10.5281/zenodo.4066363

Mattiroli F, Bhattacharyya S, Dyer PN, White AE, Sandman K, Burkhart BW, Byrne KR, Lee T, Ahn NG, Santangelo TJ, Reeve JN, Luger K. 2017. Structure of Histone-based Chromatin in Archaea. *Science* **357**:609–612. doi:10.1126/science.aaj1849

McCauley MJ, Huo R, Becker N, Holte MN, Muthurajan UM, Rouzina I, Luger K, Maher LJ, Israeloff NE, Williams MC. 2019. Single and double box HMGB proteins differentially destabilize nucleosomes. *Nucleic Acids Res* **47**:666–678. doi:10.1093/nar/gky1119

McCauley MJ, Morse M, Becker N, Hu Q, Botuyan MV, Navarrete E, Huo R, Muthurajan UM, Rouzina I, Luger K, Mer G, Maher LJ, Williams MC. 2022. Human FACT subunits coordinate to catalyze both disassembly and reassembly of nucleosomes. *Cell Reports* **41**:111858. doi:10.1016/j.celrep.2022.111858

McCullough LL, Connell Z, Xin H, Studitsky VM, Feofanov AV, Valieva ME, Formosa T. 2018. Functional roles of the DNA-binding HMGB domain in the histone chaperone FACT in nucleosome reorganization. *J Biol Chem* **293**:6121–6133. doi:10.1074/jbc.RA117.000199

Michaelis C, Ciosk R, Nasmyth K. 1997. Cohesins: Chromosomal Proteins that Prevent Premature Separation of Sister Chromatids. *Cell* **91**:35–45. doi:10.1016/S0092-8674(01)80007-6

Miller OL, Beatty BR. 1969. Visualization of Nucleolar Genes. *Science* **164**:955–957. doi:10.1126/science.164.3882.955

Minamino M, Bouchoux C, Canal B, Diffley JFX, Uhlmann F. 2023. A replication fork determinant for the establishment of sister chromatid cohesion. *Cell* **186**:837-849.e11. doi:10.1016/j.cell.2022.12.044

Miron E, Oldenkamp R, Brown JM, Pinto DMS, Xu CS, Faria AR, Shaban HA, Rhodes JDP, Innocent C, de Ornellas S, Hess HF, Buckle V, Schermelleh L. 2020. Chromatin arranges in chains of mesoscale domains with nanoscale functional topography independent of cohesin. *Science Advances* **6**:eaba8811. doi:10.1126/sciadv.aba8811

Mitter M, Gasser C, Takacs Z, Langer CCH, Tang W, Jessberger G, Beales CT, Neuner E, Ameres SL, Peters J-M, Goloborodko A, Micura R, Gerlich DW. 2020. Conformation of sister chromatids in the replicated human genome. *Nature* **586**:139–144. doi:10.1038/s41586-020-2744-4

Mizuguchi T, Fudenberg G, Mehta S, Belton J-M, Taneja N, Folco HD, FitzGerald P, Dekker J, Mirny L, Barrowman J, Grewal SIS. 2014. Cohesin-dependent globules and heterochromatin shape 3D genome architecture in S. pombe. *Nature* **516**:432–435. doi:10.1038/nature13833

Morao AK, Kim J, Obaji D, Sun S, Ercan S. 2022. Topoisomerases I and II facilitate condensin DC translocation to organize and repress X chromosomes in C. elegans. *Mol Cell* **82**:4202-4217.e5. doi:10.1016/j.molcel.2022.10.002

Muñoz S, Jones A, Bouchoux C, Gilmore T, Patel H, Uhlmann F. 2022. Functional crosstalk between the cohesin loader and chromatin remodelers. *Nat Commun* **13**:7698. doi:10.1038/s41467-022-35444-6

Muñoz S, Minamino M, Casas-Delucchi CS, Patel H, Uhlmann F. 2019. A Role for Chromatin Remodeling in Cohesin Loading onto Chromosomes. *Molecular Cell* **74**:664-673.e5. doi:10.1016/j.molcel.2019.02.027

Murawska M, Greenstein RA, Schauer T, Olsen KCF, Ng H, Ladurner AG, Al-Sady B, Braun S. 2021. The histone chaperone FACT facilitates heterochromatin spreading by regulating histone turnover and H3K9 methylation states. *Cell Rep* **37**:109944. doi:10.1016/j.celrep.2021.109944

Murawska M, Schauer T, Matsuda A, Wilson MD, Pysik T, Wojcik F, Muir TW, Hiraoka Y, Straub T, Ladurner AG. 2020. The Chaperone FACT and Histone H2B Ubiquitination Maintain S. pombe Genome Architecture through Genic and Subtelomeric Functions. *Mol Cell* **77**:501-513.e7. doi:10.1016/j.molcel.2019.11.016

Murayama Y, Samora CP, Kurokawa Y, Iwasaki H, Uhlmann F. 2018. Establishment of DNA-DNA Interactions by the Cohesin Ring. *Cell* **172**:465-477.e15. doi:10.1016/j.cell.2017.12.021

Mylonas C, Lee C, Auld AL, Cisse II, Boyer LA. 2021. A dual role for H2A.Z.1 in modulating the dynamics of RNA polymerase II initiation and elongation. *Nat Struct Mol Biol* **28**:435–442. doi:10.1038/s41594-021-00589-3

Nagasaka K, Davidson IF, Stocsits RR, Tang W, Wutz G, Batty P, Panarotto M, Litos G, Schleiffer A, Gerlich DW, Peters J-M. 2023. Cohesin mediates DNA loop extrusion and sister chromatid cohesion by distinct mechanisms. *Molecular Cell*. doi:10.1016/j.molcel.2023.07.024

Nagasaka K, Hossain MJ, Roberti MJ, Ellenberg J, Hirota T. 2016. Sister chromatid resolution is an intrinsic part of chromosome organization in prophase. *Nat Cell Biol* **18**:692–699. doi:10.1038/ncb3353

Nakazawa N, Arakawa O, Yanagida M. 2019. Condensin locates at transcriptional termination sites in mitosis, possibly releasing mitotic transcripts. *Open Biology* **9**:190125. doi:10.1098/rsob.190125

Nakazawa N, Nakamura T, Kokubu A, Ebe M, Nagao K, Yanagida M. 2008. Dissection of the essential steps for condensin accumulation at kinetochores and rDNAs during fission yeast mitosis. *J Cell Biol* **180**:1115–1131. doi:10.1083/jcb.200708170

Nakazawa N, Sajiki K, Xu X, Villar-Briones A, Arakawa O, Yanagida M. 2015. RNA pol II transcript abundance controls condensin accumulation at mitotically up-regulated and heat-shock-inducible genes in fission yeast. *Genes Cells* **20**:481–499. doi:10.1111/gtc.12239

Nasmyth K. 2001. Disseminating the Genome: Joining, Resolving, and Separating Sister Chromatids During Mitosis and Meiosis. *Annu Rev Genet* **35**:673–745. doi:10.1146/annurev.genet.35.102401.091334

Naumova N, Imakaev M, Fudenberg G, Zhan Y, Lajoie BR, Mirny LA, Dekker J. 2013. Organization of the mitotic chromosome. *Science* **342**:948–953. doi:10.1126/science.1236083

Nekrasov M, Amrichova J, Parker BJ, Soboleva TA, Jack C, Williams R, Huttley GA, Tremethick DJ. 2012. Histone H2A.Z inheritance during the cell cycle and its impact on promoter organization and dynamics. *Nat Struct Mol Biol* **19**:1076–1083. doi:10.1038/nsmb.2424

Nielsen CF, Zhang T, Barisic M, Kalitsis P, Hudson DF. 2020. Topoisomerase IIα is essential for maintenance of mitotic chromosome structure. *Proc Natl Acad Sci U S A* **117**:12131–12142. doi:10.1073/pnas.2001760117

Niki H, Jaffé A, Imamura R, Ogura T, Hiraga S. 1991. The new gene mukB codes for a 177 kd protein with coiled-coil domains involved in chromosome partitioning of E. coli. *EMBO J* **10**:183–193. doi:10.1002/j.1460-2075.1991.tb07935.x

Niki H, Yano K. 2016. In vitro topological loading of bacterial condensin MukB on DNA, preferentially single-stranded DNA rather than double-stranded DNA. *Sci Rep* **6**:29469. doi:10.1038/srep29469

Nishibuchi G, Machida S, Nakagawa R, Yoshimura Y, Hiragami-Hamada K, Abe Y, Kurumizaka H, Tagami H, Nakayama J. 2019. Mitotic phosphorylation of HP1α regulates its cell cycle-dependent chromatin binding. *The Journal of Biochemistry* **165**:433–446. doi:10.1093/jb/mvy117

Nozaki T, Imai R, Tanbo M, Nagashima R, Tamura S, Tani T, Joti Y, Tomita M, Hibino K, Kanemaki MT, Wendt KS, Okada Y, Nagai T, Maeshima K. 2017. Dynamic Organization of Chromatin Domains Revealed by Super-Resolution Live-Cell Imaging. *Molecular Cell* **67**:282-293.e7. doi:10.1016/j.molcel.2017.06.018

Oberbeckmann E, Niebauer V, Watanabe S, Farnung L, Moldt M, Schmid A, Cramer P, Peterson CL, Eustermann S, Hopfner K-P, Korber P. 2021. Ruler elements in chromatin remodelers set nucleosome array spacing and phasing. *Nat Commun* **12**:3232. doi:10.1038/s41467-021-23015-0

Ohsumi K, Katagiri C. 1991. Characterization of the ooplasmic factor inducing decondensation of and protamine removal from toad sperm nuclei: Involvement of nucleoplasmin. *Developmental Biology* **148**:295–305. doi:10.1016/0012-1606(91)90338-4

Olins DE, Olins AL. 1978. Nucleosomes: The Structural Quantum in Chromosomes: Virtually all the DNA of eukaryotic cells is organized into a repeating array of nucleohistone particles called nucleosomes. These chromatin subunits are close-packed into higher-order fibers and are modified during chromosome expression. *American Scientist* **66**:704–711.

Ono T, Fang Y, Spector DL, Hirano T. 2004. Spatial and Temporal Regulation of Condensins I and II in Mitotic Chromosome Assembly in Human Cells. *MBoC* **15**:3296–3308. doi:10.1091/mbc.e04-03-0242

Ono T, Losada A, Hirano M, Myers MP, Neuwald AF, Hirano T. 2003. Differential contributions of condensin I and condensin II to mitotic chromosome architecture in vertebrate cells. *Cell* **115**:109–121. doi:10.1016/S0092-8674(03)00724-4

Ono T, Yamashita D, Hirano T. 2013. Condensin II initiates sister chromatid resolution during S phase. *J Cell Biol* **200**:429–441. doi:10.1083/jcb.201208008

Open2C, Abdennur N, Abraham S, Fudenberg G, Flyamer IM, Galitsyna AA, Goloborodko A, Imakaev M, Oksuz BA, Venev SV. 2022. Cooltools: enabling high-resolution Hi-C analysis in Python. doi:10.1101/2022.10.31.514564

Orphanides G, LeRoy G, Chang CH, Luse DS, Reinberg D. 1998. FACT, a factor that facilitates transcript elongation through nucleosomes. *Cell* **92**:105–116. doi:10.1016/s0092-8674(00)80903-4

Orsi GA, Tortora MMC, Horard B, Baas D, Kleman J-P, Bucevičius J, Lukinavičius G, Jost D, Loppin B. 2023. Biophysical ordering transitions underlie genome 3D re-organization during cricket spermiogenesis. *Nat Commun* **14**:4187. doi:10.1038/s41467-023-39908-1

Oudet P, Gross-Bellard M, Chambon P. 1975. Electron microscopic and biochemical evidence that chromatin structure is a repeating unit. *Cell* **4**:281–300. doi:10.1016/0092-8674(75)90149-X

Paldi F, Alver B, Robertson D, Schalbetter SA, Kerr A, Kelly DA, Baxter J, Neale MJ, Marston AL. 2020. Convergent genes shape budding yeast pericentromeres. *Nature* **582**:119–123. doi:10.1038/s41586-020-2244-6

Palozola KC, Donahue G, Liu H, Grant GR, Becker JS, Cote A, Yu H, Raj A, Zaret KS. 2017. Mitotic transcription and waves of gene reactivation during mitotic exit. *Science* **358**:119–122. doi:10.1126/science.aal4671

Palozola KC, Lerner J, Zaret KS. 2019. A changing paradigm of transcriptional memory propagation through mitosis. *Nat Rev Mol Cell Biol* **20**:55–64. doi:10.1038/s41580-018-0077-z

Panday A, Grove A. 2016. Yeast HMO1: Linker Histone Reinvented. *Microbiol Mol Biol Rev* **81**:e00037-16. doi:10.1128/MMBR.00037-16

Parsons T, Zhang B. 2019. Critical role of histone tail entropy in nucleosome unwinding. *J Chem Phys* **150**:185103. doi:10.1063/1.5085663

Patel AB, Moore CM, Greber BJ, Luo J, Zukin SA, Ranish J, Nogales E. 2019. Architecture of the chromatin remodeler RSC and insights into its nucleosome engagement. *eLife* **8**:e54449. doi:10.7554/eLife.54449

Paulson JR, Hudson DF, Cisneros-Soberanis F, Earnshaw WC. 2021. Mitotic chromosomes. *Semin Cell Dev Biol* **117**:7–29. doi:10.1016/j.semcdb.2021.03.014

Paulson JR, Laemmli UK. 1977. The structure of histone-depleted metaphase chromosomes. *Cell* **12**:817–828. doi:10.1016/0092-8674(77)90280-X

Peng Y, Li S, Onufriev A, Landsman D, Panchenko AR. 2021. Binding of regulatory proteins to nucleosomes is modulated by dynamic histone tails. *Nat Commun* **12**:5280. doi:10.1038/s41467-021-25568-6

Pereira SL, Grayling RA, Lurz R, Reeve JN. 1997. Archaeal nucleosomes. *Proc Natl Acad Sci U S A* **94**:12633–12637.

Peters J-M. 2021. How DNA loop extrusion mediated by cohesin enables V(D)J recombination. *Current Opinion in Cell Biology*, Cell Nucleus **70**:75–83. doi:10.1016/j.ceb.2020.11.007

Petrova B, Dehler S, Kruitwagen T, Hériché J-K, Miura K, Haering CH. 2013. Quantitative analysis of chromosome condensation in fission yeast. *Mol Cell Biol* **33**:984–998. doi:10.1128/MCB.01400-12

Phengchat R, Hayashida M, Ohmido N, Homeniuk D, Fukui K. 2019. 3D observation of chromosome scaffold structure using a 360° electron tomography sample holder. *Micron* **126**:102736. doi:10.1016/j.micron.2019.102736

Piazza I, Rutkowska A, Ori A, Walczak M, Metz J, Pelechano V, Beck M, Haering CH. 2014. Association of condensin with chromosomes depends on DNA binding by its HEAT-repeat subunits. *Nat Struct Mol Biol* **21**:560–568. doi:10.1038/nsmb.2831

Piskadlo E, Tavares A, Oliveira RA. 2017. Metaphase chromosome structure is dynamically maintained by condensin I-directed DNA (de)catenation. *eLife* **6**:e26120. doi:10.7554/eLife.26120

Piunti A, Shilatifard A. 2021. The roles of Polycomb repressive complexes in mammalian development and cancer. *Nat Rev Mol Cell Biol* **22**:326–345. doi:10.1038/s41580-021-00341-1

Pobegalov G, Chu L-Y, Peters J-M, Molodtsov MI. 2023. Single cohesin molecules generate force by two distinct mechanisms. *Nat Commun* **14**:3946. doi:10.1038/s41467-023-39696-8

Poonperm R, Takata H, Hamano T, Matsuda A, Uchiyama S, Hiraoka Y, Fukui K. 2015. Chromosome Scaffold is a Double-Stranded Assembly of Scaffold Proteins. *Sci Rep* **5**:11916. doi:10.1038/srep11916

Poorey K, Viswanathan R, Carver MN, Karpova TS, Cirimotich SM, McNally JG, Bekiranov S, Auble DT. 2013. Measuring Chromatin Interaction Dynamics on the Second Time Scale at Single Copy Genes. *Science* **342**:369–372. doi:10.1126/science.1242369

Pradhan B, Barth R, Kim E, Davidson IF, Bauer B, van Laar T, Yang W, Ryu J-K, van der Torre J, Peters J-M, Dekker C. 2022a. SMC complexes can traverse physical roadblocks bigger than their ring size. *Cell Reports* **41**:111491. doi:10.1016/j.celrep.2022.111491

Pradhan B, Barth R, Kim E, Davidson IF, Torre J van der, Peters J-M, Dekker C. 2022b. Can pseudotopological models for SMC-driven DNA loop extrusion explain the traversal of physical roadblocks bigger than the SMC ring size? doi:10.1101/2022.08.02.502451

Pradhan B, Kanno T, Umeda Igarashi M, Loke MS, Baaske MD, Wong JSK, Jeppsson K, Björkegren C, Kim E. 2023. The Smc5/6 complex is a DNA loop-extruding motor. *Nature* **616**:843–848. doi:10.1038/s41586-023-05963-3

Price BD, D'Andrea AD. 2013. Chromatin Remodeling at DNA Double-Strand Breaks. *Cell* **152**:1344–1354. doi:10.1016/j.cell.2013.02.011

Psakhye I, Kawasumi R, Abe T, Hirota K, Branzei D. 2023. PCNA recruits cohesin loader Scc2 to ensure sister chromatid cohesion. *Nat Struct Mol Biol*. doi:10.1038/s41594-023-01064-x

Ramírez F, Ryan DP, Grüning B, Bhardwaj V, Kilpert F, Richter AS, Heyne S, Dündar F, Manke T. 2016. deepTools2: a next generation web server for deep-sequencing data analysis. *Nucleic Acids Res* **44**:W160-165. doi:10.1093/nar/gkw257

Rangasamy D, Berven L, Ridgway P, Tremethick DJ. 2003. Pericentric heterochromatin becomes enriched with H2A.Z during early mammalian development. *EMBO J* **22**:1599–1607. doi:10.1093/emboj/cdg160

Rao SSP, Huang S-C, Glenn St Hilaire B, Engreitz JM, Perez EM, Kieffer-Kwon K-R, Sanborn AL, Johnstone SE, Bascom GD, Bochkov ID, Huang X, Shamim MS, Shin J, Turner D, Ye Z, Omer AD, Robinson JT, Schlick T, Bernstein BE, Casellas R, Lander ES, Aiden EL. 2017a. Cohesin Loss Eliminates All Loop Domains. *Cell* **171**:305-320.e24. doi:10.1016/j.cell.2017.09.026

Rao SSP, Huang S-C, Glenn St Hilaire B, Engreitz JM, Perez EM, Kieffer-Kwon K-R, Sanborn AL, Johnstone SE, Bascom GD, Bochkov ID, Huang X, Shamim MS, Shin J, Turner D, Ye Z, Omer AD, Robinson JT, Schlick T, Bernstein BE, Casellas R, Lander ES, Aiden EL. 2017b. Cohesin Loss Eliminates All Loop Domains. *Cell* **171**:305-320.e24. doi:10.1016/j.cell.2017.09.026

Rao SSP, Huntley MH, Durand NC, Stamenova EK, Bochkov ID, Robinson JT, Sanborn A, Machol I, Omer AD, Lander ES, Aiden EL. 2014. A three-dimensional map of the human genome at kilobase resolution reveals principles of chromatin looping. *Cell* **159**:1665. doi:10.1016/j.cell.2014.11.021

Renshaw MJ, Ward JJ, Kanemaki M, Natsume K, Nédélec FJ, Tanaka TU. 2010. Condensins promote chromosome recoiling during early anaphase to complete sister chromatid separation. *Dev Cell* **19**:232–244. doi:10.1016/j.devcel.2010.07.013

Reyes AA, Marcum RD, He Y. 2021. Structure and Function of Chromatin Remodelers. *Journal of Molecular Biology*, RNA polymerase II Transcription **433**:166929. doi:10.1016/j.jmb.2021.166929

Reyes C, Serrurier C, Gauthier T, Gachet Y, Tournier S. 2015. Aurora B prevents chromosome arm separation defects by promoting telomere dispersion and disjunction. *J Cell Biol* **208**:713–727. doi:10.1083/jcb.201407016

Rivosecchi J. 2019. Sen1-mediated RNAPIII transcription termination controls the positioning of condensin on mitotic chromosomes (phdthesis). Université de Lyon.

Rivosecchi J, Jost D, Vachez L, Gautier FD, Bernard P, Vanoosthuyse V. 2021. RNA polymerase backtracking results in the accumulation of fission yeast condensin at active genes. *Life Sci Alliance* **4**:e202101046. doi:10.26508/lsa.202101046

Robellet X, Fauque L, Legros P, Mollereau E, Janczarski S, Parrinello H, Desvignes J-P, Thevenin M, Bernard P. 2014. A genetic screen for functional partners of condensin in fission yeast. *G3 (Bethesda)* **4**:373–381. doi:10.1534/g3.113.009621

Robellet X, Thattikota Y, Wang F, Wee T-L, Pascariu M, Shankar S, Bonneil É, Brown CM, D'Amours D. 2015. A high-sensitivity phospho-switch triggered by Cdk1 governs chromosome morphogenesis during cell division. *Genes Dev* **29**:426–439. doi:10.1101/gad.253294.114

Robellet X, Vanoosthuyse V, Bernard P. 2017. The loading of condensin in the context of chromatin. *Curr Genet* **63**:577–589. doi:10.1007/s00294-016-0669-0

Rustici G, Mata J, Kivinen K, Lió P, Penkett CJ, Burns G, Hayles J, Brazma A, Nurse P, Bähler J. 2004. Periodic gene expression program of the fission yeast cell cycle. *Nat Genet* **36**:809–817. doi:10.1038/ng1377

Ryu J-K, Bouchoux C, Liu HW, Kim E, Minamino M, de Groot R, Katan AJ, Bonato A, Marenduzzo D, Michieletto D, Uhlmann F, Dekker C. 2021a. Bridging-induced phase separation induced by cohesin SMC protein complexes. *Sci Adv* **7**:eabe5905. doi:10.1126/sciadv.abe5905

Ryu J-K, Katan AJ, van der Sluis EO, Wisse T, de Groot R, Haering CH, Dekker C. 2020. The condensin holocomplex cycles dynamically between open and collapsed states. *Nat Struct Mol Biol* **27**:1134–1141. doi:10.1038/s41594-020-0508-3

Ryu J-K, Rah S-H, Janissen R, Kerssemakers JWJ, Bonato A, Michieletto D, Dekker C. 2021b. Condensin extrudes DNA loops in steps up to hundreds of base pairs that are generated by ATP binding events. *Nucleic Acids Res* **50**:820–832. doi:10.1093/nar/gkab1268

Saitoh N, Goldberg IG, Wood ER, Earnshaw WC. 1994. ScII: an abundant chromosome scaffold protein is a member of a family of putative ATPases with an unusual predicted tertiary structure. *J Cell Biol* **127**:303–318. doi:10.1083/jcb.127.2.303

Saka Y, Sutani T, Yamashita Y, Saitoh S, Takeuchi M, Nakaseko Y, Yanagida M. 1994. Fission yeast cut3 and cut14, members of a ubiquitous protein family, are required for chromosome condensation and segregation in mitosis. *The EMBO Journal* **13**:4938–4952. doi:10.1002/j.1460-2075.1994.tb06821.x

Sakai A, Hizume K, Sutani T, Takeyasu K, Yanagida M. 2003. Condensin but not cohesin SMC heterodimer induces DNA reannealing through protein–protein assembly. *EMBO J* **22**:2764–2775. doi:10.1093/emboj/cdg247

Samejima I, Spanos C, Samejima K, Rappsilber J, Kustatscher G, Earnshaw WC. 2022. Mapping the invisible chromatin transactions of prophase chromosome remodeling. *Mol Cell* **82**:696-708.e4. doi:10.1016/j.molcel.2021.12.039

Samejima K, Booth DG, Ogawa H, Paulson JR, Xie L, Watson CA, Platani M, Kanemaki MT, Earnshaw WC. 2018. Functional analysis after rapid degradation of condensins and 3D-EM reveals chromatin volume is uncoupled from chromosome architecture in mitosis. *Journal of Cell Science* **131**:jcs210187. doi:10.1242/jcs.210187

Saunders A, Werner J, Andrulis ED, Nakayama T, Hirose S, Reinberg D, Lis JT. 2003. Tracking FACT and the RNA polymerase II elongation complex through chromatin in vivo. *Science* **301**:1094–1096. doi:10.1126/science.1085712

Schier AC, Taatjes DJ. 2020. Structure and mechanism of the RNA polymerase II transcription machinery. *Genes Dev* **34**:465–488. doi:10.1101/gad.335679.119

Schmidt CK, Brookes N, Uhlmann F. 2009. Conserved features of cohesin binding along fission yeast chromosomes. *Genome Biol* **10**:R52. doi:10.1186/gb-2009-10-5-r52

Schneider MWG, Gibson BA, Otsuka S, Spicer MFD, Petrovic M, Blaukopf C, Langer CCH, Batty P, Nagaraju T, Doolittle LK, Rosen MK, Gerlich DW. 2022. A mitotic chromatin phase transition prevents perforation by microtubules. *Nature* **609**:183–190. doi:10.1038/s41586-022-05027-y

Serrano Á, Rodríguez-Corsino M, Losada A. 2009. Heterochromatin Protein 1 (HP1) Proteins Do Not Drive Pericentromeric Cohesin Enrichment in Human Cells. *PLoS One* **4**:e5118. doi:10.1371/journal.pone.0005118

Shaltiel IA, Datta S, Lecomte L, Hassler M, Kschonsak M, Bravo S, Stober C, Ormanns J, Eustermann S, Haering CH. 2022. A hold-and-feed mechanism drives directional DNA loop extrusion by condensin. *Science* **376**:1087–1094. doi:10.1126/science.abm4012

Sheinin MY, Li M, Soltani M, Luger K, Wang MD. 2013. Torque modulates nucleosome stability and facilitates H2A/H2B dimer loss. *Nat Commun* **4**:2579. doi:10.1038/ncomms3579

Shi Z, Gao H, Bai X, Yu H. 2020. Cryo-EM structure of the human cohesin-NIPBL-DNA complex. *Science* **368**:1454–1459. doi:10.1126/science.abb0981

Shintomi K, Hirano T. 2021. Guiding functions of the C-terminal domain of topoisomerase IIα advance mitotic chromosome assembly. *Nat Commun* **12**:2917. doi:10.1038/s41467-021-23205-w

Shintomi K, Hirano T. 2011. The relative ratio of condensin I to II determines chromosome shapes. *Genes Dev* **25**:1464–1469. doi:10.1101/gad.2060311

Shintomi K, Inoue F, Watanabe H, Ohsumi K, Ohsugi M, Hirano T. 2017. Mitotic chromosome assembly despite nucleosome depletion in Xenopus egg extracts. *Science* **356**:1284–1287. doi:10.1126/science.aam9702

Shintomi K, Takahashi TS, Hirano T. 2015. Reconstitution of mitotic chromatids with a minimum set of purified factors. *Nat Cell Biol* **17**:1014–1023. doi:10.1038/ncb3187

Shogren-Knaak M, Ishii H, Sun J-M, Pazin MJ, Davie JR, Peterson CL. 2006. Histone H4-K16 Acetylation Controls Chromatin Structure and Protein Interactions. *Science* **311**:844–847. doi:10.1126/science.1124000

Shukla M, Tong P, White SA, Singh PP, Reid AM, Catania S, Pidoux AL, Allshire RC. 2018. Centromere DNA Destabilizes H3 Nucleosomes to Promote CENP-A Deposition during the Cell Cycle. *Curr Biol* **28**:3924-3936.e4. doi:10.1016/j.cub.2018.10.049

Simic R, Lindstrom DL, Tran HG, Roinick KL, Costa PJ, Johnson AD, Hartzog GA, Arndt KM. 2003. Chromatin remodeling protein Chd1 interacts with transcription elongation factors and localizes to transcribed genes. *EMBO J* **22**:1846–1856. doi:10.1093/emboj/cdg179

Singh AK, Schauer T, Pfaller L, Straub T, Mueller-Planitz F. 2021. The biogenesis and function of nucleosome arrays. *Nat Commun* **12**:7011. doi:10.1038/s41467-021-27285-6

Sivkina AL, Karlova MG, Valieva ME, McCullough LL, Formosa T, Shaytan AK, Feofanov AV, Kirpichnikov MP, Sokolova OS, Studitsky VM. 2022. Electron microscopy analysis of ATP-independent nucleosome unfolding by FACT. *Commun Biol* **5**:1–9. doi:10.1038/s42003-021-02948-8

Smith S, Stillman B. 1989. Purification and characterization of CAF-I, a human cell factor required for chromatin assembly during DNA replication in vitro. *Cell* **58**:15–25. doi:10.1016/0092-8674(89)90398-X

Solovei I, Thanisch K, Feodorova Y. 2016. How to rule the nucleus: divide et impera. *Current Opinion in Cell Biology*, Cell nucleus **40**:47–59. doi:10.1016/j.ceb.2016.02.014

Soman A, Wong SY, Korolev N, Surya W, Lattmann S, Vogirala VK, Chen Q, Berezhnoy NV, van Noort J, Rhodes D, Nordenskiöld L. 2022. Columnar structure of human telomeric chromatin. *Nature* **609**:1048–1055. doi:10.1038/s41586-022-05236-5

Song F, Chen P, Sun D, Wang M, Dong L, Liang D, Xu R-M, Zhu P, Li G. 2014. Cryo-EM Study of the Chromatin Fiber Reveals a Double Helix Twisted by Tetranucleosomal Units. *Science* **344**:376–380. doi:10.1126/science.1251413

Spencer CA, Kruhlak MJ, Jenkins HL, Sun X, Bazett-Jones DP. 2000. Mitotic Transcription Repression in Vivo in the Absence of Nucleosomal Chromatin Condensation. *J Cell Biol* **150**:13–26.

Srinivasan M, Fumasoni M, Petela NJ, Murray A, Nasmyth KA. 2020. Cohesion is established during DNA replication utilising chromosome associated cohesin rings as well as those loaded de novo onto nascent DNAs. *eLife* **9**:e56611. doi:10.7554/eLife.56611

Srinivasan M, Scheinost JC, Petela NJ, Gligoris TG, Wissler M, Ogushi S, Collier JE, Voulgaris M, Kurze A, Chan K-L, Hu B, Costanzo V, Nasmyth KA. 2018. The Cohesin Ring Uses Its Hinge to Organize DNA Using Non-topological as well as Topological Mechanisms. *Cell* **173**:1508-1519.e18. doi:10.1016/j.cell.2018.04.015

Stenström L, Mahdessian D, Gnann C, Cesnik AJ, Ouyang W, Leonetti MD, Uhlén M, Cuylen-Haering S, Thul PJ, Lundberg E. 2020. Mapping the nucleolar proteome reveals a spatiotemporal organization related to intrinsic protein disorder. *Mol Syst Biol* **16**:e9469. doi:10.15252/msb.20209469

Stigler J, Çamdere GÖ, Koshland DE, Greene EC. 2016. Single-Molecule Imaging Reveals a Collapsed Conformational State for DNA-Bound Cohesin. *Cell Rep* **15**:988–998. doi:10.1016/j.celrep.2016.04.003

St-Pierre J, Douziech M, Bazile F, Pascariu M, Bonneil É, Sauvé V, Ratsima H, D'Amours D. 2009. Polo Kinase Regulates Mitotic Chromosome Condensation by Hyperactivation of Condensin DNA Supercoiling Activity. *Molecular Cell* **34**:416–426. doi:10.1016/j.molcel.2009.04.013

Strickfaden H, Tolsma TO, Sharma A, Underhill DA, Hansen JC, Hendzel MJ. 2020. Condensed Chromatin Behaves like a Solid on the Mesoscale In Vitro and in Living Cells. *Cell* **183**:1772-1784.e13. doi:10.1016/j.cell.2020.11.027

Strom AR, Biggs RJ, Banigan EJ, Wang X, Chiu K, Herman C, Collado J, Yue F, Ritland Politz JC, Tait LJ, Scalzo D, Telling A, Groudine M, Brangwynne CP, Marko JF, Stephens AD. 2021. HP1α is a chromatin crosslinker that controls nuclear and mitotic chromosome mechanics. *eLife* **10**:e63972. doi:10.7554/eLife.63972

Strom AR, Emelyanov AV, Mir M, Fyodorov DV, Darzacq X, Karpen GH. 2017. Phase separation drives heterochromatin domain formation. *Nature* **547**:241–245. doi:10.1038/nature22989

Strunnikov AV, Larionov VL, Koshland D. 1993. SMC1: an essential yeast gene encoding a putative head-rod-tail protein is required for nuclear division and defines a new ubiquitous protein family. *J Cell Biol* **123**:1635–1648. doi:10.1083/jcb.123.6.1635

Studitsky VM, Kassavetis GA, Geiduschek EP, Felsenfeld G. 1997. Mechanism of transcription through the nucleosome by eukaryotic RNA polymerase. *Science* **278**:1960–1963. doi:10.1126/science.278.5345.1960

Stuwe T, Hothorn M, Lejeune E, Rybin V, Bortfeld M, Scheffzek K, Ladurner AG. 2008. The FACT Spt16 "peptidase" domain is a histone H3-H4 binding module. *Proc Natl Acad Sci U S A* **105**:8884–8889. doi:10.1073/pnas.0712293105

Sullivan M, Higuchi T, Katis VL, Uhlmann F. 2004. Cdc14 Phosphatase Induces rDNA Condensation and Resolves Cohesin-Independent Cohesion during Budding Yeast Anaphase. *Cell* **117**:471–482. doi:10.1016/S0092-8674(04)00415-5

Sun M, Amiri H, Tong AB, Shintomi K, Hirano T, Bustamante C, Heald R. 2023. Monitoring the compaction of single DNA molecules in Xenopus egg extract in real time. *Proc Natl Acad Sci U S A* **120**:e2221309120. doi:10.1073/pnas.2221309120

Sun M, Biggs R, Hornick J, Marko JF. 2018. Condensin controls mitotic chromosome stiffness and stability without forming a structurally contiguous scaffold. *Chromosome Res* **26**:277–295. doi:10.1007/s10577-018-9584-1

Sutani T, Kawaguchi T, Kanno R, Itoh T, Shirahige K. 2009. Budding yeast Wpl1(Rad61)-Pds5 complex counteracts sister chromatid cohesion-establishing reaction. *Curr Biol* **19**:492–497. doi:10.1016/j.cub.2009.01.062

Sutani T, Sakata T, Nakato R, Masuda K, Ishibashi M, Yamashita D, Suzuki Y, Hirano T, Bando M, Shirahige K. 2015. Condensin targets and reduces unwound DNA structures associated with transcription in mitotic chromosome condensation. *Nat Commun* **6**:7815. doi:10.1038/ncomms8815

Sutani T, Yanagida M. 1997. DNA renaturation activity of the SMC complex implicated in chromosome condensation. *Nature* **388**:798–801. doi:10.1038/42062

Suto RK, Clarkson MJ, Tremethick DJ, Luger K. 2000. Crystal structure of a nucleosome core particle containing the variant histone H2A.Z. *Nat Struct Mol Biol* **7**:1121–1124. doi:10.1038/81971

Swygert SG, Kim S, Wu X, Fu T, Hsieh T-H, Rando OJ, Eisenman RN, Shendure J, McKnight JN, Tsukiyama T. 2019. Condensin-Dependent Chromatin Compaction Represses Transcription Globally during Quiescence. *Molecular Cell* **73**:533-546.e4. doi:10.1016/j.molcel.2018.11.020

Swygert SG, Lin D, Portillo-Ledesma S, Lin P-Y, Hunt DR, Kao C-F, Schlick T, Noble WS, Tsukiyama T. 2021. Local chromatin fiber folding represses transcription and loop extrusion in quiescent cells. *eLife* **10**:e72062. doi:10.7554/eLife.72062

Tachiwana H, Dacher M, Maehara K, Harada A, Seto Y, Katayama R, Ohkawa Y, Kimura H, Kurumizaka H, Saitoh N. 2021. Chromatin structure-dependent histone incorporation revealed by a genome-wide deposition assay. *Elife* **10**:e66290. doi:10.7554/eLife.66290

Tada K, Susumu H, Sakuno T, Watanabe Y. 2011. Condensin association with histone H2A shapes mitotic chromosomes. *Nature* **474**:477–483. doi:10.1038/nature10179

Takagi M, Ono T, Natsume T, Sakamoto C, Nakao M, Saitoh N, Kanemaki MT, Hirano T, Imamoto N. 2018. Ki-67 and condensins support the integrity of mitotic chromosomes through distinct mechanisms. *Journal of Cell Science* **131**:jcs212092. doi:10.1242/jcs.212092

Takemata N, Bell SD. 2021. Multi-scale architecture of archaeal chromosomes. *Mol Cell* **81**:473-487.e6. doi:10.1016/j.molcel.2020.12.001

Takemata N, Samson RY, Bell SD. 2019. Physical and functional compartmentalization of archaeal chromosomes. *Cell* **179**:165-179.e18. doi:10.1016/j.cell.2019.08.036

Tanaka T, Fuchs J, Loidl J, Nasmyth K. 2000. Cohesin ensures bipolar attachment of microtubules to sister centromeres and resists their precocious separation. *Nat Cell Biol* **2**:492–499. doi:10.1038/35019529

Tane S, Shintomi K, Kinoshita K, Tsubota Y, Yoshida MM, Nishiyama T, Hirano T. 2022. Cell cycle-specific loading of condensin I is regulated by the N-terminal tail of its kleisin subunit. *eLife* **11**:e84694. doi:10.7554/eLife.84694

Tang M, Pobegalov G, Tanizawa H, Chen ZA, Rappsilber J, Molodtsov M, Noma K, Uhlmann F. 2023. Establishment of dsDNA-dsDNA interactions by the condensin complex. *Molecular Cell* **83**:3787-3800.e9. doi:10.1016/j.molcel.2023.09.019

Tanizawa H, Kim K-D, Iwasaki O, Noma K-I. 2017. Architectural alterations of the fission yeast genome during the cell cycle. *Nat Struct Mol Biol* **24**:965–976. doi:10.1038/nsmb.3482

Tashiro S, Nishihara Y, Kugou K, Ohta K, Kanoh J. 2017. Subtelomeres constitute a safeguard for gene expression and chromosome homeostasis. *Nucleic Acids Res* **45**:10333–10349. doi:10.1093/nar/gkx780

Tedeschi A, Wutz G, Huet S, Jaritz M, Wuensche A, Schirghuber E, Davidson IF, Tang W, Cisneros DA, Bhaskara V, Nishiyama T, Vaziri A, Wutz A, Ellenberg J, Peters J-M. 2013. Wapl is an essential regulator of chromatin structure and chromosome segregation. *Nature* **501**:564–568. doi:10.1038/nature12471

Teif VB, Vainshtein Y, Caudron-Herger M, Mallm J-P, Marth C, Höfer T, Rippe K. 2012. Genome-wide nucleosome positioning during embryonic stem cell development. *Nat Struct Mol Biol* **19**:1185–1192. doi:10.1038/nsmb.2419

Terakawa T, Bisht S, Eeftens JM, Dekker C, Haering CH, Greene EC. 2017. The condensin complex is a mechanochemical motor that translocates along DNA. *Science* **358**:672–676. doi:10.1126/science.aan6516

Thadani R, Kamenz J, Heeger S, Muñoz S, Uhlmann F. 2018. Cell-Cycle Regulation of Dynamic Chromosome Association of the Condensin Complex. *Cell Rep* **23**:2308–2317. doi:10.1016/j.celrep.2018.04.082

Thurman RE, Rynes E, Humbert R, Vierstra J, Maurano MT, Haugen E, Sheffield NC, Stergachis AB, Wang H, Vernot B, Garg K, John S, Sandstrom R, Bates D, Boatman L, Canfield TK, Diegel M, Dunn D, Ebersol AK, Frum T, Giste E, Johnson AK, Johnson EM, Kutyavin T, Lajoie B, Lee B-K, Lee K, London D, Lotakis D, Neph S, Neri F, Nguyen ED, Qu H, Reynolds AP, Roach V, Safi A, Sanchez ME, Sanyal A, Shafer A, Simon JM, Song L, Vong S, Weaver M, Yan Y, Zhang Zhancheng, Zhang Zhuzhu, Lenhard B, Tewari M, Dorschner MO, Hansen RS, Navas PA, Stamatoyannopoulos G, Iyer VR, Lieb JD, Sunyaev SR, Akey JM, Sabo PJ, Kaul R, Furey TS, Dekker J, Crawford GE, Stamatoyannopoulos JA. 2012. The accessible chromatin landscape of the human genome. *Nature* **489**:75–82. doi:10.1038/nature11232

Tomonaga T, Nagao K, Kawasaki Y, Furuya K, Murakami A, Morishita J, Yuasa T, Sutani T, Kearsey SE, Uhlmann F, Nasmyth K, Yanagida M. 2000. Characterization of fission yeast cohesin: essential anaphase proteolysis of Rad21 phosphorylated in the S phase. *Genes Dev* **14**:2757–2770.

Toselli-Mollereau E, Robellet X, Fauque L, Lemaire S, Schiklenk C, Klein C, Hocquet C, Legros P, N'Guyen L, Mouillard L, Chautard E, Auboeuf D, Haering CH, Bernard P. 2016. Nucleosome eviction in mitosis assists condensin loading and chromosome condensation. *The EMBO Journal* **35**:1565–1581. doi:10.15252/embj.201592849

Tóth A, Ciosk R, Uhlmann F, Galova M, Schleiffer A, Nasmyth K. 1999. Yeast cohesin complex requires a conserved protein, Eco1p(Ctf7), to establish cohesion between sister chromatids during DNA replication. *Genes Dev* **13**:320–333. doi:10.1101/gad.13.3.320

Tran NT, Laub MT, Le TBK. 2017. SMC Progressively Aligns Chromosomal Arms in Caulobacter crescentus but Is Antagonized by Convergent Transcription. *Cell Rep* **20**:2057–2071. doi:10.1016/j.celrep.2017.08.026

Truong DM, Boeke JD. 2017. Resetting the yeast epigenome with human nucleosomes. *Cell* **171**:1508-1519.e13. doi:10.1016/j.cell.2017.10.043

Tschiersch B, Hofmann A, Krauss V, Dorn R, Korge G, Reuter G. 1994. The protein encoded by the Drosophila position-effect variegation suppressor gene Su(var)3-9 combines domains of antagonistic regulators of homeotic gene complexes. *EMBO J* **13**:3822–3831. doi:10.1002/j.1460-2075.1994.tb06693.x

Uemura T, Ohkura H, Adachi Y, Morino K, Shiozaki K, Yanagida M. 1987. DNA topoisomerase II is required for condensation and separation of mitotic chromosomes in S. pombe. *Cell* **50**:917–925. doi:10.1016/0092-8674(87)90518-6

Uemura T, Yanagida M. 1984. Isolation of type I and II DNA topoisomerase mutants from fission yeast: single and double mutants show different phenotypes in cell growth and chromatin organization. *EMBO J* **3**:1737–1744. doi:10.1002/j.1460-2075.1984.tb02040.x

Uhlmann F, Lottspeich F, Nasmyth K. 1999. Sister-chromatid separation at anaphase onset is promoted by cleavage of the cohesin subunit Scc1. *Nature* **400**:37–42. doi:10.1038/21831

Uhlmann F, Nasmyth K. 1998. Cohesion between sister chromatids must be established during DNA replication. *Curr Biol* **8**:1095–1101. doi:10.1016/s0960-9822(98)70463-4

Umbreit NT, Zhang C-Z, Lynch LD, Blaine LJ, Cheng AM, Tourdot R, Sun L, Almubarak HF, Judge K, Mitchell TJ, Spektor A, Pellman D. 2020. MECHANISMS GENERATING CANCER GENOME COMPLEXITY FROM A SINGLE CELL DIVISION ERROR. *Science* **368**:eaba0712. doi:10.1126/science.aba0712

Vagnarelli P, Hudson DF, Ribeiro SA, Trinkle-Mulcahy L, Spence JM, Lai F, Farr CJ, Lamond AI, Earnshaw WC. 2006. Condensin and Repo-Man-PP1 co-operate in the regulation of chromosome architecture during mitosis. *Nat Cell Biol* **8**:1133–1142. doi:10.1038/ncb1475

Valieva ME, Gerasimova NS, Kudryashova KS, Kozlova AL, Kirpichnikov MP, Hu Q, Botuyan MV, Mer G, Feofanov AV, Studitsky VM. 2017. Stabilization of Nucleosomes by Histone Tails and by FACT Revealed by spFRET Microscopy. *Cancers (Basel)* **9**:3. doi:10.3390/cancers9010003

van Daal A, Elgin SC. 1992. A histone variant, H2AvD, is essential in Drosophila melanogaster. *Mol Biol Cell* **3**:593–602. doi:10.1091/mbc.3.6.593

Van Hooser A, Goodrich DW, Allis CD, Brinkley BR, Mancini MA. 1998. Histone H3 phosphorylation is required for the initiation, but not maintenance, of mammalian chromosome condensation. *J Cell Sci* **111 (Pt 23)**:3497–3506. doi:10.1242/jcs.111.23.3497

VanDemark AP, Blanksma M, Ferris E, Heroux A, Hill CP, Formosa T. 2006. The structure of the yFACT Pob3-M domain, its interaction with the DNA replication factor RPA, and a potential role in nucleosome deposition. *Mol Cell* **22**:363–374. doi:10.1016/j.molcel.2006.03.025

Vazquez Nunez R, Ruiz Avila LB, Gruber S. 2019. Transient DNA Occupancy of the SMC Interarm Space in Prokaryotic Condensin. *Mol Cell* **75**:209-223.e6. doi:10.1016/j.molcel.2019.05.001

Vian L, Pękowska A, Rao SSP, Kieffer-Kwon K-R, Jung S, Baranello L, Huang S-C, El Khattabi L, Dose M, Pruett N, Sanborn AL, Canela A, Maman Y, Oksanen A, Resch W, Li X, Lee B, Kovalchuk AL, Tang Z, Nelson S, Di Pierro M, Cheng RR, Machol I, St Hilaire BG, Durand NC, Shamim MS, Stamenova EK, Onuchic JN, Ruan Y, Nussenzweig A, Levens D, Aiden EL, Casellas R. 2018. The Energetics and Physiological Impact of Cohesin Extrusion. *Cell* **173**:1165-1178.e20. doi:10.1016/j.cell.2018.03.072

Waizenegger IC, Hauf S, Meinke A, Peters JM. 2000. Two distinct pathways remove mammalian cohesin from chromosome arms in prophase and from centromeres in anaphase. *Cell* **103**:399–410. doi:10.1016/s0092-8674(00)00132-x

Walther N, Hossain MJ, Politi AZ, Koch B, Kueblbeck M, Ødegård-Fougner Ø, Lampe M, Ellenberg J. 2018. A quantitative map of human Condensins provides new insights into mitotic chromosome architecture. *J Cell Biol* **217**:2309–2328. doi:10.1083/jcb.201801048

Wang B-D, Butylin P, Strunnikov A. 2006. Condensin Function in Mitotic Nucleolar Segregation is Regulated by rDNA Transcription. *Cell Cycle* **5**:2260–2267.

Wang F, Dai J, Daum JR, Niedzialkowska E, Banerjee B, Stukenberg PT, Gorbsky GJ, Higgins JMG. 2010. Histone H3 Thr-3 phosphorylation by Haspin positions Aurora B at centromeres in mitosis. *Science* **330**:231–235. doi:10.1126/science.1189435

Wang H, Schilbach S, Ninov M, Urlaub H, Cramer P. 2023. Structures of transcription preinitiation complex engaged with the +1 nucleosome. *Nat Struct Mol Biol* **30**:226–232. doi:10.1038/s41594-022-00865-w

Wang J, Hu C, Chen X, Li Y, Sun J, Czajkowsky DM, Shao Z. 2022. Single-Molecule Micromanipulation and Super-Resolution Imaging Resolve Nanodomains Underlying Chromatin Folding in Mitotic Chromosomes. *ACS Nano* **16**:8030–8039. doi:10.1021/acsnano.2c01025

Wang X, Brandão HB, Le TBK, Laub MT, Rudner DZ. 2017. Bacillus subtilis SMC complexes juxtapose chromosome arms as they travel from origin to terminus. *Science* **355**:524–527. doi:10.1126/science.aai8982

Wang X, Hughes AC, Brandão HB, Walker B, Lierz C, Cochran JC, Oakley MG, Kruse AC, Rudner DZ. 2018. In Vivo Evidence for ATPase-Dependent DNA Translocation by the Bacillus subtilis SMC Condensin Complex. *Mol Cell* **71**:841-847.e5. doi:10.1016/j.molcel.2018.07.006

Watson JD, Crick FHC. 1953. Molecular Structure of Nucleic Acids: A Structure for Deoxyribose Nucleic Acid. *Nature* **171**:737–738. doi:10.1038/171737a0

Weber CM, Henikoff JG, Henikoff S. 2010. H2A.Z nucleosomes enriched over active genes are homotypic. *Nat Struct Mol Biol* **17**:1500–1507. doi:10.1038/nsmb.1926

Wei Y, Yu L, Bowen J, Gorovsky MA, Allis CD. 1999. Phosphorylation of Histone H3 Is Required for Proper Chromosome Condensation and Segregation. *Cell* **97**:99–109. doi:10.1016/S0092-8674(00)80718-7

West S, Gromak N, Proudfoot NJ. 2004. Human 5′ → 3′ exonuclease Xrn2 promotes transcription termination at co-transcriptional cleavage sites. *Nature* **432**:522–525. doi:10.1038/nature03035

Whittemore K, Vera E, Martínez-Nevado E, Sanpera C, Blasco MA. 2019. Telomere shortening rate predicts species life span. *Proceedings of the National Academy of Sciences* **116**:15122–15127. doi:10.1073/pnas.1902452116

Wilkins BJ, Rall NA, Ostwal Y, Kruitwagen T, Hiragami-Hamada K, Winkler M, Barral Y, Fischle W, Neumann H. 2014. A Cascade of Histone Modifications Induces Chromatin Condensation in Mitosis. *Science* **343**:77–80. doi:10.1126/science.1244508

Yague-Sanz C, Migeot V, Larochelle M, Bachand F, Wéry M, Morillon A, Hermand D. 2023. Chromatin remodeling by Pol II primes efficient Pol III transcription. *Nat Commun* **14**:3587. doi:10.1038/s41467-023-39387-4

Yakoubi WE, Akera T. 2022. Condensin dysfunction is a reproductive isolating barrier in mice. doi:10.1101/2022.10.20.513083

Yalon M, Gal S, Segev Y, Selig S, Skorecki KL. 2004. Sister chromatid separation at human telomeric regions. *Journal of Cell Science* **117**:1961–1970. doi:10.1242/jcs.01032

Yamaguchi K, Hada M, Fukuda Y, Inoue E, Makino Y, Katou Y, Shirahige K, Okada Y. 2018. Re-evaluating the Localization of Sperm-Retained Histones Revealed the Modification-Dependent Accumulation in Specific Genome Regions. *Cell Rep* **23**:3920–3932. doi:10.1016/j.celrep.2018.05.094

Yamamoto T, Kinoshita K, Hirano T. 2023. Elasticity control of entangled chromosomes: Crosstalk between condensin complexes and nucleosomes. *Biophys J* S0006-3495(23)00506–4. doi:10.1016/j.bpj.2023.08.006

Yang TZ, Shujun C, J NA, K CJ, Jian S, Lu G. 2023. Heterogeneous non-canonical nucleosomes predominate in yeast cells in situ. *eLife* **12**. doi:10.7554/eLife.87672

Yatskevich S, Muir KW, Bellini D, Zhang Z, Yang J, Tischer T, Predin M, Dendooven T, McLaughlin SH, Barford D. 2022. Structure of the human inner kinetochore bound to a centromeric CENP-A nucleosome. *Science* **376**:844–852. doi:10.1126/science.abn3810

Yoo EJ, Jin YH, Jang YK, Bjerling P, Tabish M, Hong SH, Ekwall K, Park SD. 2000. Fission yeast Hrp1, a chromodomain ATPase, is required for proper chromosome segregation and its overexpression interferes with chromatin condensation. *Nucleic Acids Res* **28**:2004–2011.

Yoshida MM, Kinoshita K, Aizawa Y, Tane S, Yamashita D, Shintomi K, Hirano T. 2022. Molecular dissection of condensin II-mediated chromosome assembly using in vitro assays. *Elife* **11**:e78984. doi:10.7554/eLife.78984

Yuen KC, Slaughter BD, Gerton JL. 2017. Condensin II is anchored by TFIIIC and H3K4me3 in the mammalian genome and supports the expression of active dense gene clusters. *Sci Adv* **3**:e1700191. doi:10.1126/sciadv.1700191

Zaret KS, Mango S. 2016. Pioneer Transcription Factors, Chromatin Dynamics, and Cell Fate Control. *Curr Opin Genet Dev* **37**:76–81. doi:10.1016/j.gde.2015.12.003

Zencir S, Dilg D, Shore D, Albert B. 2022. Pitfalls in using phenanthroline to study the causal relationship between promoter nucleosome acetylation and transcription. *Nat Commun* **13**:3726. doi:10.1038/s41467-022-30350-3

Zhang H, Shi Z, Banigan EJ, Kim Y, Yu H, Bai X-C, Finkelstein IJ. 2023. CTCF and R-loops are boundaries of cohesin-mediated DNA looping. *Mol Cell* **83**:2856-2871.e8. doi:10.1016/j.molcel.2023.07.006

Zhang S, Übelmesser N, Barbieri M, Papantonis A. 2023. Enhancer–promoter contact formation requires RNAPII and antagonizes loop extrusion. *Nat Genet* **55**:832–840. doi:10.1038/s41588-023-01364-4

Zhang X-R, Zhao L, Suo F, Gao Y, Wu Q, Qi X, Du L-L. 2021. An improved auxin-inducible degron system for fission yeast. *G3 (Bethesda)* **12**:jkab393. doi:10.1093/g3journal/jkab393

Zhang Z, Wippo CJ, Wal M, Ward E, Korber P, Pugh BF. 2011. A Packing Mechanism for Nucleosome Organization Reconstituted Across a Eukaryotic Genome. *Science* **332**:977–980. doi:10.1126/science.1200508

Zheng G, Kanchwala M, Xing C, Yu H. 2018. MCM2–7-dependent cohesin loading during S phase promotes sister-chromatid cohesion. *eLife* **7**:e33920. doi:10.7554/eLife.33920

Zhiteneva A, Bonfiglio JJ, Makarov A, Colby T, Vagnarelli P, Schirmer EC, Matic I, Earnshaw WC. 2017. Mitotic post-translational modifications of histones promote chromatin compaction in vitro. *Open Biol* **7**:170076. doi:10.1098/rsob.170076

Zhou B-R, Feng H, Kale S, Fox T, Khant H, de Val N, Ghirlando R, Panchenko AR, Bai Y. 2021. Distinct Structures and Dynamics of Chromatosomes with Different Human Linker Histone Isoforms. *Molecular Cell* **81**:166-182.e6. doi:10.1016/j.molcel.2020.10.038

Zhou B-R, Jiang J, Feng H, Ghirlando R, Xiao TS, Bai Y. 2015. Structural Mechanisms of Nucleosome Recognition by Linker Histones. *Mol Cell* **59**:628–638. doi:10.1016/j.molcel.2015.06.025

Zhou L, Tian X, Zhu C, Wang F, Higgins JMG. 2014. Polo-like kinase-1 triggers histone phosphorylation by Haspin in mitosis. *EMBO Rep* **15**:273–281. doi:10.1002/embr.201338080

Zhu Z, Chen X, Guo A, Manzano T, Walsh PJ, Wills KM, Halliburton R, Radko-Juettner S, Carter RD, Partridge JF, Green DR, Zhang J, Roberts CWM. 2023. Mitotic bookmarking by SWI/SNF subunits. *Nature* **618**:180–187. doi:10.1038/s41586-023-06085-6

Zickler D, Kleckner N. 1999. Meiotic chromosomes: integrating structure and function. *Annu Rev Genet* **33**:603–754. doi:10.1146/annurev.genet.33.1.603

Zierhut C, Jenness C, Kimura H, Funabiki H. 2014. Nucleosomal regulation of chromatin composition and nuclear assembly revealed by histone depletion. *Nat Struct Mol Biol* **21**:617–625. doi:10.1038/nsmb.2845

9.2 Key message of the PhD thesis and relevance to the field

Taken together the results of the three Parts underscore the importance of the study of condensin in an in vivo context. In all of the scientific projects we have consistently shown that in vivo, condensin is positioned or functionally influenced by chromatin associated features and that these features have direct functional consequences on chromosome segregation, that is the shelterin component at telomeres (Part 5), the negative impact of active RNA pol II (Part 6) and of the density of nucleosomes on the chromatin fiber (Part 7).

Of main interest, the precise mechanisms by which nucleosomes and condensin interplay are certain to be investigated further in the following years judging by the most recent papers of other labs **(Sun et al., 2023; Yamamoto et al., 2023).**

9.3 Author acknowledgements and contributions to the scientific papers

I would like to reiterate my thanks to the people that have contributed to the three scientific projects, as my own contribution was necessary but not sufficient to complete these projects. For all three projects I would like to thank first **Pascal Bernard** for the supervision, visualization and writing of the papers.

Concerning Part 5, I would like to thank the **Tournier lab** for the microscopy experiments, the **Cuvier lab** for data analysis of Hi-C and the **Coulon lab** for molecular ork on telomeres. Concerning Part 6, **Jeremy Lebreton** for the data generation in Dhp1 depletion, Spt-PALM experiments and the data analysis. Concerning Part 7, **Esther Toselli** for data generation on multiple experiments and **Laurent Modolo** for help with the analysis.

I would also like to thank the people that have contributed material and technical help, notably **Jon Baxter** and **Nicola Minchell** who taught me the Hi-C procedure, and **Yasutaka Kakui** and **Frank Uhlmann** for sharing their fission yeast Hi-C protocol.

Concerning the funding, I would like to acknowledge the multiple bodies of funding that contributed to the human resources involved. Particularly I would like to thank la Ligue Contre le Cancer which funded my PhD for 3 years, the Condensin-Chromatin ANR which funded the fourth and final year and the LBMC who financed two months of salary during the uncertain period between the third and fourth year of the PhD.

Regarding the PhD manuscript I would like to thank **Stéphane Marcand** and **Frank Uhlmann** for accepting to take on the role of *rapporteurs* of my PhD jury as well as **Kerstin Bystricky**, **Armelle Lengronne** and **Benjamin Loppin** for accepting to take on the role of examiners.

9.4 Personal thanks

Here I would like to thank on a more personal note many people that have not necessarily contributed scientifically to my PhD (although sometimes they have, directly or indirectly) but have helped me personally for a good chunk of this peculiar period.

First I would like to thank the LBMC institute for hosting me and providing me both with a productive research environment. Several members of the LBMC here were instrumental to this. I would like to thank the people of the human resources who have done all the things I dislike doing myself and use CNRS software which I can only described as eldritch. Emmanuelle, Corinne, Julie all helped setting up orders & deliveries, travels and talks. I would specifically like to thank Isabelle who was always available and took time from her busy schedule to help me and ask how things were doing. I would also like to thank the people from the laverie who have likely cleaned and autoclaved… hundreds ? of my erlens and growth media and without who I could not have performed experimental work.

I would also like to thank the researchers from the LBMC who have interacted and discussed with me over the years. I would like to thank members of the Piazza team for the joint meetings – I still do not know how to draw a Holliday junction but I promise to try again at some point. I would also like to give a special mention to Laurent of the biocomputing hub. He did not only improve the calibrated chipseq pipeline, but has helped me *many* times to troubleshoot and solve issues at the PSMN when I tried to run and rerun pipes and was slowly going insane. I would like to thank him for his patience and his help.

I would also like to thank the members of my PhD commitee (CST), Fred Beckouët and Aurèle Piazza who gave me good pointers, both for my PhD project as well as my career later down the line. They kindly accepted to be present for a third comittee since I had been renewed for a fourth year. Given that I appreciated their help so much, I decided to spare them having to be members of the jury for the PhD defence.

I would like to thank my friends outside of the lab : those from Lyon, those from Lyon who have now moved, those from university, those from the karaoke and my tabletop friends. They allowed me to not think about work too much and forced me to have a social life, sometimes despite my best efforts.

I would like to thank my family, for inquiring about my PhD although explaining things in laymen's terms is not my forte. I would like to thank my parents for their love and support and being there when I had to vent about my numerous failures, both before and during the PhD. I would like to thank Constance, Pedro, Emile, Gaspard and Felix who I would have liked to see more in Spain during the PhD. I will award a special mention to Felix, born the same day I started working again in Pascal's lab for my PhD project after my long summer break of 2019.

Finally I would like to thank the Bernard team as a whole for hosting me for so long. I would like to thank past members I met (and to apologize if I forgot to mention some interns) : Clémence, Apoorva, Lauranne, Baptiste, Pierre, Laetitia, Connor, Virgile. I would like to specifically thank Julieta for her advice to me during the M2 of not being upset by stupid mistakes, but of viewing them rationally the same way one would do to an experiment. I would like to thank Xavier for being my first real bench mentor. My first internship under his supervision was not necessarily my best work but I will give myself some slack : since then the Covaris sonicator has not let me down. I would like to thank Laure for being a very easy intern to teach and wish her the best on her endeavors in plant biology. I wish the future interns/PhD students in the Bernard team the best. As of this time I have met Thomas who I hope will have as much fun as I did during his M2.

I would like to thank present members of the lab : Dana, who must now continue exploring the relationship between chromatin and condensin (and who I have selfishly titled my spiritual successor). Jeremy, who made the PhD only *slightly* more fun and with which we produced, I think, a paper of very good quality, that we both wish more people would have read. I hope we meet again at some meeting at one point. Finally I would like to thank the 'big three' of the lab, core members who have been there since before I arrived and who have withstood the test of time.

I would like to thank Vincent, who was always there for pointed and high quality feedback, as well as great insight scientifically, and for his enthusiasm and involvement in science. I have hope that

Vincent can map hybrids in cells – I am very skeptical, however, about the existence of good *haggis*. Also, if you must ask him, yes, everything is my fault.

Then I would like to thank Esther. I can only be honest when I say that I do not think I would have successfully defended my PhD without Esther. She went through the painful process of setting up library preparation, MNase, condensation assays - among many other things. We worked in close collaboration and she was always the rock during the PhD. We developed a strong solidarity through many trials : difficult time courses, tricky mitotic arrests, the occasional tear gas and not knowing when a budding yeast cell has finished dividing.

Last but not least I would like to thank Pascal for always being available, an excellent mentor that always gave me opportunities to participate in various project, as my contributions as a first co-author can attest to. As I have worked for a little while in a research environment now, I realize that a lot of time and resources are invested – and in that context I can only acknowledge the great amount of trust that Pascal gave me (although sometimes, maybe a bit too much trust ?). I am glad I discovered the SMC field thanks to Pascal, and all the fun lore that came with the literature (notably : the condensin 5%, 'God' and the interphase condensin *ts* mutants) otherwise I may have simply worked on chromatin - without ever being aware of cohesin and condensin complexes. Finally I would like to thank him overall for this PhD which was fundamental both for my career, scientific interests and also for my personal growth. My hands are not quite as shaky as they used to be.

LC